# Sustainable Management of Water Resources and Hydropower Projects in the Context of the Food-Energy-Water Nexus in the Mekong River Basin

Syed Azhar Ali

Dissertation submitted to the faculty of the Virginia Polytechnic Institute and State University in partial fulfillment of the requirements for the degree of

Doctor of Philosophy
In
Biological Systems Engineering

Venkataramana Sridhar
David J Sample
Bradford F Mills Jr
Christopher W Zobel

28th August 2020
Blacksburg, Virginia

Keywords: Remote sensing, Reservoir operation, Optimization, Variable Infiltration Capacity, Climate change

Sustainable Management of Water Resources and Hydropower Projects in the Context of the Food-Energy-Water Nexus in the Mekong River Basin

Syed Azhar Ali

## ABSTRACT

The Mekong River Basin (MRB) is one of the largest transboundary basins in the world shared between six south Asian countries. The Mekong river supports a population of more than sixty million people through irrigation and fisheries for their survival and hosts approximately 88,000 MW of unharnessed hydropower potential. The construction of the dams for the supply of energy has a wide-ranging effect on the downstream regions of reservoirs, causing unprecedented and devastating damage to the environment and livelihood of people. The dissertation examines the optimal operation of the dams for the equitable distribution of water between irrigation, domestic, and hydropower sectors with minimal effect on the downstream ecosystem by estimating the cascading effects of dams in the MRB. The hydrological characteristic of the MRB was simulated using the high resolution (1 km) Variable Infiltration Capacity (VIC) hydrological model with the Lohmann et al. (1996, 1998) routing scheme and general circulation models projection for the future till 2099. Remote sensing products were used for the derivation of the reservoir behaviors, while the net irrigation water requirement (NIWR) was simulated by the irrigation scheme embedded in the improved VIC model. The VIC-MODFLOW (VIC-MF) coupled model was used for the investigation of the interaction between the surface and groundwater movement. The hydropower potential of the dams was estimated using the modified Hanasaki et al. (2006) approach by explicitly considering the irrigation water demand from the expanding and intensifying agricultural activities. A system dynamic model for the MRB was developed for the sustainable optimization of water allocation to meet the needs from the irrigation, domestic, hydropower generation, and ecological sectors. Economic analysis was performed to evaluate the existing and future conditions over the resource surplus regions with consideration of social impacts. Streamflows in the MRB varied substantially with the peak monthly streamflow from 10 $m^3$/sec to 40,000 $m^3$/sec. The inflows to dams in both main river and tributaries are projected to increase from 1.2% to 25% under RCP 4.5 and a decrease of 28.5% - 74.7% under RCP 8.5 during

2020-2099 as compared to the historic mean. The NIWR for the MRB was calculated as 65,000 million $m^3$ for the observed period (1981-2019) with a decrease of 0.25% for the future period. The groundwater interaction is expected to enhance the surface streamflow resulting in additional inflow to dams. The multipurpose reservoirs were able to generate the desired annual energy ranging from 15 GWh to 400 GWh along with satisfying more than 80% of the irrigation water demand. Similarly, the irrigation reservoirs also satisfied more than 80% of the water demand for irrigation and hydropower reservoirs to generate the required energy between 2 GWh and 18990 GWh. Climate change will enhance the hydropower potential with an average increase of 7.3% and 5.3% in the future under RCP 4.5 and RCP 8.5, respectively. The increase in the irrigated area (5% and 10%) reduces the energy generation of the multipurpose dams by 1.5%, however, the addition of a crop cycle lowers the energy generation by more than 10%. The system dynamics model showed the multipurpose dams produced annual energy of 316 GWh and satisfied more than 60% of the irrigation, municipal, and industrial sectors water demand during 2006-2019. Similarly, irrigation dams supplying more than 60% of the irrigation water demand, and 50% of the municipal and industrial sectors demand. Climate change has a positive influence on the performance of the dams. The assessment of the shadow price shows that the dam operation in Thailand, Laos PDR, and China will be sufficient to meet the water demands of the energy, irrigation, municipal, and industrial sectors, while the energy sector of Cambodia and Vietnam may experience adverse impacts.

Sustainable Management of Water Resources and Hydropower Projects in the Context of the Food-Energy-Water Nexus in the Mekong River Basin

Syed Azhar Ali

## GENERAL AUDIENCE ABSTRACT:

The Mekong River Basin (MRB) is one of the largest transboundary basins in the world shared between six south Asian countries. The Mekong river supports more than sixty million people through irrigation and fisheries for their survival and hosts unharnessed hydropower potential. The construction of the dams has a wide-ranging effect on the downstream regions of reservoirs, causing damage to the environment and livelihood of people. The dissertation studies the optimal operation of the dams in the MRB for the equitable distribution of water between irrigation, domestic, and hydropower sectors with minimal effect on the ecosystem. The streamflow of the MRB was simulated using the hydrological model with a routing scheme and future projection till 2099. Remote sensing products were used for the derivation of the reservoir behaviors. The water requirement for the irrigation and the groundwater-surface interaction was simulated by the irrigation scheme embedded in the hydrological model and groundwater coupled model. The hydropower potential of the dams was estimated by explicitly considering the irrigation water demand from the expanding and intensifying agricultural activities. A dynamic model for the MRB was developed for the sustainable optimization of water allocation to meet the needs from the irrigation, domestic, hydropower generation, and ecological sectors. Economic analysis was performed to evaluate the existing and future conditions over the resource surplus regions with consideration of social impacts. Streamflows in the MRB varied substantially between the dams based on the location at the mainstem or tributaries. The inflows to dams in both main river and tributaries in the future is expected to increase under low-carbon emission and decrease under high-carbon emission conditions. The irrigation water for the MRB was calculated as 65,000 million $m^3$ for the period 1981-2019 and expected to decrease in the future. The groundwater interaction is expected to increase the surface streamflow resulting in additional inflow to dams. The multipurpose reservoirs were able to generate the desired annual energy ranging along with satisfying more than 80% of the irrigation water demand. Similarly, the irrigation

reservoirs also satisfied more than 80% of the water demand for irrigation and hydropower reservoirs to generate the required energy. Climate change will favor the hydropower energy potential in the future. The increase in the irrigated area and the addition of a crop cycle reduces the energy generation of the multipurpose dams. The system dynamics model showed the multipurpose dams produced 97% of the demand energy and satisfied more than 60% of the irrigation, municipal, and industrial sectors water demand during 2006-2019. Similarly, irrigation dams supplying more than 60% of the irrigation water demand, and 50% of the municipal and industrial sectors demand. Climate change has a positive influence on the performance of the dams. The assessment of the shadow price shows that the dam operation in Thailand, Laos PDR, and China will be sufficient to meet the water demands of the energy, irrigation, municipal, and industrial sectors, while the energy sector of Cambodia and Vietnam may experience adverse impacts.

Dedicated to

My Family, Teachers, and Friends

*For their endless love, support, and encouragement*

# ACKNOWLEDGEMENT

First and foremost, thanks go to God for the blessing that has bestowed upon me in all my endeavors.

I would like to express my sincere gratitude to my supervisor, Dr. Venkatramana Sridhar, for his invaluable guidance, cooperation, and constant encouragement during the course of the dissertation. I truly appreciate his esteemed guidance and support from beginning to the end of the dissertation, his knowledge and company at the time of crisis would be remembered lifelong. I would also like to thank my committee members, Dr. Bradford F Mills Jr, Dr. David J Sample, and Dr. Christopher W Zobel for accepting to serve on my committee and providing valued input and feedback.

I also thank all my friends especially Hyunwoo Kang, Parthkumar Modi, and Akhil Ahmed who made my stay at Virginia Tech cheerful and joyful.

Last but certainly not least; I would like to thank my parents who taught me the value of hard work by their example. They stood behind me for all the decisions I took and provided ever support for their loving son in all respect.

I sincerely acknowledge the opportunity provided by Virginia Tech and financial aid provided by NASA, during my Ph.D. program.

# Table of Contents

# List of Figures

**Chapter 2:**

**Chapter 3**

**Chapter 4**

**Chapter 5:**

**Appendix A:**

# List of Tables

**Chapter 2:**



**Chapter 3:**



**Chapter 4:**

**Chapter 5:**

# List of Acronyms

| | |
|---|---|
| BCSD | Bias Correction and Spatial Downscaling |
| $b_{inf}$ | VIC Infiltration parameter |
| D | Soil layer thickness |
| DHP | Developed Hydropower Potential |
| Ds | Fraction of maximum baseflow velocity |
| Dsmax | Maximum baseflow velocity |
| FDC | Flow Duration Curve |
| GCM | General Circulation Model |
| HG | Hydropower Generation |
| IGBP | International Geosphere Biosphere Programme |
| GWh | Giga Watt hour |
| LAI | Leaf Area Index |
| MODIS | Moderate Resolution Imaging Spectroradiometer |
| NSE | Nash Sutcliffe Efficiency |
| $Q_{10}$ | $10^{th}$ quantile streamflow |
| $Q_{50}$ | $50^{th}$ quantile streamflow |
| $Q_{90}$ | $90^{th}$ quantile streamflow |
| r | Correlation coefficient |
| RCP | Representative Concentration Pathway |
| VIC | Variable Infiltration Capacity model |
| Ws | Fraction of the maximum soil moisture |

# Chapter 1

# Introduction

The Mekong River Basin (MRB) is one of the largest transboundary basins in the world located in southeast Asia. The basin encompasses the region of China, Myanmar, Thailand, Lao PDR, Cambodia, and Vietnam. Sixty million people in the Lower Mekong Basin (LMB) derive their nourishment from the Mekong river for agricultural activities-rice cultivation, vegetables, livestock, fruit and nuts, and fisheries, apart from off-farm wages, (Martin & Lorenzen, 2016; Olson & Morton, 2018). In the Lower Mekong Basin (LMB), flooding, drought, and salinity intrusion are the critical problems associated with climate variability and climate change affecting crop production, local livelihood, infrastructure, and freshwater fisheries (Bastakoti et al., 2014). The hydrology of the LMB is controlled by the seasonal variability in the flow with contrasting wet and dry seasons governed by the variation in rainfall (Sridhar et al., 2019). Since the ability of the LMB to support the existing diverse ecosystem and livelihood of millions of people depends upon the unique climatic, hydrologic, and topographic characteristics of the area, various studies have been performed to understand the region and influence of vital components on the streamflow (Chen et al., 2015; Hoanh et al., 2004; Lyon et al., 2017; Minderhoud et al., 2018).

A huge pulse and depression in the mean annual flows during the wet and dry period define the hydrology of the Mekong River. Meteorological drought is a natural phenomenon caused by intense and long term scarcity of precipitation (Zargar et al., 2011). The magnitude and foreseeable peak time define the large tropical monsoonal river (Adamson et al., 2009) causing a 20-fold increase in discharge between August and September. The seasonal flood pulse and timely rainfall are the governing factors for the food production and abundant supply of fresh water and nutrients for the fisheries in lakes and rivers (Pokhrel et al., 2018).

Apart from being a lifeline for the people and ecosystems of half a dozen countries, the Mekong river hosts an incredible amount of unharnessed hydropower (more than 50,000 MW in the main stem and 30,000 MW from tributaries; Stone, 2011). More than 400 dams have been proposed or are currently being evolved along the course of the Mekong river,

including the existing 42 dams with three on the main steam of the river in China, to harness the hydropower production (Keskinen et al., 2012; Mekong River Commission, 2010). There are plans to build 16 mainstem and 110 tributary dams additionally by 2030 (Grumbine & Xu, 2011; Lauri et al., 2012; Winemiller et al., 2016). The underdeveloped condition of the MRB in terms of river impoundments (M Kummu & Sarkkula, 2008) and sensitivity of the dam information is the basic cause of archived datasets shortage in the region. Dams also protect during flood events, water availability during dry periods, and recreational activities. The construction of dams for the supply of energy has a wide-ranging effect on the downstream regions of the reservoirs, causing devastating damage to the environment and livelihood of millions of people (R Stone, 2016; Richard Stone, 2011a). Dams have catastrophic effects on agriculture, fisheries, and biodiversity (Intralawan et al., 2017; G. Ziv et al., 2012), as well as on downstream sediment delivery (M. Kummu et al., 2010; Shrestha et al., 2013), coastal groundwater (Merola et al., 2015), and flood-drought management (Wang et al., 2017).

Over the last several decades, the LMB experienced several drought events, such as in 1992, 1993, 1998, and 1999 (Mekong River Commission, 2005) with the latest occurrence in 2003 lasting until June 2006 (Te, 2007). Sin et al. (2012) utilized the monthly MODIS normalized difference vegetation (NDVI) and land surface temperature (LST) data for agricultural drought monitoring in the dry season from November 2001 to April 2010 using the temperature vegetation dryness index (TVDI). Results indicated spatially scattered moderate and severe droughts over the region from November to March but more extensive drought in Thailand and Cambodia. The 2003-2006 dry seasons caused severe drought over a larger area as compared to other years. Hapuarachchi et al (2008) highlighted the significance of the baseflow for a long term synthetically-induced drought during the investigation of the LMB hydrology for the 1980-2000 period using a grid-based distributed hydrological model called Yamanashi Hydrological Model.

The drought condition in the LMB was evaluated using a long-term high resolution ($0.05^{o}$) Climate Hazards Group Infrared Precipitation with Station data (CHIRPS) satellite product from January 1981 to 2016 through estimation of the standardized precipitation index (SPI)

at a three-month time scale (Guo et al., 2017). The LMB experienced four severe droughts during the period with a 38 months long event during 1991-1994 and driest one during 2015-2016 affecting more than 75% area of the basin. The northern and southern regions of LMB observed frequent droughts while the Delta seems to face long-term and extreme events. Thilakarathne and Sridhar (2017) conducted a multivariate analysis using copula function based on projected precipitation data from 15 GCMs and selected SPI as the drought index. The lower LMB and 3S subbasins were projected to face severe droughts, while lesser drought in the future was projected for the Chi-Mun sub-basin. According to Kiem et al. (2008), all subbasins in LMB will experience more wet days by 2099, affecting the magnitude and frequency of the extreme events, eventually resulting in increased flooding risk and reduced likelihood of droughts. Since the floods in the basin are closely related to precipitation intensities, NASA's global precipitation measurement (GPM) mission assist the flood-prone river basins to improve flood forecasting. The GPM mission initiated in 2010 comprising of high-resolution passive microwave sensors at ~3-6 temporal and 10 km spatial resolution (Hossain & Katiyar, 2006). Sakamoto et al. (2007) produced time-series inundation maps for the five annual flood seasons from 2000 to 2004 to detect a temporal change in the extent of annual flooding within Cambodia and the Vietnamese Mekong Delta using MODIS time-series imagery and wavelet-based filter approach. The result indicated an increase in the estimated area of water bodies that ranged in size between 250,000 ha to 400, 000 ha from 2000 to 2004.

The hydrological impact assessment using the Coupled Model Intercomparison Project 5 (CMIP5) climate projections and VMod hydrological model to analyze changes in river flow regimes and hydrological extremes in the LMB shows an increase in extremely high-flow events in magnitude as wells as frequency (Hoang et al., 2016). The flood risks in the basin are elevated due to higher and more frequent peak discharges. Other studies also suggested similar results showing increasing flood risks in the Cambodia and Vietnam region during the wet season due to increasing river flow (Hoanh et al., 2010; Västilä et al., 2010). Moreover, the flood variance in the MRB can be predicted by the relationship between Pacific seas surface temperature and moon variance in the basin (Delgado et al., 2012). The western Pacific monsoon is closely related to the interannual to the decadal

variance of the Mekong discharge. The projected probability of the extreme wet flood event by the end of 2039 shows large variability between different studies incorporating hydrological models accounting an increase of 5% to 76% by Eastham et al. (2008) and a small increase of 1% by Hoanh et al (2004).

A large number of quantitative models have been used for the assessment of hydrology, hydrodynamics and sediment dynamics of the LMB which were classified into four main suites of hydrological models i.e. MRC's Decision Support Framework (SWAT, IQQM, and iSIS), VIC, MIKE suite developed by DHI, and WUP-FIN suite (Johnston & Kummu, 2012). Various studies have been conducted to investigate the alteration of the flow and water availability due to climate change in the LMB (Eastham et al., 2008; Hoanh et al., 2004, 2010; Kiem et al., 2008; Västilä et al., 2010). The uncertainty study performed by Kingston et al (2011), using the semi-distributed hydrological model (SLURP) and seven different GCMs reveal the change in annual river discharge to increasing mean temperature varying from a 5.4% decrease to 4.5% increase. Similar results were obtained by Vastila et al (2010), reporting an increase of 4% in streamflow with an annual temperature increase from 1 $^{o}$C and 2 $^{o}$C in the Mekong by 2040s using the dynamically downscaled ECHAM4 climate model data. However, the impact of climate change is not confined to streamflow alteration, and it has an overwhelming effect on the sediment yield in the LMB as well. Climate change resulting in precipitation changes is expected to increase the wet season flow of the MRB by 10%, while the dry season flow remaining consistent. Chiang Saen and Luang Prabang gage stations will experience anomaly in streamflow with a reduction of up to 5% for the other flow stations (Sridhar, Kang, et al., 2019). The change in the annual sediment yield from a 27% decrease to 160% increase is predicted by Shrestha et al. (2013) employing four GCMs, a regional circulation model (PRECIS), and Soil and Water Assessment Tool (SWAT). Also, the intra-annual (monthly) variation of the sediment yield was even greater, ranging from 88% decrease to a 243% increase.

The sediment from the upstream is rich in nutrients and provides critical support to the agriculture flood plain and ecosystem in the LMB but the reliable data are not available (Kondolf et al., 2018; Kummu & Varis, 2007). The major land cover transformation from

forest area to agriculture accounting for 6.8% over the past decades is attributed to population increase with annual growth of 1-3% in member countries, urbanization, and socio-economic advancement of the countries in the LMB (Costa-Cabral et al., 2008a; Spruce et al., 2020). Spruce et al. (2018) used the MODIS and Landsat satellite data to classify regionally common forest and agricultural LULC types in the LMB. The monthly NDVI maps were derived from the 2010 MODIS MOD09 and MYD09 8-day reflectance to assess 14 classes in the MRB at a 250-m spatial resolution with 87% accuracy. The regional LULC maps were supplemented with the more detailed agriculture LULC types to enhance the application in the hydrological modeling. The Spatio-temporal dynamics of LULC change in the lower Mekong Delta from 1973 to 2011 using the high resolution (Landsat and SPOT) satellite imagery suggests an increase in the built-up areas and aquaculture lands by 120 $km^2$ and 123 $km^2$ respectively (Tran et al., 2015). Moreover, the cultivated lands reduced by 77 $km^2$ over the period but still represents the dominant class along with a decrease in bare lands, mangrove forest, and melaleuca forest. Minderhoud et al. (2018) related the land subsidence in the Mekong Delta to regional land use using the Landsat and Interferometric Synthetic Aperture Radar (InSAR) data of 20 years. The anthropogenic influence is visible in the result showing lowest mean subsidence rates for undeveloped land-use classes, like marshland and wetland forest (~6-7 mm/year), and highest rates for areas with mixed-crop agriculture and cities (~18-20 mm/year). The effect of the land transformation in the Chi river basin in Thailand was studied by Homdee et al. (2011) by considering the replacement of sugarcane crops with paddy fields using the SWAT model. It resulted in the reduction of the water flows and about a 5% increase in the ET, demanding higher water requirements for the irrigation of the rice paddies. The seasonal analysis of the variation of the water flow and ET exhibited a reduction of 12% ET and 5.1% water flow enhancement in the dry season.

Since the Mekong river basin spans over six countries, the systematic collection of the hydrological, ecological, meteorological and geographical dataset took 40 years of effort through the appointment of the Mekong River Commission (MRC) (Browder & Ortolano, 2000). The Mekong agreement aims to achieve sustainable development through the real-time sharing of data and information for planning and monitoring purpose but the

information sharing is limited (Gerlak et al., 2011; Plengsaeng et al., 2014). Moreover, the LMB is claimed to be one of the weakest monitoring regions globally and ineffective in data and information sharing (Affeltranger, 2009a, 2009b; Aliagha, 2004; Gerlak et al., 2011; Plengsaeng et al., 2014; Thu & Wehn, 2016). However, the remote sensing datasets are globally applicable and unaffected by the shortage of availability of *in-situ* data.

Remote sensing can be used to derive the reservoir parameters for the data restricted region. The reservoir water depth can be estimated using the spatial extent estimated by the optical and Synthetic Aperture Radar images (Li et al., 2016; Pipitone et al., 2018). The remotely sensed satellite data was merged with altimetry information for the monitoring of large reservoirs through unsupervised classification method (H. Gao et al., 2012). Remote sensing also helps in developing guidelines for reservoir operations. The satellite imageries and water level data set from four different satellite altimetry databases—Global Reservoir and Lake Monitor (GRLM), River-Lake Hydrology (RLH), Hydroweb, and ICESat-GLAS level 2 global land surface altimetry data (ICESat-GLAS)—are available to estimate the water volume changes in lake and reservoirs (Becker et al., 2018; Duan & Bastiaanssen, 2013; Muala et al., 2014). The streamflow variation in the LMB was explored by deriving the residence time and flow alteration with range 0.09-4.04 years and 11%-130% respectively was estimated by developing the artificial reservoir operation using the satellite data (Bonnema and Hossain, 2017)

Numerous studies have investigated the hydrological features of the Mekong river and the operations of its dams. The MRB is expected to witness a rise in streamflow (Homdee et al., 2011; Sridhar et al., 2019; Västilä et al., 2010) and annual sediment yield (Shrestha et al., 2013) due to the projected increase in future precipitation. Using satellite observations, some studies have also explored the operating pattern of reservoirs in the MRB. However, most studies were confined to a very limited number of dams and focused mainly on sediment yield changes (Kondolf et al., 2014) and fish biodiversity (Ziv et al., 2012). The overarching objective of our study is to understand the changing hydrological conditions and develop a framework for assessing water management by linking food-energy-water nexus for present and future conditions. This will be required to implement strategies to

optimally operate the dams for the equitable distribution of water between irrigation, domestic, and hydropower sectors with minimal effect on the downstream ecosystems by estimating the cascading effects of more than 400 future dams in the MRB.

### 1.1 Goals and Objectives

The goal of this research is to explore the sustainability of the MRB in fulfilling the demands of irrigation, hydropower, domestic and ecological systems under the food-energy-water nexus framework. To achieve this goal, the following objectives will be addressed:

1. To study the MRB in terms of streamflow, and land cover change using the hydrological model (VIC) for the current period and projected change in streamflow
2. To investigate the changing practices in agriculture and estimate the net irrigation water requirement (NIWR) for the irrigated area and the supply from the reservoirs and groundwater to meet the demand. This will also consider the projected NIWR based on the projected population increase in the basin.
3. To estimate the hydropower production of the MRB based on the existing dams, and to formulate supply-demand scenarios by explicitly considering the effect of irrigation growth on hydropower generation; to determine future changes in the hydropower potential considering the commissioned dams with cascading effects and expanding irrigation.
4. To develop a systems dynamic model for the sustainable optimization of water allocation to the irrigation, domestic, hydropower generation, and ecological sectors, thereby taking into account the effects of climate and land use and land cover change and satisfying the multiple criteria through feedback loops. Economic analysis of the existing and future conditions to identify the resource surplus regions with consideration of social impacts.

### 1.2 Dissertation Organization

Chapter 1 of this dissertation introduces the Mekong river basin and the literature reviews of hydrological modeling, climate change impact, irrigation, and hydropower studies.

Chapter 2-5 are specific to each of the previously mentioned four main objectives of this research. As each of these chapters shares basic input and background information, there are redundancies while describing them in the chapters. Chapter 6 contains the overall conclusion of this research.

**Reference for Chapter 1**


Adamson, P. T., Rutherfurd, I. D., Peel, M. C., & Conlan, I. A. (2009). The Hydrology of the Mekong River. In *The Mekong* (pp. 53–76). Elsevier. https://doi.org/10.1016/B978-0-12-374026-7.00004-8

Affeltranger, B. (2009a). Mekong Studies at Crossed Glances. In *4th French-MFU Seminar*. Chiang Rai, Thailand. Retrieved from https://www.ggr.ulaval.ca/sites/default/files/documents/Lasserre/Publications/actes_lasserre-affeltranger_irasec-mfu_2009.pdf

Affeltranger, B. (2009b). Sustainability of Environmental Regimes: The Mekong River Commission (pp. 593–601). Springer, Berlin, Heidelberg. https://doi.org/10.1007/978-3-540-68488-6_43

Agriculture and fishing | Open Development Mekong. (2019). Retrieved August 15, 2020, from https://opendevelopmentmekong.net/topics/agriculture-and-fishing/

Akter, A., & Babel, M. S. (2012). Hydrological modeling of the Mun River basin in Thailand. *Journal of Hydrology*, *452–453*, 232–246. https://doi.org/10.1016/J.JHYDROL.2012.05.059

Al-Ruzouq, R., Shanableh, A., Merabtene, T., Siddique, M., Khalil, M. A., Idris, A., & Almulla, E. (2019). Potential groundwater zone mapping based on geo-hydrological considerations and multi-criteria spatial analysis: North UAE. *CATENA*, *173*, 511–524. https://doi.org/10.1016/J.CATENA.2018.10.037

Alaouze, C. (1996). Shadow Prices in Linear Programming Problems. *Papers*.

Ali, Syed A., & Sridhar, V. (2019). Deriving the Reservoir Conditions for Better Water Resource Management Using Satellite-Based Earth Observations in the Lower Mekong River Basin. *Remote Sensing*, *11*(23), 2872. https://doi.org/10.3390/rs11232872

Ali, Syed Azhar, Aadhar, S., Shah, H. L., & Mishra, V. (2018). Projected Increase in Hydropower Production in India under Climate Change. *Scientific Reports*, *8*(1), 12450. https://doi.org/10.1038/s41598-018-30489-4

Aliagha, C. (2004). Environmental Clearinghouse as an Institutional Incentive for Data and Information Sharing and Conflict Reuction in the Mekong River Basin. In *OpenSIUC* (pp. 7–20). Southern Illinois University, Carbondale, Illinois. Retrieved from http://opensiuc.lib.siu.edu/ucowrconfs_2004/2

Allen, R., Pereira, L., Raes, D., & Smith, M. (1998). Crop evapotranspiration-Guidelines for computing crop water requirements-FAO Irrigation and drainage paper 56. *FAO Irrigation and Drainage Paper No. 56.* Retrieved from https://www.researchgate.net/profile/Hawre_Kiani/post/What_is_the_more_effective_way_of_deficit_irrigation/attachment/5af42706b53d2f63c3cafa73/AS%3A624694629777415%401525950214858/download/Allen_FAO1998.pdf

AQUASTAT. (2014). Irrigation water requirement and water withdrawals by country. Retrieved January 11, 2019, from http://www.fao.org/nr/water/aquastat/main/index.stm

Awawdeh, M., Obeidat, M., Al-Mohammad, M., Al-Qudah, K., & Jaradat, R. (2014). Integrated GIS and remote sensing for mapping groundwater potentiality in the Tulul al Ashaqif, Northeast Jordan. *Arabian Journal of Geosciences*, *7*(6), 2377–2392. https://doi.org/10.1007/s12517-013-0964-8

Bastakoti, R. C., Gupta, J., Babel, M. S., & van Dijk, M. P. (2014). Climate risks and

adaptation strategies in the Lower Mekong River basin. *Regional Environmental Change*, *14*(1), 207–219. https://doi.org/10.1007/s10113-013-0485-8

Becker, M., Papa, F., Frappart, F., Alsdorf, D., Calmant, S., da Silva, J. S., et al. (2018). Satellite-based estimates of surface water dynamics in the Congo River Basin. *International Journal of Applied Earth Observation and Geoinformation*, *66*, 196–209. https://doi.org/10.1016/J.JAG.2017.11.015

Birkett, C., Reynolds, C., Beckley, B., & Doorn, B. (2011). From Research to Operations: The USDA Global Reservoir and Lake Monitor. In *Coastal Altimetry* (pp. 19–50). Berlin, Heidelberg: Springer. https://doi.org/10.1007/978-3-642-12796-0_2

Bonnema, M., & Hossain, F. (2017). Inferring reservoir operating patterns across the Mekong Basin using only space observations. *Water Resources Research*, *53*(5), 3791–3810. https://doi.org/10.1002/2016WR019978

Bosch, J. M., & Hewlett, J. D. (1982). *A REVIEW OF CATCHMENT EXPERIMENTS TO DETERMINE THE EFFECT OF VEGETATION CHANGES ON WATER YIELD AND EVAPOTRANSPIRATION*. *Journal of Hydrology* (Vol. 55). Retrieved from http://coweeta.uga.edu/publications/2117.pdf

Boucher, O., Myhre, G., & Myhre, A. (2004). Direct human influence of irrigation on atmospheric water vapour and climate. *Climate Dynamics*, *22*(6–7), 597–603. https://doi.org/10.1007/s00382-004-0402-4

Box, M. J. (1965). A new method of constrained optimization and a comparison with other methods. *The Computer Journal*, *8*(1), 42–52. https://doi.org/10.1093/COMJNL/8.1.42

Brito, M. G., Costa, C. N., Almeida, J. A., Vendas, D., & Verdial, P. H. (2006). Characterization of maximum infiltration areas using GIS tools. *Engineering Geology*, *85*(1–2), 14–18. https://doi.org/10.1016/J.ENGGEO.2005.09.022

Browder, G., & Ortolano, L. (2000). *The Evolution of an International Water Resources Management Regime in the Mekong*. *Source: Natural Resources Journal* (Vol. 40). Retrieved from https://www.jstor.org/stable/pdf/24888536.pdf?refreqid=excelsior%3Af1fd62acc9ba6474184989cb5355f678

Cao, Q., Yu, D., Georgescu, M., Han, Z., & Wu, J. (2015). Impacts of land use and land cover change on regional climate: a case study in the agro-pastoral transitional zone of China. *Environmental Research Letters*, *10*(12), 124025. https://doi.org/10.1088/1748-9326/10/12/124025

Carruthers, I., Rosegrant, M. W., & Seckler, D. (1997). Irrigation and food security in the 21st century. *Irrigation and Drainage Systems*, *11*(2), 83–101. https://doi.org/10.1023/A:1005751232728

Chang, F.-J., Chen, L., & Chang, L.-C. (2005). Optimizing the reservoir operating rule curves by genetic algorithms. *Hydrological Processes*, *19*(11), 2277–2289. https://doi.org/10.1002/hyp.5674

Chapman, A., & Darby, S. (2016). Evaluating sustainable adaptation strategies for vulnerable mega-deltas using system dynamics modelling: Rice agriculture in the Mekong Delta's An Giang Province, Vietnam. *Science of the Total Environment*, *559*, 326–338. https://doi.org/10.1016/j.scitotenv.2016.02.162

Chase, T. N., Pielke Sr, R. A., F Kittel, T. G., Baron, J. S., & Stohlgren, T. J. (1999). *Potential impacts on Colorado Rocky Mountain weather due to land use changes on*

*the adjacent Great Plains*. *JOURNAL OF GEOPHYSICAL RESEARCH* (Vol. 104). https://doi.org/10.1029/1999JD900118

Chen, C.-J., Jayasekera, D. L., & Senarath, S. U. S. (2015). Assessing Uncertainty in Precipitation and Hydrological Modeling in the Mekong. In *World Environmental and Water Resources Congress 2015* (pp. 2510–2519). Reston, VA: American Society of Civil Engineers. https://doi.org/10.1061/9780784479162.246

Claverie, M., Ju, J., Masek, J. G., Dungan, J. L., Vermote, E. F., Roger, J. C., et al. (2018). The Harmonized Landsat and Sentinel-2 surface reflectance data set. *Remote Sensing of Environment*, *219*, 145–161. https://doi.org/10.1016/j.rse.2018.09.002

Cleugh, H. A., Leuning, R., Mu, Q., & Running, S. W. (2007). Regional evaporation estimates from flux tower and MODIS satellite data. *Remote Sensing of Environment*, *106*(3), 285–304. https://doi.org/10.1016/j.rse.2006.07.007

Conway, D., Van Garderen, E. A., Deryng, D., Dorling, S., Krueger, T., Landman, W., et al. (2015, August 21). Climate and southern Africa's water-energy-food nexus. *Nature Climate Change*. Nature Publishing Group. https://doi.org/10.1038/nclimate2735

Cosby, B. J., Hornberger, G. M., Clapp, R. B., & Ginn, T. R. (1984). A Statistical Exploration of the Relationships of Soil Moisture Characteristics to the Physical Properties of Soils. *Water Resources Research*, *20*(6), 682–690. https://doi.org/10.1029/WR020i006p00682

Costa-Cabral, M. C., Richey, J. E., Goteti, G., Lettenmaier, D. P., Feldkötter, C., & Snidvongs, A. (2008a). Landscape structure and use, climate, and water movement in the Mekong River basin. *Hydrological Processes*, *22*(12), 1731–1746. https://doi.org/10.1002/hyp.6740

Costa-Cabral, M. C., Richey, J. E., Goteti, G., Lettenmaier, D. P., Feldkötter, C., & Snidvongs, A. (2008b). Landscape structure and use, climate, and water movement in the Mekong River basin. *Hydrological Processes*, *22*(12), 1731–1746. https://doi.org/10.1002/hyp.6740

Crétaux, J.-F., Jelinski, W., Calmant, S., Kouraev, A., Vuglinski, V., Bergé-Nguyen, M., et al. (2011). SOLS: A lake database to monitor in the Near Real Time water level and storage variations from remote sensing data. *Advances in Space Research*, *47*(9), 1497–1507. https://doi.org/10.1016/J.ASR.2011.01.004

Dar, I. A., Sankar, K., & Dar, M. A. (2010). Remote sensing technology and geographic information system modeling: An integrated approach towards the mapping of groundwater potential zones in Hardrock terrain, Mamundiyar basin. *Journal of Hydrology*, *394*(3), 285–295. https://doi.org/10.1016/j.jhydrol.2010.08.022

Delgado, J. M., Merz, B., & Apel, H. (2012). A climate-flood link for the lower Mekong River. *Hydrology and Earth System Sciences*, *16*(5), 1533–1541. https://doi.org/10.5194/hess-16-1533-2012

Deligios, P. A., Chergia, A. P., Sanna, G., Solinas, S., Todde, G., Narvarte, L., & Ledda, L. (2019). Climate change adaptation and water saving by innovative irrigation management applied on open field globe artichoke. *Science of the Total Environment*, *649*, 461–472. https://doi.org/10.1016/j.scitotenv.2018.08.349

Dinar, A., & Letey, J. (1991). Agricultural water marketing, allocative efficiency, and drainage reduction. *Journal of Environmental Economics and Management*, *20*(3), 210–223. https://doi.org/10.1016/0095-0696(91)90009-8

Dore, John, Xiaogang Yu, and K. Y. L. (2007). China's energy reforms and hydropower expansion in Yunnan. *Democratizing Water Governance in the Mekong Region. Mekong Press*.

Duan, Z., & Bastiaanssen, W. G. M. (2013). Estimating water volume variations in lakes and reservoirs from four operational satellite altimetry databases and satellite imagery data. *Remote Sensing of Environment*, *134*, 403–416. https://doi.org/10.1016/J.RSE.2013.03.010

Eastham, J., Mpelasoka, F., Mainuddin, M., Ticehurst, C., Dyce, P., Hodgson, G., et al. (2008). Mekong River Basin water resources assessment: impacts of climate change. CSIRO: Water for a Healthy Country National Research Flagship. Retrieved from http://www.clw.csiro.au/publications/waterforahealthycountry/2008/wfhc-MekongWaterResourcesAssessment.pdf

Edet, A. E., Okereke, C. S., Teme, S. C., & Esu, E. O. (1998). Application of remote-sensing data to groundwater exploration: A case study of the Cross River State, southeastern Nigeria. *Hydrogeology Journal*, *6*(3), 394–404. https://doi.org/10.1007/s100400050162

Erban, L. E., Gorelick, S. M., & Zebker, H. A. (2014). Groundwater extraction, land subsidence, and sea-level rise in the Mekong Delta, Vietnam. *Environmental Research Letters*, *9*(8), 084010. https://doi.org/10.1088/1748-9326/9/8/084010

Fallah-Mehdipour, E., Bozorg Haddad, O., & Mariño, M. A. (2013). Extraction of Optimal Operation Rules in an Aquifer-Dam System: Genetic Programming Approach. *Journal of Irrigation and Drainage Engineering*, *139*(10), 872–879. https://doi.org/10.1061/(ASCE)IR.1943-4774.0000628

Feng, J.-M., Wang, Y.-L., Ma, Z.-G., & Liu, Y.-H. (2012). Simulating the Regional Impacts of Urbanization and Anthropogenic Heat Release on Climate across China. *Journal of Climate*, *25*(20), 7187–7203. https://doi.org/10.1175/JCLI-D-11-00333.1

Feng, M., Liu, P., Li, Z., Zhang, J., Liu, D., & Xiong, L. (2016). Modeling the nexus across water supply, power generation and environment systems using the system dynamics approach: Hehuang Region, China. *Journal of Hydrology*, *543*, 344–359. https://doi.org/10.1016/j.jhydrol.2016.10.011

Fischer, G., Tubiello, F. N., van Velthuizen, H., & Wiberg, D. A. (2007). Climate change impacts on irrigation water requirements: Effects of mitigation, 1990–2080. *Technological Forecasting and Social Change*, *74*(7), 1083–1107. https://doi.org/10.1016/J.TECHFORE.2006.05.021

Franchini, M., & Pacciani, M. (1991). Comparative analysis of several conceptual rainfall-runoff models. *Journal of Hydrology*, *122*(1–4), 161–219. https://doi.org/10.1016/0022-1694(91)90178-K

Fu, L.-L., & Cazenave, A. (2001). *Satellite altimetry and earth sciences : a handbook of techniques and applications*. Academic.

Ganapuram, S., Kumar, G. T. V., Krishna, I. V. M., Kahya, E., & Demirel, M. C. (2009). Mapping of groundwater potential zones in the Musi basin using remote sensing data and GIS. *Advances in Engineering Software*, *40*(7), 506–518. https://doi.org/10.1016/J.ADVENGSOFT.2008.10.001

Gao, B. (1996). NDWI—A normalized difference water index for remote sensing of vegetation liquid water from space. *Remote Sensing of Environment*, *58*(3), 257–266. https://doi.org/10.1016/S0034-4257(96)00067-3

Gao, H., Birkett, C., & Lettenmaier, D. P. (2012). Global monitoring of large reservoir storage from satellite remote sensing. *Water Resources Research*, *48*(9). https://doi.org/10.1029/2012WR012063

Gerlak, A. K., Lautze, J., & Giordano, M. (2011). Water resources data and information exchange in transboundary water treaties. *International Environmental Agreements: Politics, Law and Economics*, *11*(2), 179–199. https://doi.org/10.1007/s10784-010-9144-4

Gleeson, T., Wada, Y., Bierkens, M. F. P., & van Beek, L. P. H. (2012). Water balance of global aquifers revealed by groundwater footprint. *Nature*, *488*(7410), 197–200. https://doi.org/10.1038/nature11295

Goteti, G., & Lettenmaier, D. P. (2001). *Effects of streamflow regulation and land cover change on the hydrology of the Mekong river basin*. University of Washington. Retrieved from https://www.ce.washington.edu/sites/cee/files/pdfs/research/hydrology/water-resources/WRS169.pdf

Grumbine, R. E., & Xu, J. (2011). Mekong Hydropower Development. *Science*, *332*(6026), 178–179. https://doi.org/10.1126/science.1200990

Guo, H., Bao, A., Liu, T., Ndayisaba, F., He, D., Kurban, A., et al. (2017). Meteorological Drought Analysis in the Lower Mekong Basin Using Satellite-Based Long-Term CHIRPS Product. *Sustainability*, *9*(6), 901. https://doi.org/10.3390/su9060901

Habibi Davijani, M., Banihabib, M. E., Nadjafzadeh Anvar, A., & Hashemi, S. R. (2016). Multi-Objective Optimization Model for the Allocation of Water Resources in Arid Regions Based on the Maximization of Socioeconomic Efficiency. *Water Resources Management*, *30*(3), 927–946. https://doi.org/10.1007/s11269-015-1200-y

Haddeland, I., Skaugen, T., & Lettenmaier, D. P. (2006). Anthropogenic impacts on continental surface water fluxes. *Geophysical Research Letters*, *33*(8), L08406. https://doi.org/10.1029/2006GL026047

Haddeland, I., Lettenmaier, D. P., & Skaugen, T. (2006). Effects of irrigation on the water and energy balances of the Colorado and Mekong river basins. *Journal of Hydrology*, *324*(1–4), 210–223. https://doi.org/10.1016/j.jhydrol.2005.09.028

Hanasaki, N., Kanae, S., & Oki, T. (2006). A reservoir operation scheme for global river routing models. *Journal of Hydrology*, *327*(1–2), 22–41. https://doi.org/10.1016/j.jhydrol.2005.11.011

Hanim, F., & Rahim, A. (2017). *Supply and Demand of Rice in Malaysia: A System Dynamics Approach*. *International Journal of Supply Chain Management* (Vol. 6). Retrieved from http://excelingtech.co.uk/

Hapuarachchi, H. A. P., Takeuchi, K., Zhou, M., Kiem, A. S., Georgievski, M., Magome, J., & Ishidaira, H. (2008). Investigation of the Mekong River basin hydrology for 1980–2000 using the YHyM. *Hydrological Processes*, *22*(9), 1246–1256. https://doi.org/10.1002/hyp.6934

Harbaugh, A. W. (2005). *MODFLOW-2005, The U.S. Geological Survey Modular Ground-Water Model-the Ground-Water Flow Process*. Retrieved from http://water.usgs.gov/software/ground_water.html/.

Heinimann, A., Messerli, P., Schmidt-Vogt, D., & Wiesmann, U. (2007). The Dynamics of Secondary Forest Landscapes in the Lower Mekong Basin. *Mountain Research and Development*, *27*(3), 232–241. https://doi.org/10.1659/mrd.0875

Hempel, S., Frieler, K., Warszawski, L., Schewe, J., & Piontek, F. (2013). A trend-preserving bias correction – the ISI-MIP approach. *Earth System Dynamics*, *4*(2), 219–236. https://doi.org/10.5194/esd-4-219-2013

Henriksen, H. J., Troldborg, L., Højberg, A. L., & Refsgaard, J. C. (2008). Assessment of exploitable groundwater resources of Denmark by use of ensemble resource indicators and a numerical groundwater–surface water model. *Journal of Hydrology*, *348*(1–2), 224–240. https://doi.org/10.1016/J.JHYDROL.2007.09.056

Heywood, I., Corneluis, S., & Carver, S. (2003). An introduction to geographic information systems, 1st Indian Ed. Retrieved from https://scholar.google.com/scholar?hl=en&as_sdt=0%2C47&q=Heywood+I%2C+Corneluis+S%2C+Carver+S+%282003%29+An+introduction+to+geographic+information+systems%2C+1st+Indian+Ed.+Pearson+Education%2C+Delhi&btnG=

Hibbert, A. R. (1983). WATER YIELD IMPROVEMENT POTENTIAL BY VEGETATION MANAGEMENT ON WESTERN RANGELANDS. *Journal of the American Water Resources Association*, *19*(3), 375–381. https://doi.org/10.1111/j.1752-1688.1983.tb04594.x

Hoang, L. P., Lauri, H., Kummu, M., Koponen, J., van Vliet, M. T. H., Supit, I., et al. (2016). Mekong River flow and hydrological extremes under climate change. *Hydrology and Earth System Sciences*, *20*(7), 3027–3041. https://doi.org/10.5194/hess-20-3027-2016

Hoanh, C. T., Guttman, H., Droogers, P., & Aerts, J. (2004). Will we produce sufficient food under climate change?: Mekong Basin (South-east Asia). Retrieved from https://cgspace.cgiar.org/handle/10568/37433

Hoanh, C. T., Jirayoot, K., Lacombe, G., Srinetr, V., Hoanh, C. T., Jirayoot, K., et al. (2010). Impacts of climate change and development on Mekong flow regimes. First assessment - 2009. Retrieved from https://econpapers.repec.org/paper/iwtrerpts/h043262.htm

Hoekema, D. J., & Sridhar, V. (2013a). A System Dynamics Model for Conjunctive Management of Water Resources in the Snake River Basin. *JAWRA Journal of the American Water Resources Association*, *49*(6), 1327–1350. https://doi.org/10.1111/jawr.12092

Hoekema, D. J., & Sridhar, V. (2013b). A System Dynamics Model for Conjunctive Management of Water Resources in the Snake River Basin. *JAWRA Journal of the American Water Resources Association*, *49*(6), 1327–1350. https://doi.org/10.1111/jawr.12092

Homdee, T., Pongput, K., & Kanae, S. (2011). Impacts of Land Cover Changes on Hydrologic Responses: A Case Study of Chi River Basin, Thailand. *Journal of Japan Society of Civil Engineers, Ser. B1 (Hydraulic Engineering)*, *67*(4), I_31-I_36. https://doi.org/10.2208/jscejhe.67.I_31

Hook, J., Novak, S., & Johnston, R. (2003). Social Atlas of the Lower Mekong Basin. In *Mekong River Commission* (pp. 1727–1800). Phnom Penh.

Hossain, F., & Katiyar, N. (2006). Improving flood forecasting in international river basins. *Eos, Transactions American Geophysical Union*, *87*(5), 49. https://doi.org/10.1029/2006EO050001

Huffman, G., Adler, R., Stocker, E., Bolvin, D., & Nelkin, E. (2003). Analysis of TRMM 3-hourly multi-satellite precipitation estimates computed in both real and post-real

time. In *12th Conf. on Satellite Meteorology and Oceanography* (pp. 4–11). Long Beach, CA: Amer. Meteor. Soc., CD-ROM. Retrieved from https://ntrs.nasa.gov/search.jsp?R=20040026654

Huffman, G. J., Adler, R. F., Morrissey, M. M., Bolvin, D. T., Curtis, S., Joyce, R., et al. (2001). Global Precipitation at One-Degree Daily Resolution from Multisatellite Observations. *Journal of Hydrometeorology*, *2*(1), 36–50. https://doi.org/10.1175/1525-7541(2001)002<0036:GPAODD>2.0.CO;2

Intralawan, A., Wood, D., & Frankel, R. (2017). *Economic Evaluation of Hydropower Projects in the Lower Mekong Basin*. Retrieved from http://www.mrcmekong.org/assets/Uploads/Final-report-Mekong-Study-March-2017-8.pdf

Ioslovich, I., & Gutman, P. O. (2001). A model for the global optimization of water prices and usage for the case of spatially distributed sources and consumers. *Mathematics and Computers in Simulation*, *56*(4–5), 347–356. https://doi.org/10.1016/S0378-4754(01)00306-8

Jackson, R. B., Carpenter, S. R., Dahm, C. N., McKnight, D. M., Naiman, R. J., Postel, S. L., & Running, S. W. (2001). WATER IN A CHANGING WORLD. *Ecological Applications*, *11*(4), 1027–1045. https://doi.org/10.1890/1051-0761(2001)011[1027:WIACW]2.0.CO;2@10.1002/(ISSN)1939-5582(CAT)SPECIALCOLLECTION(VI)VIRTUALISSUE

Jain, P. K. (1998). Remote sensing techniques to locate ground water potential zones in upper Urmil River Basin, district Chhatarpur — Central India. *Journal of the Indian Society of Remote Sensing*, *26*(3), 135–147. https://doi.org/10.1007/BF03026671

Jaksa, W. T., & Sridhar, V. (2015). Effect of irrigation in simulating long-term evapotranspiration climatology in a human-dominated river basin system. *Agricultural and Forest Meteorology*, *200*, 109–118. https://doi.org/10.1016/j.agrformet.2014.09.008

Jha, M. K., Chowdhury, A., Chowdary, V. M., & Peiffer, S. (2007). Groundwater management and development by integrated remote sensing and geographic information systems: prospects and constraints. *Water Resources Management*, *21*(2), 427–467. https://doi.org/10.1007/s11269-006-9024-4

Ji, L., Zhang, L., & Wylie, B. (2009). Analysis of Dynamic Thresholds for the Normalized Difference Water Index. *Photogrammetric Engineering & Remote Sensing*, *75*(11), 1307–1317. https://doi.org/10.14358/PERS.75.11.1307

Jin, X., & Sridhar, V. (2010). An integrated model coupling VIC and MODFLOW to study the hydrological prediction at the Snake River Basin. Retrieved from https://www.researchgate.net/profile/Xin_Jin48/publication/267410713_An_integrated_model_coupling_VIC_and_MODFLOW_to_study_the_hydrological_prediction_at_the_Snake_River_Basin/links/55c69e9b08aea2d9bdc548ec/An-integrated-model-coupling-VIC-and-MODFLOW-to-

Jin, Y., Schaaf, C. B., Gao, F., Li, X., Strahler, A. H., Lucht, W., et al. (2003). Consistency of MODIS surface bidirectional reflectance distribution function and albedo retrievals: 1. Algorithm performance. *J. Geophys. Res*, *108*(D5), 4158. https://doi.org/10.1029/2002JD002803

Johnston, R., & Kummu, M. (2012). Water Resource Models in the Mekong Basin: A Review. *Water Resources Management*, *26*(2), 429–455.

https://doi.org/10.1007/s11269-011-9925-8
Kaiser, B., & Roumasset, J. (2002). Valuing indirect ecosystem services: The case of tropical watersheds. *Environment and Development Economics, 7*(4), 701–714. https://doi.org/10.1017/S1355770X02000426
Kalnay, E., Kanamitsu, M., Kistler, R., Collins, W., Deaven, D., Gandin, L., et al. (1996). The NCEP/NCAR 40-Year Reanalysis Project. *Bulletin of the American Meteorological Society*, *77*(3), 437–471. https://doi.org/10.1175/1520-0477(1996)077<0437:TNYRP>2.0.CO;2
Kang, H., & Sridhar, V. (2019). Drought assessment with a surface-groundwater coupled model in the Chesapeake Bay watershed. *Environmental Modelling and Software*, *119*, 379–389. https://doi.org/10.1016/j.envsoft.2019.07.002
Kang, H., Sridhar, V., Mills, B. F., Hession, W. C., & Ogejo, J. A. (2019). Economy-wide climate change impacts on green water droughts based on the hydrologic simulations. *Agricultural Systems*, *171*, 76–88. https://doi.org/10.1016/j.agsy.2019.01.006
Keskinen, M., Kummu, M., Käkönen, M., & Varis, O. (2012). Mekong at the Crossroads: Next Steps for Impact Assessment of Large Dams. *AMBIO*, *41*(3), 319–324. https://doi.org/10.1007/s13280-012-0261-x
Khandelwal, A., Karpatne, A., Wei, Z., Kuang, H., Ghosh, R., Dugan, H., et al. (2019). *GLADD-R: A new Global Lake Dynamics Database for Reservoirs created using machine learning and satellite data GLADD-R: A new Global Lake Dynamics Database for Reservoirs*. Retrieved from http://umnlcc.cs.umn.edu/GlobalReservoirDatabase/
Kiem, A. S., Ishidaira, H., Hapuarachchi, H. P., Zhou, M. C., Hirabayashi, Y., & Takeuchi, K. (2008). Future hydroclimatology of the Mekong River basin simulated using the high-resolution Japan Meteorological Agency (JMA) AGCM. *Hydrological Processes*, *22*(9), 1382–1394. https://doi.org/10.1002/hyp.6947
Kingston, D. G., Thompson, J. R., & Kite, G. (2011). Uncertainty in climate change projections of discharge for the Mekong River Basin. *Hydrology and Earth System Sciences*, *15*(5), 1459–1471. https://doi.org/10.5194/hess-15-1459-2011
Kondolf, G. M., Rubin, Z. K., & Minear, J. T. (2014). Dams on the Mekong: Cumulative sediment starvation. *Water Resources Research*, *50*(6), 5158–5169. https://doi.org/10.1002/2013WR014651
Kondolf, G. Mathias, Schmitt, R. J. P., Carling, P., Darby, S., Arias, M., Bizzi, S., et al. (2018). Changing sediment budget of the Mekong: Cumulative threats and management strategies for a large river basin. *Science of the Total Environment*, *625*, 114–134. https://doi.org/10.1016/j.scitotenv.2017.11.361
Kueppers, L. M., Snyder, M. A., & Sloan, L. C. (2007). Irrigation cooling effect: Regional climate forcing by land-use change. *Geophysical Research Letters*, *34*(3). https://doi.org/10.1029/2006GL028679
Kuhn, A., & Britz, W. (2012). Can hydro-economic river basin models simulate water shadow prices under asymmetric access? *Water Science and Technology*, *66*(4), 879–886. https://doi.org/10.2166/wst.2012.251
Kummu, M., Lu, X. X., Wang, J. J., & Varis, O. (2010). Basin-wide sediment trapping efficiency of emerging reservoirs along the Mekong. *Geomorphology*, *119*(3–4), 181–197. https://doi.org/10.1016/J.GEOMORPH.2010.03.018
Kummu, M, & Sarkkula, J. (2008). Impact of the Mekong River Flow Alteration on the

Tonle Sap Flood Pulse. *AMBIO*, *37*(3), 185–192. https://doi.org/10.1579/0044-7447(2008)37[185:IOTMRF]2.0.CO;2

Kummu, Matti, & Varis, O. (2007). Sediment-related impacts due to upstream reservoir trapping, the Lower Mekong River. *Geomorphology*, *85*(3–4), 275–293. https://doi.org/10.1016/J.GEOMORPH.2006.03.024

Lauri, H., de Moel, H., Ward, P. J., Räsänen, T. A., Keskinen, M., & Kummu, M. (2012). Future changes in Mekong River hydrology: impact of climate change and reservoir operation on discharge. *Hydrology and Earth System Sciences*, *16*(12), 4603–4619. https://doi.org/10.5194/hess-16-4603-2012

Leck, H., Conway, D., Bradshaw, M., & Rees, J. (2015). Tracing the Water-Energy-Food Nexus: Description, Theory and Practice. *Geography Compass*, *9*(8), 445–460. https://doi.org/10.1111/gec3.12222

Li, D., Long, D., Zhao, J., Lu, H., & Hong, Y. (2017). Observed changes in flow regimes in the Mekong River basin. *Journal of Hydrology*, *551*, 217–232. https://doi.org/10.1016/j.jhydrol.2017.05.061

Li, Han, Wei, Y. D., & Korinek, K. (2018). Modelling urban expansion in the transitional Greater Mekong Region. *Urban Studies*, *55*(8), 1729–1748. https://doi.org/10.1177/0042098017700560

Li, Hongyi, Wu, H., Huang, M., & Leung, L. R. (2012). Irrigation & Drainage Systems Engineering Representing Natural and Manmade Drainage Systems in an Earth System Modeling Framework, *1*(2), 1–2. https://doi.org/10.4172/2168-9768.1000e107

Li, W., Qin, Y., Sun, Y., Huang, H., Ling, F., Tian, L., & Ding, Y. (2016). Estimating the relationship between dam water level and surface water area for the Danjiangkou Reservoir using Landsat remote sensing images. *Remote Sensing Letters*, *7*(2), 121–130. https://doi.org/10.1080/2150704X.2015.1117151

Liang, X., Lettenmaier, D. P., Wood, E. F., & Burges, S. J. (1994). A simple hydrologically based model of land surface water and energy fluxes for general circulation models. *Journal of Geophysical Research*, *99*(D7), 14415. https://doi.org/10.1029/94JD00483

Lipscomb, M., Mobarak, A. M., & Barham, T. (2013). Development Effects of Electrification: Evidence from the Topographic Placement of Hydropower Plants in Brazil. *American Economic Journal: Applied Economics*, *5*(2), 200–231. https://doi.org/10.1257/app.5.2.200

Liu, Xingcai, Tang, Q., Voisin, N., & Cui, H. (2016). Projected impacts of climate change on hydropower potential in China. *Hydrology and Earth System Sciences*, *20*(8), 3343–3359. https://doi.org/10.5194/hess-20-3343-2016

Liu, Xiuli, Chen, X., & Wang, S. (2009). Evaluating and predicting shadow prices of water resources in China and its nine major river basins. *Water Resources Management*, *23*(8), 1467–1478. https://doi.org/10.1007/s11269-008-9336-7

Liu, Y., Xiao, J., Ju, W., Xu, K., Zhou, Y., & Zhao, Y. (2016). Recent trends in vegetation greenness in China significantly altered annual evapotranspiration and water yield. *Environmental Research Letters*, *11*(9), 094010. https://doi.org/10.1088/1748-9326/11/9/094010

Lobell, D. B., & Bonfils, C. (2008). The effect of irrigation on regional temperatures: A spatial and temporal analysis of trends in California, 1934-2002. *Journal of Climate*, *21*(10), 2063–2071. https://doi.org/10.1175/2007JCLI1755.1

Lohmann, D., Raschke, E., Nijssen, B., & Lettenmaier, D. P. (1998). Regional scale hydrology: II. Application of the VIC-2L model to the Weser River, Germany. *Hydrological Sciences Journal*, *43*(1), 143–158. https://doi.org/10.1080/02626669809492108

Lohmann, Dag, Nolte-Holube, R., & Raschke, E. (1996). A large-scale horizontal routing model to be coupled to land surface parametrization schemes. *Tellus, Series A: Dynamic Meteorology and Oceanography*. https://doi.org/10.1034/j.1600-0870.1996.t01-3-00009.x

Lyon, S. W., King, K., Polpanich, O., & Lacombe, G. (2017). Assessing hydrologic changes across the Lower Mekong Basin. *Journal of Hydrology: Regional Studies*, *12*, 303–314. https://doi.org/10.1016/J.EJRH.2017.06.007

Ma, L., Wang, H., Qi, C., Zhang, X., & Zhang, H. (2019). Characteristics and Adaptability Assessment of Commonly Used Ecological Flow Methods in Water Storage and Hydropower Projects, the Case of Chinese River Basins. *Water*, *11*(10), 2035. https://doi.org/10.3390/w11102035

Manh, N. Van, Dung, N. V., Hung, N. N., Kummu, M., Merz, B., & Apel, H. (2015). Future sediment dynamics in the Mekong Delta floodplains: Impacts of hydropower development, climate change and sea level rise. *Global and Planetary Change*, *127*, 22–33. https://doi.org/10.1016/J.GLOPLACHA.2015.01.001

Marhaento, H., Booij, M. J., Rientjes, T. H. M., & Hoekstra, A. Y. (2017). Attribution of changes in the water balance of a tropical catchment to land use change using the SWAT model. *Hydrological Processes*, *31*(11), 2029–2040. https://doi.org/10.1002/hyp.11167

Martin, S. M., & Lorenzen, K. (2016). Livelihood Diversification in Rural Laos. *World Development*, *83*, 231–243. https://doi.org/10.1016/J.WORLDDEV.2016.01.018

Mekong River Commission. (2005). *Overview of the Hydrology of the Mekong Basin Mekong River Commission Meeting the Needs, Keeping the Balance*. Retrieved from http://www.mekonginfo.org/assets/midocs/0001968-inland-waters-overview-of-the-hydrology-of-the-mekong-basin.pdf

Mekong River Commission. (2010). Assessment of basin-wide development scenarios–main report. *Mekong River Commission, Vientiane, Lao PDR*.

Merola, R. B., Hien, T. T., Quyen, D. T. T., & Vengosh, A. (2015). Arsenic exposure to drinking water in the Mekong Delta. *Science of The Total Environment*, *511*, 544–552. https://doi.org/10.1016/J.SCITOTENV.2014.12.091

Minderhoud, P. S. J., Coumou, L., Erban, L. E., Middelkoop, H., Stouthamer, E., & Addink, E. A. (2018). The relation between land use and subsidence in the Vietnamese Mekong delta. *Science of The Total Environment*, *634*, 715–726. https://doi.org/10.1016/J.SCITOTENV.2018.03.372

Ming, B., Liu, P., Chang, J., Wang, Y., & Huang, Q. (2017). Deriving Operating Rules of Pumped Water Storage Using Multiobjective Optimization: Case Study of the Han to Wei Interbasin Water Transfer Project, China. *Journal of Water Resources Planning and Management*, *143*(10), 05017012. https://doi.org/10.1061/(ASCE)WR.1943-5452.0000828

Mitchell, T. D., & Jones, P. D. (2005). An improved method of constructing a database of monthly climate observations and associated high-resolution grids. *International Journal of Climatology*, *25*(6), 693–712. https://doi.org/10.1002/joc.1181

Monteith, L. J. (1965). Evaporation and environment, In The state and movement of water in living organisms. *Symp. Soc. Exp. Biol.*, 205–234. Retrieved from https://ci.nii.ac.jp/naid/10007810939/

MRC. (2018). *Irrigation database improvement for the lower Mekong basin*. Retrieved from http://www.mrcmekong.org/publications/

Mu, Q., Heinsch, F. A., Zhao, M., & Running, S. W. (2007). Development of a global evapotranspiration algorithm based on MODIS and global meteorology data. *Remote Sensing of Environment*, *111*(4), 519–536. https://doi.org/10.1016/J.RSE.2007.04.015

Mu, Q., Zhao, M., & Running, S. W. (2011). Improvements to a MODIS global terrestrial evapotranspiration algorithm. *Remote Sensing of Environment*, *115*(8), 1781–1800. https://doi.org/10.1016/J.RSE.2011.02.019

Muala, E., Mohamed, Y. A., Duan, Z., & Van der Zaag, P. (2014). Estimation of Reservoir Discharges from Lake Nasser and Roseires Reservoir in the Nile Basin Using Satellite Altimetry and Imagery Data. *Remote Sensing*, *6*(8), 7522–7545. https://doi.org/10.3390/rs6087522

Myneni, R. ., Hoffman, S., Knyazikhin, Y., Privette, J. ., Glassy, J., Tian, Y., et al. (2002). Global products of vegetation leaf area and fraction absorbed PAR from year one of MODIS data. *Remote Sensing of Environment*, *83*(1), 214–231. https://doi.org/10.1016/S0034-4257(02)00074-3

Narendra, K., Nageswara Rao, K., & Swarna Latha, P. (2013). Integrating remote sensing and GIS for identification of groundwater prospective zones in the Narava basin, Visakhapatnam region, Andhra Pradesh. *Journal of the Geological Society of India*, *81*(2), 248–260. https://doi.org/10.1007/s12594-013-0028-4

Nash, J. E., & Sutcliffe, J. V. (1970). River flow forecasting through conceptual models part I — A discussion of principles. *Journal of Hydrology*, *10*(3), 282–290. https://doi.org/10.1016/0022-1694(70)90255-6

Nesbitt, H., R. Johnston, and M. S. (2004). Mekong River water: will river flows meet future agriculture needs in the Lower Mekong Basin? *Water in Agriculture, Seng, V., Craswell, E., Fukai, S., and Fisher, K.(Eds), Australian Centre of International Agricultural Research Proceedings 116*.

Oikonomidis, D., Dimogianni, S., Kazakis, N., & Voudouris, K. (2015). A GIS/Remote Sensing-based methodology for groundwater potentiality assessment in Tirnavos area, Greece. *Journal of Hydrology*, *525*, 197–208. https://doi.org/10.1016/j.jhydrol.2015.03.056

Olson, K. R., & Morton, L. W. (2018). Tonle Sap Lake and River and confluence with the Mekong River in Cambodia Soil management View project. *Article in Journal of Soil and Water Conservation*, *73*(3), 60A-66A. https://doi.org/10.2489/jswc.73.3.60A

Paper, W. (2009). *GoldSim: Engineering and Environmental Simulation Software for Water Resource Applications*.

Pech, S., & Sunada, K. (2008). Population Growth and Natural-Resources Pressures in the Mekong River Basin. *Ambio*. SpringerRoyal Swedish Academy of Sciences. https://doi.org/10.2307/25547886

Pham, H. T., Marshall, L., Johnson, F., & Sharma, A. (2018). Deriving daily water levels from satellite altimetry and land surface temperature for sparsely gauged catchments: A case study for the Mekong River. *Remote Sensing of Environment*, *212*, 31–46.

https://doi.org/10.1016/j.rse.2018.04.034
Pipitone, C. I., Maltese, A., Dardanelli, G. I., Lo Brutto, M. I., & La Loggia, G. I. (2018). Monitoring Water Surface and Level of a Reservoir Using Different Remote Sensing Approaches and Comparison with Dam Displacements Evaluated via GNSS. *Remote Sensing*, *10*(1), 71. https://doi.org/10.3390/rs10010071
Pittock, J., Dumaresq, D., & Bassi, A. (2016). Modeling the Hydropower–Food Nexus in Large River Basins: A Mekong Case Study. *Water*, *8*(10), 425. https://doi.org/10.3390/w8100425
Plengsaeng, B., Wehn, U., & van der Zaag, P. (2014). Data-sharing bottlenecks in transboundary integrated water resources management: a case study of the Mekong River Commission's procedures for data sharing in the Thai context. *Water International*, *39*(7), 933–951. https://doi.org/10.1080/02508060.2015.981783
Pokhrel, Y., Burbano, M., Roush, J., Kang, H., Sridhar, V., & Hyndman, D. (2018). A Review of the Integrated Effects of Changing Climate, Land Use, and Dams on Mekong River Hydrology. *Water*, *10*(3), 266. https://doi.org/10.3390/w10030266
Quinn, J. D., Reed, P. M., Giuliani, M., Castelletti, A., Oyler, J. W., & Nicholas, R. E. (2018). Exploring How Changing Monsoonal Dynamics and Human Pressures Challenge Multireservoir Management for Flood Protection, Hydropower Production, and Agricultural Water Supply. *Water Resources Research*, *54*(7), 4638–4662. https://doi.org/10.1029/2018WR022743
Rasul, G., & Sharma, B. (2016). The nexus approach to water–energy–food security: an option for adaptation to climate change. *Climate Policy*, *16*(6), 682–702. https://doi.org/10.1080/14693062.2015.1029865
Richter, B., & Thomas, G. (2007). Restoring environmental flows by modifying dam operations. *JSTOR*. Retrieved from https://www.jstor.org/stable/26267852?casa_token=aiozWKMVOdAAAAAA:pnbt3UP1Bk1W1O0fEKoMA6xl41grmqT_XdN7ngBGS43u5Yg6Nn_7lw0OJ4y3T01IQamjIzNU6wXvvmHQ2-oRgMM64_XbHnasRSAGgJ8nQlWeSVcJxGQr
Ringler, C., von Braun, J., & Rosegrant, M. W. (2004). Water Policy Analysis for the Mekong River Basin. *Water International*, *29*(1), 30–42. https://doi.org/10.1080/02508060408691746
Rosegrant, M. W., Ringler, C., McKinney, D. C., Cai, X., Keller, A., & Donoso, G. (2000). Integrated economic-hydrologic water modeling at the basin scale: the Maipo river basin. *Agricultural Economics*, *24*(1), 33–46. https://doi.org/10.1111/j.1574-0862.2000.tb00091.x
Sabo, J. L., Ruhi, A., Holtgrieve, G. W., Elliott, V., Arias, M. E., Ngor, P. B., et al. (2017). Designing river flows to improve food security futures in the Lower Mekong Basin. *Science (New York, N.Y.)*, *358*(6368), eaao1053. https://doi.org/10.1126/science.aao1053
Sacks, W. J., Cook, B. I., Buenning, N., Levis, S., & Helkowski, J. H. (2009). Effects of global irrigation on the near-surface climate. *Climate Dynamics*, *33*(2–3), 159–175. https://doi.org/10.1007/s00382-008-0445-z
Sakamoto, T., Van Nguyen, N., Kotera, A., Ohno, H., Ishitsuka, N., & Yokozawa, M. (2007). Detecting temporal changes in the extent of annual flooding within the Cambodia and the Vietnamese Mekong Delta from MODIS time-series imagery. *Remote Sensing of Environment*, *109*(3), 295–313.

https://doi.org/10.1016/J.RSE.2007.01.011
Salomon, J. G., Schaaf, C. B., Strahler, A. H., Feng Gao, & Yufang Jin. (2006). Validation of the MODIS bidirectional reflectance distribution function and albedo retrievals using combined observations from the aqua and terra platforms. *IEEE Transactions on Geoscience and Remote Sensing*, *44*(6), 1555–1565. https://doi.org/10.1109/TGRS.2006.871564
Schubert, S. D., Suarez, M. J., Pegion, P. J., Koster, R. D., & Bacmeister, J. T. (2004). Causes of Long-Term Drought in the U.S. Great Plains. *Journal of Climate*, *17*(3), 485–503. https://doi.org/10.1175/1520-0442(2004)017<0485:COLDIT>2.0.CO;2
Senanayake, I. P., Dissanayake, D. M. D. O. K., Mayadunna, B. B., & Weerasekera, W. L. (2016). An approach to delineate groundwater recharge potential sites in Ambalantota, Sri Lanka using GIS techniques. *Geoscience Frontiers*, *7*(1), 115–124. https://doi.org/10.1016/j.gsf.2015.03.002
Sener, E., Davraz, A., & Ozcelik, M. (2005). An integration of GIS and remote sensing in groundwater investigations: A case study in Burdur, Turkey. *Hydrogeology Journal*, *13*(5–6), 826–834. https://doi.org/10.1007/s10040-004-0378-5
Shaban, A., Khawlie, M., & Abdallah, C. (2006). Use of remote sensing and GIS to determine recharge potential zones: the case of Occidental Lebanon. *Hydrogeology Journal*, *14*(4), 433–443. https://doi.org/10.1007/s10040-005-0437-6
Sheffield, J., Goteti, G., & Wood, E. F. (2006). Development of a 50-Year High-Resolution Global Dataset of Meteorological Forcings for Land Surface Modeling. *Journal of Climate*, *19*(13), 3088–3111. https://doi.org/10.1175/JCLI3790.1
Shrestha, B., Babel, M. S., Maskey, S., van Griensven, A., Uhlenbrook, S., Green, A., & Akkharath, I. (2013). Impact of climate change on sediment yield in the Mekong River basin: a case study of the Nam Ou basin, Lao PDR. *Hydrology and Earth System Sciences*, *17*(1), 1–20. https://doi.org/10.5194/hess-17-1-2013
Siebert, S., Burke, J., Faures, J. M., Frenken, K., Hoogeveen, J., Döll, P., & Portmann, F. T. (2010). Groundwater use for irrigation – a global inventory. *Hydrology and Earth System Sciences*, *14*(10), 1863–1880. https://doi.org/10.5194/hess-14-1863-2010
Sigvaldson, O. T. (1976). A simulation model for operating a multipurpose multireservoir system. *Water Resources Research*, *12*(2), 263–278. https://doi.org/10.1029/WR012i002p00263
Solomon, S., & Quiel, F. (2006). Groundwater study using remote sensing and geographic information systems (GIS) in the central highlands of Eritrea. *Hydrogeology Journal*, *14*(5), 729–741. https://doi.org/10.1007/s10040-005-0477-y
Son, N. T., Chen, C. F., Chen, C. R., Chang, L. Y., & Minh, V. Q. (2012). Monitoring agricultural drought in the Lower Mekong Basin using MODIS NDVI and land surface temperature data. *International Journal of Applied Earth Observation and Geoinformation*, *18*, 417–427. https://doi.org/10.1016/J.JAG.2012.03.014
Spruce, J., Bolten, J., Srinivasan, R., Lakshmi, V., Spruce, J., Bolten, J., et al. (2018). Developing Land Use Land Cover Maps for the Lower Mekong Basin to Aid Hydrologic Modeling and Basin Planning. *Remote Sensing*, *10*(12), 1910. https://doi.org/10.3390/rs10121910
Spruce, J., Bolten, J., Mohammed, I. N., Srinivasan, R., & Lakshmi, V. (2020). Mapping Land Use Land Cover Change in the Lower Mekong Basin From 1997 to 2010. *Frontiers in Environmental Science*, *8*, 21. https://doi.org/10.3389/fenvs.2020.00021

Sridhar, V. (2013). Tracking the Influence of Irrigation on Land Surface Fluxes and Boundary Layer Climatology. *Journal of Contemporary Water Research & Education*, *152*(1), 79–93. https://doi.org/10.1111/j.1936-704X.2013.03170.x

Sridhar, V., & Anderson, K. A. (2017). Human-induced modifications to land surface fluxes and their implications on water management under past and future climate change conditions. *Agricultural and Forest Meteorology*, *234–235*, 66–79. https://doi.org/10.1016/j.agrformet.2016.12.009

Sridhar, V., Billah, M. M., & Hildreth, J. W. (2018). Coupled Surface and Groundwater Hydrological Modeling in a Changing Climate. *Groundwater*, *56*(4), 618–635. https://doi.org/10.1111/gwat.12610

Sridhar, V., Ali, S. A., & Lakshmi, V. (2019). Assessment and validation of total water storage in the Chesapeake Bay watershed using GRACE. *Journal of Hydrology: Regional Studies*, *24*, 100607. https://doi.org/10.1016/J.EJRH.2019.100607

Sridhar, V., Kang, H., & Ali, S. A. (2019). Human-Induced Alterations to Land Use and Climate and Their Responses for Hydrology and Water Management in the Mekong River Basin. *Water*, *11*(6), 1307. https://doi.org/10.3390/w11061307

Stackhouse, P. W., Gupta, S. K., Cox, S. J., Mikowitz, J. C., Zhang, T., & Chiacchio, M. (2004). 12-year surface radiation budget data se. *GEWEX News*, *14*(4), 10–12.

Stone, R. (2016). Dam-building threatens Mekong fisheries. Retrieved from http://science.sciencemag.org/content/354/6316/1084.summary

Stone, Richard. (2011a). Mayhem on the Mekong. *Science*, *333*(6044), 814–818. https://doi.org/10.1126/science.333.6044.814

Stone, Richard. (2011b, August 12). Mayhem on the Mekong. *Science*. https://doi.org/10.1126/science.333.6044.814

Subba Rao, N. (2006). Groundwater potential index in a crystalline terrain using remote sensing data. *Environmental Geology*, *50*(7), 1067–1076. https://doi.org/10.1007/s00254-006-0280-7

Sun, S., Yan, X., Cui, P., & Feng, J. (2011). A four-step method for optimising the normal water level of reservoirs based on a mathematical programming model--a case study for the Songyuan backwater dam in Jilin Province, China. *International Journal of Environmental Research and Public Health*, *8*(4), 1049–60. https://doi.org/10.3390/ijerph8041049

Tatsumi, K., & Yamashiki, Y. (2015a). Effect of irrigation water withdrawals on water and energy balance in the Mekong River Basin using an improved VIC land surface model with fewer calibration parameters. *Agricultural Water Management*, *159*, 92–106. https://doi.org/10.1016/J.AGWAT.2015.05.011

Tatsumi, K., & Yamashiki, Y. (2015b). Effect of irrigation water withdrawals on water and energy balance in the Mekong River Basin using an improved VIC land surface model with fewer calibration parameters. *Agricultural Water Management*, *159*, 92–106. https://doi.org/10.1016/j.agwat.2015.05.011

Te, N. (2007). *Drought management in the Lower Mekong Basin*. The 3rd Southeast Asia Water Forum, Kuala Lumpur, Malaysia.

Teeuw, R. M. (1995). Groundwater Exploration Using Remote Sensing And A Low-Cost Geographical Information System. *Hydrogeology Journal*, *3*(3), 21–30. https://doi.org/10.1007/s100400050057

Thanh, T. N., Tri, V. P. D., Kim, S., Phuong, T. N., Mong, T. L., & Tuan, P. V. (2020). A

subregional model of system dynamics research on surface water resource assessment for paddy rice production under climate change in the Vietnamese mekong delta. *Climate*, *8*(3). https://doi.org/10.3390/cli8030041

Thiery, W., Visser, A. J., Fischer, E. M., Hauser, M., Hirsch, A. L., Lawrence, D. M., et al. (2020). Warming of hot extremes alleviated by expanding irrigation. *Nature Communications*, *11*(1), 1–7. https://doi.org/10.1038/s41467-019-14075-4

Thilakarathne, M., & Sridhar, V. (2017). Characterization of future drought conditions in the Lower Mekong River Basin. *Weather and Climate Extremes*, *17*, 47–58. https://doi.org/10.1016/J.WACE.2017.07.004

Thu, H. N., & Wehn, U. (2016). Data sharing in international transboundary contexts: The Vietnamese perspective on data sharing in the Lower Mekong Basin. *Journal of Hydrology*, *536*, 351–364. https://doi.org/10.1016/j.jhydrol.2016.02.035

Tran, H., Tran, T., Kervyn, M., Tran, H., Tran, T., & Kervyn, M. (2015). Dynamics of Land Cover/Land Use Changes in the Mekong Delta, 1973–2011: A Remote Sensing Analysis of the Tran Van Thoi District, Ca Mau Province, Vietnam. *Remote Sensing*, *7*(3), 2899–2925. https://doi.org/10.3390/rs70302899

Tsur, Y., Dinar, A., Doukkali, R. M., Roe, T. L., Tsur, Y., Dinar, A., et al. (2004). Irrigation water pricing: policy implications based on international comparison. *Environment and Development Economics*, *9*(6), 735–755.

Västilä, K., Kummu, M., Sangmanee, C., & Chinvanno, S. (2010). Modelling climate change impacts on the flood pulse in the Lower Mekong floodplains. https://doi.org/10.2166/wcc.2010.008

van Vuuren, D. P., Edmonds, J., Kainuma, M., Riahi, K., Thomson, A., Hibbard, K., et al. (2011). The representative concentration pathways: An overview. *Climatic Change*, *109*(1), 5–31. https://doi.org/10.1007/s10584-011-0148-z

Wang, W., Lu, H., Ruby Leung, L., Li, H.-Y., Zhao, J., Tian, F., et al. (2017). Dam Construction in Lancang-Mekong River Basin Could Mitigate Future Flood Risk From Warming-Induced Intensified Rainfall. *Geophysical Research Letters*, *44*(20), 10,378-10,386. https://doi.org/10.1002/2017GL075037

Winemiller, K. O., McIntyre, P. B., Castello, L., Fluet-Chouinard, E., Giarrizzo, T., Nam, S., et al. (2016). Balancing hydropower and biodiversity in the Amazon, Congo, and Mekong. *Science*, *351*(6269), 128–129. https://doi.org/10.1126/science.aac7082

Wood, E. F., Lettenmaier, D. P., & Zartarian, V. G. (1992). A land-surface hydrology parameterization with subgrid variability for general circulation models. *Journal of Geophysical Research*, *97*(D3), 2717. https://doi.org/10.1029/91JD01786

Wu, C. S., Chen, Y., Jeng, M. R., Hwong, J. L., & Lee, K. C. (2004). Evaluating the economic benefit of water resource nourishment by forests. *Taiwan Journal of Forest Science*, *19*(3), 187–197.

Wu, L., Feng, J., & Miao, W. (2018). Simulating the Impacts of Irrigation and Dynamic Vegetation Over the North China Plain on Regional Climate. *Journal of Geophysical Research: Atmospheres*, *123*(15), 8017–8034. https://doi.org/10.1029/2017JD027784

Yang, B., Zhang, Y., Qian, Y., Tang, J., & Liu, D. (2016). Climatic effects of irrigation over the Huang-Huai-Hai Plain in China simulated by the weather research and forecasting model. *Journal of Geophysical Research: Atmospheres*, *121*(5), 2246–2264. https://doi.org/10.1002/2015JD023736

Yang, Y., Zhang, M., Zhu, L., Liu, W., Han, J., & Yang, Y. (2017). Influence of Large

Reservoir Operation on Water-Levels and Flows in Reaches below Dam: Case Study of the Three Gorges Reservoir. *Scientific Reports*, *7*(1), 15640. https://doi.org/10.1038/s41598-017-15677-y

Zargar, A., Sadiq, R., Naser, B., & Khan, F. I. (2011). A review of drought indices. *Environmental Reviews*, *19*(NA), 333–349. https://doi.org/10.1139/a11-013

Zatarain Salazar, J., Reed, P. M., Quinn, J. D., Giuliani, M., & Castelletti, A. (2017). Balancing exploration, uncertainty and computational demands in many objective reservoir optimization. *Advances in Water Resources*, *109*, 196–210. https://doi.org/10.1016/J.ADVWATRES.2017.09.014

Zhao, R., & Chen, S. (2008). Fuzzy pricing for urban water resources: Model construction and application. *Journal of Environmental Management*, *88*(3), 458–466. https://doi.org/10.1016/j.jenvman.2007.03.004

Zhou, T., Haddeland, I., Nijssen, B., & Lettenmaier, D. P. (2016). Human-Induced Changes in the Global Water Cycle (pp. 55–69). American Geophysical Union (AGU). https://doi.org/10.1002/9781118971772.ch4

Zhou, T., Nijssen, B., Gao, H., Lettenmaier, D. P., Zhou, T., Nijssen, B., et al. (2016). The Contribution of Reservoirs to Global Land Surface Water Storage Variations. *Journal of Hydrometeorology*, *17*(1), 309–325. https://doi.org/10.1175/JHM-D-15-0002.1

Ziolkowska, J. R. (2015). Shadow price of water for irrigation-A case of the High Plains. *Agricultural Water Management*, *153*, 20–31. https://doi.org/10.1016/j.agwat.2015.01.024

Ziv, G., Baran, E., Nam, S., Rodriguez-Iturbe, I., & Levin, S. A. (2012). Trading-off fish biodiversity, food security, and hydropower in the Mekong River Basin. *Proceedings of the National Academy of Sciences*, *109*(15), 5609–5614. https://doi.org/10.1073/pnas.1201423109

Ziv, Guy, Baran, E., Nam, S., Rodríguez-Iturbe, I., & Levin, S. A. (2012). Trading-off fish biodiversity, food security, and hydropower in the Mekong River Basin. *Proceedings of the National Academy of Sciences of the United States of America*, *109*(15), 5609–14. https://doi.org/10.1073/pnas.1201423109

# Chapter 2

# Implications for streamflow and water management from land use and land cover change and climate change impacts

**Keywords:** VIC, land cover, remote sensing, GCM, rule curve.

## 2.1 Introduction

Anthropogenic activities markedly affect the exchanges of energy, mass, and momentum across the land and atmosphere interface at different spatial and temporal scales, and these modification causes significant impacts on water and energy balance through the land-atmosphere interaction (Cao et al., 2015; Yang et al., 2016). Quantifying streamflow changes due to land cover and climate change has been of interest for many decades. The changing land cover and irrigation alter the water balance of the basin due to noticeable variations in the evapotranspiration (ET), soil water content, and groundwater recharge (Marhaento et al., 2017). The hydrological cycle is influenced by the change in vegetation cover and productivity through the alteration in the interception, evaporation, and transpiration processes (Liu et al., 2016). In combination with the variability of the precipitation, the ET transforms the third component of the water balance, i.e. streamflow, modifying the duration and magnitude of the peak flow and low flow conditions due to the unavailability of the water flux.

The Mekong river basin (MRB) is one of the largest transboundary basins in the world located in southeast Asia. The basin encompasses the region of China, Myanmar, Thailand, Lao PDR, Cambodia, and Vietnam. Sixty million people in the Lower Mekong Basin (LMB) derive their nourishment from the Mekong river for agricultural activities-rice cultivation, vegetables, livestock, fruit and nuts, and fisheries, apart from off-farm wages, (Martin & Lorenzen, 2016; Olson & Morton, 2018). The MRB has high hydropower potential (more than 50,000 MW in the main stem and 30,000 MW from tributaries) (Stone, 2011a) and hosts 42 dams in the basin with three on the main stem of the river in China, to harness the hydropower production (Keskinen et al., 2012; Mekong River Commission, 2010). The construction of dams has catastrophic effects on agriculture, fisheries, and

biodiversity (Intralawan et al., 2017; Ziv et al., 2012), along with changes in downstream sediment delivery (Kummu & Varis, 2007; Manh et al., 2015; Shrestha et al., 2013; Västilä et al., 2010), coastal groundwater (Erban et al., 2014; Merola et al., 2015), and flood and drought management (Li et al., 2017; Wang et al., 2017). The crop yield of the MRB is confined by inferior soil and water availability during the dry season. The heterogeneous variability of the yield in the basin caused low agricultural productivity in Cambodia and Thailand, while moderate production in Lao PDR and central Vietnam. On the other hand, Vietnam delta is the highest rice producer of the region and exports 10% of the global rice market. The paddy rice production of the lower Mekong countries was more than 109 million tons in 2017 with Vietnam, Thailand, and Myanmar ranking $5^{th}$, $6^{th}$, and $7^{th}$ largest producers in the world, respectively. Apart from rice cultivation, the rubber production of Thailand was more than 4.4 million tons in 2017, accounting for 33% of global production. Also, Vietnam is the third-largest rubber producer and second-largest exporter of coffee, followed by Lao PDR ("Agriculture and fishing | Open Development Mekong," 2019).

Various studies have been conducted to investigate the alteration of the flow and water availability due to climate change in the LMB (Eastham et al., 2008; Hoanh et al., 2004, 2010; Kiem et al., 2008; Västilä et al., 2010). The uncertainty study performed by Kingston et al (2011), using the semi-distributed hydrological model (SLURP) and seven different GCMs reveal the change in annual river discharge to increasing mean temperature varying from a 5.4% decrease to 4.5% increase. Similar results were obtained by Vastila et al (2010), reporting an increase of 4% in annual streamflow with an annual average temperature increase from 1 $^{o}$C and 2 $^{o}$C in the Mekong by 2040s using the dynamically downscaled ECHAM4 climate model data. However, the impact of climate change is not confined to streamflow alteration, it has an overwhelming effect on the sediment yield in the LMB as well. The change in the annual sediment yield from a 27% decrease to 160% increase is predicted by Shrestha et al. (2013) employing four GCMs, a regional circulation model (PRECIS), and Soil and Water Assessment Tool (SWAT). Also, the intra-annual (monthly) variation of the sediment yield was even greater, ranging from 88% decrease to a 243% increase. The MRB is projected to face a wide range of variations in the temperature and precipitation accounting 1-6 $^{o}$C and -5-20%, respectively, between 2020

and 2099 with respect to the historic period. Using the VIC and SWAT hydrologic models, the region may experience flooding and inundation due to the increase in peak flows ranging from 10-70% between RCP 4.5 and RCP 8.5 in the response of climate change. The reservoir operation will affect the streamflow through 35% and 16% reduction in flow during the dry and wet season, respectively (Sridhar et al., 2019).

Despite the limited studies that were carried out using hydrological and hydraulic models to explore the dam characteristics, real time monitoring, and modeling of the water diversion for the irrigation, electricity, municipal and domestic demand with the performance during the extreme events is required for developing reservoir operation plans. Bonnema and Hossain (2017) used the satellite data to develop the operating pattern of reservoirs in the LMB through the study of two parameters, residence time and flow alteration, impacting the streamflow. The range of the residence times of the individual reservoirs was between 0.09 to 4.04 years with the streamflow alteration between 11 and 130% of its natural variability. The assessment of reservoir operation using a remote sensing approach has been majorly confined to the reservoirs of the United States, Europe, and Africa. Also, the water extraction from the reservoirs was not explicitly inferred from these studies.

To explore the hydrological characteristics of the Mekong River basin, a high-resolution ($0.05^{o}$ spatial and daily timestep) hydrological model is required with the GCMs projection to study the impact of climate change for the precise simulation of the impact of dams on both tributaries and mainstem flows. The novelty of this study is embedded in the implementation of the high-resolution hydrological model (Variable Infiltration Capacity at $0.05^{o}$ resolution) for the simulation of the inflow and outflow from the dams and the use of remote sensing products to derive the reservoir operations. We used meteorological variables including temperature and precipitation and observed streamflow from 1981 to 2019, land cover maps from 1992 to 2015, satellite imageries and altimetry data from 2008 to 2018, and climate model data from 1951 to 2099, the objectives of the study are to:

- quantify land use and land cover (LULC) change using the remotely sensed land cover maps.

- implement the hydrological model to assess the hydrological, and investigation of the impact of dams.
- project the impact of climate change on streamflow.
- derive the dam characteristics using satellite imageries and altimetry data to compensate for the observed data.

## 2.2 Materials and Methods

### 2.2.1 Study Area

The Mekong is a transboundary river in Southeast Asia, ranking 7th in Asia and 12th globally in terms of river length. The river originates in southeastern Qinghai province in China and flows through Tibetan Plateau, and Yunnan province to empty into the South China Sea at the Mekong Delta in Vietnam. It courses through China, Myanmar, Laos, Thailand, Cambodia, and Vietnam, covering a total length of approximately 4800 km with a catchment area of nearly 765,000 $km^2$. The MRB is divided into two parts by the intersection point of China, Laos and Myanmar boundaries, namely Upper Mekong River Basin (UMB) spanning a length of closely 2200 km, and Lower Mekong River Basin (LMB) having the remaining length of 2600 km. The MRB is associated with high discharge having an annual mean flow value of approximately 15,000 $km^3$/year. The precipitation in the region is defined by the monsoon season (June to November) during which the basin receives the majority of the rainfall. The spatial variation of the precipitation is remarkable, following east-to-west gradient, with the annual precipitation of 3,000 mm for uplands in the central MRB region and 1000 to 1600 mm in northeast Thailand in the LMB, whereas in UMB, the Tibetan Plateau receives 600 mm and mountains of Yunnan gets 1700 mm mean annual rainfall. On the other hand, the variation of the temperature follows a north-to-south gradient with 30 $^oC$ and 38 $^oC$ during March-April, and November to February marked with the coolest temperature, while the winter temperate at higher elevations of the Lao PDR is around 15 $^oC$. As a result, the climate of LMB is classified as tropical monsoonal, i.e. hot and humid and the portion of UMB is glaciated, which provides the snowmelt runoff during the dry season.

In this study, the selection of the dams for the analysis was primarily based on the function of the reservoirs. We have selected 31 dams commissioned for irrigation and hydropower

purpose to estimate the inflow and outflow with the impact of climate change (Figure 1, Table 1). Based on the Food and Agriculture Organization (FAO) and Mekong River Commission (MRC) database, the established and operational dams located in the six countries and falling within the boundaries of the Mekong basin were determined. The selected dams were operational for more than 10 years with the evolved rule curve and streamflow impacts. Out of these dams, 3 dams namely Lam Pao, Sirindhorn, and Ubol Ratana, were selected based on the reservoir capacity of more than 1000 million $m^3$ and reservoir area more than 200 $km^2$ for the derivation of reservoir operation using the remote sensing data.

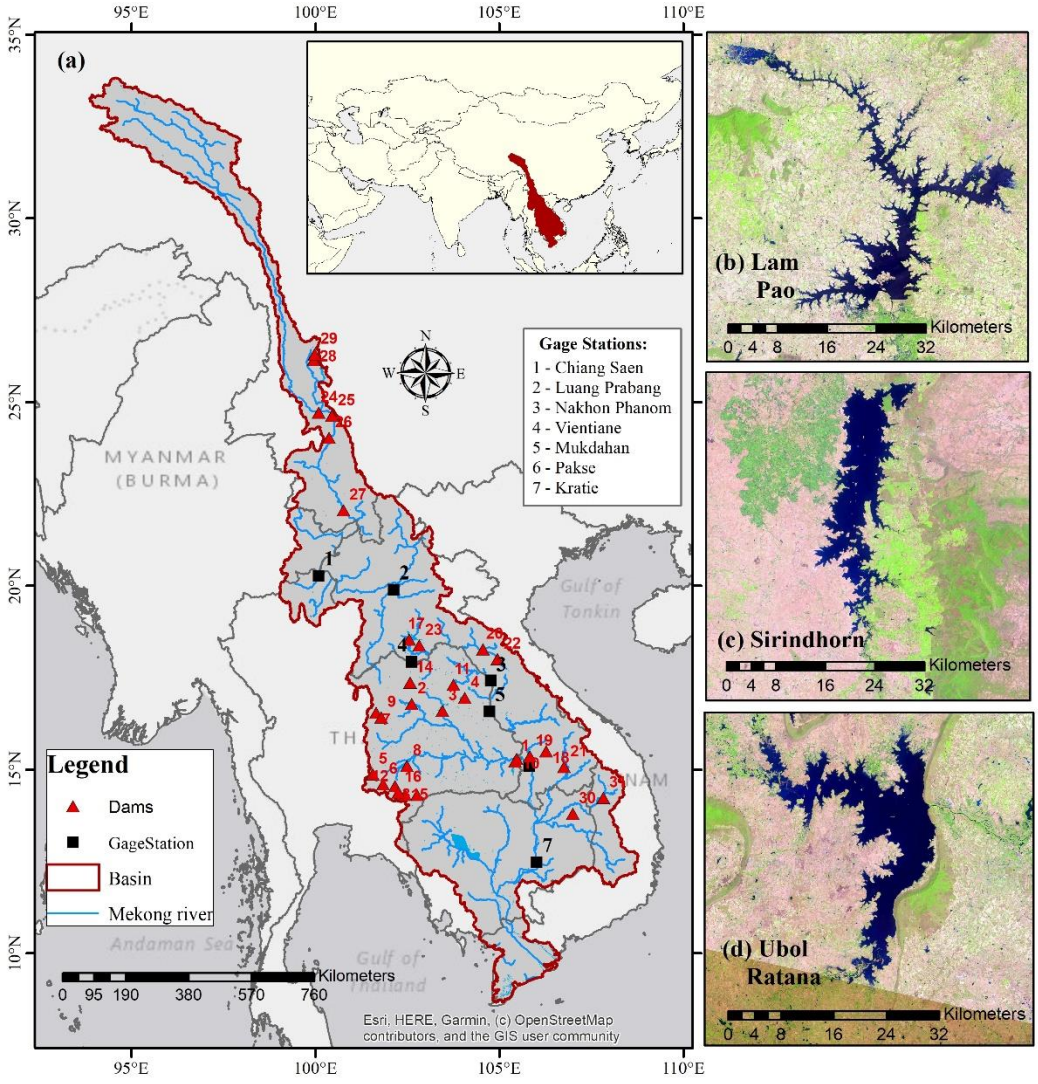


*Figure 1: (a) Geographical map of the Mekong River basin and satellite images of (b) Lam Pao, (c) Sirindhorn, and (d) Ubol Ratana from the official US Geological Survey*

*Table 1: List of the dams considered in this study*

| S.No. | Name of dam | Country | Function | Completed /operational since | Dam height (m) | Reservoir capacity (million $m^3$) | Reservoir area ($km^2$) |
|---|---|---|---|---|---|---|---|
| 1 | Sirindhorn | Thailand | Multipurpose | 1971 | 42 | 1966 | 288 |
| 2 | Ubol Ratana | Thailand | Multipurpose | 1966 | 32 | 2.559 | 41 |
| 3 | Lam Pao | Thailand | Irrigation | 1969 | 33 | 1430 | 240 |
| 4 | Nam Pung | Thailand | Multipurpose | 1965 | 40 | 165 | 2.165 |
| 5 | Lam Takhong | Thailand | Multipurpose | 1969 | 40.3 | 310 | 3.7 |
| 6 | Lam Phra Phloeng | Thailand | Multipurpose | 1970 | 50 | 110 | 1.31 |
| 7 | Chulabhorn | Thailand | Multipurpose | 1972 | 70 | 188 | 31 |
| 8 | Lam Chang Han | Thailand | Multipurpose | 1992 | 18 | 26 | 4.8 |
| 9 | Huai Kum | Thailand | Hydroelectricity | 1982 | 36 | 22.8 | 1.8 |
| 10 | Pakmun | Thailand | Hydroelectricity | 1994 | 17 | 114.3 | 1.7 |
| 11 | Nam Un | Thailand | Irrigation | 1973 | 29.5 | 520 | 8.5 |
| 12 | Upper Mun | Thailand | Irrigation | 1980 | 32.7 | 141 | 1.275 |
| 13 | Lam Nang Rong | Thailand | Irrigation | 1982 | 23 | 150 | 11.6 |
| 14 | Huai Luang | Thailand | Irrigation | 1984 | 12.5 | 113 | 3.2 |
| 15 | Lam Plai Mas | Thailand | Irrigation | 1988 | 32 | 98 | 1.04 |
| 16 | Lam Sae | Thailand | Irrigation | 1998 | 29.5 | 275 | 2.95 |
| 17 | Nam Ngum | Laos PDR | Hydroelectricity | 1985 | 45 | 7010 | |
| 18 | Xeset 1 | Laos PDR | Hydroelectricity | 1991 | | 30 | |
| 19 | Selabam | Laos PDR | Hydroelectricity | 1993 | | 30 | |
| 20 | Theun-Hinboun | Laos PDR | Hydroelectricity | 1998 | | 20 | |
| 21 | Houay-Ho | Laos PDR | Hydroelectricity | 1998 | 80 | | |
| 22 | Nam Leuk | Laos PDR | Hydroelectricity | 2000 | | | |
| 23 | Nam Mang 3 | Laos PDR | Hydroelectricity | 2004 | 22 | | 10 |
| 24 | Xiaowan | China | Hydroelectricity | | 292 | 15043 | 190 |
| 25 | Manwan | China | Hydroelectricity | 1995 | 132 | 662 | |
| 26 | Dachaoshan | China | Hydroelectricity | 2004 | 111 | 933 | |
| 27 | Jinghong | China | Hydroelectricity | 2008 | 108 | 1233 | 510 |
| 28 | Cibihe (Zibihe) | China | Irrigation | | | 93.22 | 7.9 |
| 29 | Haixihai | China | Irrigation | | | 61.854 | 4 |
| 30 | Ochum | Cambodia | Hydroelectricity | | | | |
| 31 | Yaly | Viet Nam | Hydroelectricity | 2002 | 69 | 1037 | 64.5 |

### 2.2.2 Data

*Landcover Maps:*

Global landcover data from the Earth's Change Atmosphere – Climate Change Initiative (ESA-CCI) available at www. cci.esa.int with 300 m spatial resolution and annual time

step was used for the analysis of change in the land use pattern in the Mekong River basin from 1992 to 2015. ESA-CCI is the only database that has continuous long-term annual land cover maps from 1992-2015 for the analysis of land transformation. The ESA-CCI land use had 21 classes that were clipped to the Mekong basin and reclassified to IGBP classes reducing the number of classes to 11. The conversion to IGBP classification helped in developing the vegetation parameters for the VIC model to study the streamflow and its relationship with the land cover. Figure 2 shows the schematic diagram of the methodology adopted to obtain Land Use Map for the Mekong river basin with IGBP classes. The re-classification mainly combined the classes of the ESA-CCI with different coverage percentages into a single class. The dominant classes from the land cover map were cropland, evergreen broadleaf forest, grassland, and closed shrubland, while the other classes comprised less than 5% of the total land cover. The cropland class was derived by combining six ESA-CCI classes, while the evergreen broadleaf forest, grassland, and closed shrublands were obtained by combining four, two, and three classes, respectively. Since the reclassification of the land cover classes was done by combining the existing spatial resolution grids of different categories, the resolution was not compromised. The grouping of the ESA-CCI classes to derive IGBP classes is summarized in Table 2.

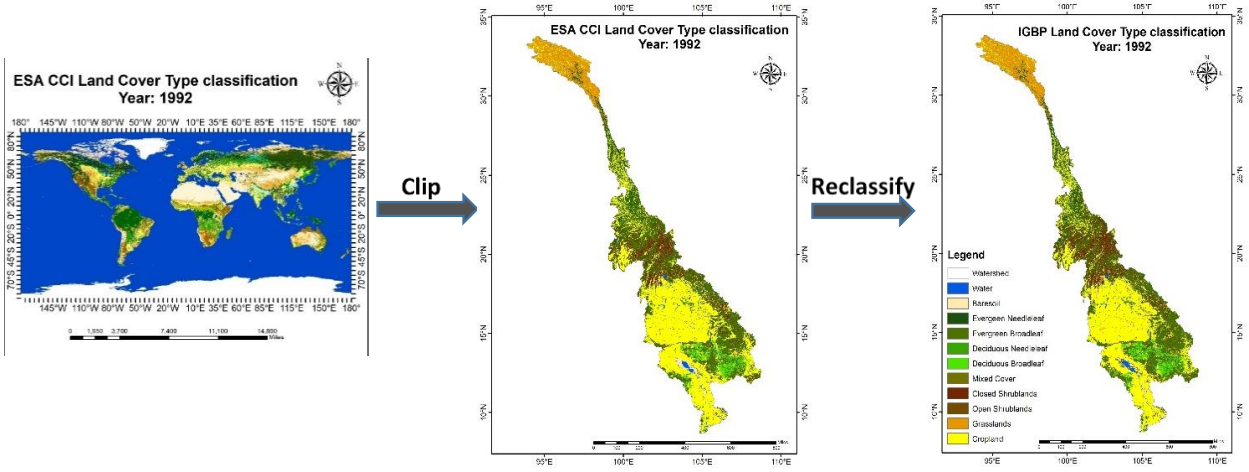


*Figure 2: Schematic diagram for the derivation of the IGBP land use classes*

*Table 2: Classification of the ESA-CCI classes into IGBP classes*

| ID | ESA-CCI Class | IGBP Class | New class |
|---|---|---|---|
| 70 | Tree cover needle leaved evergreen closed to open (>15%) | Evergreen Needleleaf | 401 |
| 50 | Tree cover broadleaved evergreen closed to open (>15%) | Evergreen Broadleaf | 402 |
| 100 | Mosaic tree and shrub (>50%) / herbaceous cover (<50%) | | |
| 160 | Tree cover flooded fresh or brakish water | | |
| 170 | Tree cover flooded saline water | | |
| 80 | Tree cover needle leaved deciduous closed to open (>15%) | Deciduous Needleleaf | 403 |
| 60 | Tree cover broadleaved deciduous closed to open (>15%) | Deciduous Broadleaf | 404 |
| 61 | Tree cover broadleaved deciduous closed (>40%) | | |
| 62 | Tree cover broadleaved deciduous open (15-40%) | | |
| 90 | Tree cover, mixed leaf type (broadleaved and needle leaved) | Mixed Cover | 405 |
| 120 | Shrubland | Closed Shrublands | 408 |
| 121 | Shrubland evergreen | | |
| 122 | Shrubland deciduous | | |
| 150 | Sparse vegetation (tree shrub herbaceous cover) (<15%) | Open Shrublands | 409 |
| 110 | Mosaic herbaceous cover (>50%) / tree and shrub (<50%) | Grasslands | 410 |
| 130 | Grassland | | |
| 10 | Cropland, rainfed | Cropland | 411 |
| 11 | Herbaceous cover | | |
| 12 | Tree or shrub cover | | |
| 20 | Cropland, irrigated or post-flooding | | |
| 30 | Mosaic cropland (>50%) / natural vegetation (tree shrub,herbaceous cover) (<50%) | | |
| 40 | Mosaic natural vegetation (tree shrub herbaceous cover) (>50%) / cropland (<50%) | | |
| 180 | Shrub or herbaceous cover flooded fresh/saline/brakish water | Bare soil | 400 |
| 190 | Urban areas | | |
| 200 | Bare areas | | |
| 201 | Consolidated bare areas | | |
| 202 | Unconsolidated bare areas | | |
| 210 | Water bodies | Water | 399 |
| 220 | Permanent snow and ice | | |

*Reflectance images:*

The surface area of the reservoirs was calculated using the reflectance images of LandSat 8 and Sentinel-2(Claverie et al., 2018). The LandSat 8 mission was started in February 2013, to provide timely, high quality visible and infrared images of all landmass and near-coastal areas on the Earth, continually refreshing an existing Landsat database. The satellite has two main sensors, namely, the Operational Land Imager (OLI) and the Thermal Infrared Sensor (TIRS). 11 bands are sensing the spectral details of the landscape with

green signature (0.533-0.590 µm) in Band 3 and near-infrared signals (0.851-0.879 µm) in Band 5. The spatial resolution of this product was 30 m and temporal resolution was 15 days. The images with high cloud cover were discarded and Sentinel-2 reflectance images were employed to fill the date gaps between the LandSat 8 images. The Sentinel-2 began in March 2017, to perform terrestrial observations for forest monitoring, land cover changes detection, and natural disaster management. The images were captured under thirteen spectral bands with green signature (0.5425-0.5775µm) in Band 3 and near-infrared signals (0.7845-0.8995µm) in Band 8. The presence of two identical satellites, namely, Sentinel-2A and Sentinel-2B, improved the temporal resolution to 5 days, as also the spatial resolution was improved to 10 m. The satellite images of LandSat 8 and Sentinel-2 were collected for the period 2013-2018 from https://remotepixel.ca/projects/index.html.

*Altimetry:*

The altimetry datasets were used to generate the time series of water level variation of the reservoirs (Birkett et al., 2011). The altimetry data for some of the reservoirs in the MRB have been archived in the Global Reservoir and Lake Monitor (GRLM), and Hydroweb databases using the altimetry information from different satellites at a temporal resolution of 10 days. These satellites were operational for different periods and had an overlapping period, which contributed towards the generation of continuous altimetry data from 1992 to 2018. However, in this analysis, the dataset from 2013 to 2018 was utilized to coincide with the surface area data from LandSat 8 and Sentinel-2. Duan and Bastiannssen (2013) can be referred for the discussion of the altimetry water level databases.

Hydroweb is created by LEOS/GOHS (Laboratoire d'études en géophysique et océanographie spatiales/ Géophysique, Océanographie et Hydrologie Spatiales), using the altimetry data from ERS-1 (1991-1996), Topex/Poseidon (1992-2006), ERS-2 (1995-2011), GFO (2000-present), Jason-1 (2001-2013), Envisat (2002-2012), Jason-2 (2008-present) and Saral/Altika (2013-present). Cretaux et al. (2011) describe the procedure for obtaining the water level in Hydroweb. The GRLM is developed by the United States Department of Agriculture's Foreign Agricultural Service (USDA-FAS) in collaboration

with NASA and the University of Maryland. The database uses the altimetry data from Topex/Poseidon (T/P) (1992-2006), Jason-1 (2001-2013), Envisat (2002-2012), and Jason-2 (2008-present) to derive the 10-day time series of the reservoir water levels. However, the conversion factors were used to convert from satellite product to an orthometric/mean sea level datum. The relative height of the reservoir from mean sea level was used to derive the absolute water level of the reservoirs, which was validated through the back-calculation from dead storage of the reservoirs (Section 4.1). Birkett et al. (2011) describe water level processing in GRLM. The processing of the raw data from the satellite requires a complex sequence of steps necessary for extracting usable water level information. Primarily, the objective of the procedure is to remove unwanted effects caused by the instrument, atmosphere, and ocean. The water level derivation from the satellite altimeters is based on the principle presented in Fu and Cazenave (Fu & Cazenave, 2001). The surface height (h) with reference to an ellipsoid is based on the arithmetic sum of satellite altitude (A), range between the satellite and the surface (R), and corrections (C). The local undulation of the geoid is reduced from surface height for estimation of physical height from the ellipsoidal height (Pham et al., 2018). The reference of water for Hydroweb is the GRACE Gravity Model 02 geoid, while the GRLM has a mean 9-year T/P water level as a reference.

*Reservoir storage:*

The total storage of the reservoir was estimated by combining the live storage derived from the surface area and water level anomaly with the dead storage. The daily time series of the observed total storage of the reservoirs situated in Thailand are available through the reservoir database (http://app.rid.go.th:88/reservoir/) from 2008 to 2018. The variation of the total storage of the reservoirs was used for the validation of the results obtained through the developed methodology.

*Evapotranspiration:*

The total evaporation was required to calculate the amount of water lost as evaporation from the surface of reservoirs used for the estimation of outflow. Besides, the net irrigation water requirement was considered as a surrogate variable to ET, since ET estimates from croplands needed to be included in the analysis to account for the crop water use (Allen et

al., 1998). To this effect, variations in ET were compared with the water diversion from the reservoirs for irrigation purposes. The total ET was estimated using an 8-day composite MODIS product produced at 500-meter pixel resolution (MOD16A2 Version 6). The MOD16A ET products represent total transpiration by vegetation and evaporation from the canopy and soil surfaces at the land surfaces. The monthly series of the ET for the dams was derived from the global MOD16A dataset for the period 2008-2016 and ensemble mean was used for the evaluation of the monthly variation throughout the year. The estimation of the MOD16 ET product was carried out using the improved ET algorithm by Mu et al. (2011) using global MODIS land cover, a fraction of photosynthetically active radiation/leaf area index (FPAR/LAI) data (Myneni et al., 2002), albedo data (Y. Jin et al., 2003; Salomon et al., 2006) and global surface meteorology from the Global Modeling and Assimilation Office (GMAO) meteorological data. The current algorithm (Mu et al., 2007) used for the estimation of the MOD16 is the revised version of the algorithm proposed by Cleugh et al. (2007) based on the Penman-Monteith (PM) method (Monteith, 1965).

### 2.2.3 Hydrological and routing model

The Variable Infiltration Capacity (VIC) model was implemented for the estimation of the water budget components and streamflow at the dam and gage station locations for the observed climate. The VIC is a semi-distributed physically-based hydrological model that solves water and energy balance for each grid (here, $0.05^{o}$ spatial resolution) separately at a daily time step (Liang et al., 1994). The model requires meteorological parameters including precipitation, minimum, and maximum temperature and wind speed from the Global Meteorological Forcing Dataset (GMFD) gridded dataset available at $0.25^{o}$ spatial and daily temporal resolution (Sheffield et al., 2006). The GMFD dataset was statistically downscaled to $0.05^{o}$ spatial resolution. The GMFD dataset was developed by assembling various reanalysis and observed datasets such as the NCEP-NCAR reanalysis (Kalnay et al., 1996), CRU TS3.0 (Mitchell & Jones, 2005), the GPCP (G. J. Huffman et al., 2001), the TRMM (G. Huffman et al., 2003), and the NASA Langley SRB (Stackhouse et al., 2004). Precipitation and temperature data for the recent period (2017 to 2019 October) was derived from Climate Hazards Group InfraRed Precipitation with Station (CHIRPS) and Climate Prediction Center (CPC) gridded dataset respectively. The vegetation texture

containing the land cover type, leaf area index, and albedo was developed using Advanced Very High-Resolution Radiometer (AVHRR) at a 1 km spatial resolution. The soil class from the United States Department of Agriculture (USDA) classification and pedo-transfer functions (Cosby et al., 1984) applied to Harmonized World Soil Database (HWSD) were combined to extract soil parameters.

The VIC model takes into consideration the vegetation variability within a grid cell, as the fractional value of the grid covered by the particular vegetation class. Also, the VIC model has three soil layers (0.1 m to 1.5 m); the rainfall is responded quickly by the top two layers with diffusion from the middle to the top layer, and the bottom layer corresponds to baseflow calculated using the Arno model formulation (Franchini & Pacciani, 1991). The total ET is calculated based on the Penman-Monteith approach and considered as the sum of evaporation from bare soil and canopy, and transpiration from vegetation features. Since VIC is a one-dimensional hydrologic model, the exchange of the fluxes is considered only vertically, i.e. the interaction between the adjacent grids is assumed to be negligible. Therefore, the water can enter the grid cell from the atmosphere with trivial lateral movement in the subsurface layer. The infiltration of water into the soil layer is defined by the variable infiltration curve (Wood et al., 1992), which is a non-linear function of the fractional saturated area. The VIC model provides only the fluxes for each grid at a daily temporal resolution based on the forcing parameters, therefore to extract the accumulated effect at the particular location, a separate routing scheme developed by Lohmann et al. (1998; 1996) was used on the VIC simulated fluxes. The VIC model has been implemented over numerous basins around the globe (Syed Azhar Ali et al., 2018; Kang et al., 2019; Kang & Sridhar, 2019; Sridhar, Ali, et al., 2019). The VIC model has been used for the hydrological assessment of the MRB (Bonnema & Hossain, 2017; Haddeland, Lettenmaier, et al., 2006; Tatsumi & Yamashiki, 2015a; Västilä et al., 2010; Zhou, Haddeland, et al., 2016).

The water (runoff and baseflow) and energy fluxes were simulated by VIC forced with meteorological, soil, and vegetation data for each grid cell independently without any lateral exchange of evaporation, runoff, baseflow, soil moisture, shortwave, and longwave

radiation fluxes. The routing model developed by Lohmann et al. (1998; 1996) was employed for the estimation of the streamflow at the desired location by routing the fluxes of each grid generated by the VIC model. The routing scheme explicitly routed the surface and subsurface flow within a grid using a unit hydrograph that contributed to a channel network where the node of the channel network represented each grid-cell of the VIC model. The unit hydrograph governed the distribution of travel time within the grid cell and implicitly assimilated the travel time across hill slope and tributaries that connected the hill slopes and main channel (Hongyi Li et al., 2012). The water no longer considered as part of the water budget, once it reached the channel. Using the linearized Saint Venant equation, the channel routing was simulated for the whole network within the study area at the basin outlet assuming all runoff exits in a single flow direction. The parameters required for the routing model were (a) fraction of the grid-cell that flows into the basin being routed; (b) flow direction defining the connectivity between the grid-cells; (c) velocity (m/s) for the river routing component of the model; (d) flow diffusion ($m^2/s$) parameter for the routing component of the model; (e) location of the grid-cell to be routed to and, (f) grid cell impulse response function.

### 2.2.4 General Circulation Models

Four global circulation models (GCM) from two Representative Concentration Pathways (RCPs) 4.5 and 8.5 were used for future meteorological parameters in this analysis and they are GFDL-ESM2M, IPSL-CM5A-LR, MIROC-ESM-CHEM, and NorESM1-M. To access the future impact of climate change, certain scenarios based on greenhouse gas was developed for scientific investigations. These scenarios are known to be RCPs. RCPs are referred to as pathways to emphasize that their primary purpose is to provide time-dependent projections of atmospheric greenhouse gas (GHG) concentrations (IPCC expert meeting report, 2007). According to these four RCPs are RCP 8.5 (high pathway) for which radiative forcing reaches >8.5 $W/m^2$ by 2100 and continues to rise for some amount of time; RCP 6 and RCP 4.5 (intermediate “stabilization pathways”) in which radiative forcing is stabilized at approximately 6 $W/m^2$ and 4.5 $W/m^2$ after 2100; and RCP 2.6 pathway where radiative forcing peaks at approximately 3 $W/m^2$ before 2100 and then declines(van Vuuren et al., 2011).

The selection of the climate models was based on the collection of the distribution of wet/dry and cold/hot climate conditions defined using the precipitation and temperature change for five future periods between 2006 and 2099. The meteorological parameters of the GCMs were bias-corrected and statistically downscaled to 0.25-degree resolution using the Intersectoral Impact Model Intercomparison Project (ISI-MIP) approach (Hempel et al., 2013). Since the future period temperature was higher for all the GCMs relative to the historic period, the cool climate scenario was not analyzed. The climate change impact on the hydrological characteristics of the basin was well captured by the wide range of the temperature and precipitation changes, exhibited by the climate models, ranging between 0 °C and 6 °C, and -7% and 15%, respectively. The change in the meteorological parameters was considerable for RCP 8.5 as compared to RCP 4.5 with hottest and wettest scenario exhibited by IPSL-CMA-LR, while NorESM1-M covering the driest climate conditions (Figure 3). Clearly, MIROC-ESM-CHEM showed high precipitation and temperature for the later part of the century but GFDL-ESM2M and IPSL-CMA-LR projected drier and cooler conditions through 2040.

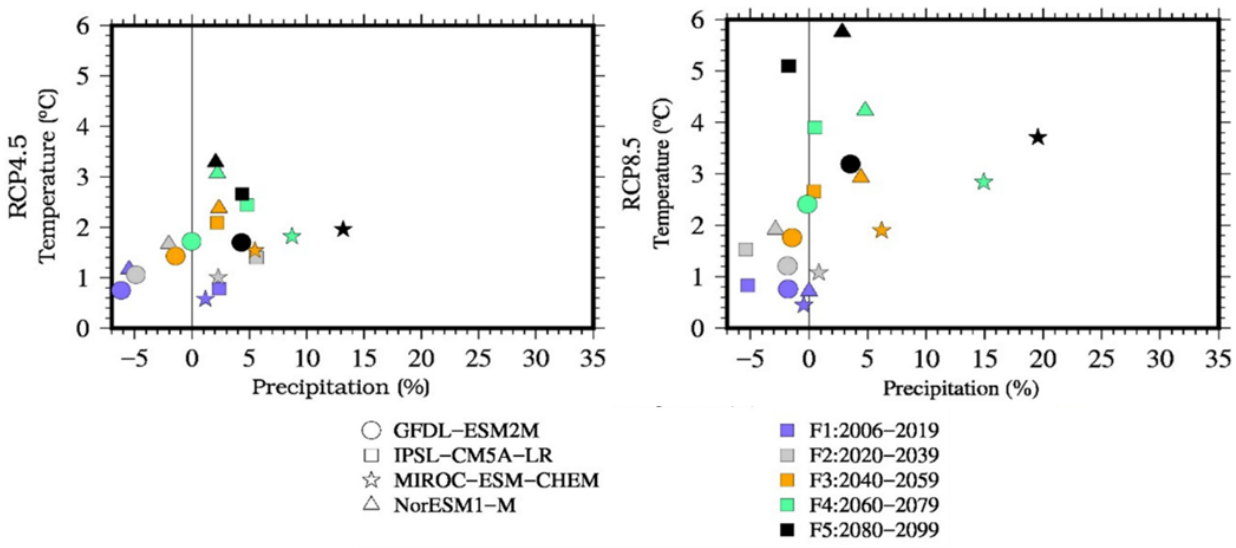


*Figure 3: Choice of wet (cold) and dry (hot) global circulation models (GCM) from two Representative Concentration Pathways (RCPs), 4.5 and 8.5, showing changing precipitation and temperature for five future periods, F1 through F5 between 2006 and 2099.*

### 2.2.5 Estimation of reservoir storage

The methodology adopted to estimate the impact of dams can be primarily classified into three major approaches; i.e. (a) estimation of the total storage variation of the reservoirs using the surface area (from LandSat 8 and Sentinel-2) and water level (from altimetry) fluctuation information through the development of relationship by carrying out regression analysis, (b) simulations from the VIC model for the estimation of the inflow to the reservoirs, and (c) the modification of the routing scheme of Lohmann et al. (1998; 1996) for the combination of the natural streamflow from the catchment and the outflow from the upstream reservoirs. The results from the mentioned approaches were blended to estimate the outflow from the reservoir. The graphical algorithm of the methodology is provided in Figure 4.

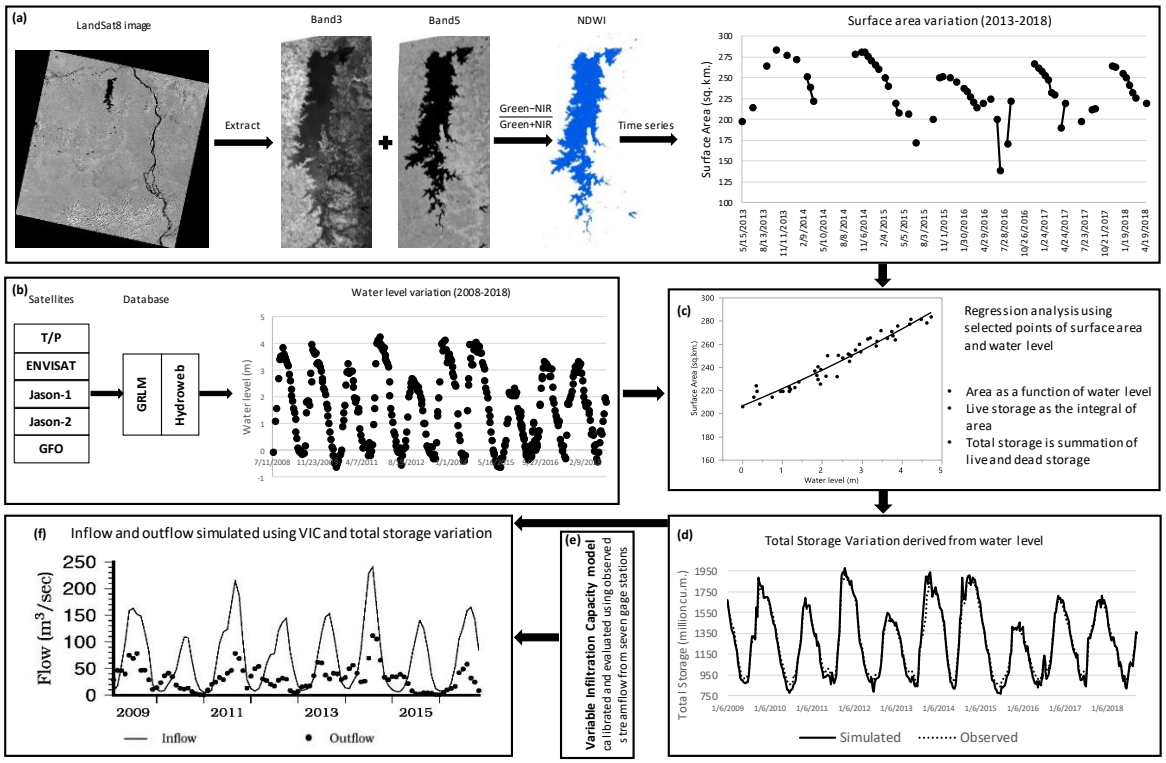


*Figure 4: The graphical representation of the sequential execution of the operations adopted to assess the impact of dams*

The estimation of the variation of the storage of the reservoirs was performed by segregating the total storage ($S_{total}$) into a variable component which fluctuates with the water level, i.e. live storage ($S_{live}$), and the minimum fixed amount of water available

throughout the period, i.e. dead storage ($S_{dead}$). Since the variation of the water level in the reservoirs is contained in the live storage component of the total storage of the reservoirs, it was estimated by employing a simple statistical tool using the altimetry and surface area data from remote sensing products. The overall procedure for the derivation of the total storage of the reservoirs can be split into the following steps:

*Surface Area variation:*

The extraction of the extent (surface area) of the reservoirs was performed by estimating the normalized difference water index (NDWI; B. Gao, 1996) using the reflectance images. Considering the spatial coverage of the LandSat 8 and Sentinel-2 images and the size of the reservoirs, the image processing was performed over a small region, called as the region of interest (ROI), containing the reservoirs with a buffer area of the images using ArcGIS. The NDWI is a remote sensing indicator, calculated as the ratio of the green band subtracted from the near-infrared (NIR) band to the sum of the green band and the NIR band, which is expressed as:

$$NDWI = \frac{Green - NIR}{Green + NIR} \quad (1)$$

The reflectance of the water feature is higher in the green band as compared to the NIR band. As a result, the NDWI value is positive for the pixels with major proportion occupied by the water feature, while negative values of NDWI indicates non-water features (soil and vegetation) because of less reflectance in the green band. However, the threshold value of NDWI for the classification of water features is affected by the atmosphere (clouds and aerosols), and water quality of the reservoirs (sediments and algae). Moreover, manual adjustment of the NDWI threshold value for the accurate extraction of the features is suggested by Ji et al (2009). Therefore, the NDWI range from 0.01 to 1, from visual inspection, was used for the extraction of the water bodies. The estimation of the area of the reservoir based on the classification of the pixels as water based on the above range was performed by multiplication of the number of water pixels with the spatial resolution of the image. The procedure was employed for all the images to obtain the series of the reservoir area defining the fluctuation of the surface area. Some of the reservoirs were not completely captured by a single image, therefore, the mosaicking was performed to extract

the ROI for those reservoirs. The surface area was estimated for the period 2013 to 2018 with an interval of 15 days (Figure 4a). However, discontinuity exists in the estimated time series due to non-usable satellite images, primarily cause by could cover inherence. The generation of the relationship between the surface area and water level is not impacted by the gaps in the time series as the individual surface area values at a specific time are considered for the regression analysis. The surface area of the reservoir is denoted by 'A'.

*Water level variation:*

The water level of the reservoirs was extracted, indirectly, from the altimetry dataset available from a different satellite. As compared to the reflectance images of LandSat 8 and Sentinel-2, the altimetry information was available for a longer time duration, from 2008 to 2018, and higher frequency, i.e. 10 days. Also, the existence of the non-available data (gaps in the time series) was minimal, fabricating this dataset as more consistent. The altimetry data is with reference to the reference ellipsoid which was converted into orthometric height by removing geoid height. The geoid approximately coincides with the mean sea level in the absence of all forces except gravity and centrifugal forces. The altimetry data was marked with both, positive and negative, values indicating that the water level yielded by the dataset was relative to the satellite reference level (Figure 4b). However, the conversion factor between the satellite reference datum and mean sea level was provided with the dataset, but the relative values were used in this analysis as the live storage was governed by the change in the water level with respect to an arbitrary reference. Hence, the zero water level was considered as the arbitrary reference datum (details in the next step). The relative water level from the altimetry dataset is denoted by 'h'.

*Regression Analysis:*

Since the altimetry data and surface area data were derived from different satellites, the datasets were inherited with disagreement in the date of acquisition of data. The data for the regression analysis were selected based on the date of acquisition of surface area data and the corresponding altimetry data with the tolerance of ±2 days. The filtering of the data to match the dates ensured the behavior of the reservoirs correctly captured by both the parameters. The selected altimetry data were assumed to reflect the variation of the live

storage, therefore the minimum value of the selected altimetry data ($h_{min}$) is corresponding to the null live storage ($S_{live}$= 0). Hence, the $h_{min}$ is subtracted from the altimetry data to have the range of $S_{live}$ initialing from zero. Mathematically, when h-$h_{min}$ = 0, $S_{live}$ =0. The regression analysis was carried out to fit surface area 'A' and h-$h_{min}$ values using the polynomial with degree 2. The correlation coefficient ($r^2$) was used as the performance parameter to infer the goodness of the fit. The surface area of the reservoir 'A' was expressed as the function of h-$h_{min}$ (Figure 4c). However, the h-$h_{min}$ for the data other than those selected for the regression analysis can have negative values suggesting the depletion of the dead storage ($S_{dead}$). Here, the surface area is not zero, when h-$h_{min}$ and $S_{live}$ are zero, indicating that the surface area is corresponding to the dead storage ($S_{dead}$).

*Estimation of live storage and total storage:*

The regression analysis yielded the relationship between the surface area (A) and water level (h-$h_{min}$) in the form of a second-polynomial function, which can be expressed as:

$$A = f(h - h_{min}) = a(h - h_{min})^2 + b(h - h_{min}) + c\ km^2 \quad (2)$$

where a, b, and c are the coefficients determined by the regression analysis. The expression for the live storage ($S_{live}$) was derived in term of water level by integrating equation 2, and

$$\text{Live storage } (S_{live}) = \int f(h - h_{min})dh = \frac{a(h - h_{min})^3}{3} + \frac{b(h - h_{min})^2}{2} + c(h - h_{min}) + d \quad (3)$$

expressed as:

where a, b, and c are the coefficients and has the same values as for equation 2. The value of d was calculated by considering the condition that $S_{live}$ =0 when h-$h_{min}$ =0; resulting in the value of d =0. Also, the total storage of the reservoir was the sum of live storage and dead storage. Mathematically, it can be expressed as:

$$Total\ storage\ (S) = \frac{a(h - h_{min})^3}{3} + \frac{b(h - h_{min})^2}{2} + c(h - h_{min}) + S_{dead} \quad (4)$$

*Validation of simulated storage:*

The time series for the total storage variation of the reservoirs were generated using equation (4) and the altimetry dataset. The total storage estimation was entirely dependent

on the altimetry data and was extracted for the same period as that of the altimetry dataset. The simulated total storage of the reservoirs was compared with the observed storage variation to assess the performance of the approach (Figure 4d). The comparison was made for the time series of the available observed storage data and the seasonal variation of total storage between the simulated and observed data.

### 2.2.6 Estimation of outflow from reservoirs

The fluxes simulated by the VIC model for the catchment area of the dams were routed to the reservoirs for the estimation of inflow to the dams. The monthly outflows from the dams were computed from the water balance equation for the reservoir accounting for the change in the reservoir storage and inflow to the dams, assuming negligible groundwater interactions:

$$Q_{out} = Q_{in} - \frac{\Delta S}{\Delta t} + A(P - E) \quad (5)$$

where $Q_{out}$ is the monthly outflow from the dam in $m^3$/sec, $Q_{in}$ is the monthly inflow to the reservoir in $m^3$/sec, $\Delta S/\Delta t$ is the change in the storage volume with time in $m^3$/sec, A is the area of the reservoir's water surface in $m^2$, and P and E are the precipitation and open evaporation in m/sec, respectively

The $Q_{in}$, P, and E on the reservoir were obtained from the simulation of the VIC model, whereas A was derived from the LandSat 8 and Sentinel2 imageries. The change in the storage of the reservoir ($\Delta S$) was computed as the difference between the storage for the month in consideration and the previous month, derived from the surface area and depth of the reservoirs from surface reflectance imageries and altimetry dataset, respectively. The $Q_{out}$ from the dams simulated from equation 5 was then validated against observed discharges from 2008 to 2016.

## 2.3 Results and Discussion

### 2.3.1 Land Cover change

The annual land use maps estimated for the Mekong river during the period 1992 to 2015 are shown in Figure 5. The dominant land cover in the region is Cropland covering more than 40% of the area, followed by Evergreen broadleaf forest with approximately 30% of

the area. Closed shrublands and grassland contribute approximately 10% of the region while other land use classes constitute a marginal proportion. Figure 6 shows the annual percentage variation of each land use class between 1992 and 2015. The highest increase during the period 1992-2015 was observed in Cropland (+2.04%), Bare soil (+0.83%), and Closed shrublands (+0.53%). The expansion of the cropland and bare soil occurred at the cost of Evergreen broadleaf forest (-3.02%) and Deciduous broadleaf forest (-0.47%). The spatial change of the land use classes was carried out to identify the regions affected by the expansion and contraction of the specific classes between 1992 and 2015 (Figure 6 (a-d)). The analysis was performed by reclassifying the target class ID to 1 and other class ID to 0 for the 1992 land use map. Similarly, the target and other classes were reclassified for the 2015 land use map. Finally, the two derived maps were subtracted ($ReclassifiedMap_{2015}$ minus $ReclassifiedMap_{1992}$) to obtain the change map with values -1,0, and 1. The index -1 indicates the extinction area, 0 indicates the area with no change, while 1 indicates the expansion of the target class between 1992 to 2015. The increase in the cropland is observed in the lower Mekong river basin, while Evergreen broadleaf forest extinction is estimated in the same region. The change in the grassland was not appreciably in the region and the upper Mekong river basin is marked with the removal of closed shrublands.

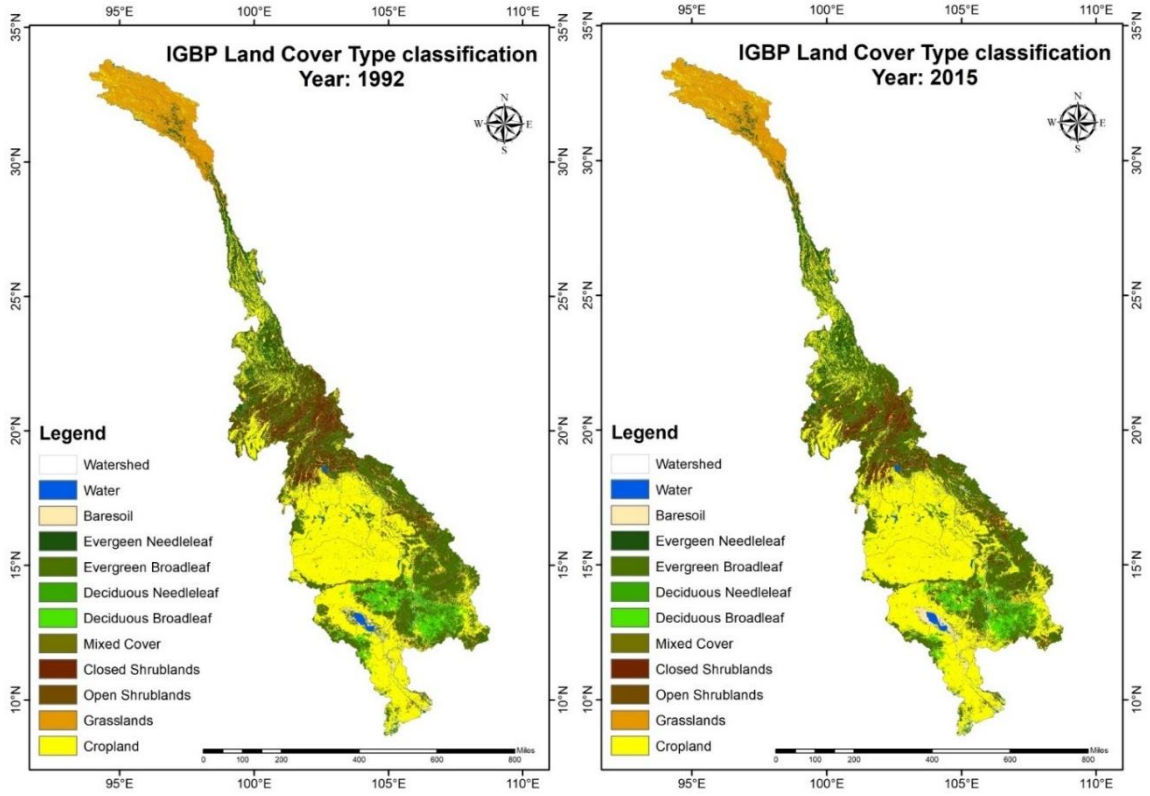


*Figure 5: Land use and land cover for the Mekong river basin for 1992 (left) and 2015 (right)*

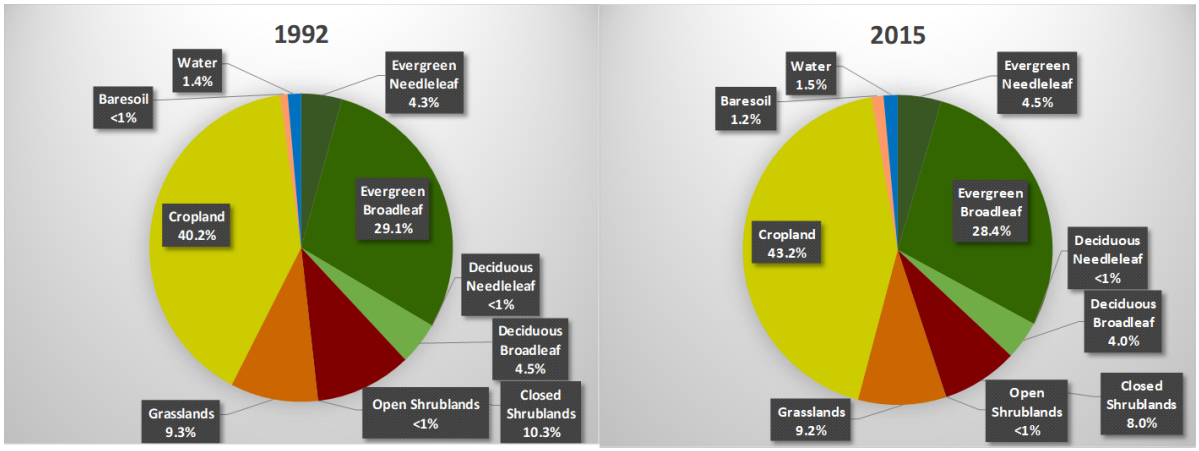


*Figure 6: Pie chart distribution of the major land cover types in the Mekong river basin for 1992 (left) and 2015 (right)*

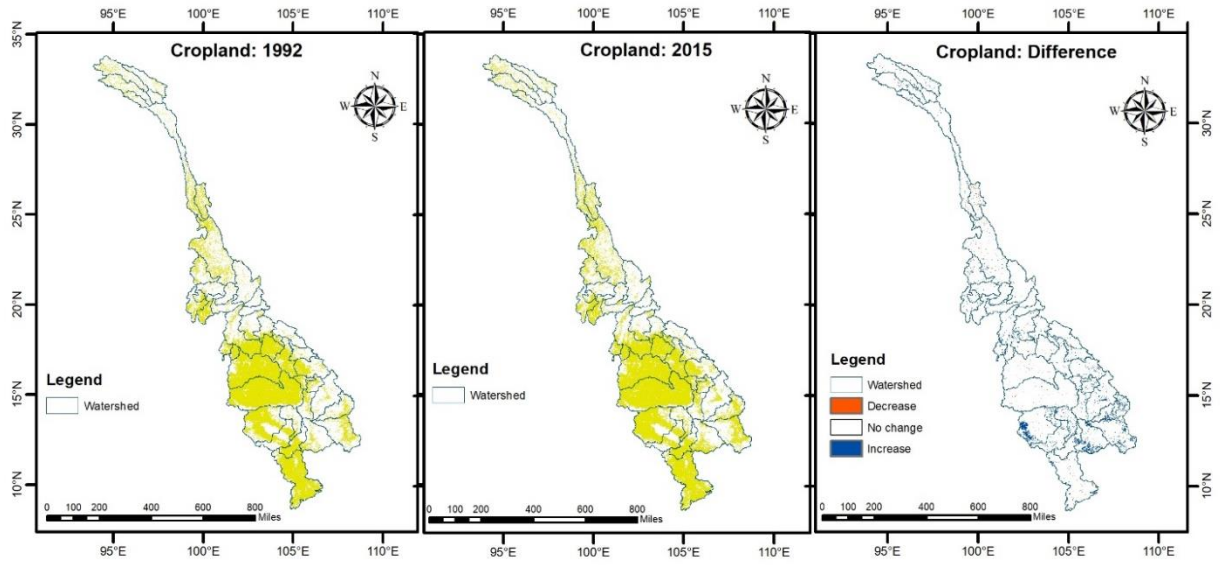


*Figure 6(a): Change in the cropland area in the MRB over the period 1992-2015*

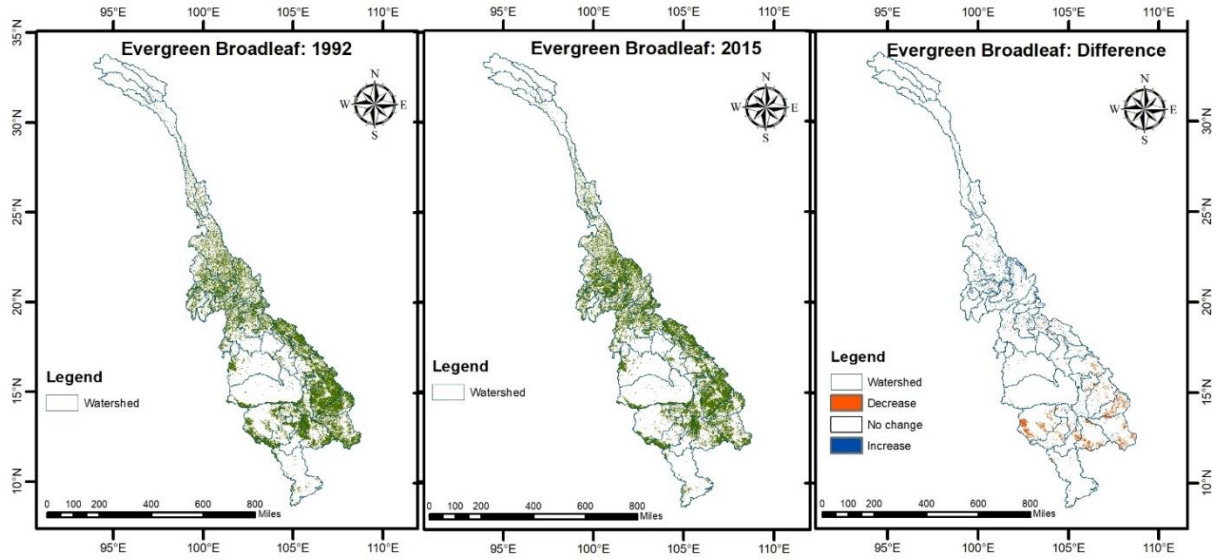


*Figure 6(b): Change in the evergreen broadleaf area in the MRB over the period 1992-2015*

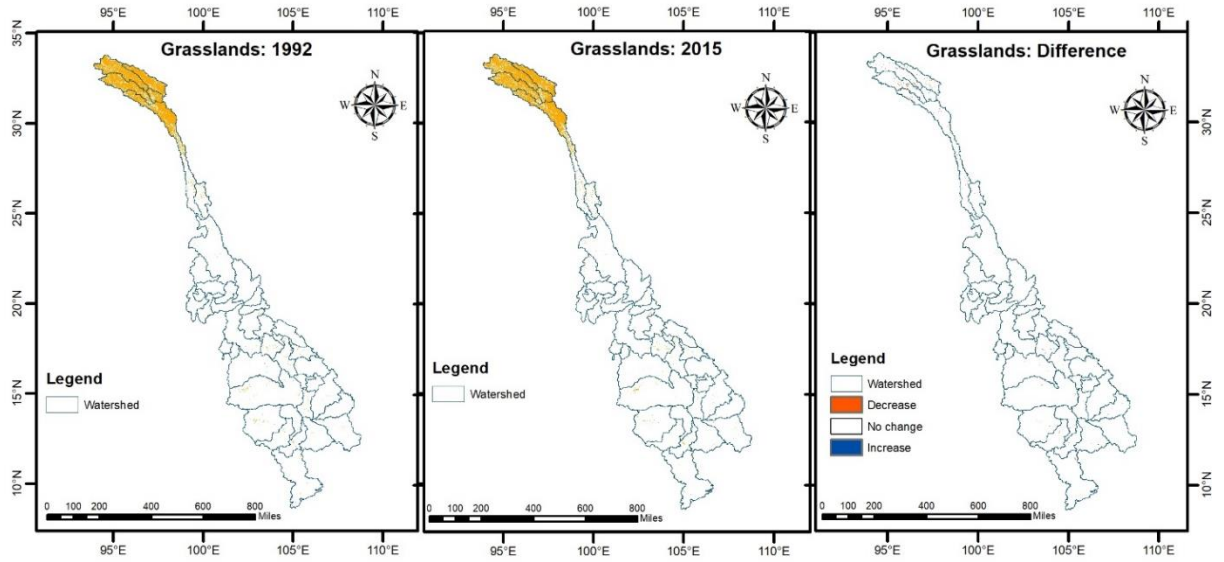


*Figure 6(c): Change in the grassland area in the MRB over the period 1992-2015*

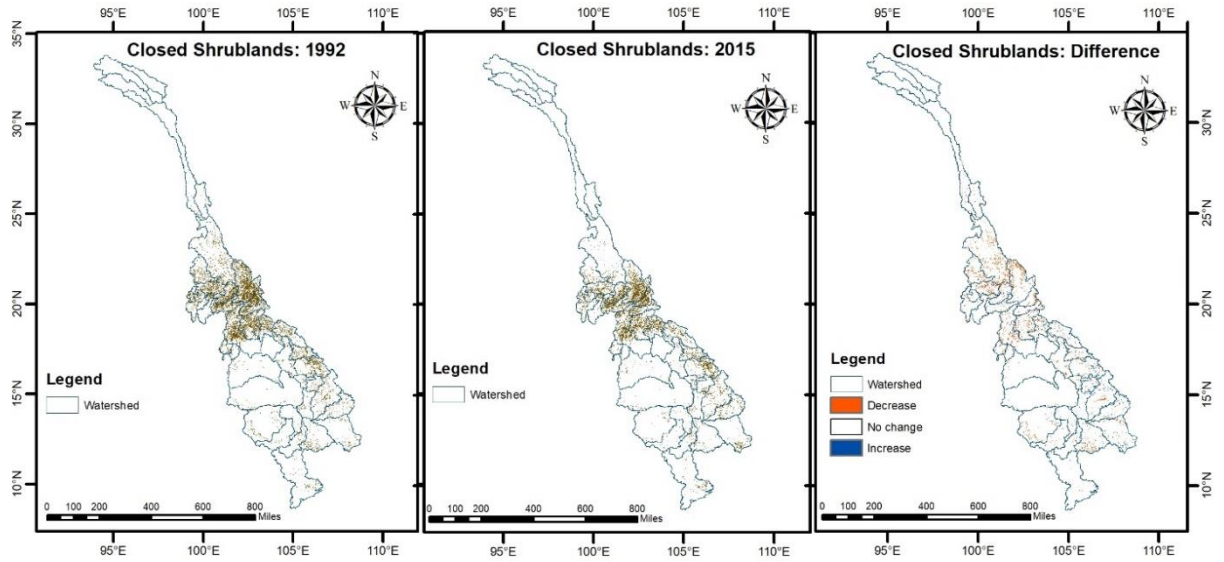


*Figure 6(d): Change in the closed shrublands area in the MRB over the period 1992-2015*

Similar results were obtained by Goteti & Lettenmaier (2001) suggested logging and agricultural expansion as the major cause of deforestation in Northern Thailand, Cambodia, Laos PDR, and Mekong delta. The analysis of the Mekong River Commission (MRC) funded by the German Agency for Technical Cooperation (GTZ) revealed a considerable decrease in secondary forest and an increase in agricultural area between 1993 to 1997. The high-density forests have seen comparatively low dynamics, whereas medium to low-density forests have experienced greater losses (Heinimann et al., 2007). The Forest Cover

Project estimated a rate of loss of forest of 0.53% per year over the basin from 1993 to 1997 (Costa-Cabral et al., 2008b).

### 2.3.2 Streamflow variation at gage and dam locations

The calibration and evaluation of the VIC model were performed using the monthly discharge data from the gauging stations distributed across the basin, namely Chiang Saen, Luang Prabang, Nakhon Phanom, Vientiane, Mukdahan, Pakse, and Kratie. The performance of the VIC model in simulating the streamflow improved substantially with the calibration of parameters such as variable infiltration curve parameter ($b_i$), the depth of the second and third soil layers (D), a fraction of maximum velocity of baseflow where non-linear baseflow begins ($D_s$), and a fraction of maximum soil moisture where non-linear baseflow occurs ($W_s$) with the allowable range as 0.1-0.5, 0.1-1.5, 0-0.4, and 0.5-1.0, respectively. The calibration was carried out for the gage stations stepwise from upstream basins and the regions already considered were excluded while calibrating the downstream locations. The period of the calibration and evaluation varied for the gage station as the data were recorded over different periods at each station, however, the calibration period was held constant from 1986 to 1991 and the evaluation period was varied based on the availability of data (Table 3). Mathematically, the capability of the VIC model was performed by the calculation of the NSE and r between the monthly simulated and observed streamflow. NSE ranges from -∞ to 1 and defined as:

$$NSE = 1 - \frac{\Sigma(Q_o^t - Q_m^t)^2}{\Sigma(Q_o^t - \overline{Q}_o)^2} \quad (6)$$

and r is defined as:

$$r = \frac{n(Q_o^t Q_m^t) - (\Sigma Q_o^t)(\Sigma Q_m^t)}{\sqrt{[n\Sigma(Q_o^t)^2 - (\Sigma Q_o^t)^2][n\Sigma(Q_m^t)^2 - (\Sigma Q_m^t)^2]}} \quad (7)$$

where $\overline{Q}_o$ is the mean of observed streamflow, $Q_o^t$ is observed streamflow at time t, $Q_m^t$ is simulated streamflow at time t, and n is the number of observations.

*Table 3: List of the gage stations used for the calibration and evaluation of the Variable Infiltration Capacity (VIC) model, Nash-Sutcliffe model efficiency coefficient (NSE) and coefficient of correlation (r) values between the observed and simulated streamflow*

| Station | Calibration | | | Evaluation | | |
|---|---|---|---|---|---|---|
| | Period | NSE | r | Period | NSE | r |
| Chiang Saen | 1986-1991 | 0.84 | 0.94 | 1992-1997 | 0.84 | 0.94 |
| Luang Prabang | 1986-1991 | 0.74 | 0.94 | 1992-1997 | 0.74 | 0.94 |
| Nakhon Phanom | 1986-1991 | 0.80 | 0.91 | 1992-1995 | 0.80 | 0.91 |
| Vientiane | 1986-1991 | 0.77 | 0.94 | 1992-1996 | 0.77 | 0.94 |
| Mukdahan | 1986-1991 | 0.86 | 0.94 | 1992-1995 | 0.86 | 0.94 |
| Pakse | 1986-1991 | 0.84 | 0.94 | 1992-1998 | 0.84 | 0.94 |
| Kratie | 1986-1991 | 0.85 | 0.92 | 1992-1998 | 0.85 | 0.92 |

Figure 7 shows the comparison of the monthly simulated streamflow with observations at seven gage stations for the calibration and evaluation period. The VIC model was able to precisely produce the observed streamflow with the NSE value of more than 0.8 except for Luang Prabang (NSE=0.74) and Vientiane (NSE=0.77), and a correlation coefficient of more than 0.91 during the calibration period. For the evaluation period, the NSE value remained greater than 0.74, while the correlation coefficient was over 0.91 between the observed and simulated streamflow. A well-calibrated model has an NSE value greater than 0.80 and the NSE values for the study locations indicated an "excellent" classification status while Luang Prabang was categorized as "very good" (Henriksen et al., 2008). Streamflows varied substantially with the peak monthly streamflow gradually increasing from Chiang Saen in the upstream region to Kratie in the lower portion of the basin ranging from 4000 $m^3$/sec to more than 40,000 $m^3$/sec. These comparisons confirmed that the VIC model was able to capture the magnitude and variations in streamflows throughout the LMB.

Since the gage stations were situated on the main stem of the Mekong River while the dams were on the tributary, the comparisons of observed and simulated inflows to the 10 dams were carried out to evaluate the VIC model. The monthly inflows to the dams were compared from 2008 to 2016. The NSE values between the observed and simulated inflow were estimated between 0.50 to 0.83 whereas the r values greater than 0.71 (Table 4). The decline in the NSE and r values for all the dams as compared to the gage station was partly due to low streamflow magnitudes. The peak inflows to the Lam Pao and Sirindhorn dams

were estimated as 450 $m^3$/sec and 1000 $m^3$/sec for Ubol Ratana, which constitute about 5.6% and 12.5% of the peak flow relative to the most upstream gage station (Chiang Saen, Figure 8). The inflow to the remaining 21 dams was simulated from 1981 to 2019 (Figure 9).

*Table 4: List of the dams used for the calibration and evaluation of the Variable Infiltration Capacity (VIC) model, Nash-Sutcliffe model efficiency coefficient (NSE) and coefficient of correlation (r) values between the observed and simulated streamflow*

| Dams | Calibration | | | Evaluation | | |
|---|---|---|---|---|---|---|
| | Period | NSE | r | Period | NSE | r |
| NamPung | 2004-2010 | 0.60 | 0.78 | 2011-2016 | 0.60 | 0.78 |
| UbolRatana | 2006-2011 | 0.63 | 0.89 | 2012-2016 | 0.63 | 0.89 |
| Chulabhorn | 2006-2011 | 0.76 | 0.88 | 2012-2016 | 0.76 | 0.88 |
| LamPao | 2004-2010 | 0.62 | 0.89 | 2011-2016 | 0.62 | 0.89 |
| LamTakhong | 2004-2010 | 0.58 | 0.77 | 2011-2016 | 0.58 | 0.77 |
| LamPhraPloeng | 2004-2010 | 0.50 | 0.71 | 2011-2016 | 0.50 | 0.71 |
| UpperMun | 2004-2010 | 0.66 | 0.82 | 2011-2016 | 0.66 | 0.82 |
| LamSae | 2006-2011 | 0.64 | 0.83 | 2012-2016 | 0.64 | 0.83 |
| LamNangRong | 2004-2010 | 0.72 | 0.89 | 2011-2016 | 0.72 | 0.89 |
| Sirindhorn | 2004-2010 | 0.83 | 0.91 | 2011-2016 | 0.83 | 0.91 |

The comparison of the VIC simulated and observed streamflow at the gage station locations has good agreements but the VIC model underestimated the flow volume during the high flow years and downstream most gage station locations, namely, Pakse and Kratie. The interannual variability of the flow was not considerably distinguishable but the basin observed high flows during 1995-97 and 2019. On the other hand, the flow was exceptionally low during 1992-93. Similar underestimation of the flows was simulated by the VIC model for the high inflow dams, namely Ubol Ratana, Lam Pao, and Sirindhorn, while the peak inflows were precisely simulated for the remaining dams. During the observed period, the inflow for 2011-12 was considerably higher than the average inflow due to the occurrence of the flood in Thailand in 2011. On the other hand, 2001-02 faced low inflows to the dams in the Thailand region. But the dams located in the upper Mekong region in China observed a peak inflow during 1993 followed by the low flow conditions in 1994. Moreover, Theun-Hiboun, Nam Leuk, and Huai Kum experienced the flood conditions during 2006-07 caused by the high inflow to the dams. Most of the dams

suffered from the reduced inflow during 2009-10. As the dams are sparsely located from each other at different meteorological and geographical conditions, the inflow characteristics varied widely. The inflow magnitude of the dams is characterized by their locations based on the mainstem, tributaries, or secondary tributaries. The classification of the dams based on the historic inflows is described in section 2.3.4.

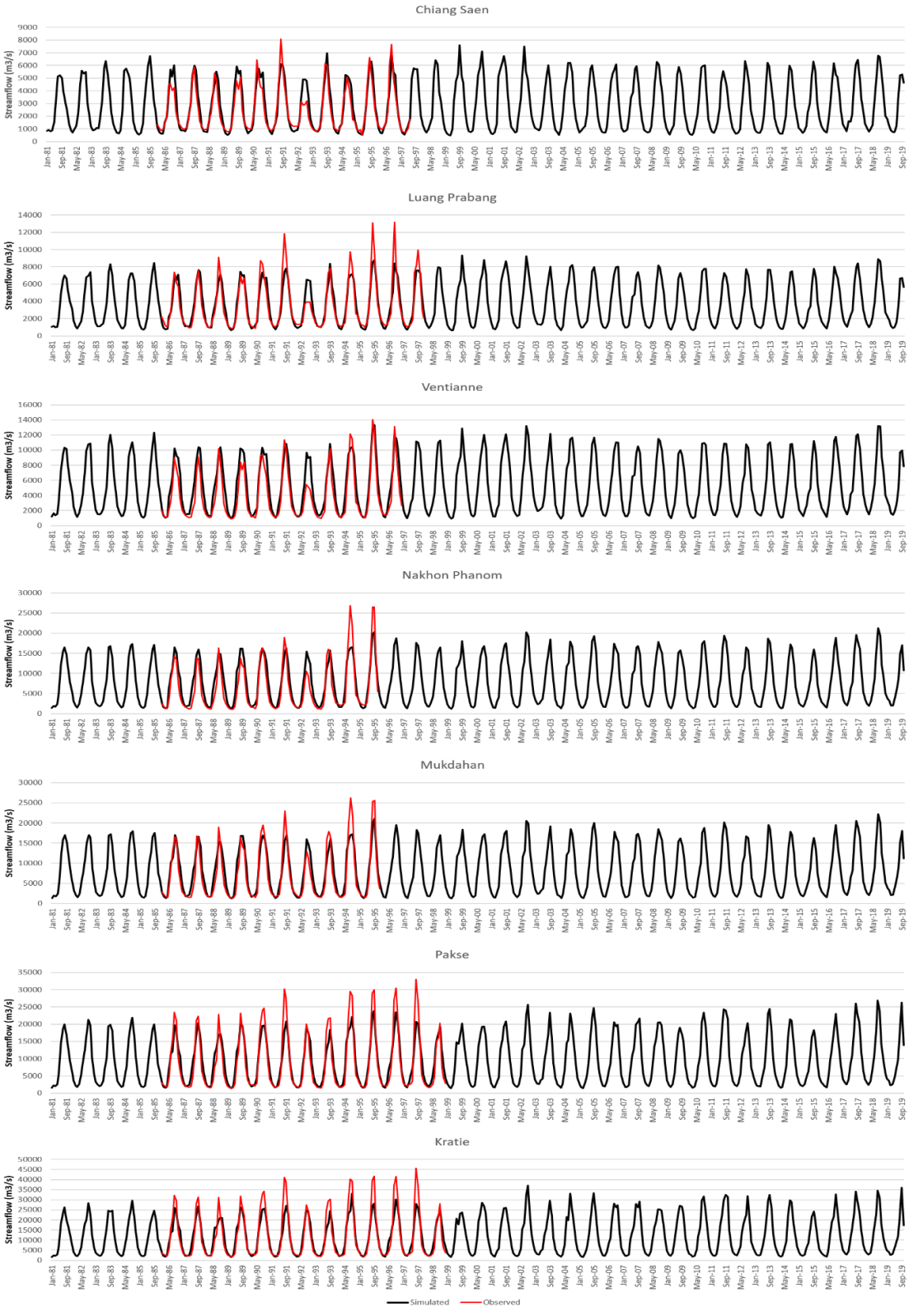


*Figure 7: Evaluation of the Variable Infiltration Capacity (VIC) model with the comparisons of the simulated and observed streamflow for calibration (1986-1992) and evaluation (1993-1998) periods at seven gage station locations*

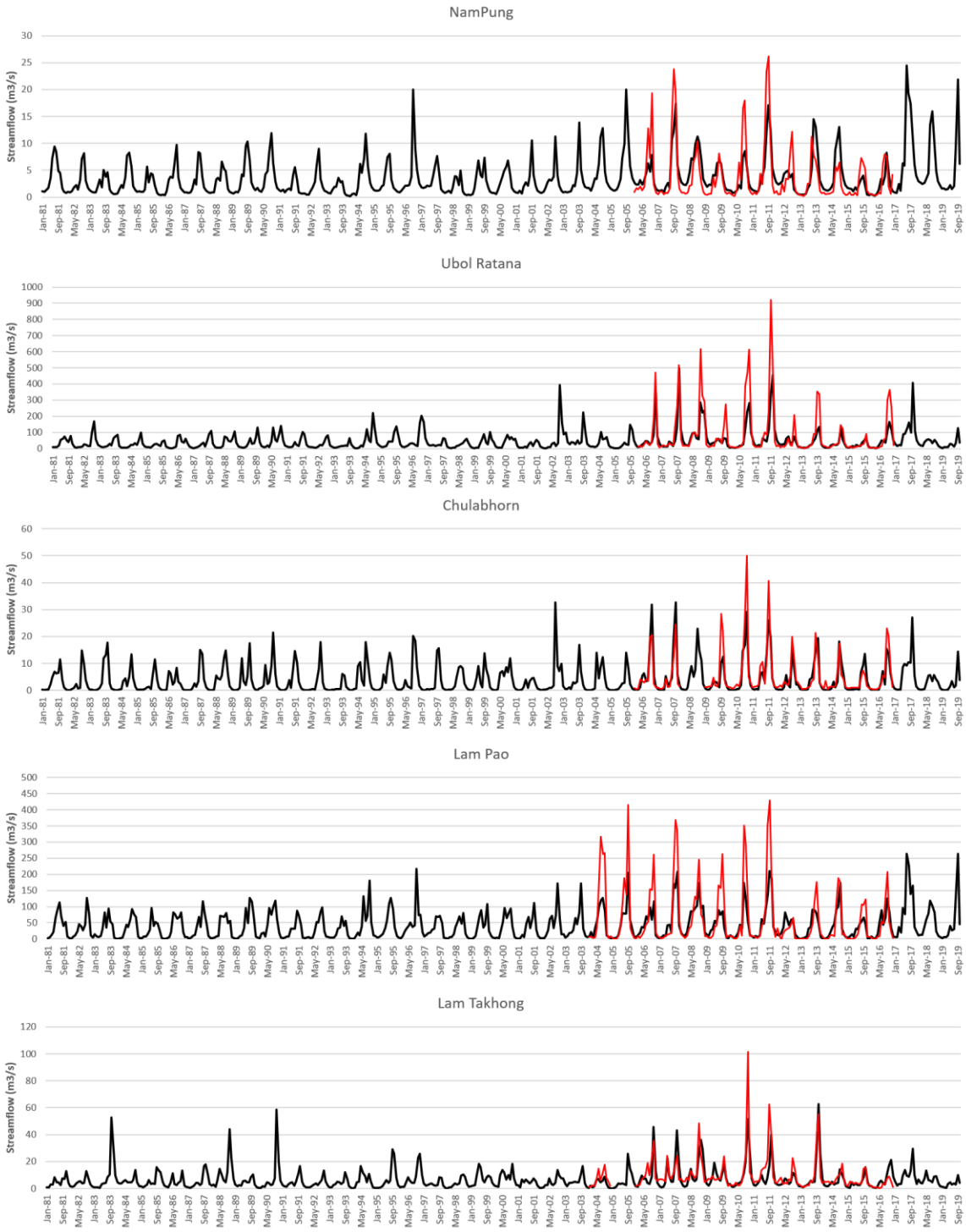


*Figure 8(a): Evaluation of the Variable Infiltration Capacity (VIC) model with the comparisons of the simulated and observed streamflow for calibration and evaluation periods at dam locations*

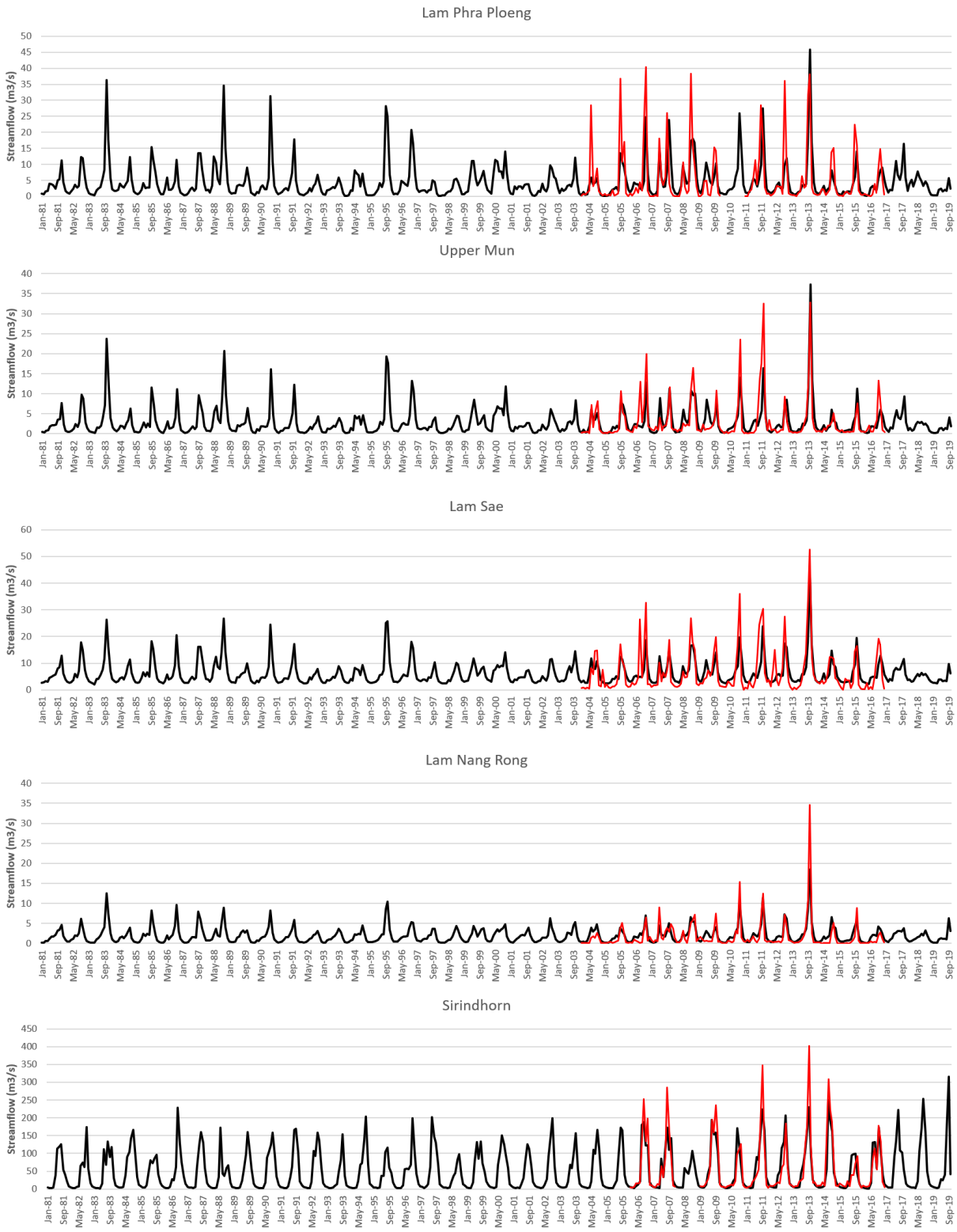


*Figure 8(b): Evaluation of the Variable Infiltration Capacity (VIC) model with the comparisons of the simulated and observed streamflow for calibration and evaluation periods at dam locations*

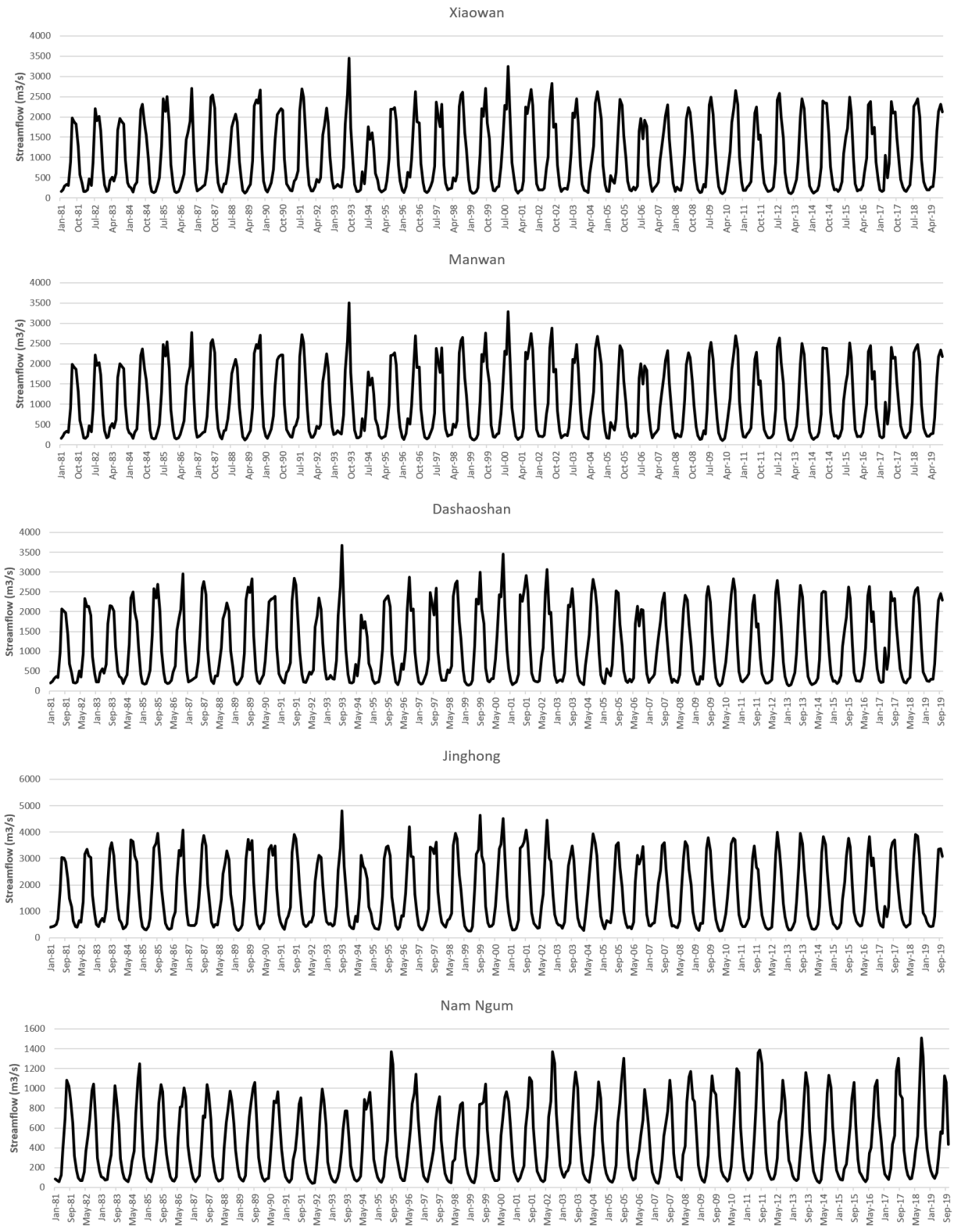


*Figure 9(a): Variable Infiltration Capacity (VIC) model simulated inflow at dam locations*

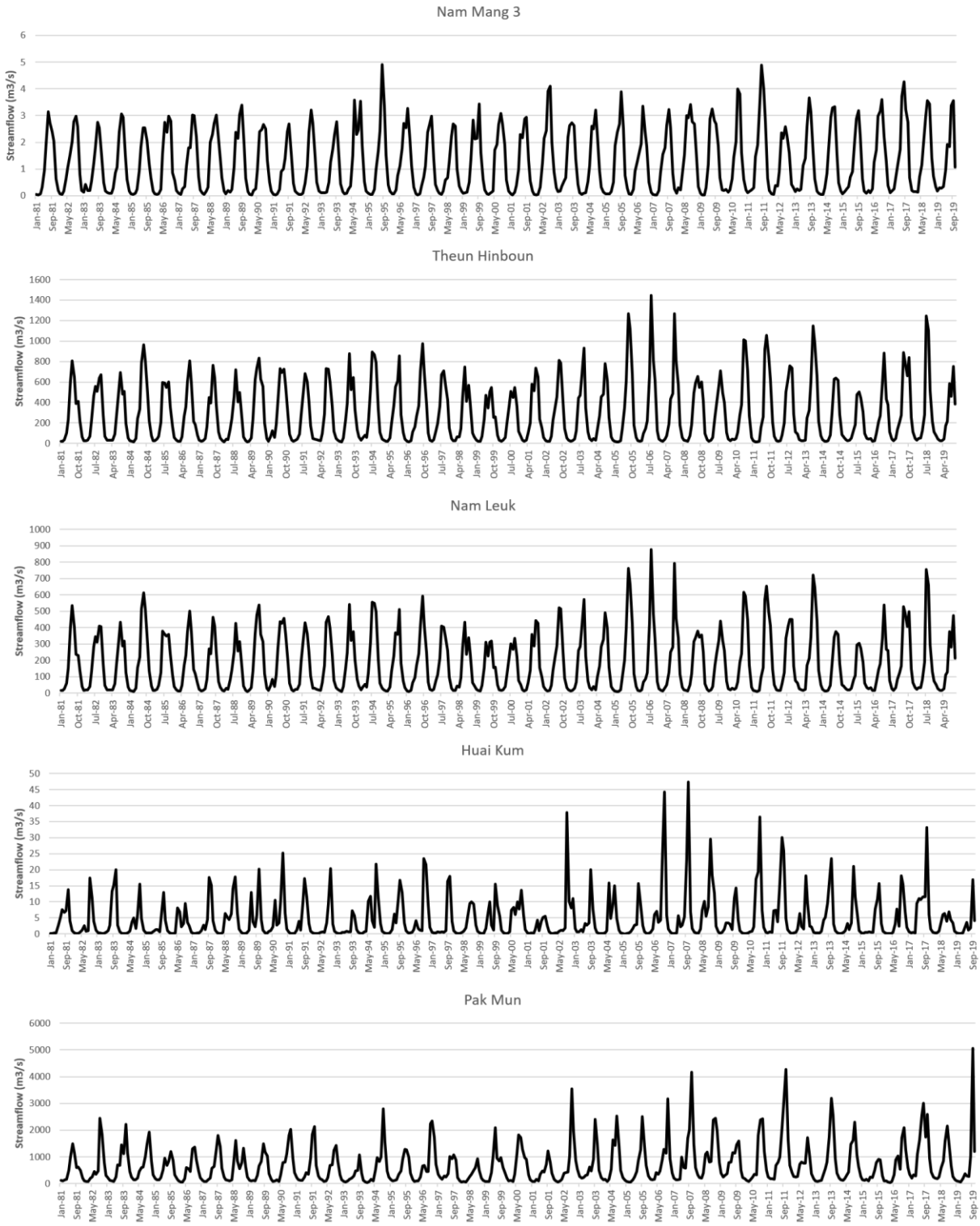


*Figure 9(b): Variable Infiltration Capacity (VIC) model simulated inflow at dam locations*

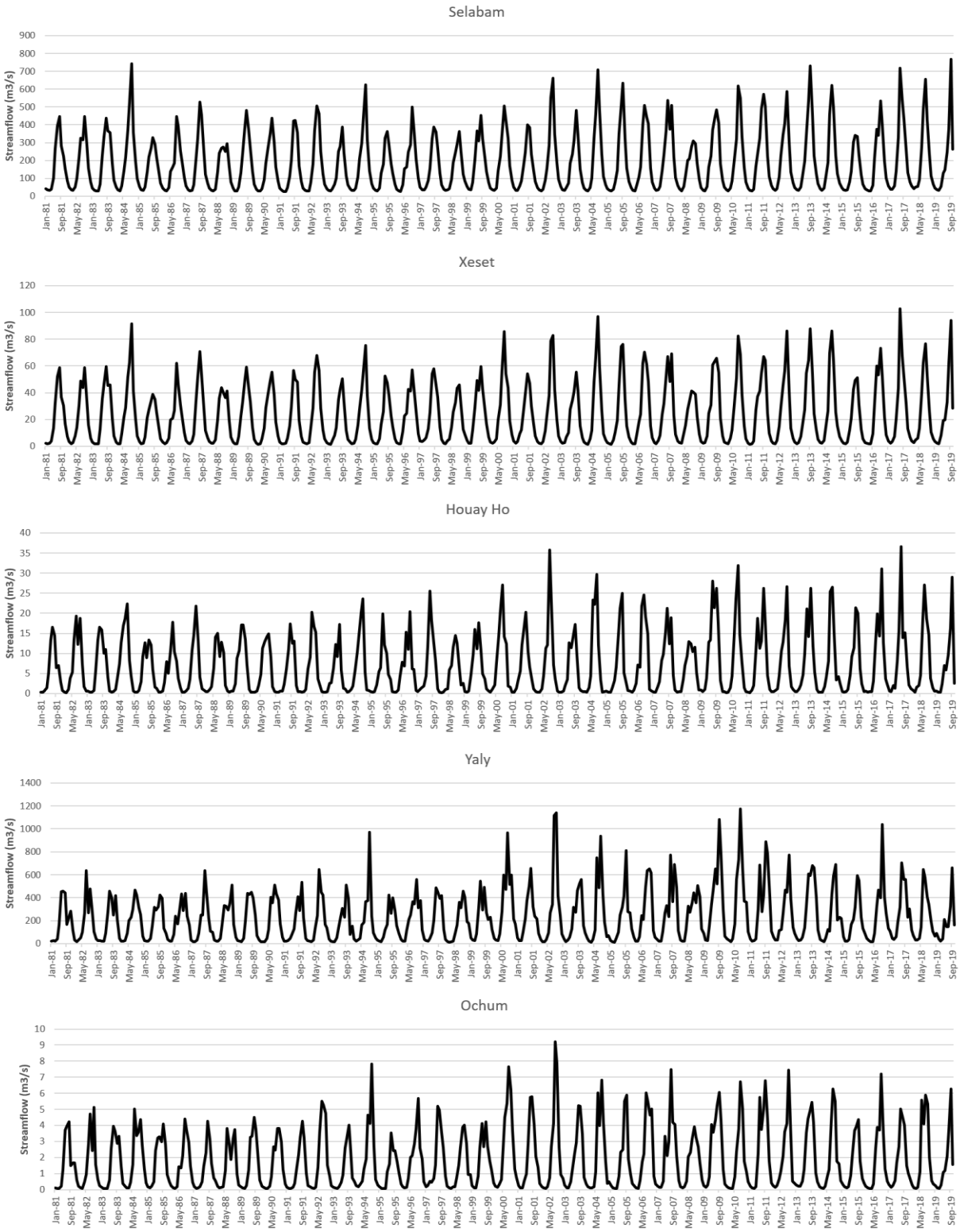


*Figure 9(c): Variable Infiltration Capacity (VIC) model simulated inflow at dam locations*

### 2.3.3 Climate change during the future period

Compared with the historic period of 1950-2005 with mean daily precipitation average of 4.16 mm/day, a modest increase in precipitation was expected in the future between 2006 and 2099 and these increases were 4.26 mm/day for RCP 4.5 and 4.25 mm/day for RCP 8.5. NorESM1-M showed the highest increase in precipitation under RCP 4.5 and RCP 8.5 in the basin, whereas GFDL-ESM2M projected a decline in precipitation. Increase in monthly precipitation for all the months except February to May under RCP 4.5 and RCP 8.5 (Figure 10). Mean Annual precipitation for the historic period is 1520 mm, while for the future period is 1551 mm and 1548 mm under RCP 4.5 and RCP 8.5, respectively. The mean annual temperature for the historic period was 22.2 °C, while for the future period it was estimated to be about 23.9 °C and 24.7 °C under RCP 4.5 and RCP 8.5, respectively. The average increase in monthly temperature of 1.8 °C and 2.6 °C were projected between now and the end of the century for RCP 4.5 and RCP 8.5, respectively. The highest increase is predicted for April month (Figure 10). Figure S1 shows the spatial variation of the precipitation and temperature in the Mekong River basin.

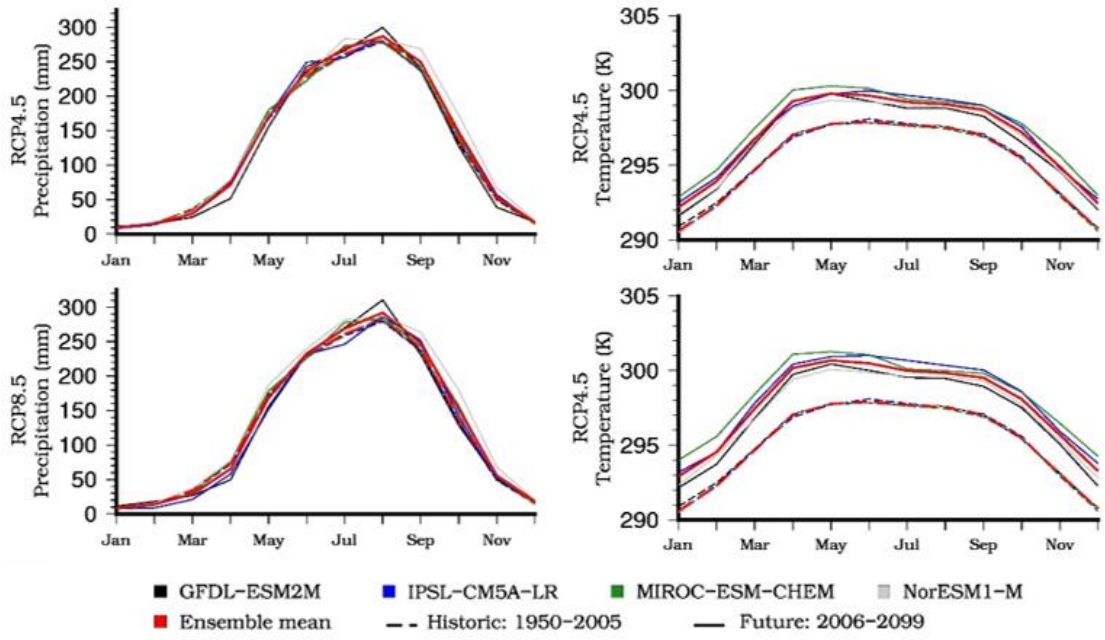


*Figure 10: Seasonal variation of precipitation and temperature projected by the GCMs*

### 2.3.4 Streamflow variation during the future period

The streamflow change at the gage station locations and inflow to the dams for the future period was projected using the four GCMs under RCP 4.5 and RCP 8.5 scenarios. Table 5 shows the statistics of the impact of climate change on the streamflow at seven gage station locations using the ensembled mean of the GCMs. The annual streamflow increases between 3.7% and 5.2% under RCP 4.5, while the RCP 8.5 projects the reduction from 7.9% to 34.4% caused by the projected increase in precipitation under RCP 4.5 and decrease under RCP 8.5. The highest variability in the streamflow is projected for Vientiane (from +5% to -34.4%), on the other hand, the uppermost gage stations, i.e., Chiang Saen (from +3.7% to -9.1%) and Luang Prabang (from +4% to -7.9%) will experience the low variability inflows. For the downstream most gage stations, the streamflow is forecasted to varying between +5±0.2% and -26.9±2%. The higher variation in the streamflow towards the downstream locations is due to the large catchment area with heterogeneous precipitation. RCP 4.5 projects the highest flood at all the gage locations in 2090, while 2097 is forecasted as the highest flow year under RCP 8.5. On the other hand, 2045 (RCP 4.5) and 2028 (RCP 8.5) will experience the driest flow conditions. On an average, RCP 4.5 project the flood as 1.5 times higher than the mean historic flow, while flood under RCP 8.5 is confined to the maximum increase in historic flow to 15%. The drought conditions are higher under RCP 8.5 with the average flow approximately 50% of the mean historic flow, however, the RCP 4.5 projects the flows to reduce up to 80% of the mean historic flow during dry years.

*Table 5: Statistics of the impact of climate change on the streamflow at gage locations*

| S. No. | Gage Station | Flow | Change | | RCP 4.5 | | | | RCP 8.5 | | | |
|---|---|---|---|---|---|---|---|---|---|---|---|---|
| | | Hist | RCP 4.5 | RCP 8.5 | Flood | Year | Drought | Year | Flood | Year | Drought | Year |
| 1 | Chiang Saen | 2901 | 3.7 | -9.1 | 4067 | 2090 | 2362 | 2009 | 3316 | 2079 | 2137 | 2028 |
| 2 | Luang Prabang | 3734 | 4.0 | -7.9 | 5447 | 2090 | 3095 | 2009 | 4324 | 2097 | 2763 | 2028 |
| 3 | Nakhon Phanom | 9572 | 5.0 | -28.6 | 13834 | 2090 | 8289 | 2096 | 9526 | 2097 | 4895 | 2006 |
| 4 | Vientiane | 6183 | 5.0 | -34.4 | 9236 | 2090 | 5387 | 2018 | 5696 | 2097 | 2866 | 2006 |
| 5 | Mukdahan | 9847 | 5.0 | -28.3 | 14227 | 2090 | 8518 | 2096 | 9829 | 2097 | 5084 | 2006 |

| | | | | | | | | | | | | |
|---|---|---|---|---|---|---|---|---|---|---|---|---|
| 6 | Pakse | 12073 | 5.2 | -27.7 | 18101 | 2090 | 9675 | 2045 | 12125 | 2097 | 6204 | 2017 |
| 7 | Kratie | 15369 | 4.9 | -24.9 | 22868 | 2090 | 11705 | 2045 | 15042 | 2046 | 8427 | 2017 |

Table 6 shows the statistics of the inflow variation to the 31 dams due to climate change under RCP 4.5 and RCP 8.5. The historic inflows to the dams varied from 1942.1 $m^3$/sec (Jinghong, China) to 1.5 $m^3$/sec (Lam Plai Mas, Thailand). The change in the inflow to the dams shows an increase under RCP 4.5 and a decrease under RCP 8.5. The percentage change in the inflow ranges from +25% to +1.2% under RCP 4.5, while the change under RCP 8.5 is projected as -28.5% to -74.7%. However, the dams located in Thailand will experience a higher increase in the inflow under RCP 4.5 (12.9%), at the same time, Thailand dams will suffer the lowest decrease (55.6%) under extreme temperature conditions (RCP 8.5). Similar flow variations will be experienced by China dams with the average reduction in inflow as 52.4% under RCP 8.5, but the increase in the inflow will be averaged as 6% as compared to the historic inflows. Dams in Laos PDR, Cambodia, and Vietnam are projected to experience similar flow conditions under climate change with an average increase in inflows as 3.7% under RCP 4.5 and decrease as 31.7% under RCP 8.5. The fluctuation in the inflow is not constrained by the storage capacity or the purpose of the dams. The potential for flood in most of the dams in Thailand and China is high during the end of the 21st century (2075 – 2090), while Laos PDR dams flood years are projected around 2090-2093 under RCP 4.5. On the other hand, Cambodia and Vietnam dams will experience flood situations during the 2030s. Most of the dams in the MRB is projected to experience drought conditions during the mid-21st century (2030-2060) under RCP 4.5 and RCP 8.5.

*Table 6: Statistics of the impact of climate change on the inflow to the dams*

| S. No. | Name of dam | Flow | Change | | RCP 4.5 | | | | RCP 8.5 | | | |
|---|---|---|---|---|---|---|---|---|---|---|---|---|
| | | Hist | RCP 4.5 | RCP 8.5 | Flood | Year | Drought | Year | Flood | Year | Drought | Year |
| 1 | Sirindhorn | 75 | 4 | -37 | 108 | 2080 | 48 | 2045 | 68 | 2023 | 30 | 2042 |
| 2 | Ubol Ratana | 126 | 15 | -60 | 281 | 2090 | 54 | 2045 | 119 | 2080 | 2 | 2078 |
| 3 | Lam Pao | 97 | 8 | -53 | 166 | 2043 | 45 | 2045 | 94 | 2080 | 14 | 2078 |
| 4 | Nam Pung | | | | | | | | | | | |
| 5 | Lam Takhong | 23 | 14 | -69 | 63 | 2090 | 9 | 2045 | 18 | 2072 | -18 | 2027 |

| | | | | | | | | | | | | |
|---|---|---|---|---|---|---|---|---|---|---|---|---|
| 6 | Lam Phra Phloeng | 15 | 13 | -71 | 38 | 2090 | 5 | 2045 | 11 | 2072 | -9 | 2027 |
| 7 | Chulabhorn | 7 | 14 | -47 | 13 | 2090 | 4 | 2011 | 6 | 2080 | 1 | 2027 |
| 8 | Lam Chang Han | 2 | 22 | -71 | 5 | 2090 | 1 | 2045 | 1 | 2072 | -1 | 2027 |
| 9 | Huai Kum | 8 | 16 | -52 | 19 | 2090 | 4 | 2011 | 8 | 2066 | 1 | 2027 |
| 10 | Pakmun | 1509 | 11 | -53 | 2917 | 2090 | 677 | 2045 | 1401 | 2068 | 162 | 2027 |
| 11 | Nam Un | 32 | 5 | -32 | 48 | 2043 | 23 | 2045 | 33 | 2079 | 14 | 2078 |
| 12 | Upper Mun | 7 | 20 | -73 | 20 | 2090 | 3 | 2045 | 5 | 2079 | -5 | 2027 |
| 13 | Lam Nang Rong | 4 | 25 | -66 | 11 | 2090 | 2 | 2019 | 3 | 2079 | -2 | 2027 |
| 14 | Huai Luang | 19 | 8 | -30 | 27 | 2090 | 14 | 2045 | 19 | 2079 | 7 | 2078 |
| 15 | Lam Plai Mas | 1 | 6 | -74 | 3 | 2090 | 1 | 2017 | 1 | 2067 | -1 | 2027 |
| 16 | Lam Sae | 10 | 12 | -46 | 20 | 2090 | 6 | 2045 | 9 | 2079 | 0 | 2027 |
| 17 | Nam Ngum | 591 | 5 | -30 | 868 | 2090 | 489 | 2045 | 639 | 2046 | 263 | 2017 |
| 18 | Xeset 1 | 26 | 1 | -33 | 37 | 2090 | 18 | 2045 | 25 | 2009 | 12 | 2042 |
| 19 | Selabam | 268 | 2 | -32 | 399 | 2090 | 192 | 2045 | 257 | 2009 | 123 | 2042 |
| 20 | Theun-Hinboun | 405 | 6 | -32 | 586 | 2093 | 316 | 2011 | 408 | 2081 | 159 | 2098 |
| 21 | Houay-Ho | 8 | 2 | -33 | 12 | 2090 | 6 | 2024 | 8 | 2009 | 4 | 2027 |
| 22 | Nam Leuk | 255 | 6 | -32 | 365 | 2093 | 199 | 2011 | 255 | 2046 | 103 | 2098 |
| 23 | Nam Mang 3 | 2 | 6 | -29 | 2 | 2090 | 1 | 2021 | 2 | 2046 | 1 | 2017 |
| 24 | Xiaowan | 1213 | 8 | -72 | 1685 | 2075 | 1040 | 2062 | 422 | 2098 | 257 | 2031 |
| 25 | Manwan | 1235 | 7 | -70 | 1705 | 2075 | 1058 | 2062 | 453 | 2079 | 276 | 2031 |
| 26 | Dachaoshan | 1316 | 7 | -66 | 1775 | 2075 | 1125 | 2062 | 570 | 2079 | 346 | 2031 |
| 27 | Jinghong | 1942 | 5 | -47 | 2509 | 2097 | 1626 | 2010 | 1328 | 2079 | 782 | 2016 |
| 28 | Cibihe (Zibihe) | 19 | 4 | -29 | 28 | 2066 | 14 | 2010 | 17 | 2093 | 10 | 2080 |
| 29 | Haixihai | 5 | 4 | -30 | 7 | 2066 | 3 | 2010 | 4 | 2093 | 3 | 2080 |
| 30 | Ochum | 3 | 2 | -31 | 4 | 2031 | 2 | 2024 | 2 | 2023 | 1 | 2027 |
| 31 | Yaly | 280 | 5 | -32 | 426 | 2031 | 222 | 2018 | 263 | 2072 | 118 | 2069 |

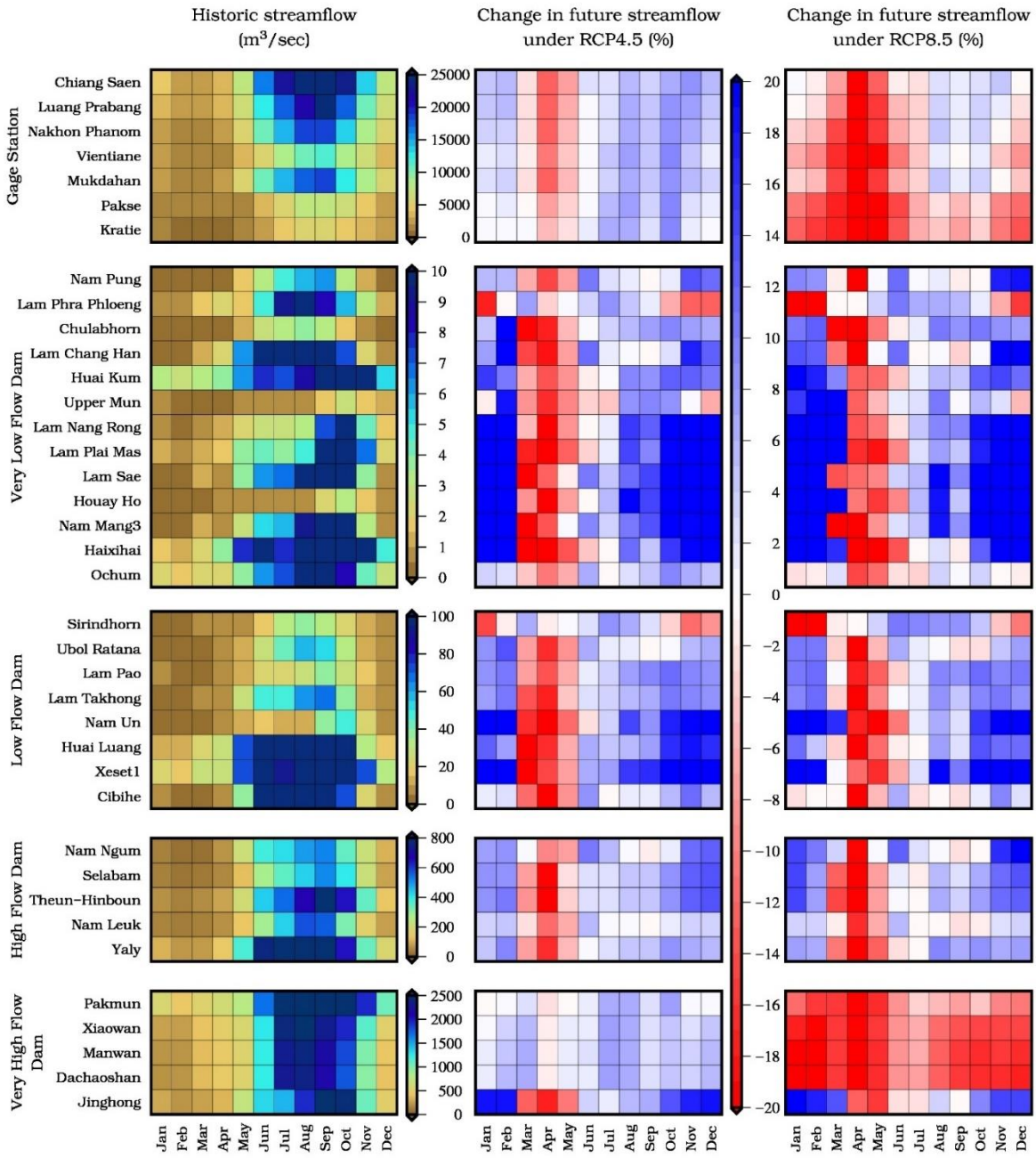


*Figure 11: Classification and change in the streamflow at gage station locations and inflow to the dams for the historic (1951-2005) and future period (2006-2099) under RCP 4.5 and RCP 8.5 using the four climate models.*

The climate change influences the streamflow of the Mekong mainstem and tributaries flowing into the dams. Figure 11 shows the change in the streamflow at the gage station locations and the inflow to the dams for the historic period (1951-2005) with the change in the future period (2006-2099) under RCP 4.5 and RCP 8.5 using the four climate models. The classification of the dams into four classes was done based on the inflow magnitude

during the historic period. The dams under the very low flow class had the peak historic inflow of 10 $m^3$/sec, while, the peak inflow for the low flow, high flow, and very high flow classes are 100 $m^3$/sec, 800 $m^3$/sec, and 2500 $m^3$/sec, respectively. 13 dams were classified as low flow dams, 8 dams fell under the low flow class, 5 dams had the high flow, and 5 dams on the mainstem of the Mekong river were sorted under the very high flow category. As observed during the observed period, the inflow to the dams and streamflow at gage station locations were dominantly driven by the monsoon with peak flow during July-October. Although the magnitude of the inflow varied vastly between the dams, the change in the flow during the future period is projected to be similar for the dams and gage stations.

Generally, the summer period (March-May) is expected to experience a considerable decrease in the flows. The streamflow at the gage station locations will decrease by 5.8% and 17.8% in the future under RCP 4.5, and RCP 8.5, respectively, as compared to the historic period. Also, the decrease in the inflow to the very low flow class dams will be 13.5% under RCP 4.5 and 6.1% under RCP 8.5. Similarly, the decrease for the low flow, high flow, and very high flow dams will be 11.4% (9%), 8.8% (12.3%), and 1.5% (14.8%) in the future under RCP 4.5 (RCP 8.5) with respect to the long-term historic flows. On the other hand, the gage station locations are expected to face an increase in the projected streamflow during the monsoon season accounting for 5.8% under RCP 4.5 and a marginal decrease of 0.8% under RCP 8.5. While the dams will experience an increase in the inflow after the monsoon season (October-February). The increase in the inflow for the very low flow dams will be 19% and 28.9% during October-February in the future under RCP 4.5 and RCP 8.5, respectively. Furthermore, the increase in the future inflow to the low flow and high flow dams will be 11.2% and 7.8% under RCP 4.5, and 12.9% and 8.6% under RCP 8.5 as compared to the historic inflows. However, the future inflow to the very high low dams are expected to have contrasting characteristics under RCP 4.5 and RCP 8.5 with a change of +6.1% and -9.6%, respectively. In conclusion, the impacts of climate change include a seasonal effect on the inflow to the dams with the surplus inflow volume after the monsoon season and dry flows during the summer period. The reservoir operation can be optimized to take advantage of the extra flows to meet the water demand of the various sector and avoid water shortage during the summer period.

### 2.3.5 Surface area and storage variation of reservoirs

The fluctuation of the surface area of the Lam Pao, Sirindhorn, and Ubol Ratana reservoirs followed the monsoon season, resulting in the shrinkage of the reservoir before the onset of the monsoon (May) and swelling at the end of the season (November). The time series of the variation of the surface area of the Lam Pao reservoir using the 15-day interval satellite imageries and some missing data due to high cloud impacted images is shown in Figure 12a. The surface area of the Lam Pao reservoir, estimated by the satellite imageries from 2013 to early 2018, exhibited a range between 80 $km^2$ and 236 $km^2$. The water depth of the reservoir extracted from the GRLM and Hydroweb databases, from 2008 to 2018, showed a similar variation as the surface area and correlated well (Figure 12b). The Lam Pao reservoir experienced a gradual increase in the surface area from 2015 to 2017 due to the increase in the annual precipitation in the catchment area.

The surface of the Sirindhorn reservoir varies from 206 $km^2$ to 285 $km^2$ from 2013 to 2017 (Figure 12c). The lesser range of the surface area of the Sirindhorn (79 $km^2$), as compared to Lam Pao (154 $km^2$), was due to a smaller catchment area of the Sirindhorn dam with respect to Lam Pao catchment area, and the minimum surface area remained consistent possibly due to the management of the reservoir. The seasonal variation of the surface area of Sirindhorn reservoir and gradual increase from 2015 to 2017 is similar to the Lam Pao reservoir. The time series of the surface area variation of the Ubol Ratana reservoir was constructed using the 70 satellite imageries and it showed the highest surface area of 370 $km^2$ in November 2017 and lowest as 120 $km^2$ in May 2016 The large variation of the surface area of the reservoirs is caused by the high water volume collected by the large catchment area of the Ubol Ratana dam. The variation between the maximum and minimum surface area of the reservoirs accounts for 64%, 27%, and 58% of the maximum reservoir area of the Lam Pao, Sirindhorn and Ubol Ratana, respectively. The maximum surface area of the reservoirs simulated by the satellite imageries was 239.6 $km^2$, 283.6 $km^2$, and 369.2 $km^2$ for Lam Pao, Sirindhorn, and Ubol Ratana, respectively, with a bias of 0.4 $km^2$, 4.4 $km^2$, and 40.8 $km^2$. The water depth anomaly of the Ubol Ratana reservoir was not analyzed in the study due to the non-availability of the data in the GRLM and Hydroweb databases Non-availability of the data for Ubol Ratana in the GRLM and

Hydroweb databases restricts the reservoir depth analysis and estimation of the total storage. However, the observed total storage of the Ubol Ratana from 2008 to 2018 is used for further analysis. The water depth variation of the reservoirs inferred from the altimetry dataset is more consistent as compared to the surface area, providing the information at high frequency (Figure 12).

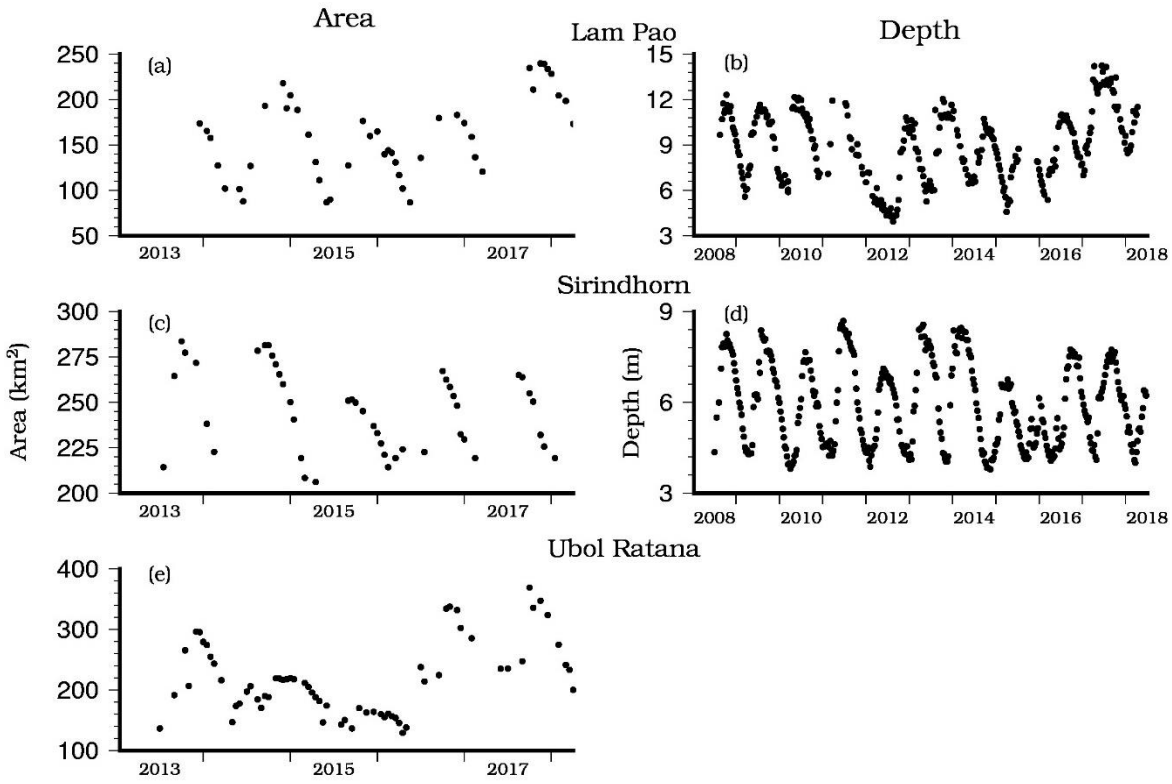


*Figure 12: Time series of the surface area and water level variation of Lam Pao (a, b), Sirindhorn (c, d), and Ubol Ratana (e) reservoirs. The water level of the reservoirs is with respect to the satellite reference datum derived from the altimetry data from different satellites. The archived dataset from Global Reservoir and Lake Monitor (GRLM), and Hydroweb databases, along with the individual satellite data from 2008 to 2018 with the temporal resolution of 10 days were used for the analysis. The surface area was extracted from LandSat 8 and Sentinel-2 satellite imageries from 2013 to 2018 at 15-day frequency*

The relationship between the surface area and water depth of the reservoirs was used for the estimation of the live storage and total storage of the reservoirs. Since the date of capture of satellite imageries differed from the altimetry data collection, more than 45 pairs of coincident surface area and water level for Lam Pao and Sirindhorn were selected for regression analysis (Figure 13). The data point of the surface area and water level matched well, similar to the variation in the reservoir conditions. The coefficient of determination

($r^2$) was used to evaluate the goodness of fit with the regression line. The relationships between the area and depth expressed as quadratic equations are shown in Figure 13, with an $r^2$ value greater than 0.90 for both Lam Pao and Sirindhorn. The depth-area equations were used to derive the volume-depth relationships and those equations are given below (equations 8 and 9). The live storages for these reservoirs were estimated from the water levels available from GRLM and Hydroweb datasets and using the cubic equations of volume-depth relationships and they are provided below (equations 10 and 11)

$$A_{Lam\ Pao} = -0.2342468 \times h^2 + 19.90271519 \times h + 83.40634555\ km^2 \quad (8)$$

$$A_{Sirindhorn} = 0.5980226 \times h^2 + 14.19245909 \times h + 206.988042\ km^2 \quad (9)$$

$$S_{live,Lam\ Pao} = -0.078082 \times h^3 + 9.951357 \times h^2 + 83.406345 \times h\ million\ m^3 \quad (10)$$

$$S_{live,Sirindhorn} = 0.199340 \times h^3 + 7.096225 \times h^2 + 206.988042 \times h\ million\ m^3 \quad (11)$$

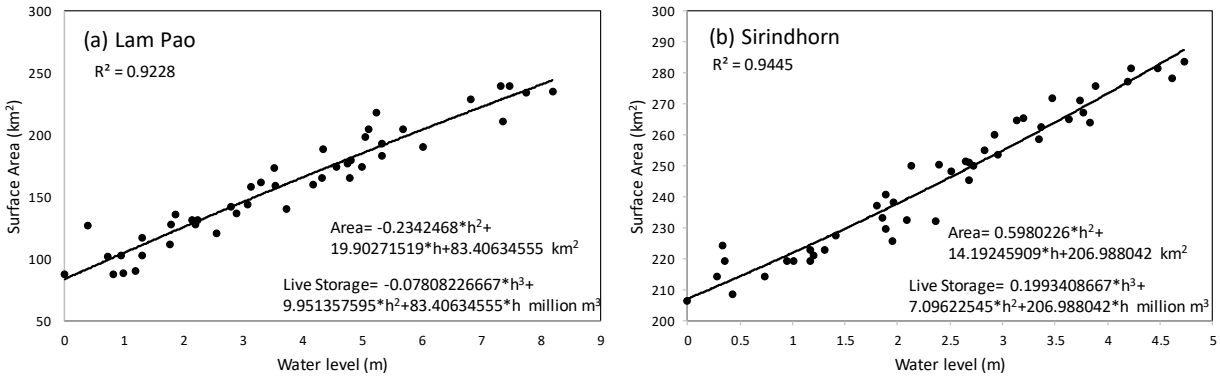


*Figure 13: The regression analysis curve developed by fitting the surface area and water level values selected on the basis of availability of both the data at a particular time. The quality of fit was indicated by the correlation index, $R^2$. The relationship between the surface area and water level, and live storage and water level were estimated for the (a) Lam Pao, and (b) Sirindhorn reservoirs using the curve fitted between the surface area and water level.*

The water level anomaly from the altimetry dataset was used for the estimation of the total storage of the reservoirs (total storage = live storage + dead storage) at 10-days interval from 2008 to 2018. The time series of the simulated total storage variation of the Lam Pao and Sirindhorn reservoirs were validated by comparing it with the observed storage from the reservoir database (Figure 14). The Nash-Sutcliffe efficiency coefficient (NSE) and the correlation coefficient (r) between the observed and simulated total storages were used to measure the efficiencies of the approach in estimating the reservoir storages. The total storage of the Lam Pao reservoir varied from 245 million $m^3$ to 1790 million $m^3$, accounting

for the dead storage as 245 million $m^3$ (Figure 14a). The simulated total storage of the reservoir agreed well with the observed storage with NSE and r values greater than 0.9. The ensemble mean was used to estimate the monthly variation of the total storage variation of the Lam Pao reservoir (Figure 14b). The lowest volume in the reservoir is observed during May (450 million $m^3$) to host inflow water during the monsoon period and highest volume during October (1170 million $m^3$) after accumulating monsoon flow, which can be released till the onset of next monsoon.

For the Sirindhorn reservoir, the NSE and r values between the observed and simulated total storages were estimated as 0.98 and 0.99, respectively (Figure 14c). Estimates of the monthly variation in the total storage of the Sirindhorn reservoir suggested higher predictability of volume-depth aided by area-depth relationships and a lesser fluctuation in the surface area. Since the water depth information was not derived for the Ubol Ratana reservoir, the total storage was not available from the area-depth relationship hence, the observed total storage of the Ubol Ratana reservoir from 2008 to 2018 was used for the subsequent analysis. The fluctuation in the total storage of the reservoir ranged between 500 million $m^3$ and 2800 million $m^3$, however, the average total storage was 990 million $m^3$ from 2013 to 2015 (Figure 14e). The annual maximum total storage of the reservoirs was in close agreement with the annual precipitation over the catchment and the range of the storage variation was dependent on the size of the catchment area. Simulation of the total storage of the reservoir was substantially better with higher coefficients of determination ($R^2 > 0.9$) values between observed and simulated storage for Lam Pao and Sirindhorn reservoirs (Figure 14g and 14h).

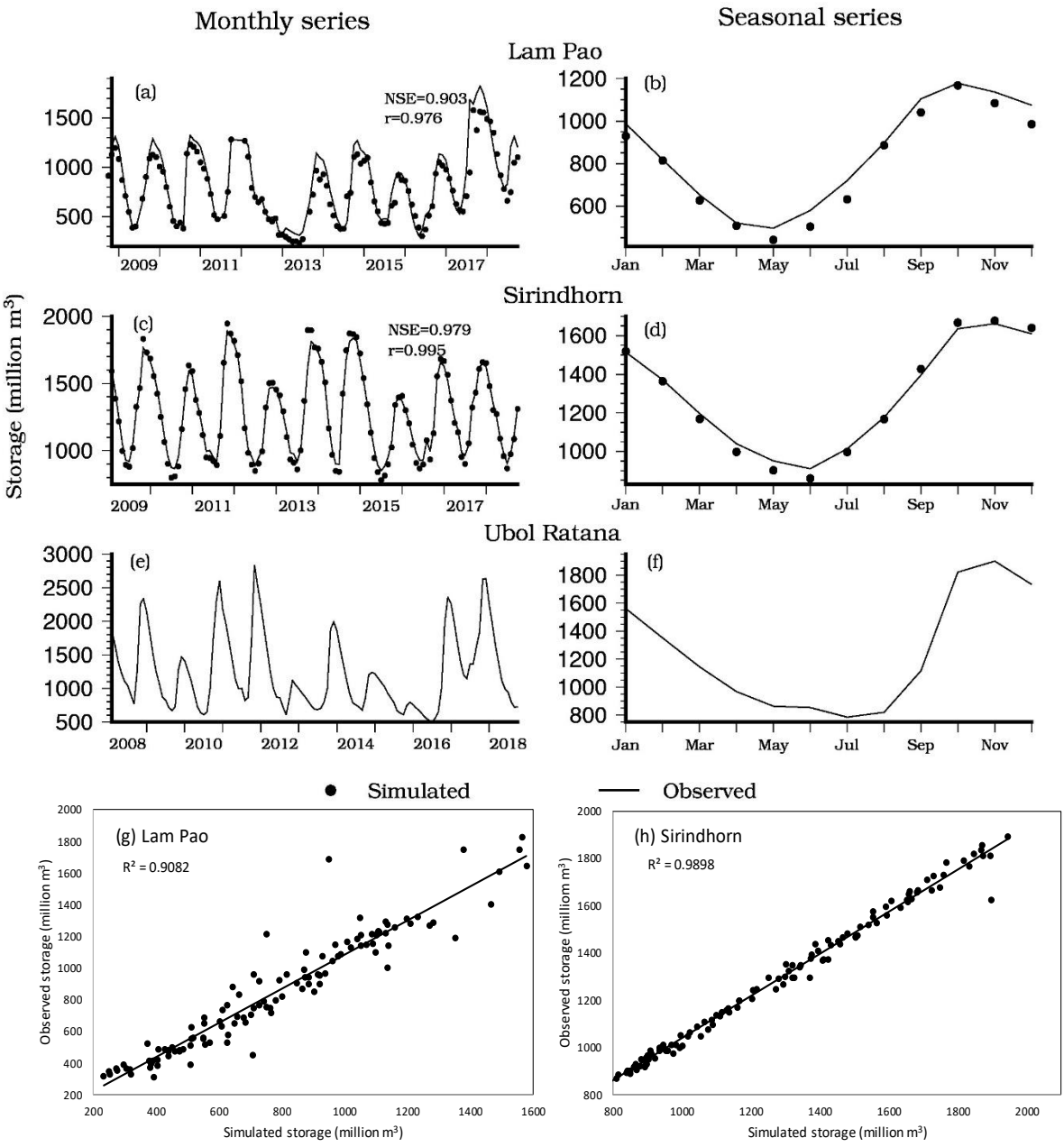


*Figure 14: Comparison of the simulated and observed total storage of Lam Pao (a,b), Sirindhorn (c,d), and Ubol Ratana (e,f) reservoirs. The time series of the total storage of the reservoirs simulated (dotted line) using the expression derived from the regression analysis was compared with the observed (continuous line) total storage for the reservoirs (a, c, and e) for the period 2008 to 2018. The series was ensemble to generate the annual curve representing the seasonal variation of the total storage (b, d, and f). The scatter plot between the observed and simulated total storage for Lam Pao (g) and Sirindhorn (h) reservoirs show good correlation with $R^2$ values greater than 0.9.*

### 2.3.6 Rule Curve

Operating rule curves generally serve as a guiding principle for regulating the flow and maintain dam operations. Figure 15 a, b, and c show the rule curve for Lam Pao, Sirindhorn, and Ubol Ratana reservoirs, respectively, derived from the monthly total storage based on eight years between 2008 and 2016. The simulated rule curve closely resembled the current rule curves for the reservoirs as shown in Figure 15. Since the cumulative impact of the inflow and outflow from the reservoirs was quantified implicitly from total storage changes, the rule curve was useful to estimate the discharge from the reservoirs based on the inflow to the reservoirs. The average storage of the Lam Pao varied from 410 million $m^3$ to 1025 million $m^3$ with a mean value of 720 million $m^3$ (Figure 15a). For Sirindhorn, the minimum and maximum value of the reservoir storage were estimated as 850 million $m^3$ and 1630 million $m^3$, respectively and the mean value was observed as 1250 million $m^3$. Highest A wide range in the total storage of the reservoir was noticeable for Ubol Ratana from 720 million $m^3$ to 1750 million $m^3$, constituting the mean storage of 1150 million $m^3$.

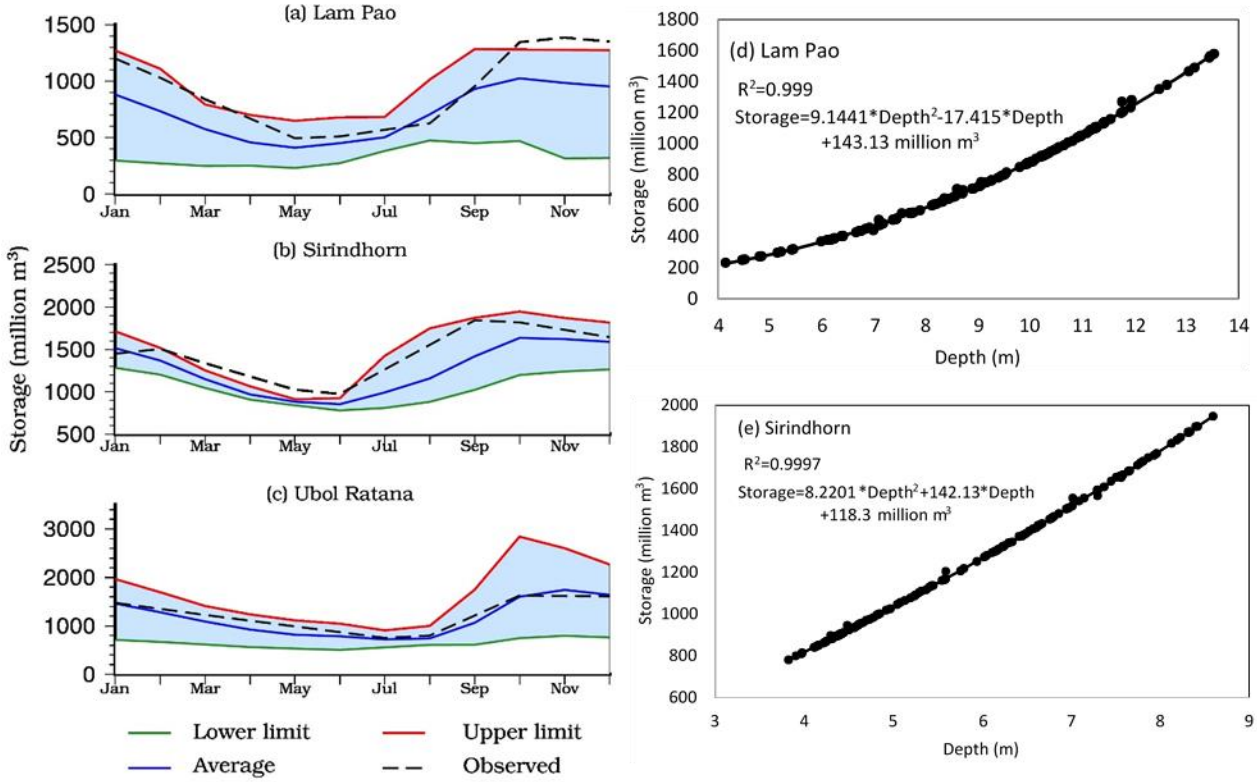

*Figure 15: The mean monthly variation of the total storage for each month during the year along with upper and lower limits, defined as the rule curve, for (a) Lam Pao, (b) Sirindhorn, and (c) Ubol Ratana derived from the surface area and water level variation of the reservoirs during the period 2008 to 2018. The relationships between the total storage and water level at the reservoirs were developed for (d) Lam Pao and (e) Sirindhorn.*

Estimates of storage showing seasonal differences were similar for all the reservoirs with the increasing magnitude from May to October resulting from the lower outflow as compared to the inflow. On the contrary, there was decreasing storage from November to April as discharges were regulated with higher outflows. Furthermore, the change in the variation of the storage of the reservoirs is negative for May-October and positive for November-April with respect to the mean annual storage. The total storage declined up to 43%, 32%, and 38% below the mean annual storage for Lam Pao, Sirindhorn, and Ubol Ratana, respectively, however, the average declines during May-October were estimated as 28%, 21%, and 28%. On the other hand, the highest increases in the storage were computed as 43%, 30%, and 51% above the mean storage for Lam Pao, Sirindhorn and Ubol Ratana, respectively. Since the dry period and wet period experienced both the positive and negative fluctuation in the total storage with respect to mean storage, the cumulative increase in Lam Pao, Sirindhorn, and Ubol Ratana during dry-wet periods were calculated as 6.8%, 1.3%, and 4%, respectively. The range of the spread between the upper limit and lower limit of the rule curve varied from 300 million $m^3$ to 970 million $m^3$ for Lam Pao, whereas the range for the spread was 71-860 million $m^3$ and 350-2100 million $m^3$ for Sirindhorn and Ubol Ratana, respectively. The monthly range of the rule curve of the reservoirs was primarily governed by the magnitude of the inflow. Since the monsoon season (June-November) generated a large volume of inflow to the reservoir, the spread between the lower limit and upper limit of the rule curve was large enough to accommodate the uncertainty associated with the fluctuation in the catchment response during the extreme events. Since the inflow during the dry period is low in magnitude and fluctuation, the uncertainty in the rule curve is less. The low reservoir storage during the dry period helps to accommodate the high inflows during the monsoon period. Figure 15d and Figure 15e show the relationship between the storage and water level of the Lam Pao and Sirindhorn reservoirs. The rule curve of the Lam Pao and Sirindhorn can be transformed

into the water level variation using the quadratic equations 12 and 13, respectively with an $R^2$ value greater than 0.99.

$$Storage = 9.1441 \times Depth^2 - 17.415 \times Depth + 143.13\ million\ m^3 \quad (12)$$

$$Storage = 8.2201 \times Depth^2 - 142.13 \times Depth + 118.30\ million\ m^3 \quad (8)$$

where, Storage is the total storage of the reservoir in million $m^3$ defining the rule curve, and Depth is the water level of the reservoir in meters.

### 2.3.7 Water extraction from reservoir and ET resemblance

The comparison of the seasonal variation of the inflow and outflow from the reservoirs showed high outflows during the dry season relative to inflows (Figure 18). However, the difference between the inflow and outflow from the reservoir was more during the wet season, which indicated more impoundment occurred during the wet season. Even the outflow was less than the inflow for the reservoirs during the dry period, i.e. 2016 in Lam Pao, 2015-2016 in Sirindhorn and 2014-2016 in Ubol Ratana (Figure 19). As a result, the total storage capacity of the reservoir increased, especially during the period of inflow exceeding outflow in the dry season. Despite these dynamic inter-seasonal and inter-annual changes, the storage variation of the reservoirs showed no response to any particular situation, even when the storage volume in the Ubol Ratana reservoir declined during 2013-2016. Figure 16 shows the annual and monthly variation of the excess water which remained unaccounted in the flow estimation from the Lam Pao, Sirindhorn, and Ubol Ratana dams between 2008 and 2016. Storage depletion can be attributed to diversion for irrigation, domestic, and industrial sectors, and quantifying them from the reservoir also pose a potential source for the unaccountability.

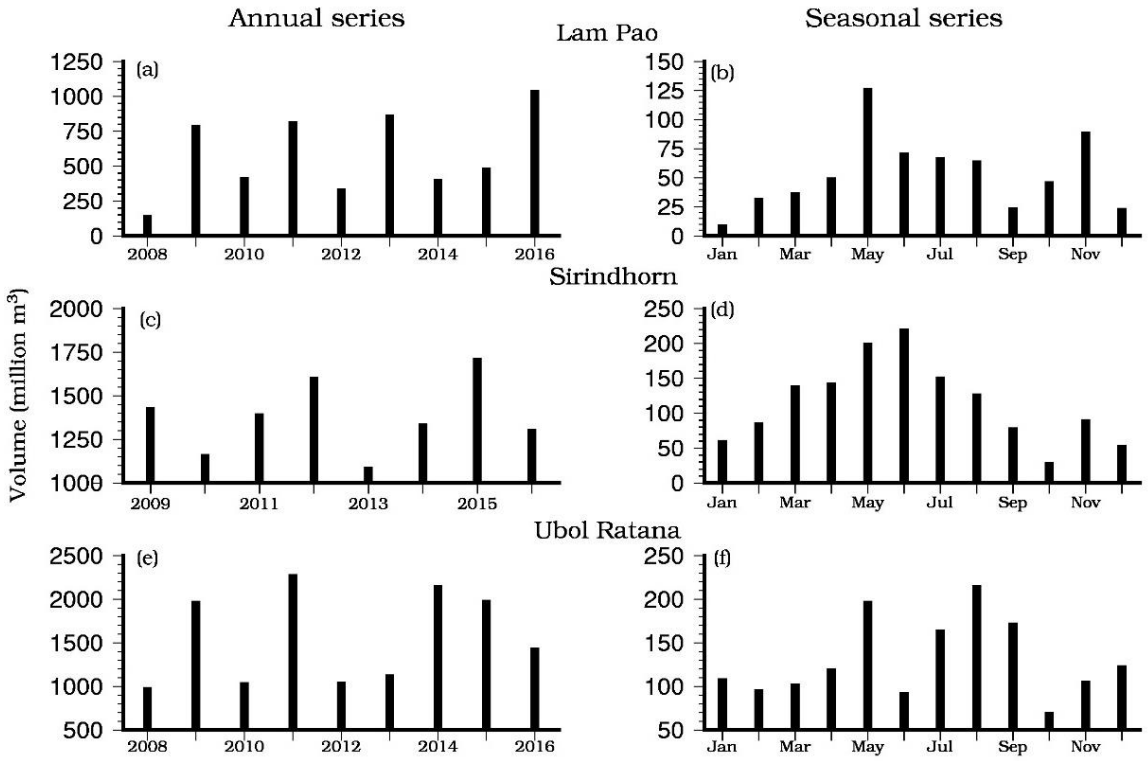


*Figure 16: The volume of water extracted from the reservoir, which was not accounted in the outflow, annually during 2008-2016 from (a) Lam Pao (c) Sirindhorn (e) Ubol Ratana. The seasonal series of the extracted volume (b, d, f) from the ensemble means for each month resemble the evapotranspiration variation over the year.*

The annual variation in storage from the reservoirs to meet various above-mentioned demands demonstrated some randomness with the extent of fluctuation that ranges from 150 to 1050 million $m^3$ for Lam Pao, 1100 to 1700 million $m^3$ for Sirindhorn, and 990 to 2300 million $m^3$ for Ubol Ratana reservoirs, respectively. The mean annual diversions from Lam Pao (600 million $m^3$), Sirindhorn 1380 million $m^3$), and Ubol Ratana (1560 million $m^3$) were proportional to the total storage capacity of the reservoirs. The variation in monthly diversions was similar in all three reservoirs. The magnitude of diversions increased gradually from January to May, i.e. ahead of the monsoon period, and then decreased during the monsoon season (June-October) followed with the moderate withdrawal during November and December (Figure 16). The highest diversion of 128 million $m^3$, 220 million $m^3$, and 215 million $m^3$ occurred during May-June for Lam Pao, Sirindhorn, and Ubol Ratana, respectively, while the lowest withdrawal ranged from 10 million $m^3$ to 70 million $m^3$ during September-October.

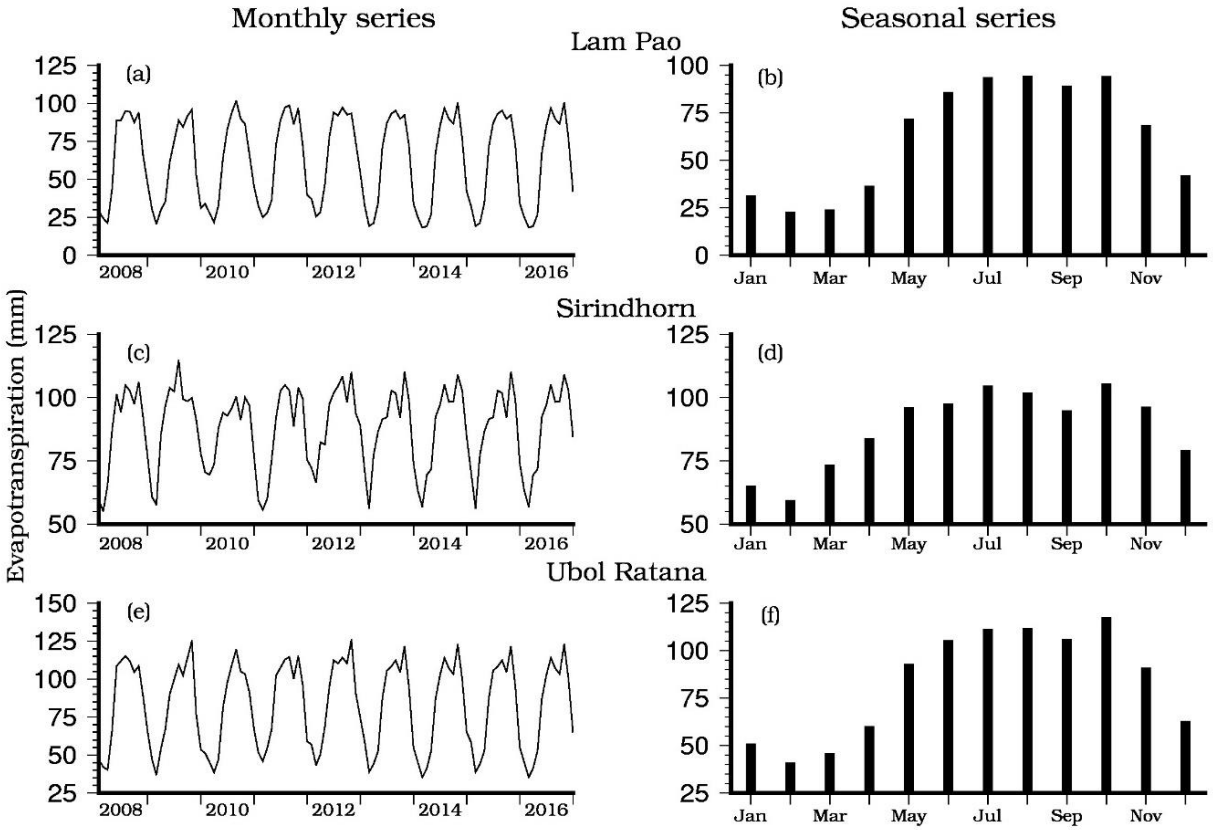


*Figure 17: The monthly variation in the estimated evapotranspiration for (a &b) Lam Pao, (c & d) Sirindhorn, and (e & f) Ubol Ratana from 2008 to 2016 using the MODIS (MODerate resolution Imaging Spectroradiometer) Evapotranspiration product MOD16A2, which is an 8-day composite product produced at 500-meter pixel resolution.*

As crop water requirements can be mapped implicitly through ET estimation, monthly ET was calculated from 2008 to 2016 using the remotely sensed-MODIS ET. The monthly series of ET showed no significant variation from year to year but the monthly variation was captured by the estimation of the ensemble mean for each month from 2008 to 2016 (Figure 17). Monthly ET estimates were the lowest during January- March, which increased gradually between May and October, afterward the ET decreased during the last two months of the year. The variation of the ET was in good agreement with the crop calendar for the Thailand region. The sowing and growing period of the main rice crop occurred from May to September followed by harvesting. Therefore, the ET was the highest from May to October with an estimation of 88 mm/month, 100 mm/month, and 107 mm/month for Lam Pao, Sirindhorn, and Ubol Ratana, respectively. Also, the second crop of rice or maize or sorghum was grown over the year. The assessment of the monthly water in irrigation diversion (Figure 16b, d, f) and ET (Figure 17b, d, f) showed similar patterns

during January-April and November-December. But the water extraction is suppressed as compared to ET from May to October. Although the availability of water during the monsoon season was not limited, the demand was still high but diminished slightly which resulted in gradual reductions in irrigation demand.

### 2.3.8 Effect of dams on outflows

Simulated inflows were used in combination with the total storage change to estimate the monthly outflow as shown in equation 5. The period of estimation of the outflow from the dams remained as that of the inflow except for Lam Pao as the total storage variation of Lam Pao reservoir starts from 2009. Simulated outflows were validated with observed flows by computing NSE and r values. The NSE values improved at the two locations Sirindhorn and Ubol Ratana dams, with values up to 0.65 and 0.67, respectively. However, the NSE value for the Lam Pao dam remained the same as the inflow but the improvement was evidenced in the correlation coefficient (r=0.92) because of marginally low NSE value between observed and simulated total storage of Lam Pao as compared to other reservoirs. The inflow to the Ubol Ratana reservoir was impacted partly by the Chulabhorn dam situated on the upstream of the same river network. Since the catchment area and storage capacity of the Chulabhorn reservoir was relatively insignificant, the dam influence on the flows was considered minimal. However, the compounding effect of these dams as considered in this study suggested that the series of dams on the tributaries and mainstem of the river system could still be accounted systematically to provide reasonable estimates of inflows downstream.

While the characteristics of the monthly outflows and inflows were similar, the reduction in the magnitude of outflows due to impoundments was noticeable. The peak flow occurred during 2010-2011 for Lam Pao and Ubol Ratana while Sirindhorn observed peak flows during 2011, and 2013-2014. High precipitation during the peak flow period is the primary cause of high inflow and outflow in the reservoirs. The common peak flow period for the Lam Pao and Ubol Ratana is due to the adjacent catchment area of the dams. Although the anomaly of the monthly inflow and outflow remained similar, the seasonal variation of the flows exhibited contrasting characteristics during the wet and dry periods within a year (Figure 18). During the wet period (June – November), the basin received a major

proportion (79%) of the annual precipitation resulting in the large streamflow from the catchment to the river channels. Therefore, the inflows to the dams were considerably larger than the outflows during the wet period (Figure 18b, d, f). Also, the total storage of the reservoirs was at a minimum level before the onset of the monsoon (May-June), allowing the monsoon flows to accumulate into the reservoirs to their capacities. As a result, the outflow from the dams was less than the inflows, after the minimum ecological flow requirements were met. On the other hand, the inflows to the reservoirs were negligible during the dry period (December- May) due to the decreased precipitation and snowmelt. But the demand for the water for domestic, industrial, and energy generation purpose needed to be met during this period, and outflows were generally higher than inflows. Also, the higher outflows during the dry period enabled in the retention of a surge in flows from monsoonal rain events in the following season.

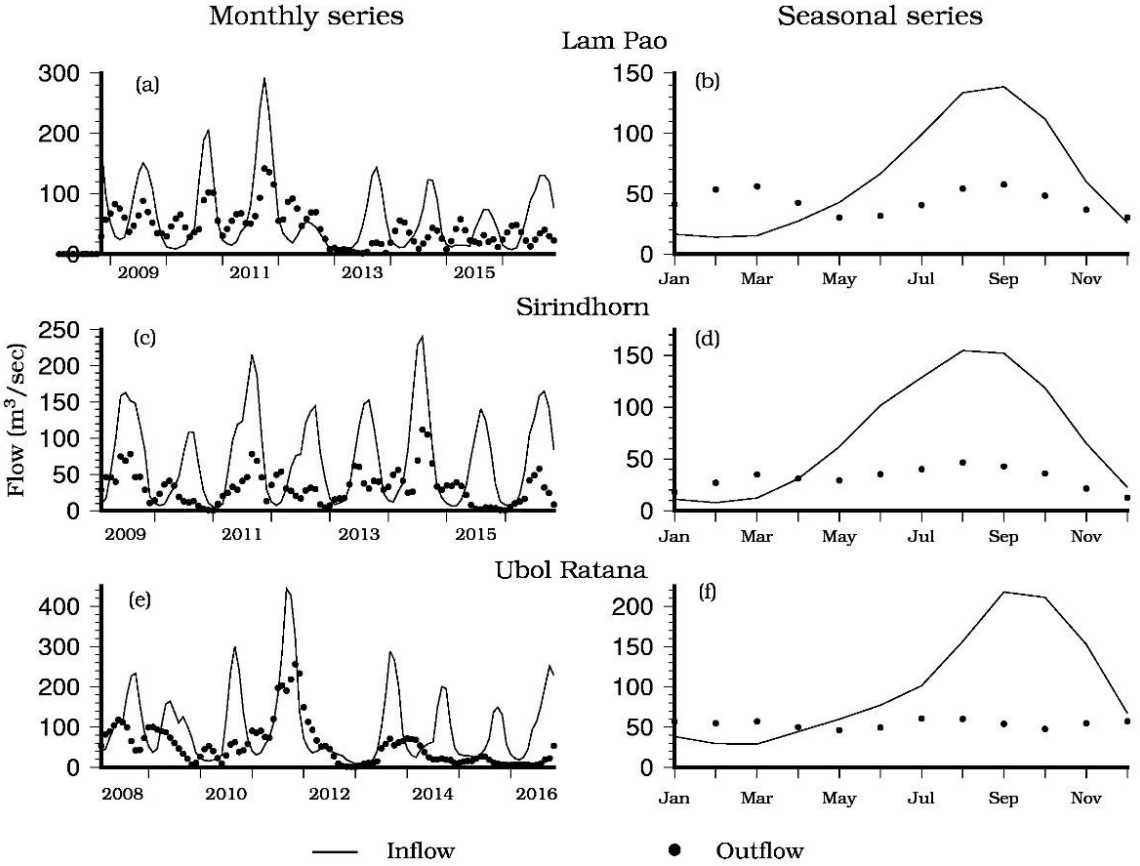


*Figure 18: Comparison of the monthly inflows and outflows from Lam Pao (a), Sirindhorn (c), and Ubol Ratana (e) from 2008 to 2016 based on the Variable Infiltration Capacity (VIC) simulated flow and the water balance. The seasonal cycle (b, d, f) shows the variation in inflows and outflows from the reservoirs for each month, derived from the monthly ensemble mean between 2008 and 2016.*

Figure 19 shows the percentage change in outflows from the dams with respect to inflows during the wet (blue) and the dry (red) period from 2008 to 2016 for Lam Pao, Sirindhorn, and Ubol Ratana. The average increase in the outflow during the dry period was estimated as 94% with respect to the inflow to the Lam Pao reservoir, but the outflow decreased by 55% during the wet period from 2008 to 2016. However, the average outflow magnitudes between the dry and the wet periods remained almost equal with the monthly discharge of 42 $m^3$/sec and 47 $m^3$/sec, respectively (Figure 18b). Management of reservoirs between seasons had an impact on maintaining the flows, despite natural and anthropogenic-induced changes to the climate and monsoon rains.

The change in the outflow from the Lam Pao reservoir was always negative with respect to inflow for the wet period except during 2012. The annual precipitation during 2012 (31% less as compared to historical average) is lowest for the period of analysis generating low inflow to the Lam Pao from the small catchment, but the average outflow was maintained throughout the year, causing an increase of 29% in the outflows relative to the inflows during the wet period. Also, the outflow remained equal to the inflow during the dry period (1.4% increase in outflow). Storage from these reservoirs during the low precipitation year enabled flows to be maintained from the proceeding high precipitation year (2011), but the effect was reflected with decreased storage in the reservoir during 2012-2013. For the Sirindhorn dam, the average outflow from the reservoirs varied from -70% during the wet period to 36% during the dry period with an average outflow of 40 $m^3$/sec and 25 $m^3$/sec during the wet and dry period, respectively (Figure 19c). The change in the flow during the dry period was governed by the annual precipitation, evident during the high precipitation years of 2009, 2011, and 2014 (Figure 19d), while the outflow change remained negative for the rest of the years. For the Ubol Ratana dam, the outflow from the reservoir varied from -23% to 93% with an average value of 60% during the dry season from 2008 to 2016. However, the change in flows during the wet season showed an increase of 54% from 2008 to 2011 then a gradual decrease of 44% for the remaining period (Figure 19e). The average outflow from the reservoir was estimated as 54 $m^3$/sec, which remained the same throughout the year, but the considerable fluctuation in the inflow, especially during 2010, 2011, and 2013, enhanced the flow difference between inflow and outflow from the

reservoir. Also, the total storage in the Ubol Ratana reservoir diminished during 2012-2016, with average storage of 990 million $m^3$. Fluctuation in the annual precipitation and large size of the catchment area of the Ubol Ratana reservoir minimized the variability imposed by climate and anthropogenic factors.

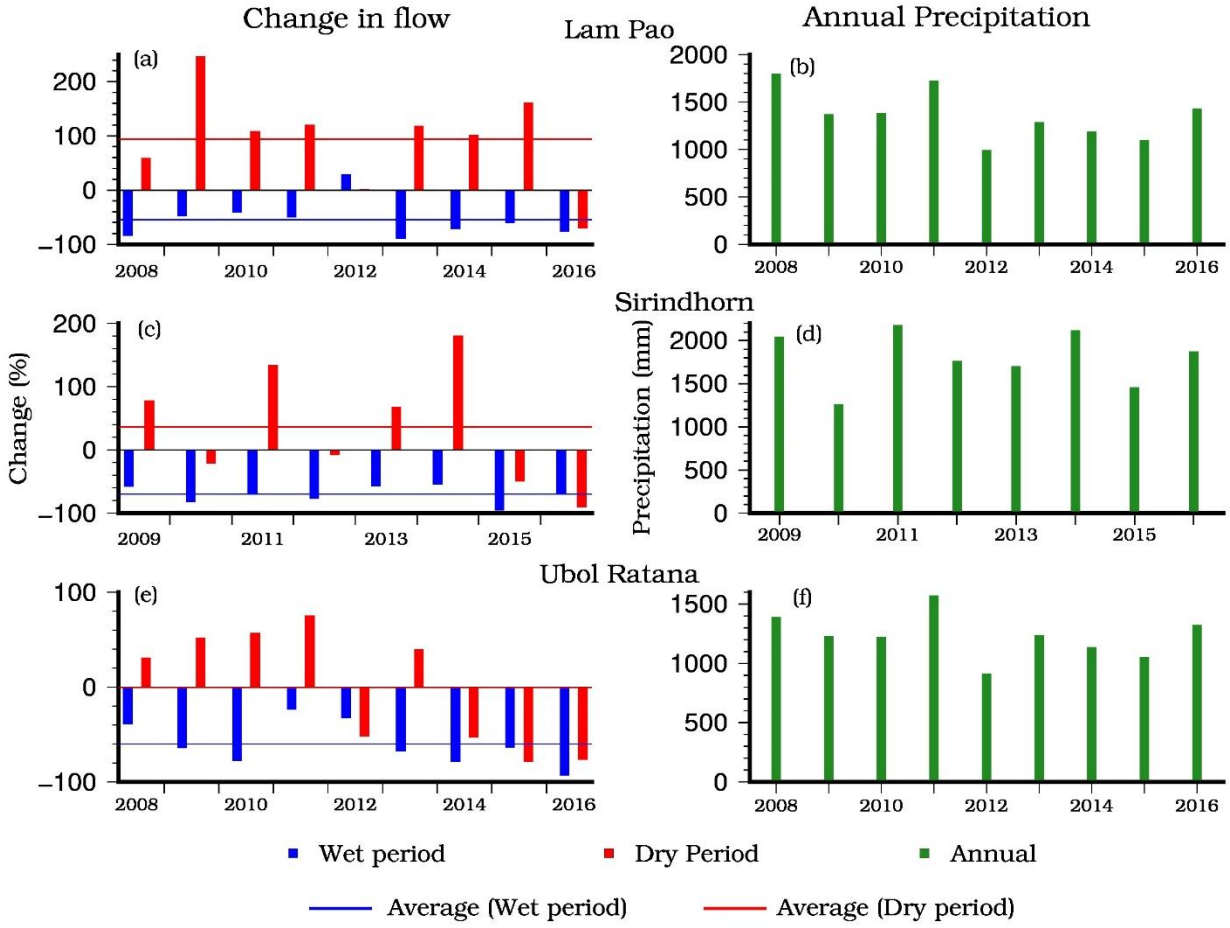


*Figure 19: Percentage change in the outflow relative to inflow from the reservoirs (a) Lam Pao (c) Sirindhorn (e) Ubol Ratana during wet (June – November) and dry (December – May) periods from 2008 to 2016. Annual precipitation for the catchments of Lam Pao (b), Sirindhorn (d), and Ubol Ratana (f) is also shown from 2008 to 2016.*

The analysis for the future period was performed using the inflow projected using the four GCMs under RCP 4.5 and RCP 8.5. For the future period (2006-2099), the rule curve of the reservoir was assumed to be the same as during the observed period (2008 to 2016). Figure 20 shows the monthly variation of the inflow and outflow for the three dams for historic and future period under two RCPs. The seasonal pattern of the outflow for the future period is similar to the pattern observed from 2006 to 2018. The outflow is lower during the wet period and higher during the dry period as compared to the inflow. As the

storage variation of the reservoir is the key factor governing the impact of the dams, a similar pattern of the outflow for the future period is the result of assuming a constant rule curve. However, the mean value of the projected outflow changes in the future as compared to the historic period because of the dependency on the inflow, which makes the system non-stationary Moreover, the degree of the impact of the dams is also influenced by the magnitude of the projected inflow.

The average inflow for Lam Pao during the historic period was 72.5 $m^3$/sec and the average outflow was 70.5 $m^3$/sec, while the inflow and outflow values for the observed period were 62.5 $m^3$/sec and 43.6 $m^3$/sec, respectively. The inflow to Lam Pao increased for the future period by 4.3% under RCP 4.5 and 2.0% under RCP 8.5. The increase in the inflow is caused by the high precipitation in the catchment area of Lam Pao accounting 2% and 1.1% increasing under RCP 4.5 and RCP 8.5, respectively, as compared to the historic precipitation. The dam operation caused the suppression of flow pulse during the wet season and increase flow in the downstream during the dry season. On average, the increase in the outflow for the future period was projected as 10.6% under RCP 4.5 and 4.4% under RCP 8.5 as compared to the historic period. The change in the flow due to Lam Pao operation was estimated as +280% during the dry season and -46% during the wet season during the historic period, while for the future period the change during the dry season is projected as +281% under RCP 4.5 (+276% under RCP 8.5), and -42% under RCP 4.5 (-45% under RCP 8.5) during the wet period. Similar behavior was exhibited by Sirindhorn with average inflow values as 63.1 $m^3$/sec during the historic period against the observed 72.3 $m^3$/sec, on the other hand, the outflow value was 39 $m^3$/sec and 31.3 $m^3$/sec for the historic and observed period, respectively. The Sirindhorn is projected to experience a marginal decrease in the inflow for the future period with respect to the historic period (0.62% under RCP 4.5 and 1.7% under RCP 8.5).

On the other hand, the outflow is projected to increase by 0.75% under RCP 4.5 and decrease by 1.3% under RCP 8.5 as compared to the historic period. The impact of the Sirindhorn operation was estimated as a 372.5% increase in the flow downstream during the dry season but a 32.8% decrease during the wet season for the historic period. For future periods, the change in the outflow with respect to inflow is projected as +372% (376% under RCP 8.5) for the dry season and -32.1% (-32.7% under RCP 8.5) for the wet season

under RCP 4.5. For the Ubol Ratana dam, the average inflow and outflow during the historic period were estimated as 87.7 $m^3$/sec and 57.3 $m^3$/sec, respectively, with the values during the observed period as 98.7 $m^3$/sec for inflow and 54.1 $m^3$/sec for outflow. The inflow from the Ubol Ratana dam is projected to increase in the future period causing the relative increase in the outflow. Under RCP 4.5, the projected increase in the inflow and outflow is 9.6% and 18%, respectively, while under RCP 8.5, there will be a 10.7% increase in inflow and 18.8% increase in the outflow. The seasonal variation of the influence of the dam was estimated as the 20.4% increase in outflow under RCP 4.5 and 18.5% increase under RCP 8.5 during the dry season as compared to inflow. On the other hand, the decrease in the outflow during the wet is projected as 25.9% and 26.2% under RCP 4.5 and RCP 8.5, respectively. For all the dams, the highest increase in the inflow and outflow for the future period with respect to the historic period is projected during October-November, while March-April will experience the largest reduction in the flows. The projected alteration in inflow to the dams will be caused by the heterogenous change in the precipitation over the different months. In addition, the water diversion to meet the demand for crop irrigation during the growing season (March-April) will be high, resulting in the suppression of the outflow during the dry season. On the other hand, the crop water demand will be reduced during the wet season due to projected increase precipitation. The increased inflow and outflow during October-November can provide a beneficial outcome to other sectors in improving the production of the electricity and fulfilling the municipal and industrial water demand. While the dry season is projected to suffer from the conflicting conditions of water struggle between the demanding sectors.

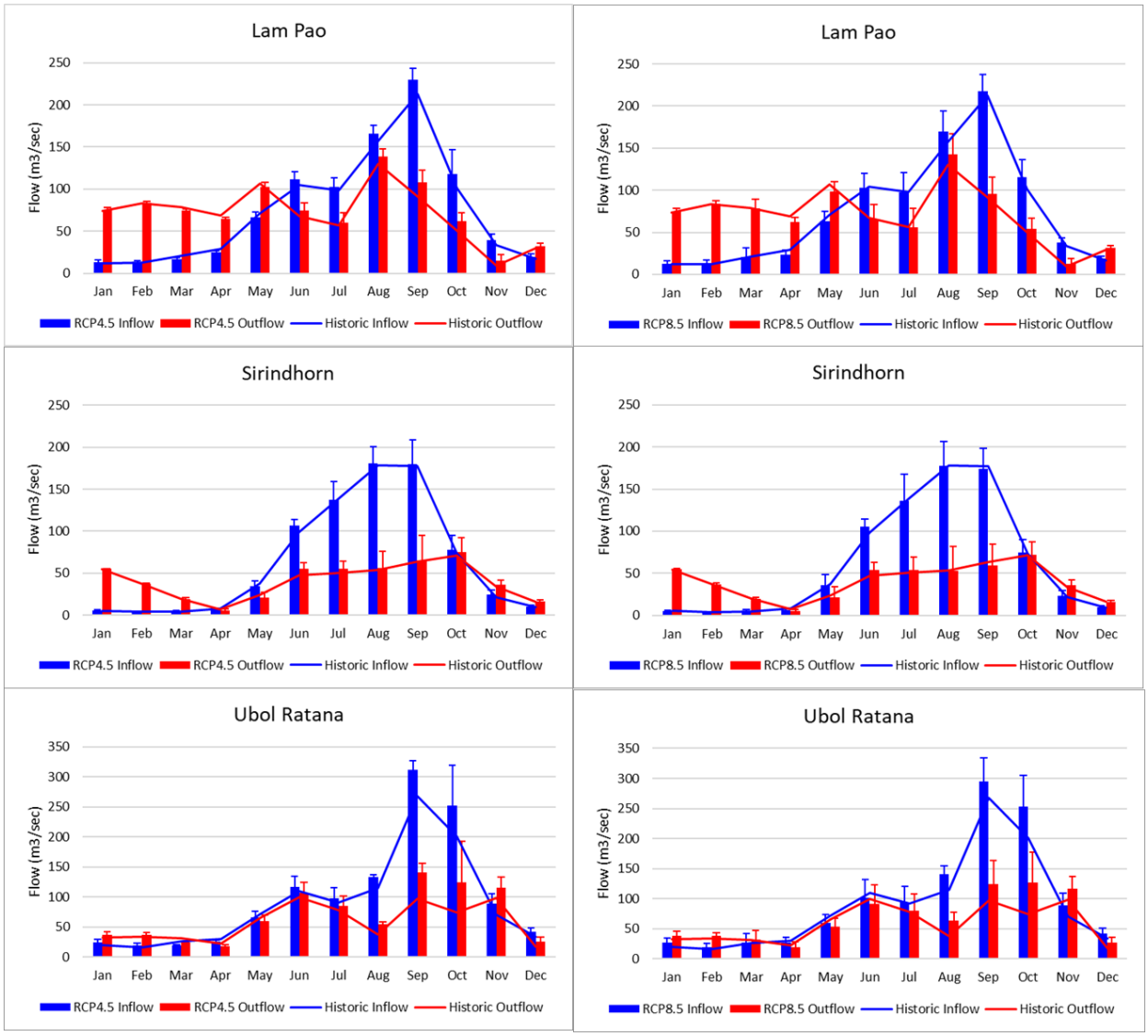


*Figure 20: The seasonal cycle shows the variation in inflows and outflows from the reservoirs for each month, derived from the monthly ensemble mean for historic and future period (RCP 4.5 and RCP 8.5).*

## 2.4 Conclusion

The major findings of this investigation are summarized below.

- The Mekong river basin has undergone a major land transformation during the period 1992-2015 with the expansion of the agriculture land over the forest area. Though the variation of the land use was less than 5% for each class over the 23 years, the trend is changing over the recent period. Particularly, cropland and closed shrub have increased, while deciduous forest has undergone a moderate decrease.

- High resolution (0.05$^{o}$) VIC model was able to accurately simulate the flow at mainstem and major tributaries of the Mekong river with the Nash-Sutcliffe model efficiency coefficient (NSE) more than 0.6 and coefficient of correlation (r) more than 0.7 as compared to the observed inflow at nine dam locations. However, the magnitude of the flow varied considerably with peak values 10 $m^3$/sec at Upper Mun to 1000 $m^3$/sec at Ubol Ratana.
- The precipitation in the MRB is defined by the monsoon season (June–November), during which the basin receives the majority of the rainfall. The spatial variability of precipitation is high, with the mean annual rainfall of 3,000 mm in the uplands in the Lao PDR and Cambodia and 1,000 to 1,600 mm in northeastern Thailand. The temperatures during the warmest months (March and April) fluctuate between 30$^{o}$C and 38$^{o}$C and in the winter around 15$^{o}$C. The temperature is projected to change between 1$^{o}$c and 6$^{o}$c and precipitation changes to be -5 to 20 % in the basin between 2020 and 2099.
- The variation of the total storage of the reservoirs was simulated exclusively using the remote sensing products viz, LandSat 8 satellite imagery for the estimation of the surface area fluctuation and altimetry datasets (ERS-1, T/P, ERS-2, GFO, Jason-1, Envisat, Jason-2, and Saral/Altika) defining the water level change. The regression analysis, using the selected area and depth data of the coinciding dates, provided the relationship between the two parameters, and storage was estimated as the integral function. The simulated total storage precisely depicted the observed storage with NSE and *r* values of 0.90 or higher. The total storage of the reservoir was minimum during May-June, prior to the onset of the monsoon. The storage gradually increased and reached the optimal values by the monsoon termination (October-November); however, storages declined to satisfy water demand for domestic and irrigation purposes. The variation between the minimum and maximum storage ranges from 600 million $m^3$ (for Lam Pao) to more than 1000 million $m^3$ (for Ubol Ratana)
- The monthly comparison of the inflow to and outflow from the reservoirs showed a general reduction in outflows during the observed period. The peak flow for the inflow during the period 2008 to 2016 was more than two-fold the peak outflow. The seasonal cycle of the inflow and outflow from the reservoirs exhibited the lesser outflow during

the wet period (June-November) and more outflow during the dry period (December-May) as compared to inflow. Lam Pao had an average decrease of 54% in the outflow during the wet period and a 94% increase during the dry period; these values were 70% and 36%, respectively for Sirindhorn. Also, Ubol Ratana had a decrease of 60% in the outflow during the wet period without much change in flows during the dry period.

- Based on the rule curve analysis, the total storage was minimum during June-July, increased by November, and then decreased for the remainder of the year. The average storage of the reservoir decreases by 54% during June-July and swells by 92% during September-October. As the precipitation and irrigation water demand has a huge impact on the dam operation, the difference between the lower limit and upper limit is higher during the monsoon period, with values approximately 1000 million $m^3$, 850 million $m^3$, and 2000 million $m^3$ for Lam Pao, Sirindhorn and Ubol Ratana dam respectively. Also, the minimum (maximum) value of the average curve for Lam Pao, Sirindhorn, and Ubol Ratana were observed as 400 (1025) million $m^3$, 850 (1630) million $m^3$, and 700 (1750) million $m^3$ respectively.

**Reference for Chapter 2**


Agriculture and fishing | Open Development Mekong. (2019). Retrieved August 15, 2020, from https://opendevelopmentmekong.net/topics/agriculture-and-fishing/

Ali, S. A., Aadhar, S., Shah, H. L., & Mishra, V. (2018). Projected Increase in Hydropower Production in India under Climate Change. *Scientific Reports*, *8*(1), 12450. https://doi.org/10.1038/s41598-018-30489-4

Allen, R., Pereira, L., Raes, D., & Smith, M. (1998). Crop evapotranspiration-Guidelines for computing crop water requirements-FAO Irrigation and drainage paper 56. *FAO Irrigation and Drainage Paper No. 56.* Retrieved from https://www.researchgate.net/profile/Hawre_Kiani/post/What_is_the_more_effective_way_of_deficit_irrigation/attachment/5af42706b53d2f63c3cafa73/AS%3A624694629777415%401525950214858/download/Allen_FAO1998.pdf

Birkett, C., Reynolds, C., Beckley, B., & Doorn, B. (2011). From Research to Operations: The USDA Global Reservoir and Lake Monitor. In *Coastal Altimetry* (pp. 19–50). Berlin, Heidelberg: Springer. https://doi.org/10.1007/978-3-642-12796-0_2

Bonnema, M., & Hossain, F. (2017). Inferring reservoir operating patterns across the Mekong Basin using only space observations. *Water Resources Research*, *53*(5), 3791–3810. https://doi.org/10.1002/2016WR019978

Cao, Q., Yu, D., Georgescu, M., Han, Z., & Wu, J. (2015). Impacts of land use and land cover change on regional climate: a case study in the agro-pastoral transitional zone of China. *Environmental Research Letters*, *10*(12), 124025. https://doi.org/10.1088/1748-9326/10/12/124025

Claverie, M., Ju, J., Masek, J. G., Dungan, J. L., Vermote, E. F., Roger, J. C., et al. (2018). The Harmonized Landsat and Sentinel-2 surface reflectance data set. *Remote Sensing of Environment*, *219*, 145–161. https://doi.org/10.1016/j.rse.2018.09.002

Cleugh, H. A., Leuning, R., Mu, Q., & Running, S. W. (2007). Regional evaporation estimates from flux tower and MODIS satellite data. *Remote Sensing of Environment*, *106*(3), 285–304. https://doi.org/10.1016/j.rse.2006.07.007

Cosby, B. J., Hornberger, G. M., Clapp, R. B., & Ginn, T. R. (1984). A Statistical Exploration of the Relationships of Soil Moisture Characteristics to the Physical Properties of Soils. *Water Resources Research*, *20*(6), 682–690. https://doi.org/10.1029/WR020i006p00682

Costa-Cabral, M. C., Richey, J. E., Goteti, G., Lettenmaier, D. P., Feldkötter, C., & Snidvongs, A. (2008). Landscape structure and use, climate, and water movement in the Mekong River basin. *Hydrological Processes*, *22*(12), 1731–1746.

https://doi.org/10.1002/hyp.6740

Crétaux, J.-F., Jelinski, W., Calmant, S., Kouraev, A., Vuglinski, V., Bergé-Nguyen, M., et al. (2011). SOLS: A lake database to monitor in the Near Real Time water level and storage variations from remote sensing data. *Advances in Space Research*, *47*(9), 1497–1507. https://doi.org/10.1016/J.ASR.2011.01.004

Duan, Z., & Bastiaanssen, W. G. M. (2013). Estimating water volume variations in lakes and reservoirs from four operational satellite altimetry databases and satellite imagery data. *Remote Sensing of Environment*, *134*, 403–416. https://doi.org/10.1016/J.RSE.2013.03.010

Eastham, J., Mpelasoka, F., Mainuddin, M., Ticehurst, C., Dyce, P., Hodgson, G., et al. (2008). Mekong River Basin water resources assessment: impacts of climate change. CSIRO: Water for a Healthy Country National Research Flagship. Retrieved from http://www.clw.csiro.au/publications/waterforahealthycountry/2008/wfhc-MekongWaterResourcesAssessment.pdf

Erban, L. E., Gorelick, S. M., & Zebker, H. A. (2014). Groundwater extraction, land subsidence, and sea-level rise in the Mekong Delta, Vietnam. *Environmental Research Letters*, *9*(8), 084010. https://doi.org/10.1088/1748-9326/9/8/084010

Feng, J.-M., Wang, Y.-L., Ma, Z.-G., & Liu, Y.-H. (2012). Simulating the Regional Impacts of Urbanization and Anthropogenic Heat Release on Climate across China. *Journal of Climate*, *25*(20), 7187–7203. https://doi.org/10.1175/JCLI-D-11-00333.1

Franchini, M., & Pacciani, M. (1991). Comparative analysis of several conceptual rainfall-runoff models. *Journal of Hydrology*, *122*(1–4), 161–219. https://doi.org/10.1016/0022-1694(91)90178-K

Fu, L.-L., & Cazenave, A. (2001). *Satellite altimetry and earth sciences : a handbook of techniques and applications*. Academic.

Gao, B. (1996). NDWI—A normalized difference water index for remote sensing of vegetation liquid water from space. *Remote Sensing of Environment*, *58*(3), 257–266. https://doi.org/10.1016/S0034-4257(96)00067-3

Goteti, G., & Lettenmaier, D. P. (2001). *Effects of streamflow regulation and land cover change on the hydrology of the Mekong river basin*. University of Washington. Retrieved from https://www.ce.washington.edu/sites/cee/files/pdfs/research/hydrology/water-resources/WRS169.pdf

Haddeland, I., Lettenmaier, D. P., & Skaugen, T. (2006). Effects of irrigation on the water and energy balances of the Colorado and Mekong river basins. *Journal of*

*Hydrology*, *324*(1–4), 210–223. https://doi.org/10.1016/j.jhydrol.2005.09.028

Heinimann, A., Messerli, P., Schmidt-Vogt, D., & Wiesmann, U. (2007). The Dynamics of Secondary Forest Landscapes in the Lower Mekong Basin. *Mountain Research and Development*, *27*(3), 232–241. https://doi.org/10.1659/mrd.0875

Hempel, S., Frieler, K., Warszawski, L., Schewe, J., & Piontek, F. (2013). A trend-preserving bias correction – the ISI-MIP approach. *Earth System Dynamics*, *4*(2), 219–236. https://doi.org/10.5194/esd-4-219-2013

Henriksen, H. J., Troldborg, L., Højberg, A. L., & Refsgaard, J. C. (2008). Assessment of exploitable groundwater resources of Denmark by use of ensemble resource indicators and a numerical groundwater–surface water model. *Journal of Hydrology*, *348*(1–2), 224–240. https://doi.org/10.1016/J.JHYDROL.2007.09.056

Hoanh, C. T., Guttman, H., Droogers, P., & Aerts, J. (2004). Will we produce sufficient food under climate change?: Mekong Basin (South-east Asia). Retrieved from https://cgspace.cgiar.org/handle/10568/37433

Hoanh, C. T., Jirayoot, K., Lacombe, G., Srinetr, V., Hoanh, C. T., Jirayoot, K., et al. (2010). Impacts of climate change and development on Mekong flow regimes. First assessment - 2009. Retrieved from https://econpapers.repec.org/paper/iwtrerpts/h043262.htm

Huffman, G., Adler, R., Stocker, E., Bolvin, D., & Nelkin, E. (2003). Analysis of TRMM 3-hourly multi-satellite precipitation estimates computed in both real and post-real time. In *12th Conf. on Satellite Meteorology and Oceanography* (pp. 4–11). Long Beach, CA: Amer. Meteor. Soc., CD-ROM. Retrieved from https://ntrs.nasa.gov/search.jsp?R=20040026654

Huffman, G. J., Adler, R. F., Morrissey, M. M., Bolvin, D. T., Curtis, S., Joyce, R., et al. (2001). Global Precipitation at One-Degree Daily Resolution from Multisatellite Observations. *Journal of Hydrometeorology*, *2*(1), 36–50. https://doi.org/10.1175/1525-7541(2001)002<0036:GPAODD>2.0.CO;2

Intralawan, A., Wood, D., & Frankel, R. (2017). *Economic Evaluation of Hydropower Projects in the Lower Mekong Basin*. Retrieved from http://www.mrcmekong.org/assets/Uploads/Final-report-Mekong-Study-March-2017-8.pdf

Ji, L., Zhang, L., & Wylie, B. (2009). Analysis of Dynamic Thresholds for the Normalized Difference Water Index. *Photogrammetric Engineering & Remote Sensing*, *75*(11), 1307–1317. https://doi.org/10.14358/PERS.75.11.1307

Jin, Y., Schaaf, C. B., Gao, F., Li, X., Strahler, A. H., Lucht, W., et al. (2003).

Consistency of MODIS surface bidirectional reflectance distribution function and albedo retrievals: 1. Algorithm performance. *J. Geophys. Res*, *108*(D5), 4158. https://doi.org/10.1029/2002JD002803

Kalnay, E., Kanamitsu, M., Kistler, R., Collins, W., Deaven, D., Gandin, L., et al. (1996). The NCEP/NCAR 40-Year Reanalysis Project. *Bulletin of the American Meteorological Society*, *77*(3), 437–471. https://doi.org/10.1175/1520-0477(1996)077<0437:TNYRP>2.0.CO;2

Kang, H., & Sridhar, V. (2019). Drought assessment with a surface-groundwater coupled model in the Chesapeake Bay watershed. *Environmental Modelling and Software*, *119*, 379–389. https://doi.org/10.1016/j.envsoft.2019.07.002

Kang, H., Sridhar, V., Mills, B. F., Hession, W. C., & Ogejo, J. A. (2019). Economy-wide climate change impacts on green water droughts based on the hydrologic simulations. *Agricultural Systems*, *171*, 76–88. https://doi.org/10.1016/j.agsy.2019.01.006

Keskinen, M., Kummu, M., Käkönen, M., & Varis, O. (2012). Mekong at the Crossroads: Next Steps for Impact Assessment of Large Dams. *AMBIO*, *41*(3), 319–324. https://doi.org/10.1007/s13280-012-0261-x

Kiem, A. S., Ishidaira, H., Hapuarachchi, H. P., Zhou, M. C., Hirabayashi, Y., & Takeuchi, K. (2008). Future hydroclimatology of the Mekong River basin simulated using the high-resolution Japan Meteorological Agency (JMA) AGCM. *Hydrological Processes*, *22*(9), 1382–1394. https://doi.org/10.1002/hyp.6947

Kingston, D. G., Thompson, J. R., & Kite, G. (2011). Uncertainty in climate change projections of discharge for the Mekong River Basin. *Hydrology and Earth System Sciences*, *15*(5), 1459–1471. https://doi.org/10.5194/hess-15-1459-2011

Kummu, M., & Varis, O. (2007). Sediment-related impacts due to upstream reservoir trapping, the Lower Mekong River. *Geomorphology*, *85*(3–4), 275–293. https://doi.org/10.1016/J.GEOMORPH.2006.03.024

Li, D., Long, D., Zhao, J., Lu, H., & Hong, Y. (2017). Observed changes in flow regimes in the Mekong River basin. *Journal of Hydrology*, *551*, 217–232. https://doi.org/10.1016/j.jhydrol.2017.05.061

Li, H., Wu, H., Huang, M., & Leung, L. R. (2012). Irrigation & Drainage Systems Engineering Representing Natural and Manmade Drainage Systems in an Earth System Modeling Framework, *1*(2), 1–2. https://doi.org/10.4172/2168-9768.1000e107

Liang, X., Lettenmaier, D. P., Wood, E. F., & Burges, S. J. (1994). A simple

hydrologically based model of land surface water and energy fluxes for general circulation models. *Journal of Geophysical Research*, *99*(D7), 14415. https://doi.org/10.1029/94JD00483

Liu, Y., Xiao, J., Ju, W., Xu, K., Zhou, Y., & Zhao, Y. (2016). Recent trends in vegetation greenness in China significantly altered annual evapotranspiration and water yield. *Environmental Research Letters*, *11*(9), 094010. https://doi.org/10.1088/1748-9326/11/9/094010

Lohmann, D., Raschke, E., Nijssen, B., & Lettenmaier, D. P. (1998). Regional scale hydrology: II. Application of the VIC-2L model to the Weser River, Germany. *Hydrological Sciences Journal*, *43*(1), 143–158. https://doi.org/10.1080/02626669809492108

Lohmann, Dag, Nolte-Holube, R., & Raschke, E. (1996). A large-scale horizontal routing model to be coupled to land surface parametrization schemes. *Tellus, Series A: Dynamic Meteorology and Oceanography*. https://doi.org/10.1034/j.1600-0870.1996.t01-3-00009.x

Manh, N. Van, Dung, N. V., Hung, N. N., Kummu, M., Merz, B., & Apel, H. (2015). Future sediment dynamics in the Mekong Delta floodplains: Impacts of hydropower development, climate change and sea level rise. *Global and Planetary Change*, *127*, 22–33. https://doi.org/10.1016/J.GLOPLACHA.2015.01.001

Marhaento, H., Booij, M. J., Rientjes, T. H. M., & Hoekstra, A. Y. (2017). Attribution of changes in the water balance of a tropical catchment to land use change using the SWAT model. *Hydrological Processes*, *31*(11), 2029–2040. https://doi.org/10.1002/hyp.11167

Martin, S. M., & Lorenzen, K. (2016). Livelihood Diversification in Rural Laos. *World Development*, *83*, 231–243. https://doi.org/10.1016/J.WORLDDEV.2016.01.018

Mekong River Commission. (2010). Assessment of basin-wide development scenarios–main report. *Mekong River Commission, Vientiane, Lao PDR*.

Merola, R. B., Hien, T. T., Quyen, D. T. T., & Vengosh, A. (2015). Arsenic exposure to drinking water in the Mekong Delta. *Science of The Total Environment*, *511*, 544–552. https://doi.org/10.1016/J.SCITOTENV.2014.12.091

Mitchell, T. D., & Jones, P. D. (2005). An improved method of constructing a database of monthly climate observations and associated high-resolution grids. *International Journal of Climatology*, *25*(6), 693–712. https://doi.org/10.1002/joc.1181

Monteith, L. J. (1965). Evaporation and environment, In The state and movement of water in living organisms. *Symp. Soc. Exp. Biol.*, 205–234. Retrieved from

https://ci.nii.ac.jp/naid/10007810939/

Mu, Q., Heinsch, F. A., Zhao, M., & Running, S. W. (2007). Development of a global evapotranspiration algorithm based on MODIS and global meteorology data. *Remote Sensing of Environment*, *111*(4), 519–536. https://doi.org/10.1016/J.RSE.2007.04.015

Mu, Q., Zhao, M., & Running, S. W. (2011). Improvements to a MODIS global terrestrial evapotranspiration algorithm. *Remote Sensing of Environment*, *115*(8), 1781–1800. https://doi.org/10.1016/J.RSE.2011.02.019

Myneni, R. ., Hoffman, S., Knyazikhin, Y., Privette, J. ., Glassy, J., Tian, Y., et al. (2002). Global products of vegetation leaf area and fraction absorbed PAR from year one of MODIS data. *Remote Sensing of Environment*, *83*(1), 214–231. https://doi.org/10.1016/S0034-4257(02)00074-3

Olson, K. R., & Morton, L. W. (2018). Tonle Sap Lake and River and confluence with the Mekong River in Cambodia Soil management View project. *Article in Journal of Soil and Water Conservation*, *73*(3), 60A-66A. https://doi.org/10.2489/jswc.73.3.60A

Pham, H. T., Marshall, L., Johnson, F., & Sharma, A. (2018). Deriving daily water levels from satellite altimetry and land surface temperature for sparsely gauged catchments: A case study for the Mekong River. *Remote Sensing of Environment*, *212*, 31–46. https://doi.org/10.1016/j.rse.2018.04.034

Salomon, J. G., Schaaf, C. B., Strahler, A. H., Feng Gao, & Yufang Jin. (2006). Validation of the MODIS bidirectional reflectance distribution function and albedo retrievals using combined observations from the aqua and terra platforms. *IEEE Transactions on Geoscience and Remote Sensing*, *44*(6), 1555–1565. https://doi.org/10.1109/TGRS.2006.871564

Sheffield, J., Goteti, G., & Wood, E. F. (2006). Development of a 50-Year High-Resolution Global Dataset of Meteorological Forcings for Land Surface Modeling. *Journal of Climate*, *19*(13), 3088–3111. https://doi.org/10.1175/JCLI3790.1

Shrestha, B., Babel, M. S., Maskey, S., van Griensven, A., Uhlenbrook, S., Green, A., & Akkharath, I. (2013). Impact of climate change on sediment yield in the Mekong River basin: a case study of the Nam Ou basin, Lao PDR. *Hydrology and Earth System Sciences*, *17*(1), 1–20. https://doi.org/10.5194/hess-17-1-2013

Sridhar, V., Ali, S. A., & Lakshmi, V. (2019). Assessment and validation of total water storage in the Chesapeake Bay watershed using GRACE. *Journal of Hydrology: Regional Studies*, *24*, 100607. https://doi.org/10.1016/J.EJRH.2019.100607

Sridhar, V., Kang, H., & Ali, S. A. (2019). Human-Induced Alterations to Land Use and Climate and Their Responses for Hydrology and Water Management in the Mekong River Basin. *Water*, *11*(6), 1307. https://doi.org/10.3390/w11061307

Stackhouse, P. W., Gupta, S. K., Cox, S. J., Mikowitz, J. C., Zhang, T., & Chiacchio, M. (2004). 12-year surface radiation budget data se. *GEWEX News*, *14*(4), 10–12.

Stone, R. (2011). Mayhem on the Mekong. *Science*, *333*(6044), 814–818. https://doi.org/10.1126/science.333.6044.814

Tatsumi, K., & Yamashiki, Y. (2015). Effect of irrigation water withdrawals on water and energy balance in the Mekong River Basin using an improved VIC land surface model with fewer calibration parameters. *Agricultural Water Management*, *159*, 92–106. https://doi.org/10.1016/J.AGWAT.2015.05.011

Västilä, K., Kummu, M., Sangmanee, C., & Chinvanno, S. (2010). Modelling climate change impacts on the flood pulse in the Lower Mekong floodplains. https://doi.org/10.2166/wcc.2010.008

van Vuuren, D. P., Edmonds, J., Kainuma, M., Riahi, K., Thomson, A., Hibbard, K., et al. (2011). The representative concentration pathways: An overview. *Climatic Change*, *109*(1), 5–31. https://doi.org/10.1007/s10584-011-0148-z

Wang, W., Lu, H., Ruby Leung, L., Li, H.-Y., Zhao, J., Tian, F., et al. (2017). Dam Construction in Lancang-Mekong River Basin Could Mitigate Future Flood Risk From Warming-Induced Intensified Rainfall. *Geophysical Research Letters*, *44*(20), 10,378-10,386. https://doi.org/10.1002/2017GL075037

Wood, E. F., Lettenmaier, D. P., & Zartarian, V. G. (1992). A land-surface hydrology parameterization with subgrid variability for general circulation models. *Journal of Geophysical Research*, *97*(D3), 2717. https://doi.org/10.1029/91JD01786

Yang, B., Zhang, Y., Qian, Y., Tang, J., & Liu, D. (2016). Climatic effects of irrigation over the Huang-Huai-Hai Plain in China simulated by the weather research and forecasting model. *Journal of Geophysical Research: Atmospheres*, *121*(5), 2246–2264. https://doi.org/10.1002/2015JD023736

Zhou, T., Haddeland, I., Nijssen, B., & Lettenmaier, D. P. (2016). Human-Induced Changes in the Global Water Cycle (pp. 55–69). American Geophysical Union (AGU). https://doi.org/10.1002/9781118971772.ch4

Ziv, G., Baran, E., Nam, S., Rodríguez-Iturbe, I., & Levin, S. A. (2012). Trading-off fish biodiversity, food security, and hydropower in the Mekong River Basin. *Proceedings of the National Academy of Sciences of the United States of America*, *109*(15), 5609–14. https://doi.org/10.1073/pnas.1201423109

# Chapter 3
# Estimation of the net irrigation water requirement for the irrigated area and supply for reservoir and groundwater to meet the demand

**Keywords:** VIC, NIWR, ModFlow, groundwater, Mekong, GCMs

## 3.1 Introduction

The rise in the global food price and worse malnutrition will result from even a small shortfall in crop production (Carruthers et al., 1997). Therefore, enhanced food production from irrigation is essential through the expansion of irrigated areas and water supplies. To meet food production needs, the intensification and expansion of the irrigated agriculture would pressurize land and water resources and degrade the environment. Anthropogenic activities (e.g., urbanization, deforestation, and irrigation) markedly alter the underlying surface characteristics, and these changes produce significant impacts on water and energy balance through the land-atmosphere interaction (Cao et al., 2015; Feng et al., 2012; Jaksa & Sridhar, 2015; Sridhar, 2013; Sridhar & Anderson, 2017; Yang et al., 2016). Irrigation affects the natural hydrological cycle and the partitioning of surface energy and has been recognized as an important factor that affects water partitioning (Wu et al., 2018). Hence, the estimation of the water requirement for the irrigation purpose is necessary to ensure the food security of the region. Due to the meteorological condition of Southeast Asia and Mekong region, the rainfed agriculture can be practiced only during the monsoon season (Pokhrel et al., 2018).

The dams and diversion structures play a significant role in assuring the water availability for crop production throughout the year. But the finite volume of water needs to be distributed for various purposes such as energy generation, domestic water needs, and industrial demands. So, the estimates of the net irrigation water requirement (NIWR) is crucial for water resource management as it has to compete with multiple sectors. Groundwater is a form of water occupying all the voids within a geological stratum. Water bearing formation of the earth's crust acts as conduits for transmission and as reservoirs for storing water (Ganapuram et al., 2009). Though the groundwater reserves are not uniform over the globe, the regions with high water table level enjoy the water availability over a long period of time. Groundwater is a primary resource for agricultural, domestic,

and industrial uses worldwide (Gleeson et al., 2012). However, the groundwater can be an alternative to partially satisfy the water needs of the irrigation, the extensive extraction of the water leads to land subsidence, saltwater intrusion, and salinity.

The Mekong river basin (MRB) is one of the largest transboundary basins in the world shared between six countries, viz. China, Myanmar, Thailand, Lao PDR, Cambodia, and Vietnam. Agriculture is the primary occupation of more than 60 million inhabitants of the Lower Mekong River Basin (LMRB) accounting for approximately 10 million hectares of land (Martin & Lorenzen, 2016; Olson & Morton, 2018). With a total irrigated area of 6,414,880 hectares, Thailand is the leading cultivated region among the countries in the LMRB. Also, the Thailand host all the 6 multipurpose dams commissioned for irrigation purpose in the LMBR. Irrigation plays an important role in regulating the water supply during the wet season and supplementing the crop water requirements in the dry season. With the consumption of more than 70 percent of the total available water, irrigation is the leading use of water in the lower MRB. From a technical perspective, investments into irrigated agriculture in northeast Thailand has (for the last 50 years) been a continuous attempt to balance the seasonality of rainfall, make wet season production less risky through supplementary irrigation, and allow for dry season agricultural production.

The crisis for the water management exaggerates with the increasing population of the MRB. The growth of the population was estimated as 45% between 1980 and 2000, which is further expected to extend in the next two decades, exerting extensive pressure on the land and water for supplementary food production (Han Li et al., 2018; Nesbitt, H., R. Johnston, 2004; Pech & Sunada, 2008). Over the past few decades, the conversion of large forest areas into agricultural lands is devoted to rapid population growth, urbanization, and socio-economic development in the countries of the MRB (Sabo et al., 2017). Sridhar et al. (2019) estimated the conversion of land use as a 3% increase in the cropland and a 1-2% decline in the grasslands, shrublands, and forests. The changing climate is expected to increase the wet season flow of the MRB by 10%, while the dry season flow remaining consistent. Chiang Saen and Luang Prabang gage stations will experience anomaly in streamflow with a reduction of up to 5% in streamflow for the other flow stations. The

increase in the flows during wet season and reduction during the dry season will alter the reservoir management during the peak irrigation periods. Furthermore, the fulfillment of the growing food demand of the population in the MRB is satisfied by the cultivation of additional rice crops in the basin. The total irrigated area in the basin is approximately 4 million hectares, and irrigated areas are expanding steadily in all four Member Countries (MRC, 2005). The expanding agricultural area and intensification of the crop cycle demand enormous water requirements for the cultivation of crops. Land use change, through influencing storage patterns and water discharge transforms the hydrological cycle and its surrounding aquatic systems in the Mun River basin in Thailand (Akter & Babel, 2012).

The large temporal and spatial variation in global rainfall has a significant impact on agriculture and the "intersection between irrigation, water resource, and climate" has been the focus of much recent attention (Fischer et al., 2007). Soil saturation in the wet season leads to extensive runoff, whilst irrigation is necessary for the dry season to prevent crop losses. Irrigation-intensive farming increases the soil water content and evapotranspiration rates and reduces run-off: in turn, these effects have the potential to change both the surface water and energy balance within the soils. Chase et al. (1999) reported that regional-scale increases in irrigation have the potential to induce a cooler and wetter climate on the northern Colorado plains in the United States. Similar results have been obtained by Kueppers et al. (2007), Sacks et al. (2009), Lobell & Bonfils (2008), Deligios et al. (2019), and Thiery et al. (2020). Changes in vegetation and land use also affect runoff and water yields within a watershed (Bosch & Hewlett, 1982; Hibbert, 1983). Jackson et al. (2001) found that approximately half of the global water diverted for the irrigation of crops is lost through evapotranspiration and is therefore unavailable for further use. Schubert et al. (2004) suggest that evaporation is controlled by net radiative energy, rather than soil moisture, in wet climate regions, but that it is sensitive to soil moisture in dry regions of the U.S. Great Plains. Using idealized climate simulations, Boucher et al. (2004) found a global mean radiative forcing in the range of 0.03–0.1 W $m^{-2}$ could be attributed to the increase in water vapor due to irrigation, accompanied by a change in the vertical temperature profile and surface cooling of up to 0.8 K over irrigated land. The anthropogenic impacts on surface water fluxes in North America were studied by

Haddeland et al. (2006) using the VIC model. Also, the VIC model with the irrigation scheme was implemented at a global scale to study the impact of reservoirs on global water storage variations (Nijssen, et al., 2016). The impact of irrigation water withdrawals on water and energy balance in the MRB was investigated by Tatsumi and Yamashiki (2015a) using the improved VIC model. However, these studies were done at a coarse spatial resolution ($0.25^{o}$), accounting for only a few major dams.

As compared to the non-irrigation area, irrigation plays an important role in portioning the water budget, especially increasing the evapotranspiration (ET) from the irrigated fields. The elevated ET has a direct influence on the water availability to the downstream region. Hence, the irrigation reservoirs suffer due to higher water demand from agricultural fields. In addition, the estimate of the water requirement for the irrigation fields contributes towards efficient water resources management. The net irrigation water requirement (NIWR) constitutes a major portion of the water demand from the reservoirs. Based on the available water for supply, the accuracy in the supply-demand scenario assessment can be achieved to ensure the food security of the region, especially under drought conditions. As the various sectors are interdependent to fulfill the water requirement from the water available in the reservoir, the NIWR affects the ecological impacts, hydropower production, municipal and industrial supplies. Therefore, it is important to estimate the effect of irrigation on the water budget components as the agricultural area is expanding over the forest lands in the basin.

The exploration of the additional source of water to satisfy the growing demand is the key to the sustainable management of the MRB. According to Seibert et al. (2010), groundwater remains largely underutilized in the Mekong basin. Sridhar et al. (2018) developed a new coupled framework, namely VIC-MF, using Variable Infiltration Capacity (VIC) and MODFLOW models to study the influence of groundwater on water and energy balance components and the effect of changing hydrology on the recharge and groundwater levels in the Snake River Basin (SRB), Idaho, US. In the regions of the dominant groundwater contribution in adding moisture in the vadose zone, the soil moisture is altered by the surface water movement through the upward flux from below.

The limitation of the VIC model in simulating the hydrologic processes related to groundwater was overcome by coupling with MODFLOW for a more accurate understanding of the physical processes with surface-groundwater interactions. The VIC model simulates the infiltration to act as recharge to the groundwater zone. Finally, the MODFLOW model combined the recharge to simulate groundwater dynamics. As compared to the VIC model, a 4.4% increase in base flow and a 10.3% decrease in peak flow was estimated by VIC-MF in SRB. Kang & Sridhar (2019) implemented the VIC-MF model to evaluate the response of soil moisture and groundwater dynamics in the Northern Atlantic Plain in the Chesapeake Bay watershed for the comprehensive understanding of impacts of drought due to surface and subsurface water exchanges. Since the MRB is associated with the data scares region (Affeltranger, 2009a, 2009b; Aliagha, 2004; Gerlak et al., 2011), recent advances in remote sensing (RS) and geographic information science (GIS) provide effective tools for groundwater exploration and mapping (Dar et al., 2010; Ganapuram et al., 2009; Jain, 1998; Jha et al., 2007; Oikonomidis et al., 2015; Senanayake et al., 2016).

Awawdwh et al. (2014) investigated groundwater potential areas in the Tulul al Ashaqif area, Jordan, using the multicriteria evaluation techniques. Eight thematic layers, namely lithology, geomorphology, lineaments density, drainage density, soil texture, rainfall, elevation, and slope, were combined using the weighted overlay approach to develop the groundwater potential map (GPM) for the study area. Similarly, the groundwater availability for agriculture was explored in the Musi basin by Ganapuram et al. (2009) using the digital elevation model (DEM) and Landsat 7 thematic mapper data. The potential groundwater zone mapping showed a high accuracy of 81.7% in the northern United Arab Emirates (UAE) based on geo-hydrological considerations (Al-Ruzouq et al., 2019). Along with the groundwater potential mapping in the arid and semi-arid countries, the technique has been used in the tropical climate regions such as India. Narendra et al. (2013) delineated groundwater prospective zones in Narava basin, Visakhapatnam, India using geomorphology, geology, lineament density, drainage density, slope, and land use/land cover (LULC) thematic layers. Though the groundwater potentiality zone is a widely used approach to explore the water below the earth's surface, the technique has not been applied to large basins.

The overarching aim of this study is to evaluate the water budget components variation due to irrigation in the Mekong River basin. The novelty of this study is embedded in the implementation of the high-resolution hydrological model (Variable Infiltration Capacity at $0.05^{o}$ resolution) with the irrigation scheme to investigate the irrigation effects. In this study, we explored the topographical, hydrological, meteorological, and geoenvironmental characteristics of the MRB and combined the elevation, slope, drainage density, land cover, soil texture, lineament density, and precipitation maps using the weighted overlay analysis to develop the GPM for the MRB. The objectives of the study are to:

- estimate the water requirement (NIWR) for irrigation purposes using the irrigated maps and hydrological model
- develop the groundwater potential map (GPM) for the MRB

## 3.2 Materials and Methods

### 3.2.1 Study Area

MRB covers an area of about 800,000 $km^2$ and the mainstem and their tributaries drain six countries, namely China, Myanmar, Thailand, Laos, Cambodia, and Vietnam. The Mekong River originates in southeastern Qinghai province in China and flows a distance of 4800 km through Tibetan Plateau, and Yunnan province to empty into the South China Sea at the Mekong Delta in Vietnam. The mean annual discharge from the basin is approximately 15,000 $km^3$/year. The heterogeneous distribution of the precipitation follows the east-to-west gradient with a mean annual value of 1200 mm. Nearly 70% of the annual precipitation in the MRB occurs during the monsoon season. However, the temperature and elevation variation follow a north-to-south gradient. The temperature in the MRB varies from 38 $^{o}$C during March-April to 15 $^{o}$C during November-February. Since the condition in the MRB is hot and humid with the glaciated portion for the upper region, the climate is classified as tropical monsoonal. The elevation drop of more than 4900 m in the MRB also affects the climate heterogeneity.

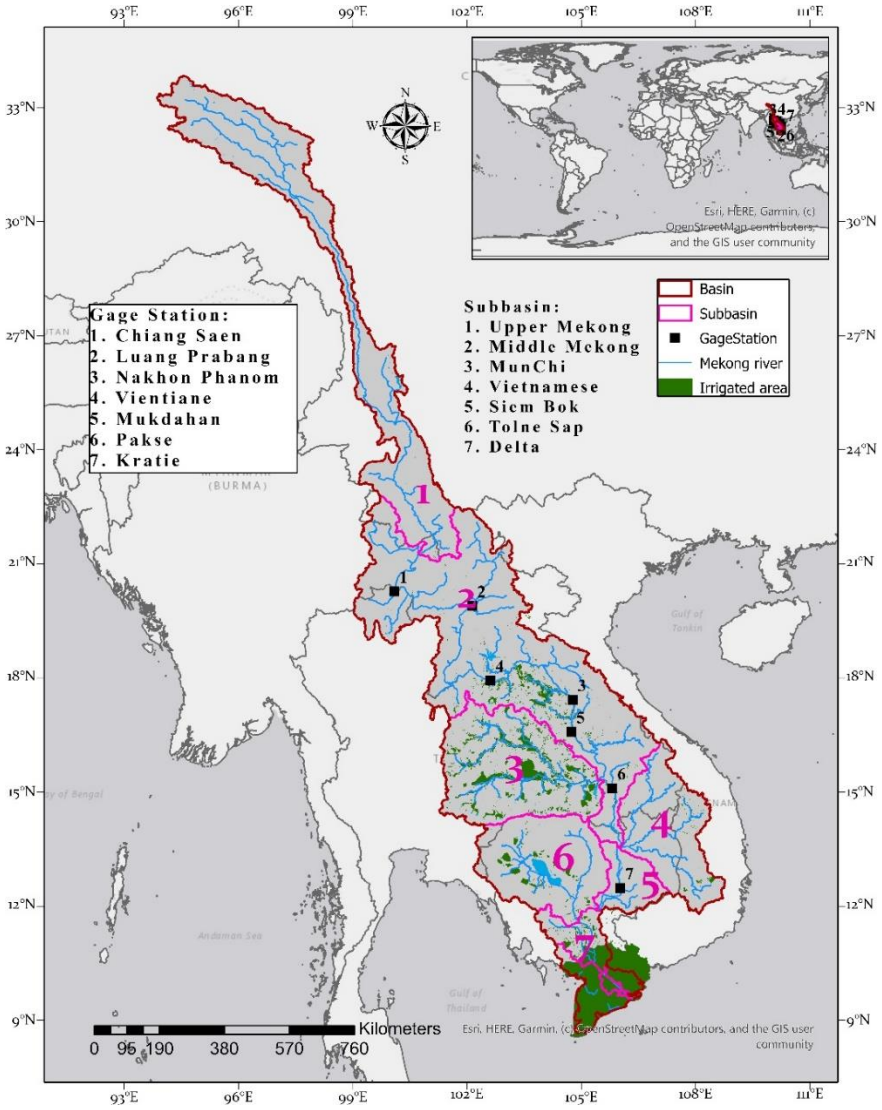


*Figure 1: The Mekong river basin with the irrigated area (2004) and geographical location of the gage stations and subbasins*

A major portion of the MRB is covered with the croplands (40%), followed by evergreen broadleaf forest (28%), closed shrublands (10.3%), and grasslands (9.3%). Irrigated wet season rice is grown throughout the year and fish catch (4.4 million tons per year) provide food security to more than 60 million people residing in the MRB (Martin & Lorenzen, 2016; Olson & Morton, 2018). The total irrigated area of the Mekong river basin is estimated at 66,000 km$^2$ in 2004 according to MRC (2004). For the sake of analysis, the MRB was classified into seven subbasins, viz., Upper Mekong, Middle Mekong, Mun Chi, Vietnamese, Siem Bok, Tolne Sap, and Delta. The major portion of the irrigated area is located in the delta comprising 52% of the total irrigated area, followed by Mun Chi basin

with 30%, and Middle Mekong with 12%, while the remaining basins host less than 5% of the total irrigated area of the basin.

### 3.2.2 Variable Infiltration Capacity

The VIC model (version 4.2.a) was used for the estimation of the water budget components for the observed and future climate. The VIC is a semi-distributed physically-based hydrological model that solves water and energy balance for each grid (here, $0.05^{o}$ spatial resolution) separately at a daily time step (Liang et al., 1994). The water (runoff and baseflow) and energy fluxes were simulated by VIC for each grid cell independently without any lateral exchange of these fluxes. The routing model developed by Lohmann et al. (1998; 1996) was used for the estimation of the streamflow at the desired location by routing the fluxes of each grid generated by the VIC model.

The water withdrawal for irrigation is influenced by land use and would increase necessarily during periods of water scarcity. Furthermore, the indirect influence through the alteration of river discharge and irrigation schemes were imposed by the presence of reservoirs, hydropower schemes, urbanization, and groundwater pumping. There is a lack of information on the uncertainty around crop water withdrawal (Tatsumi & Yamashiki, 2015b). In this study, an improved VIC model including the irrigation scheme developed by Haddeland et al. (2006) was used to simulate the impact of irrigation on the water budget components and water abstraction for irrigation purposes. The irrigated area of the MRB was derived from the Mekong River Commission (MRC) database for the year 2004 and was used for the estimation of crop fraction in the grids for irrigation scheme implementation. The main objective of the irrigation scheme is to provide additional moisture to the water-stressed vegetation caused by limited soil moisture availability. The irrigation process is designed to initiate when soil moisture of the top layer falls below the level at which transpiration is limited. The modified VIC model allows for irrigation water use based on the predicted soil moisture content for agricultural grid cells at every computational step. Specifically, when the soil moisture drops below the wilting point, irrigation is represented in the model as additional precipitation until the soil moisture reaches field capacity. The additional precipitation continues on a daily basis until soil

moisture reaches field capacity (Nijssen, et al., 2016). Based on water availability, Haddeland et al. (2006) introduced two modules for the extraction of the water i.e. free-irrigation, where unlimited water availability was assumed, and limited-irrigation, where the withdrawal was restricted by the amount available as runoff or from river channels and dams. The free-irrigation module of the irrigation scheme was used in this study and the estimated irrigation water requirement was compared with the storage capacity of the reservoirs in the basin.

### 3.2.3 General Circulation Models

Four global circulation models (GCM) from two Representative Concentration Pathways (RCPs) 4.5 and 8.5 were used for future meteorological parameters in this analysis and they are GFDL-ESM2M, IPSL-CM5A-LR, MIROC-ESM-CHEM, and NorESM1-M. The selection of the climate models was based on the collection of the distribution of wet/dry and cold/hot climate conditions defined using the precipitation and temperature change for five future periods between 2006 and 2099. The precipitation, minimum, and maximum temperature from the GCMs were bias-corrected and statistically downscaled to 0.25-degree resolution using the Intersectoral Impact Model Intercomparison Project (ISI-MIP) approach (Hempel et al., 2013). Since the future period temperature was higher for all the GCMs with respect to the historic period, the cool climate scenario was not analyzed.

### 3.2.4 Groundwater potential zone

Figure 2 shows the methodology followed for this study. Overall, the raw data of the factors (elevation, slope, precipitation, soil, land cover, geology, drainage stream density, and lineament density) describing the features of the MRB were prepared through multiple processing methods to acquire the required thematic maps for the study area. Thematic maps were then processed to develop GPM for the MRB. The raw data for the development of the thematic maps were acquired through different sources. The spatial data such as elevation, slope, drainage stream density were prepared using the Shuttle Radar Topography Mission (SRTM) digital elevation map available from https://opentopography.org/. The soil map at 0.25º spatial resolution was derived using the classification defined by Hybrid State Soil Geographic (STATSGO) / Food and Agriculture

Organization (FAO) soil texture and is freely available at https://ldas.gsfc.nasa.gov/gldas/GLDASsoils.php. The land cover map showing the spatial distribution of the vegetation in the MRB was extracted from the European Space Agency Climate Change Initiative-Land Cover (ESA CCI-LC) dataset (https://www.esa-landcover-cci.org/?q=node/164). The Landsat 8 Operational Land Imager (OLI) and Thermal Infrared Sensor (TIRS) images (available at https://www.usgs.gov/land-resources/nli/landsat) were classified using the USGS (United States Geological Survey) geological map from https://certmapper.cr.usgs.gov/geoportal/catalog/main/home.page for developing the spatial geological map. The lineaments in the MRB were prepared using the Advanced Space-Borne Thermal Emission and Reflection (ASTER) dataset available from https://terra.nasa.gov/data/aster-data. The precipitation variation spatial map showing the monthly precipitation was derived from the APHRODITE's (Asian Precipitation - Highly-Resolved Observational Data Integration Towards Evaluation) daily gridded precipitation at 0.25$^{o}$ resolution downloaded from http://www.chikyu.ac.jp/. The validation of the GPM resulted from the processing of the thematic maps was carried out through the comparison of the observational wells locations available at the Mekong River Commission (MRC) database (http://portal.mrcmekong.org/).

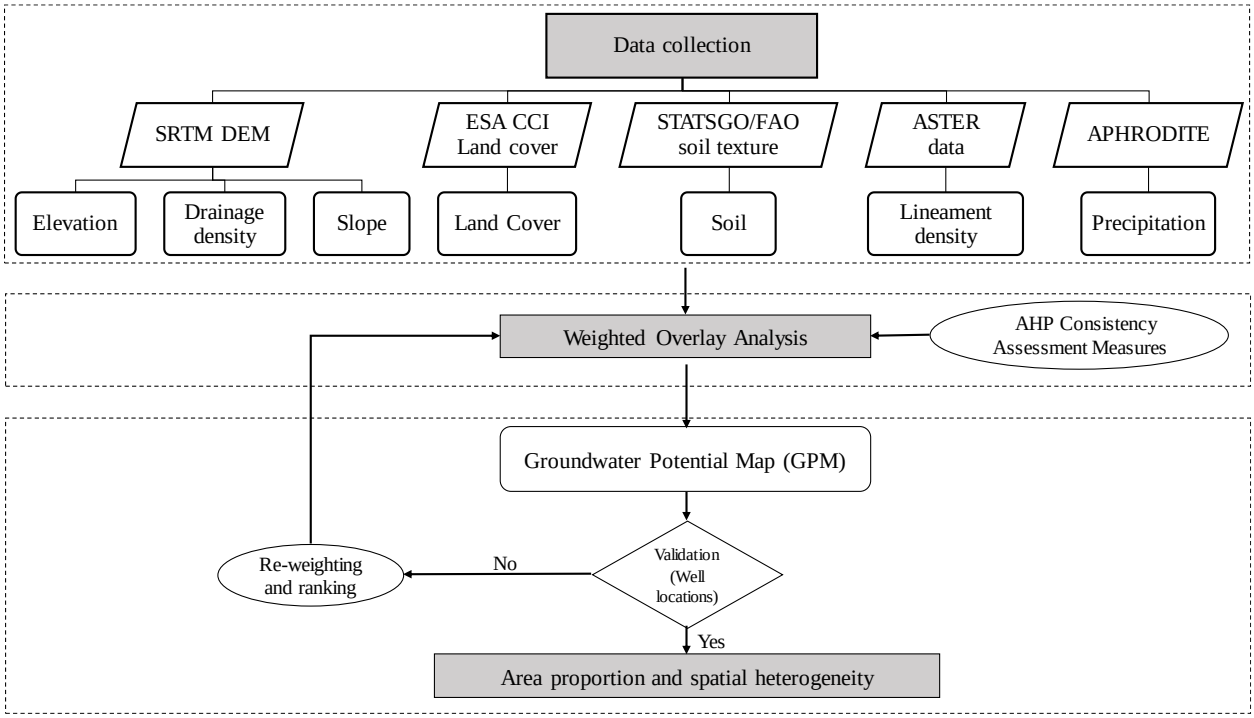


*Figure 2: Flowchart of methodology for the preparation of groundwater potential map*

Spatial analysis software, such as ArcMap 10.5 package of ArcGIS, Focus 2019 package of PCI Geomatics, and ENVI 4.2 was used for the processing of remote sensing data. After preparation, the weighted overlay analysis scheme was used for processing the thematic layers to generate the GPM. The continuous thematic layers (all the factors except the land cover) were classified into five classes to overcome the differentiation between the measurement units between each thematic layer. The mathematical background of the weighting overlay is illustrated in equation 1:

$$GPM = \sum_{k \in f} W_k \times r_k \quad (1)$$

where:

$k$ = element of thematic layer set,

$f$ = set of all thematic layers,

$W$ = weight of each thematic layer, and

$r$ = rating of the subclasses of each thematic layer.

Since all the above-mentioned factors do not contribute equally towards the groundwater occurrence and storage, a multicriteria evaluation technique (MCET) was adopted to prepare the final maps of the groundwater potential map (GPM). MCET is a numerical algorithm that defines the suitability of a particular solution on the basis of the input criteria and weights together with some mathematical or logical means of determining trade-offs when conflicts arise (Heywood et al., 2003). In this technique, the importance of each data layer relative to other data layers is reflected through the assigned "weight" to the layer. Moreover, a rank is given to reflect the importance of a class within a data layer. It is important to understand the control of these factors on the groundwater regime of any area for optimal exploitation and aquifer management. The method used to assign weights of the parameters was the analytical hierarchy principle (AHP). Using the APH nine-point scale (Table 1), a paired comparison matrix was created for the seven factors selected for the analysis, and then maps weights were then developed (Table 2). The assignment of the rating scale for the paired comparison matrix for the majority of the factors was derived from Awawdeh et al. (2014).

*Table 1: Rating scale used in Saaty's APH model*

| S. No. | Weight | Definition |
|---|---|---|
| **1** | 1 | Equally likely occurrence |
| **2** | 3 | Moderately likely occurrence |
| **3** | 5 | Strongly likely occurrence |
| **4** | 7 | Very strongly likely occurrence |
| **5** | 9 | Extremely strongly likely occurrence |

*Table 2: Paired comparison matrix of the used factors*

| Factor | Land Cover | Drainage Density | Slope | Precip--itation | Soil | Lineament Density | Eleva--tion | Weight |
|---|---|---|---|---|---|---|---|---|
| **Land Cover** | 1 | 1 | 1 | 3 | 1 | 3 | 3 | **18** |
| **Drainage Density** | 1 | 1 | 3 | 3 | 5 | 7 | 9 | **32** |
| **Slope** | 1 | 1/3 | 1 | 1 | 3 | 5 | 7 | **17** |
| **Precipitation** | 1/3 | 1/3 | 1 | 1 | 3 | 5 | 7 | **16** |
| **Soil** | 1 | 1/5 | 1/3 | 1/3 | 1 | 3 | 5 | **9** |
| **Lineament Density** | 1/3 | 1/7 | 1/5 | 1/5 | 1/3 | 1 | 3 | **5** |
| **Elevation** | 1/3 | 1/9 | 1/7 | 1/7 | 1/5 | 1/3 | 1 | **3** |

In the APH model, a reciprocal and consistent matrix A of order n, where n is the number of thematic factors in the criterion, is constructed. For each element $a_{ij}$ of the matrix, the following condition was satisfied:

$$a_{ij} = \frac{1}{a_{ij}} \quad (2)$$

By solving the matrix, the weight of each factor was calculated. In order to solve for weights, the following equation was used:

$$(A - I\lambda)X = 0 \quad (3)$$

where $I$ is an identity matrix of order n, and $X$ is the nx1 weight matrix and $\lambda$ is the eigenvalue.

Since a matrix of order n provides n number of eigenvalues, the largest value of λ was selected for the calculation of the weights. Using the geometric mean method, the weight (X) of each factor is obtained, which are then normalized so that their sum is 1. These were then utilized to calculate the largest positive eigenvalue $\lambda_{max}$. Then maximum $\lambda_{max}$ was selected to recalculate the weights. The values in the paired comparison matrix A must be checked for consistency. It was important to check for consistency because there may be

inconsistency in judgment while comparing the various classes. The following formulas were used for calculating the consistency index:

$$CI = (\lambda_{max} - n)/(n - 1) \quad (4)$$

$$CR = CI/RI \quad (5)$$

where *CI* is consistency index, *CR* is consistency ratios, and *RI* is a random index. Here, RI is the randomized consistency index for the matrix of order n. The used *RI* values in this study are shown in Table 3. For an acceptable level of consistency, the value of *CR* should be greater than 0.1.

*Table 3: Average consistency index*

| S. No. | Order of matrix | Randomized index (RI) |
|---|---|---|
| **1** | 3 | 0.9 |
| **2** | 4 | 1.12 |
| **3** | 5 | 1.24 |
| **4** | 6 | 1.32 |
| **5** | 7 | 1.41 |
| **6** | 8 | 1.45 |
| **7** | 9 | 1.51 |

As discussed earlier, MCET requires assigning ranks (scores) of the classes in the thematic layers. Every thematic layer (except landcover) were divided into 5 classes and each class in the thematic layers was placed into one of the following categories: (5) very good, (4) good, (3) moderate, (2) low, and (1) poor, depending on their groundwater potential level. The ranks were allotted based on field observation and previous similar researches on groundwater potential mapping (Al-Ruzouq et al., 2019; Awawdeh et al., 2014; Brito et al., 2006; Ganapuram et al., 2009; Narendra et al., 2013). The weights of the data layers and the ranks of the classes belonging to each layer are given in Table 4. All data relevant to groundwater potential mapping were collected or created, thoroughly examined, edited, compiled, and assembled in digital format for modeling.

*Table 4: Weights and ranks of the factors used to map groundwater potentiality*

| Parameter | Class | Rank | Weightage |
|---|---|---|---|
| **Land Cover** | Cropland | 5 | 18 |
| | Forest | 2 | |
| | Grassland | 3 | |
| | Shrubland | 3 | |

| | | | |
|---|---|---|---|
| | Bare soil | 1 | |
| **Drainage Density** | 0.7-5.0 | 1 | 32 |
| | 5.1-7.0 | 2 | |
| | 7.1-8.6 | 3 | |
| | 8.7-10.4 | 4 | |
| | 10.5-15.6 | 5 | |
| **Slope** | 0 | 5 | 17 |
| | 0.01-89.81 | 4 | |
| | 89.82-89.93 | 3 | |
| | 89.94-89.98 | 2 | |
| | 89.99-90.00 | 1 | |
| **Precipitation** | 34-54 | 1 | 16 |
| | 55-91 | 2 | |
| | 92-110 | 3 | |
| | 111-146 | 4 | |
| | 147-213 | 5 | |
| **Soil** | Sandy Loam | 5 | 9 |
| | Loam | 1 | |
| | Sandy Clay Loam | 3 | |
| | Clay Loam | 2 | |
| | Clay | 1 | |
| **Lineament Density** | 0-532 | 1 | 5 |
| | 533-2965 | 2 | |
| | 2966-12413 | 3 | |
| | 12414-24982 | 4 | |
| | 24983-54063 | 5 | |
| **Elevation** | -46-170 | 5 | 3 |
| | 171-440 | 4 | |
| | 441-1250 | 3 | |
| | 1251-3531 | 2 | |
| | 3532-6562 | 1 | |

### 3.2.5 VIC-ModFlow coupled model

MOdular Three-Dimensional Finite-Difference Ground-Water Flow model (MODFLOW) is a physically based, three-dimensional, and distributed finite-difference groundwater model that considers aquifer groundwater levels and routes groundwater flow (Harbaugh, 2005). MODFLOW facilitates the estimation of groundwater recharge, pumping, vadose zone percolation, discharge to subsurface drains, and river-aquifer interactions. However, the model lacks the estimation of surface water budget components, such as runoff and soil moisture. The VIC model was coupled with the MODFLOW to develop the VICMF for

the interaction of surface and subsurface through flux exchange by Jin and Sridhar (2010). The VICMF model is based on the interdependent equations that estimate the flow of water in a surface and groundwater hydrologic system. The upward flux (discharge) for the aquifer region from the MODFLOW grid cells for the daily stress period was integrated into the corresponding VIC model grid for the simulation period by the drainage package. The discharge amount into the unsaturated VIC soil layer generated by the MODFLOW can be represented as:

$$\frac{\partial \theta}{\partial t} = \frac{\partial}{\partial z}\left[D(\theta)\frac{\partial}{\partial z}\right] - \frac{\partial K(\theta)}{\partial z} + U_f$$

where θ is the soil moisture content ($L^3/L^3$), D(θ) is the hydraulic diffusivity ($L^2/T$), K(θ) is the hydraulic conductivity (L/T), and z is the soil depth (L).

The simulation of the surface hydrology was done at 0.05 deg resolution by the VIC model while the groundwater simulation was performed at 0.01deg resolution by the MODFLOW model. VIC-MF was simulated by initially calling MODFLOW and running a stress period to generate a flux out of the aquifer for each cell from the drainage package. The MODFLOW simulated flux was added to the soil column in the VIC model, which determines how to handle the additional water. Excess water was added as the baseflow after the unsaturated soil zones became saturated. Subsequently, the recharge flux was calculated by running the VIC model. The flux was added to MODFLOW, which was again ran to estimate the new head, and the process was repeated. The limitation for the number of iterations of the process can be set before proceeding to the next stress period.

### 3.3 Results and Discussion

#### 3.3.1 NIWR for the observed period

The efficiency of the approach in simulating the annual net irrigation water requirement for the MRB was estimated by comparing the VIC simulated and observed irrigation water volume for one crop cycle in the Mun-Chi basin for 2007. The observed volume of water used for irrigation purposes at the country level was obtained from the AQUASTAT FAO's Global Information System on Water and Agriculture database for Thailand for 2007 and was proportioned to the provinces based on the irrigated area (AQUASTAT,

2014). The volumetric estimates of the water demand for the irrigation purpose simulated from the VIC model for the Mun Chi basin for 2007 for one crop cycle were calculated as 2268 million $m^3$ as compared to the observed volume of 2452 million $m^3$ obtained from the AQUASTAT database.

The irrigation water requirement map shows the spatial distribution of the average monthly irrigation water demand for the seven sub-basins in the MRB from 1981 to 2019 (Figure 3). The map specifically coincides with the irrigated area map of the basin shown in Figure 1, exhibiting the efficiency of the irrigation module of the VIC model. The monthly irrigation water demand reaches up to 58 million $m^3$ for a 0.05 deg resolution grid in the delta portion of the basin. The irrigation water demand is higher for the delta sub-basin as the region accommodates more than 50% of the basin irrigated area, while the Mun Chi basin irrigation water demand is scattered throughout the sub-basin.

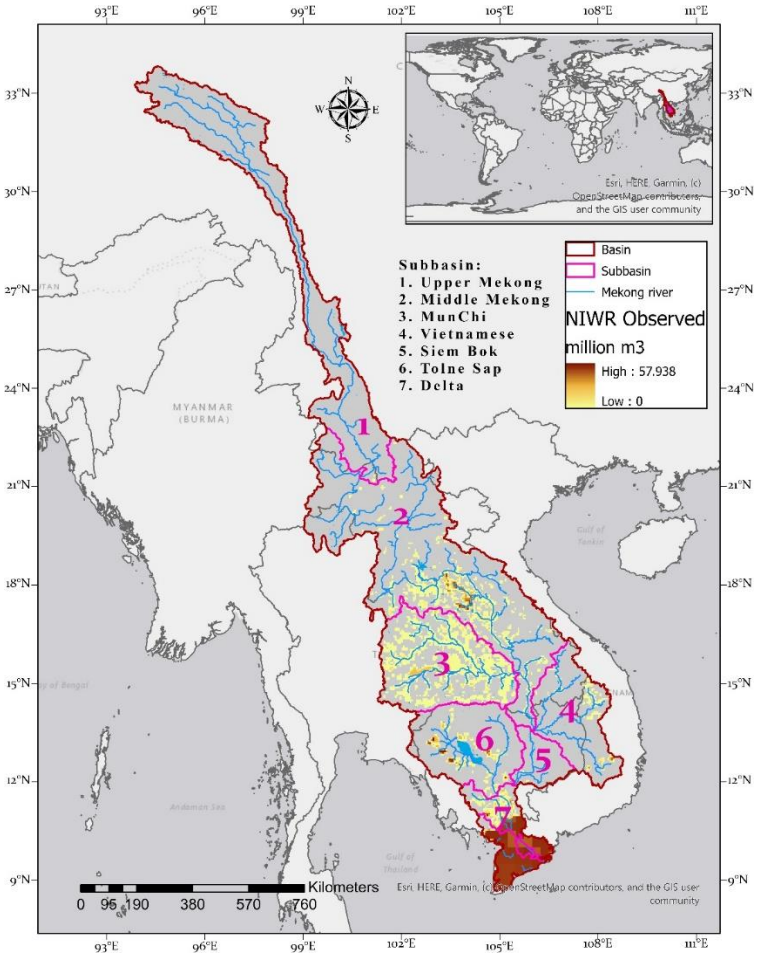


*Figure 3: The average monthly irrigation water requirement map of the Mekong river basin with seven subbasin boundaries from 1981 to 2019.*

Figure 4 shows the monthly variation of the irrigation water demand for the MRB and subbasins from 1981 to 2019. The MRB and subbasins followed a similar pattern of seasonal variation of the water demand with the contrasting demand volume for each basin signifying the proportion of the irrigation area covered within the subbasin. The water demand for irrigation was immensely affected by the monsoon season with the decrease in the demand observed during July-October and maximum value during December-January and March-April. The highest water demand for the MRB was observed in January with value 6200 million $m^3$, while the highest values for Delta, Middle Mekong, Mun Chi, and Tolne Sap subbasins were 5133 million $m^3$, 480 million $m^3$, 280 million $m^3$, and 277 million $m^3$, respectively. On the other hand, the minimum water demand for the MRB with 4750 million $m^3$ was observed during September, while the least water demand for Delta, Middle Mekong, Mun Chi, and Tolne Sap subbasins were 3980 million $m^3$, 320 million $m^3$, 145 million $m^3$, and 224 million $m^3$, respectively.

The monthly variation in the irrigation water demand is governed by the difference in the evapotranspiration between natural (no-irrigation) conditions and free-irrigation conditions. The minimum water demand occurring during August-September due to low evapotranspiration difference and abundant precipitation during the monsoon period. The elevated temperature during the summer period supports high evapotranspiration difference and minimal precipitation was the reason behind high water demand (Figure 5). For the Mun Chi subbasin, the difference in the monthly evapotranspiration between the natural (no-irrigation) and free-irrigation conditions was accounted as 1.5 mm during August-September, while the difference in March-April was 6 mm. Figure 6 shows the annual variation of the irrigation water demand of the Mekong river basin and seven subbasins from 1981 to 2019.

The mean annual irrigation water demand for the irrigation of 66,000 $km^2$ of cropland in the MRB was estimated as 65,070 million $m^3$. The combined total storage capacity of the nine dams situated in the Mun-Chi basin was estimated at 4500 million $m^3$, while the irrigation water demand for Mun Chi was 2600 million $m^3$. However, the combined capacity was sufficient to fulfill the annual water demand of the basin, but the locations of the dam were not favorable for the efficient water supply. The irrigation water demand for

the delta subbasin was highest among all the subbasins in the MRB with an annual demand of 54,000 million $m^3$, while the annual water demand of the Middle Mekong, Tolne Sap, Vietnamese, Siem Bok, and Upper Mekong was estimated as 4933 million $m^3$, 3076 million $m^3$, 3.6 million $m^3$, and 1.3 million $m^3$, respectively. The irrigation water demand of the Middle Mekong and Tolne Sap subbasins was higher than the Mun Chi basin through the irrigated area of the Mun Chi subbasin was more as the Middle Mekong and Tolne Sap host two hot spots of the high irrigation area demand.

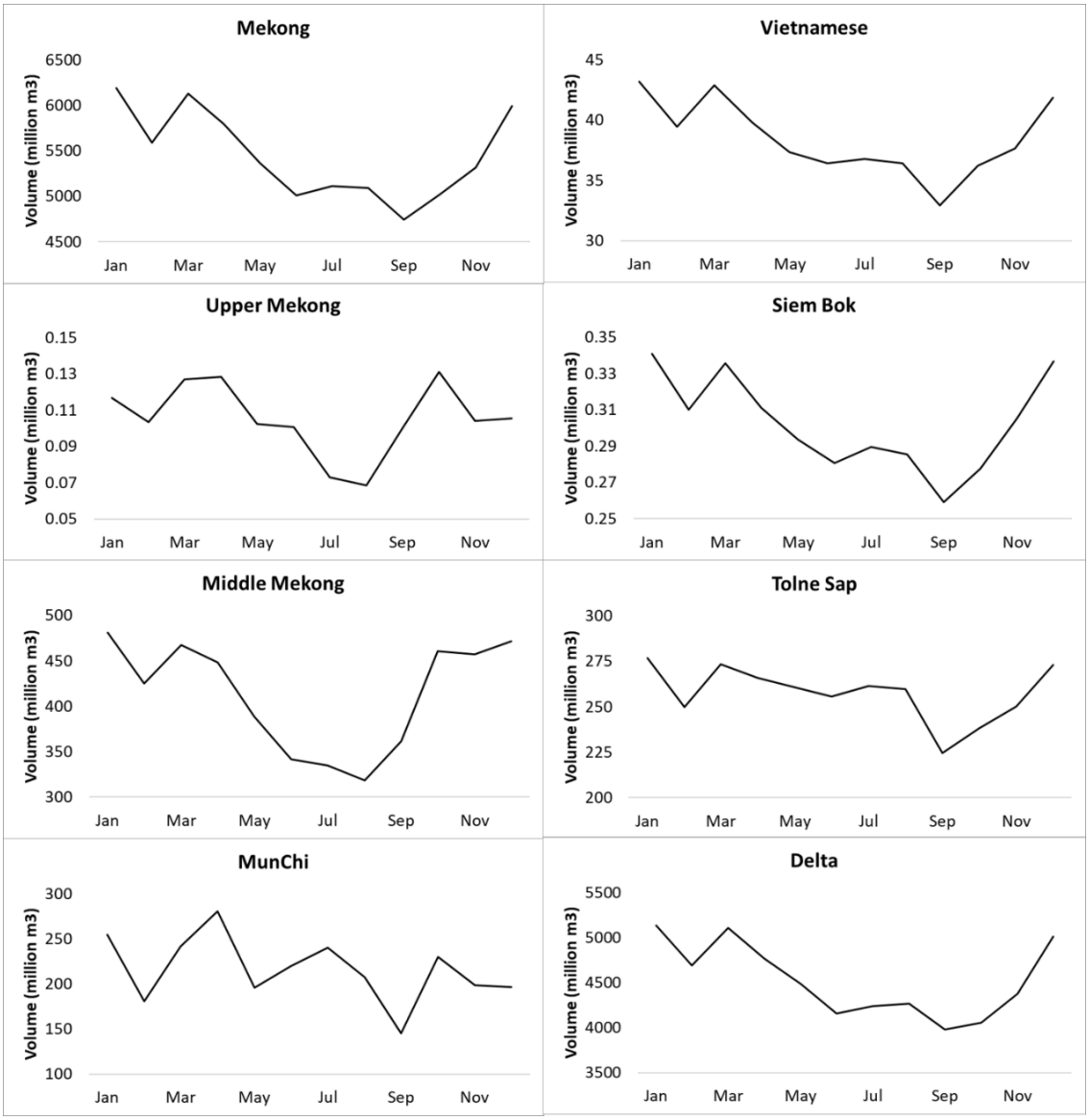


*Figure 4: Seasonal variation of the irrigation water demand of the Mekong river basin and seven subbasins from 1981 to 2019.*

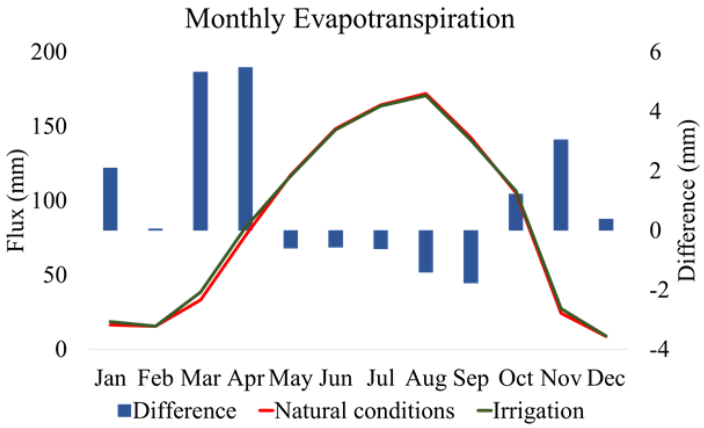


*Figure 5: Comparison of the evapotranspiration for the Mun Chi subbasin under 'irrigation' and 'no-irrigation' conditions from 1981 to 2019.*

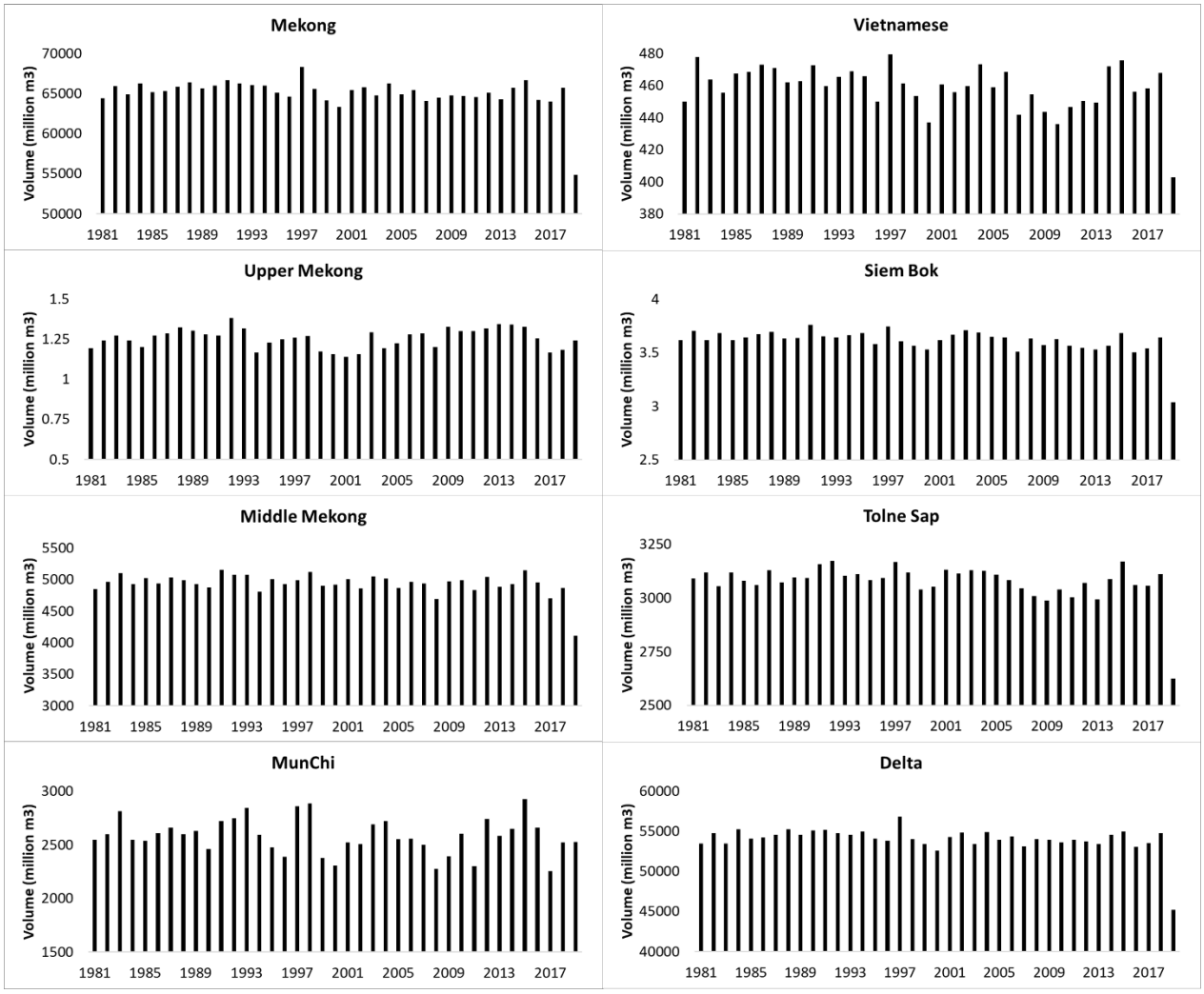


*Figure 6: Annual variation of the irrigation water demand of the Mekong river basin and seven subbasins from 1981 to 2019.*

### 3.3.2 NIWR for the future period

The net irrigation water requirement for the future period is altered by the meteorological conditions of the MRB, specifically modifying the evapotranspiration under the irrigation conditions. Figure 7 shows the monthly net irrigation water requirement map of the MRB for the historic period (1951-2005) and the change in the irrigation water requirement for the future period (2006-2099) under RCP 4.5 and RCP 8.5. The range of the projected change in the irrigation water requirement for the future is expected to be subbasin specific. The change in the water requirement is distinguishable for two subbasins, namely, Mun Chi and Delta, with the contrasting characteristics. The Mun Chi basin is expected to experience an increase in the irrigation water requirement on the concentrated irrigated area adjoining the main tributary of the Mun and Chi rivers. On the other hand, the Delta region will face a decrease in the irrigation water requirement in the future. The seasonal variation of the net irrigation water requirement will be impacted by climate change (Figure 8). The MRB is expected to experience 0.3% and 0.2% decrease in the NIWR in the future period under RCP 4.5 and RCP 8.5, respectively as compared to the historic water requirement for irrigation. The decrease in the NIWR is expected to be in all the months except the summer period, i.e. March-May, however, the decrease is expected to be the highest during the monsoon season, i.e. July-October. The average decrease in the monsoon season in NIWR will account for 0.75% and 0.89% for the MRB under RCP 4.5 and RCP 8.5, respectively. Contrarily, the increase in the NIWR for the future period is expected as 0.7% and 0.98% during the summer season under RCP 4.5 and RCP 8.5, respectively. A similar pattern of the NIWR change in the future under climate change will be experienced by the Delta, Siem Bok, Vietnamese and Middle Mekong subbasins. On the other hand, Upper Mekong and Mun Chi basin is expected to show an increase in the NIWR throughout the year. Specifically, the increase in the NIWR during the summer season will account as 6% and 9.7% for the Upper Mekong under RCP 4.5 and RCP 8.5, respectively. Similarly, the increase for the Mun Chi basin is expected to be 8.3% and 12.5% during the summer season under RCP 4.5 and RCP 8.5, respectively. Moreover, the seasonal variation of the NIWR for the MRB and subbasins will be similar for the future period as compared to the historic period.

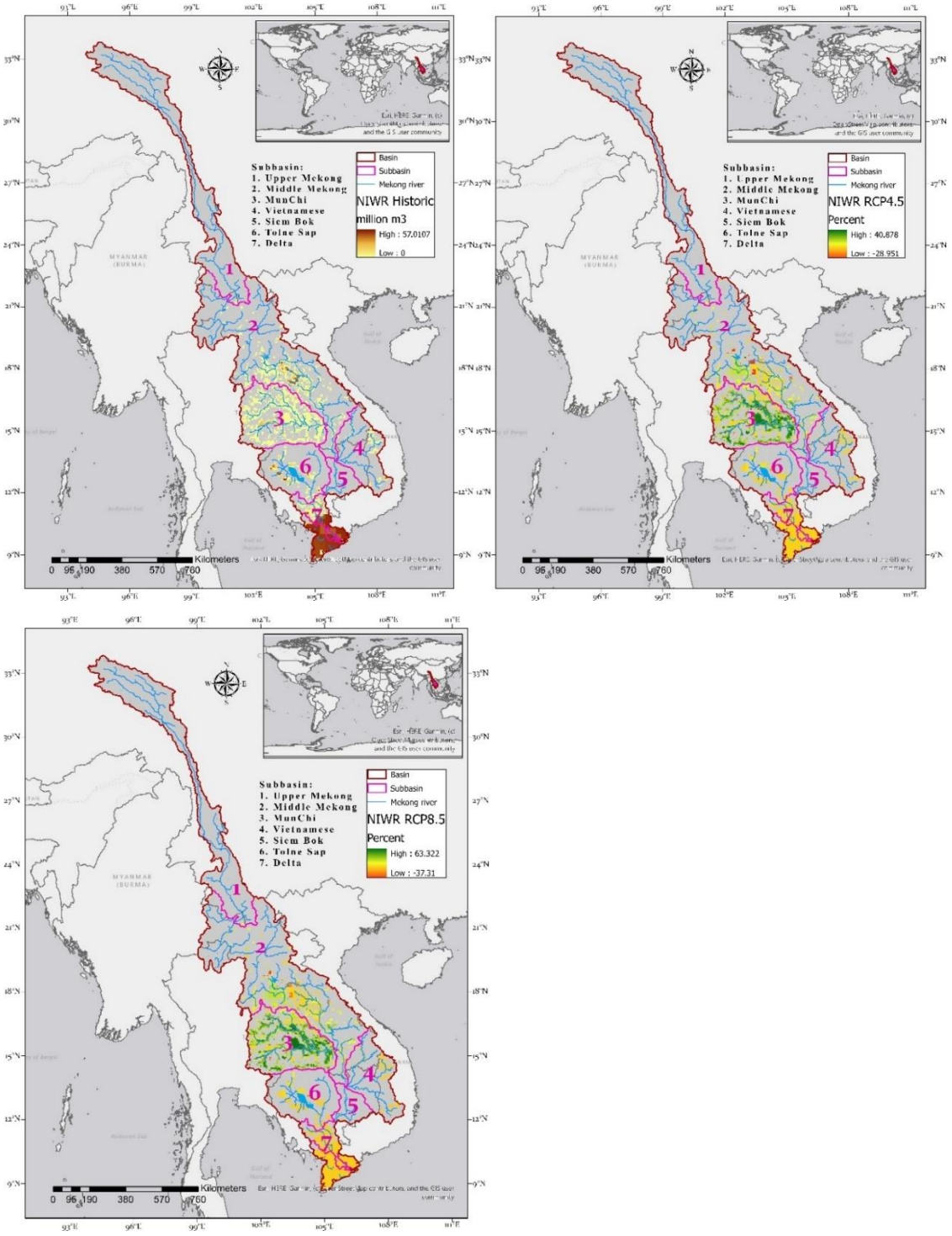


*Figure 7: The average monthly irrigation water requirement map of the Mekong river basin with seven subbasin boundaries for the historic period (1951-2005) and change in the irrigation water demand for the future period (2006-2099) under RCP 4.5 and RCP 8.5.*

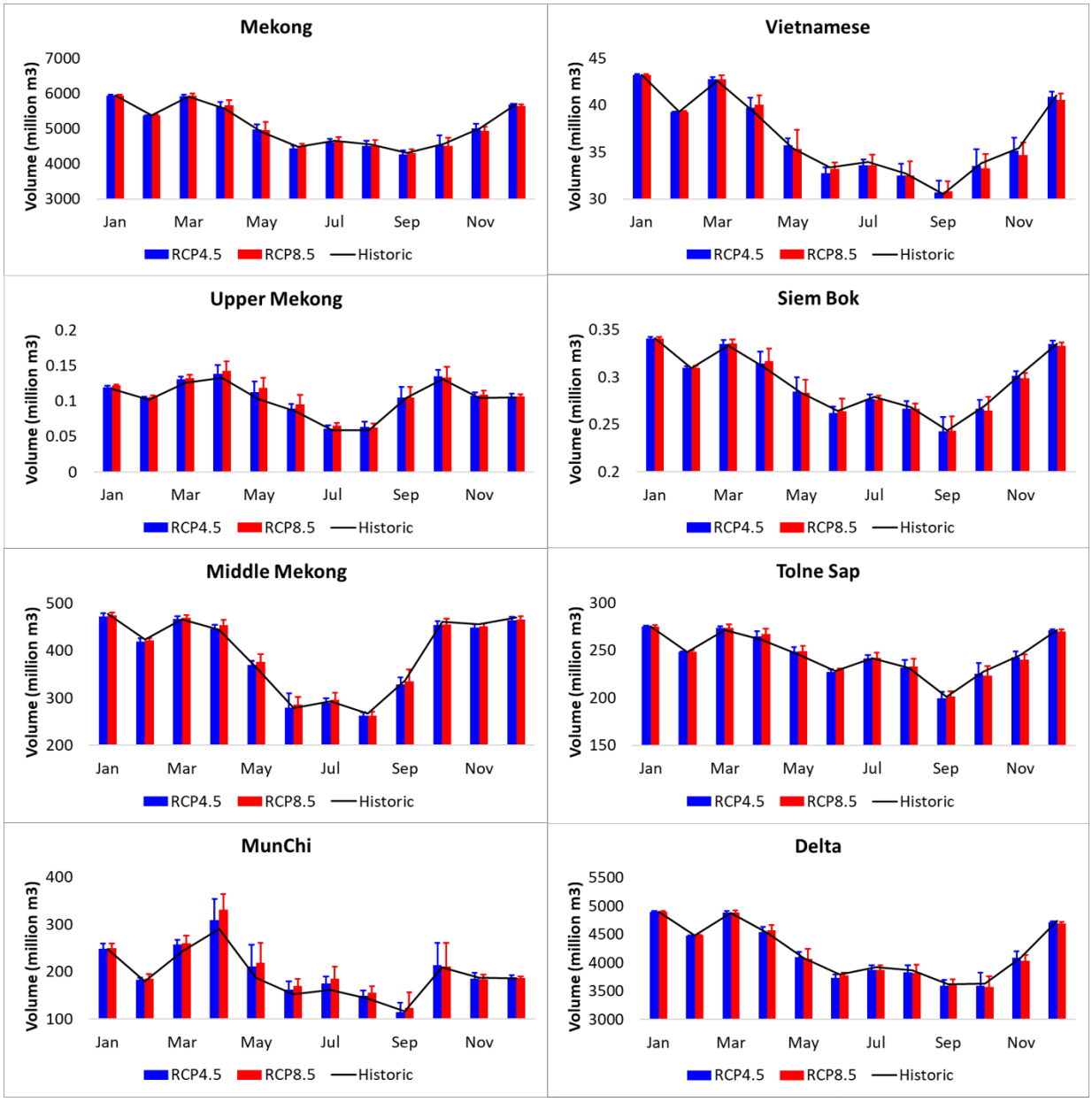


*Figure 8: Seasonal variation of the irrigation water demand of the Mekong river basin and seven subbasins for the historic period (1951-2005) and future period (2006-2099) under RCP 4.5 and RCP 8.5.*

Figure 9 shows the annual variation of the irrigation water demand of the Mekong river basin and seven subbasins for the historic period (1951-2005) and the future period (2006-2099) under RCP 4.5 and RCP 8.5. The annual fluctuation in the NIWR during the historic and future periods was due to the variation in the precipitation and temperature while the irrigated area was assumed to be the same. The mean annual NIWR for the historic period

was estimated as 60970 million $m^3$ for the Mekong river basin with the major proportion contained in the Delta and Middle Mekong subbasins. The mean historic annual irrigation water requirement was estimated as 50530 million $m^3$, 4740 million $m^3$, 2950 million $m^3$, 2300 million $m^3$, 440 million $m^3$, 3.5 million $m^3$, and 1.2 million $m^3$ for Delta, Middle Mekong, Tolne Sap, Mun Chi, Vietnamese, Siem Bok, and Upper Mekong subbasins, respectively.

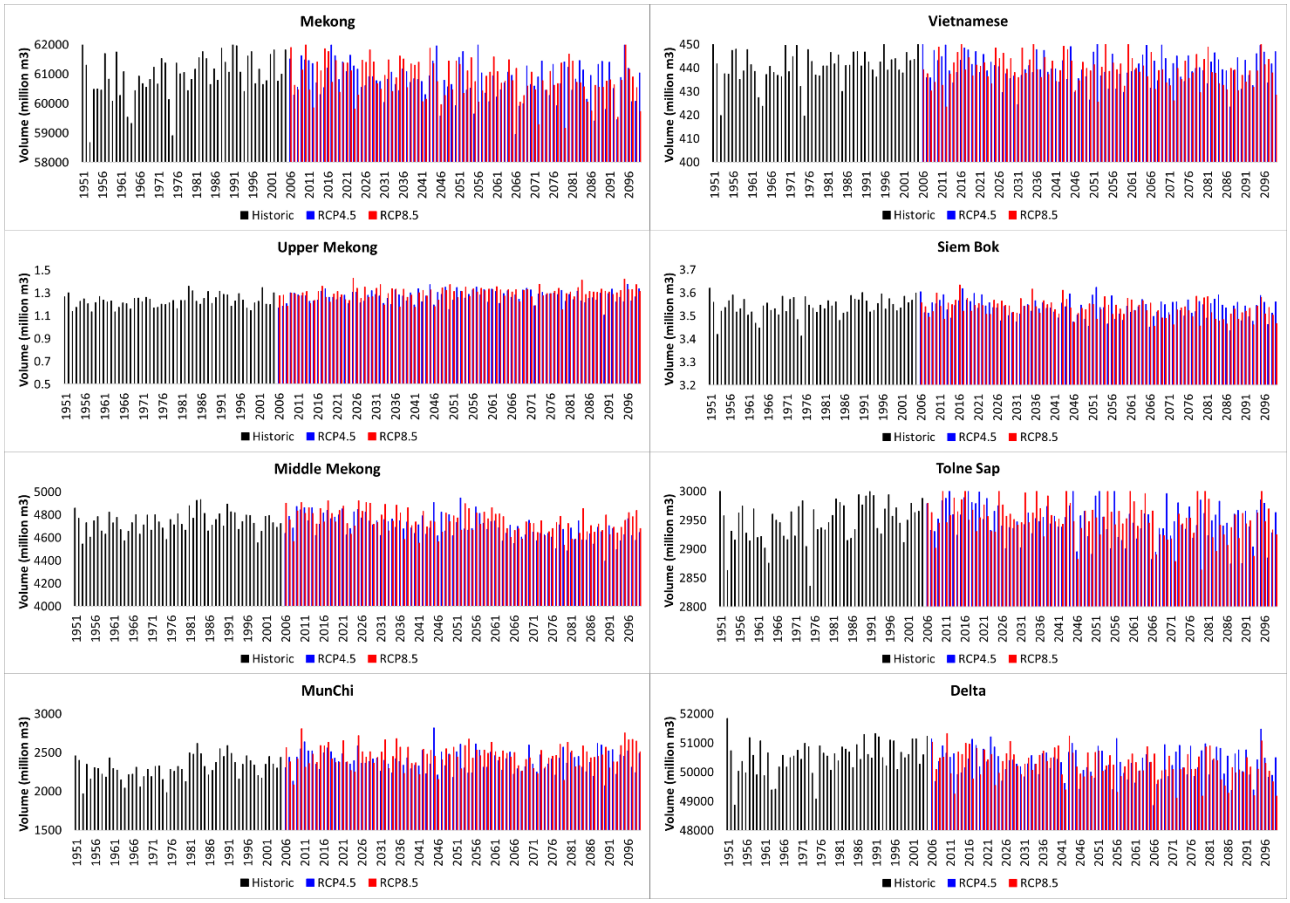


*Figure 9: Annual variation of the irrigation water demand of the Mekong river basin and seven subbasins for the historic period (1951-2005) and future period (2006-2099) under RCP 4.5 and RCP 8.5.*

The decrease in the projected NIWR is expected to be highest for the Delta region ranging between 0.46% and 0.58% for the RCP 4.5 and RCP 8.5, respectively. Vietnamese and Siem Bok are expected to experience a decrease of 0.2% and 0.3% in the projected NIWR under RCP 4.5 and RCP 8.5, respectively. However, the NIWR is projected to increase by 3.8% and 6.4% with respect to the historic mean for Upper Mekong and Mun Chi subbasins

under RCP 4.5 and RCP 8.5, respectively. Tolne Sap will also experience a positive change in the projected NIWR with a nominal increase of 0.04% under RCP 4.5 and 0.17% under RCP 8.5. While the change will be -0.85% and +0.23% for the Middle Mekong for the future period under RCP 4.5 and RCP 8.5.

### 3.3.3 Groundwater potential map

Groundwater potentiality mapping was achieved by investigating the topographical, hydrological, meteorological, and geoenvironmental conditions governing its occurrence. Therefore, the controlling factors on groundwater movement, storage, and occurrence were explored and digitally mapped as thematic layers. The layers include elevation, slope, drainage density, land cover, soil, lineament density, and precipitation. The factors used vary spatially, and it implies (1) elevation; (2) slope, which controls water flow energy; (3) drainage density, which plays a vital role in the runoff distribution and level of infiltration; (4) land cover, which defines the permeability of the surface; (5) soil texture, which determine infiltration rate of the soil; (6) lineaments (rock fractures), which enhances significantly hydraulic conductivity; and (7) precipitation as a source of water.

*Elevation:*

The elevation variation in the MRB was extracted using the 90 m SRTM elevation map. The range of the elevation varies from -46 m to 6562 m. The region falling in China is associated with a high elevation, whereas the lower Mekong region compromising Thailand and Cambodia have relatively flat terrain with an altitude of less than 170 m. The central portion of the basin had the transition characteristics from high altitude to low altitude. Therefore, the lower Mekong region had a high probability for the groundwater reserves (Solomon & Quiel, 2006; Subba Rao, 2006). The MRB is classified into five classes based on the elevation as shown in Figure 10. The weight of the elevation layer is relatively less as compared to other layers (Table 4).

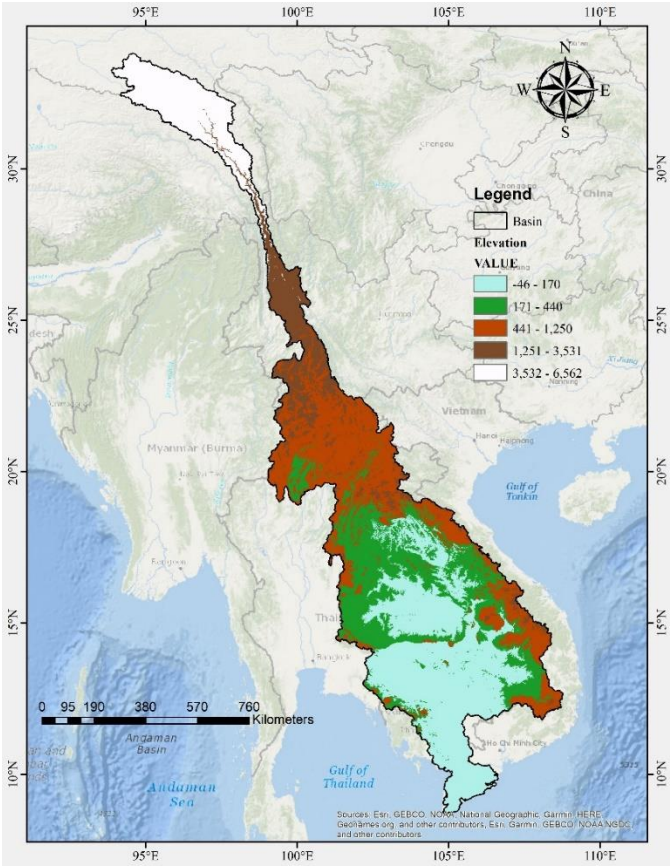


*Figure 10: Elevation map of the Mekong river basin*

*Slope:*

The slope was derived directly from the elevation map, as shown in Figure 11. The slope value varies from 0º to 89.99º. The pattern of the slope was similar to the trend of the elevation variation in the basin. Previous studies indicated that groundwater potential zones increase with a gentle slope (Sener et al., 2005; Shaban et al., 2006). The slope of the MRB had considerable weight for deriving the GPM (Table 4).

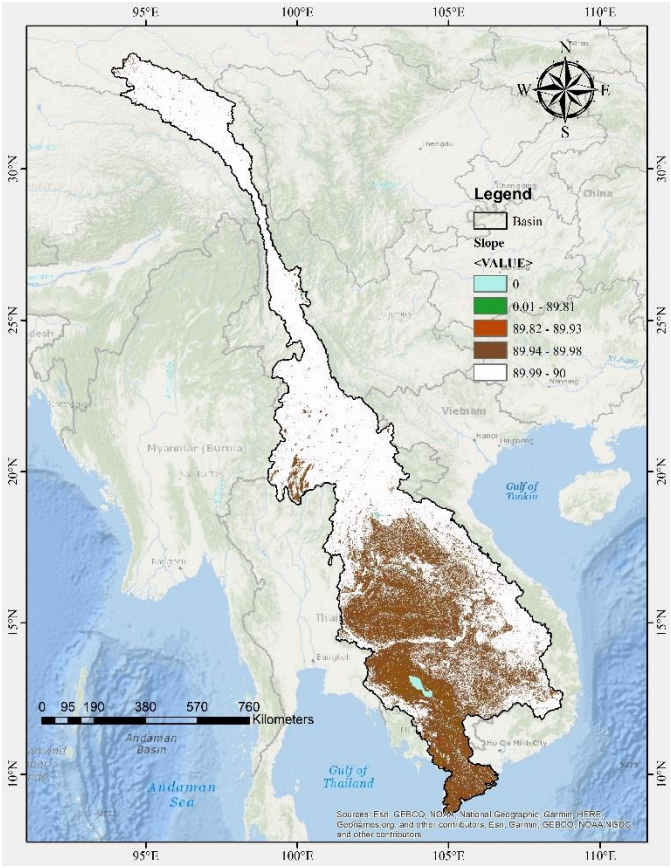


*Figure 11: Slope map of the Mekong river basin*

*Drainage density:*

Many researchers emphasize that groundwater potentiality increases in the region of high drainage density (Edet et al., 1998; Sener et al., 2005; Shaban et al., 2006). The drainage system of the MRB was developed through the watershed delineation in the ArcGIS platform using the SRTM DEM. The main stem of the Mekong River along with the tributaries are shown in Figure 12. The spatial signatures of the Mekong River and tributaries were utilized to estimate the density of the drainage varying from 0.7 to 15.6 km/km$^2$ (Figure 12). The patches of the high drainage density (10.5-15.6 km/km$^2$) area were distributed throughout the lower Mekong basin region as more of the tributaries are present due to the low slope. The drainage density map was the most sensitive layer defining the groundwater potential zones (Table 4).

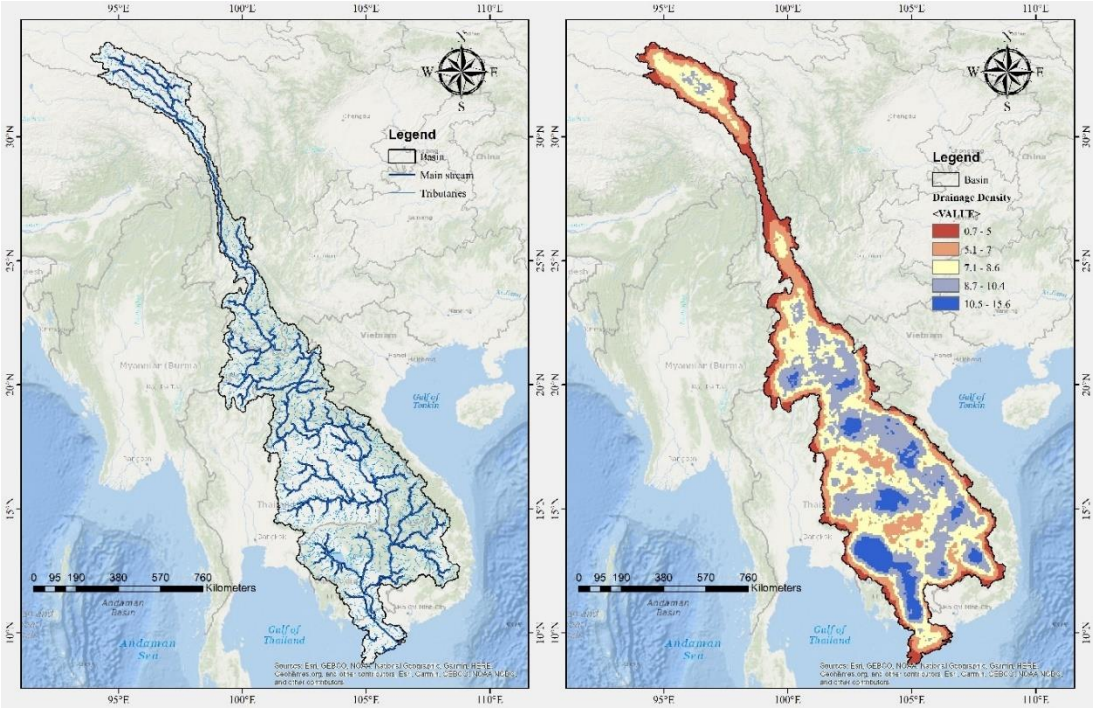


*Figure 12: The Mekong River and tributaries (left); and drainage density map of the Mekong river basin (right)*

*Land cover:*

The land cover of the area provides important indications of the extent of groundwater requirement and utilization (Ganapuram et al., 2009; Narendra et al., 2013). Also, the land cover indicates the roughness and resistance to the water flow in the region. The ESA-CCI land cover map (300 m spatial resolution) for the MRB shows the 43% area coverage by the cropland, followed by forest (37%), grassland (9%), and shrubland (8%) (Pokhrel et al., 2018). The central and delta region of the MRB is covered with the cropland, whereas the eastern region is occupied by the forest cover (Figure 13). The weight assigned to the land cover layer was 18 (Table 4).

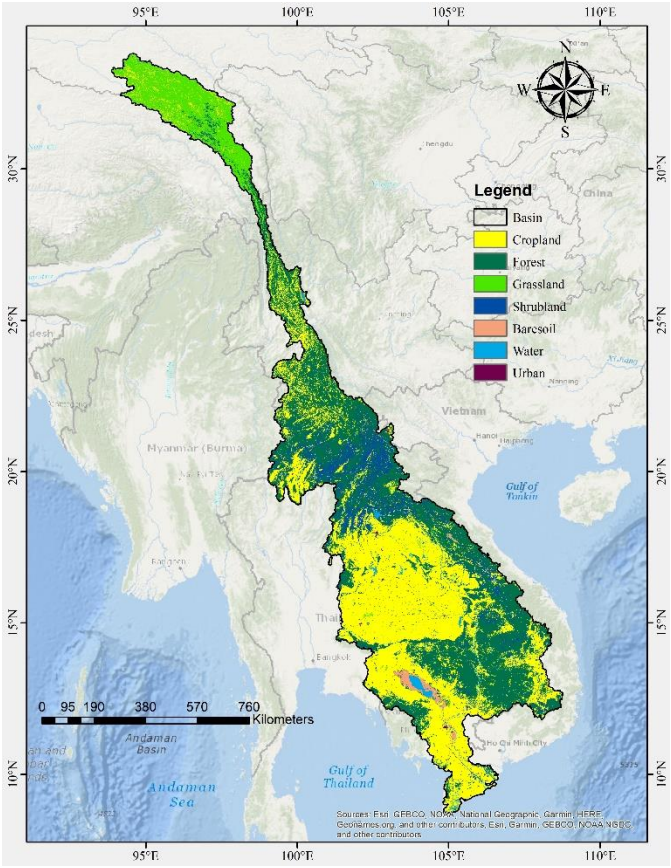


*Figure 13: Land cover map of the Mekong river basin*

*Soil:*

A digital soil map was obtained from the Hybrid State Soil Geographic (STATSGO) / Food and Agriculture Organization (FAO) at 25 km spatial resolution. Textually, the soil cover in the region consists of five soil units: clay loam (37.4%), loam (24.9%), sandy loam (17.3%), clay (12.6%), and sandy clay loam (7.8%). As the permeability of loam soil is better than clay soil, the sandy loam has the highest permeability between all the soil units in the MRB. The spatial distribution of the soil texture indicates the higher likelihood of the groundwater zone in the central MRB comprising of Thailand and Cambodia (Figure 14). The soil texture was given a weight of 9.

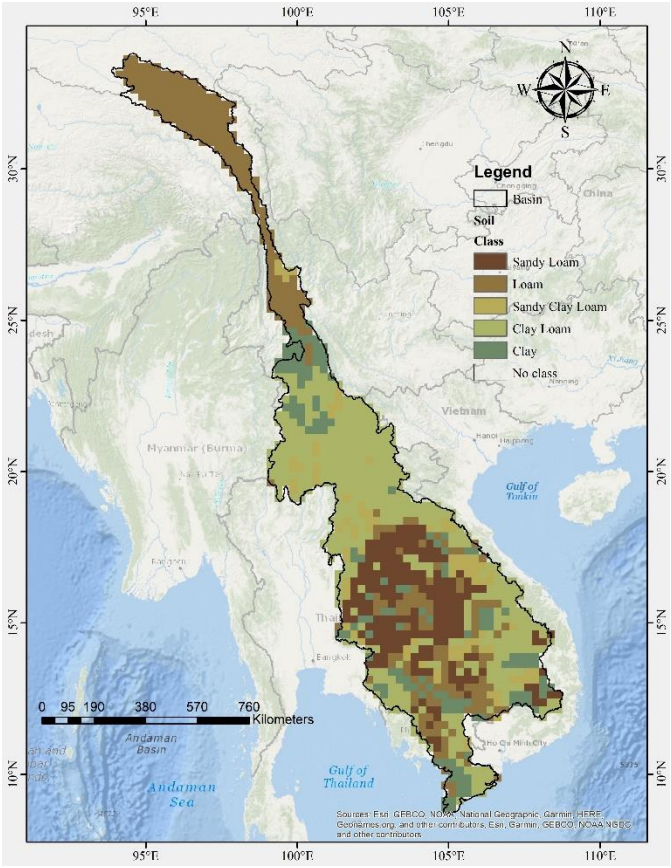


*Figure 14: Soil texture map of the Mekong river basin*

*Lineament density:*

Since structural features such as fractures act as conduits for surface water and rainfall and enhance secondary porosity of rocks, lineaments analysis for groundwater exploration is a very important step. Lineaments provide helpful clues to the movement and storage of groundwater. According to many studies, groundwater potential increases with higher lineament length density (Sener et al., 2005; Shaban et al., 2006; Teeuw, 1995). The lineament of the MRB was identified using the ASTER dataset of 30 m spatial resolution (Figure 15). In groundwater exploration studies, lineament density is used instead of lineaments solely. The lineament density map in the range of 0-54,000 ($m/km^2$) was categorized into five classes and assigned ranks according to Table 4 (Figure 15). Based on the AHP, the lineament density factor was assigned a weight value equal to 5.

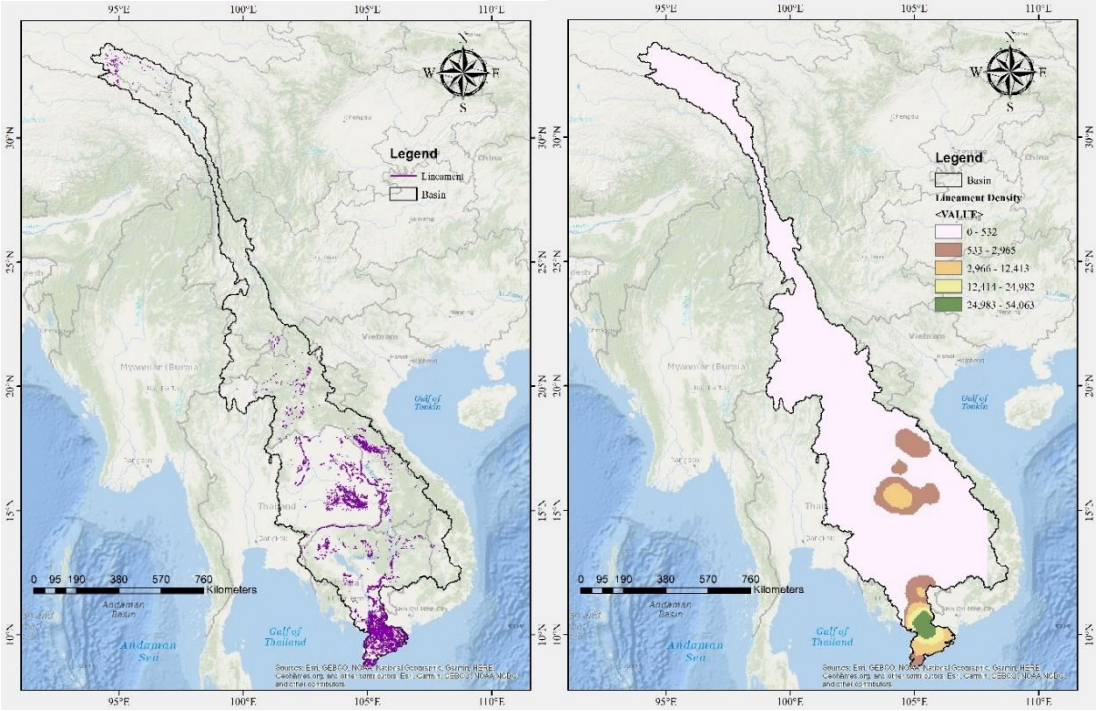


*Figure 15: Lineaments extracted from ASTER data (left); and lineament density map of the Mekong river basin (right)*

*Precipitation:*

Precipitation is the source of water in the MRB and the spatial distribution of the precipitation controls the groundwater potentiality in the basin. The regions with high precipitation are expected to have more probability for groundwater reserves. APHRODITE daily precipitation gridded product at 0.25$^{o}$ resolution was processed for the estimation of the mean monthly precipitation from 1952 to 2015. The spatial heterogeneity of precipitation is shown in Figure 16. The mean monthly precipitation varies from 35 mm (in the upper MRB) to 213 mm (eastern region of MRB). The weight assigned to the precipitation factor was 16.

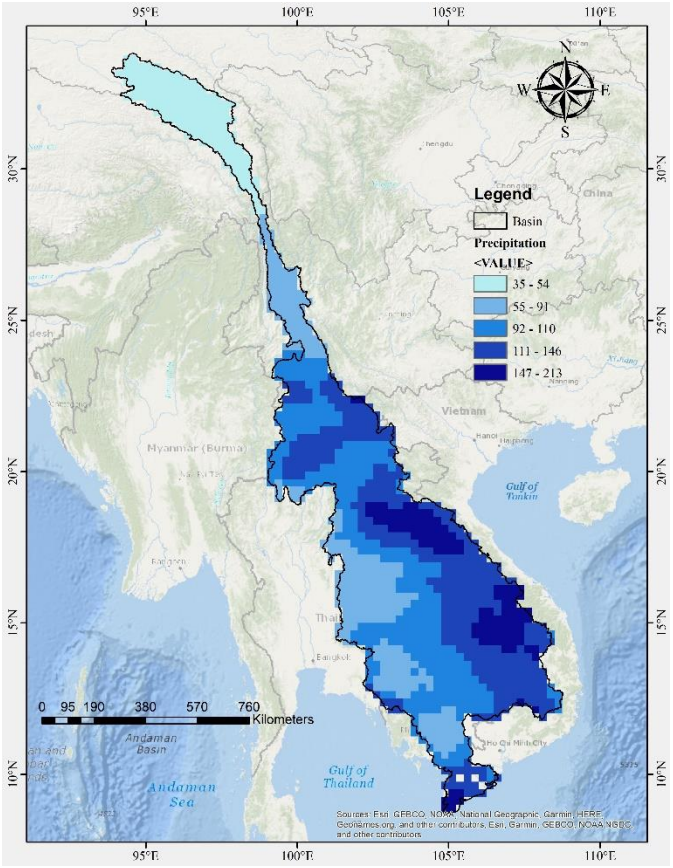


*Figure 16: Monthly Precipitation map of the Mekong river basin*

*Geology:*

The geology map provides information on the underlying rocks and structures below the earth's surface. The geology map was intended to prepare using the supervised classification of the Landsat 8 OLI TIRS images with the USGS geological map. But the majority of the area of MRB was not classified in the USGS geological map (Figure 17). Therefore, the geology factor was excluded for the estimation of the GPM for the basin.

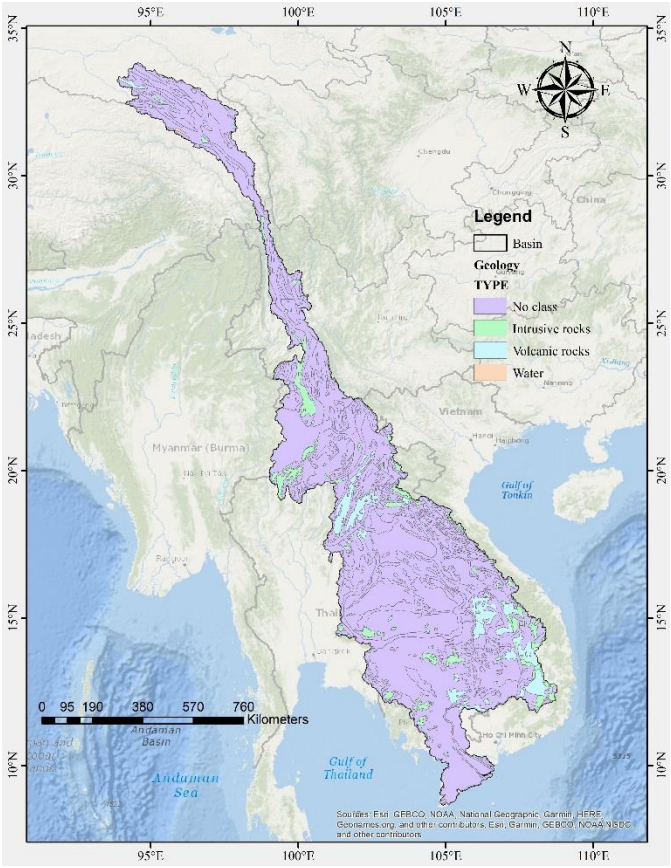


*Figure 17: Geology map of the Mekong river basin*

*Groundwater Potential Map:*

The GPM for the Mekong river basin, derived from the adopted algorithm with the assigned weighting and ranking presented in Section 3, is shown in Figure 18. Depending on the groundwater capacity, five categorical zones of potential groundwater were presented: very low, low, moderate, high, and very high. These zones delineate areas where the subsurface has varying degrees of available groundwater. Before attempting any further analysis, the resultant GPM in Figure 18 was validated through the hydrogeological map of the lower Mekong basin with the groundwater potentials. The comparison of the derived groundwater potential map with the hydrogeology map was in good agreement with the coinciding locations of the high potential zones.

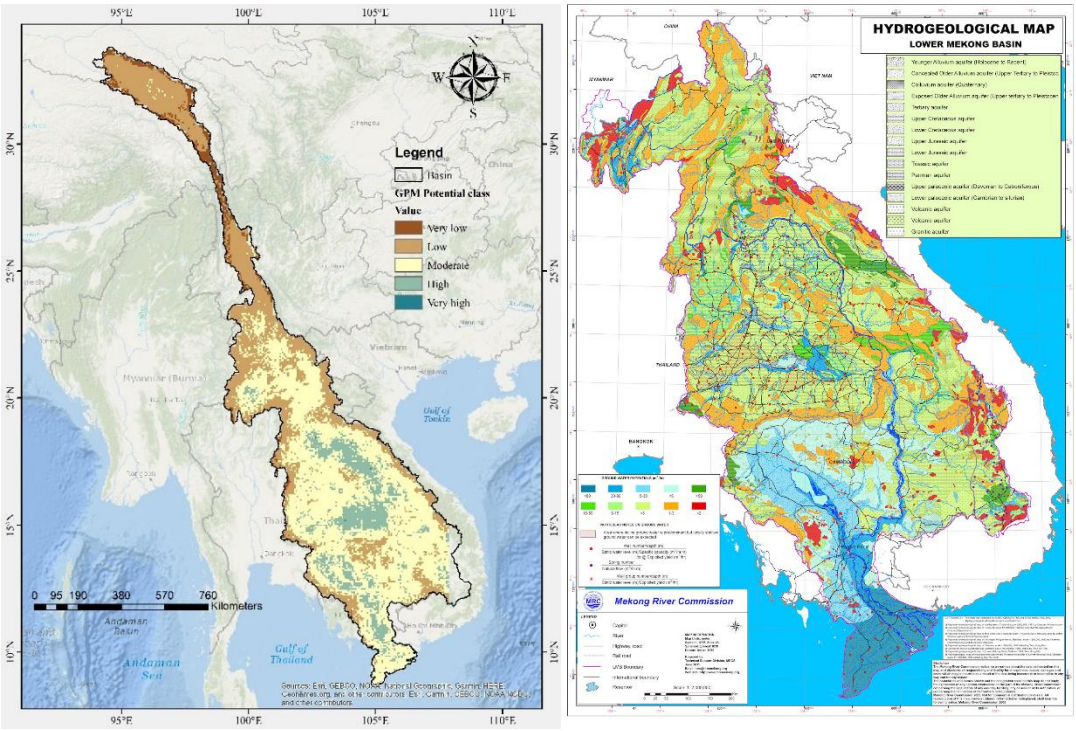


*Figure 18: Groundwater Potential Map (GPM) for the Mekong river basin (left); and Lower Mekong basin hydrogeology map with the groundwater potential (source: Mekong River Commission, obtained from [https://opendevelopmentmekong.net/topics/ground-water/](https://opendevelopmentmekong.net/topics/ground-water/)) (right)*

Table 5 shows the percentage coverage of each class of the GPM in the Mekong river basin. The map shows that most of the area is occupied by moderate potential zone (50.89%), followed by the low potential zone (33.23%), high potential zone (11.92), very low potential zone (3.94%) and a negligible amount of very high potential zone (0.02%), respectively. It can be inferred from the GPM that the upper portion of the basin, mainly consisting of the China territories had low to very low groundwater potential. High altitude with a steep slope and low drainage density caused the low groundwater potential in the area. However, the moderate potential zone was present through the central and lower portion of the MRB consisting of Thailand, Cambodia, Laos, and Vietnam. But the high potential zones were confined to the area of Laos and the central region of Thailand. The presence of a large number of tributaries and flatter land terrain increased the groundwater potentiality of this region.

Mathematically, the GPM for the Mekong river basin can be calculated using the following equation:

$$GPM = (18 \times Land\ cover) + (32 \times Drainage\ density) + (17 \times Slope) + (16 \times Precipitation) + (5 \times Lineament\ density) + (3 \times Elevation) \quad (6)$$

*Table 5: Classification of groundwater potential zones in the Mekong river basin*

| S. No. | GPM potential class | Area (%) |
|---|---|---|
| **1** | Very low | 3.94 |
| **2** | Low | 33.23 |
| **3** | Moderate | 50.89 |
| **4** | High | 11.92 |
| **5** | Very high | 0.02 |

### 3.3.4 Fluctuation in the baseflow

The interaction between the surface and subsurface fluxes was simulated using the VICMF model for dry period (November-May) from 2016 to 2019. The simulation was done for the region occupied by the Khorat aquifer in the MunChi basin in the Thailand region. The input for the model in additional to the VIC forcing were horizontal and vertical hydraulic conductivity, specific storage, storativity, specific yield, and porosity based on the subsurface soil type, classified as sandy clay loam, sandy loam, clay and loam. The effect of the groundwater on the streamflow was evaluated at the outlet point of the MunChi subbasin located at the Pakmun location.

Figure 19 shows the comparison of the streamflow simulated by the VIC and VICMF models for the dry season from 2016 to 2019 at Pakmun location. Due to non-availability of the observed data at the Pakmun location, the simulated data was compared with the difference in the streamflow observed at the upstream (Mukdahan gage station) and downstream (Pakse gage station) of the MunChi basin. The streamflow was mainly constituted of the base flow during the dry period (November-May). Due to the contribution of the groundwater fluxes, the streamflow of the MunChi region was increased by 60%, accounting a difference of 80 $m^3$/sec between the VIC and VICMF simulated streamflow. Moreover, the year-to-year change in the non-monsoon streamflow varied from +5% to +150% due to groundwater interaction from 2016 to 2019.

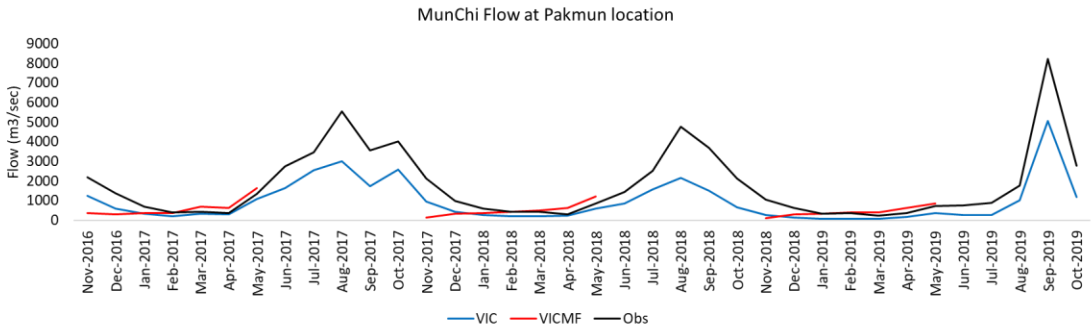


*Figure 19: Comparison of the VIC and VICMF simulated streamflow at the outlet of the MunChi subbasin*

Figure 20 shows the daily drainage and recharge volume of the Khorat aquifer in the MunChi basin from 2016 to 2019. The drainage represents volume of the water leaving the aquifer, while the recharge represents the water volume getting into the aquifer. The net effect of the drainage and recharge volume determines the change in the streamflow and water level of the aquifer. The daily drainage volume from the aquifer varied from 450 million $m^3$ in November to 500 million $m^3$ in May with the similar cycle of variation between the years. Similarly, the recharge volume initiates with nil recharge in November and reaches the maximum value during May accounting 10,000 million $m^3$ in 2017, 6000 million $m^3$ in 2018, and 3000 million $m^3$ in 2019.

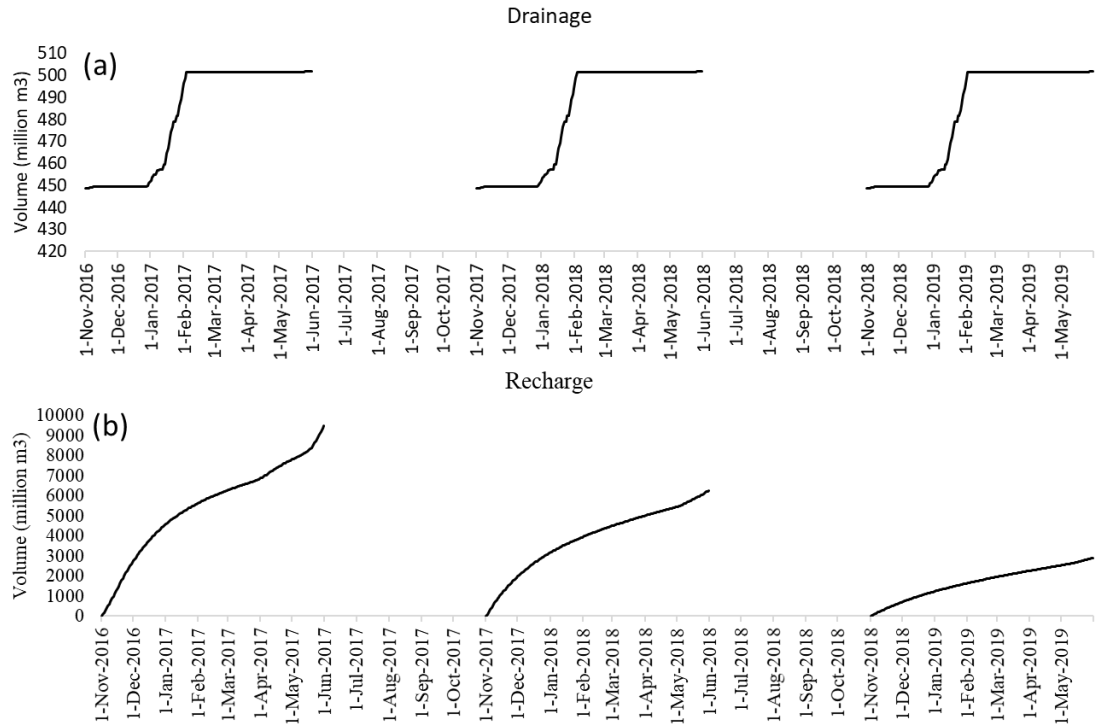

*Figure 20: Drainge volume and recharge volume for the Khorat aquifer in the MunChi basin*

The effect of the increasing drainage volume, increasing streamflow and reducing recharge volume within a year resulted in the lowering the water level of the aquifer from November to May (Figure 21). The water level of the Khorat aquifer ranges from 15.6 cm to 8.1 cm from 2016 to 2019. Figure 22(a) show the spatial distribution of the average water level of the aquifer for 2016 with the most of the central region within the same depth. The change in the water level from 2016-17 to 2017-18 is shown in figure 22(b) with majority of the region experienced a nominal change of less than 5mm, while the water level increased by more than 22mm in the southern region of the aquifer and decrease in the water level experienced by the north-eastern part. On the other hand, during 2018-19, the increase in the water level expands towards the central region of the aquifer with a value of more than 22 mm.

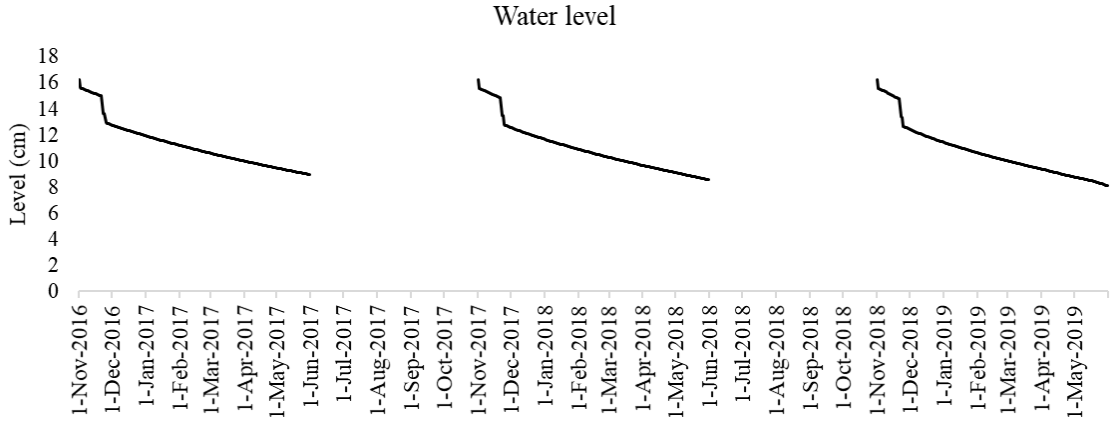


*Figure 21: Change in the water level of the Khorat aquifer in the MunChi basin*

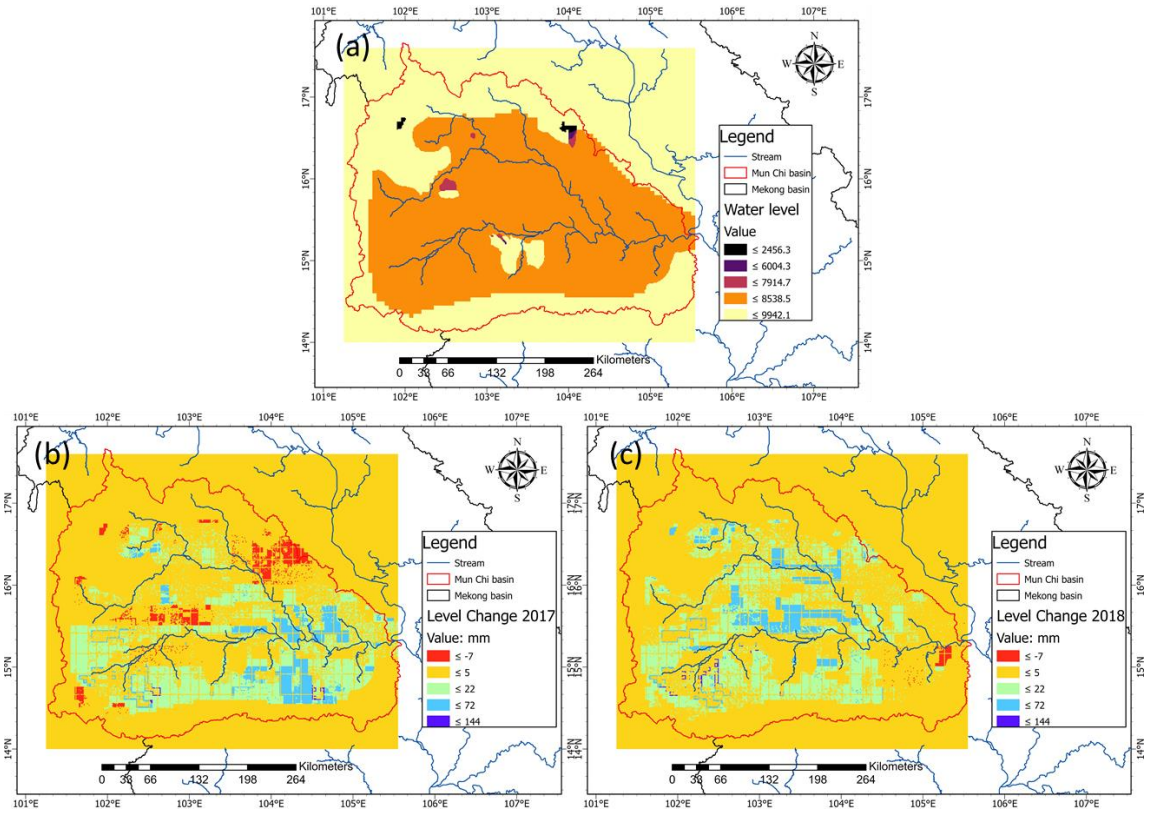


*Figure 22: Spatial distribution of the water level of the Khorat aquifer in the MunChi basin (a), and (b) change during 2017, and (c) 2018*

Figure 23 shows the daily downward flux from the soil column to the aquifer for the dry season from 2016 to 2019. The daily fluctuation of the total downward flux from the three soil layers of the VIC column was highest during November and decreases gradually to the minimum value of 0.2 mm/day during March-April, then increases till May. The range of the downward flux was 1.8 mm/day to 0.2 mm/day. The spatial variation of the average daily downward flux for the aquifer region is shown in figure 24(a). The average daily downward flux for the MunCh subbasin was less than 0.65 mm/day. The change in the downward flux ranges from -0.3 mm to 0.23 mm (figure 24b and 24c). The downward flux decreased by more than 0.5 mm/day in the south eastern region of the MunChi subbasin, while an increase of more than 0.07 mm/day was observed in the north and north western region during 2017-18. On the other the decrease in the downward flux expands to central and northern region of the MunChi subbasin during 2018-19.

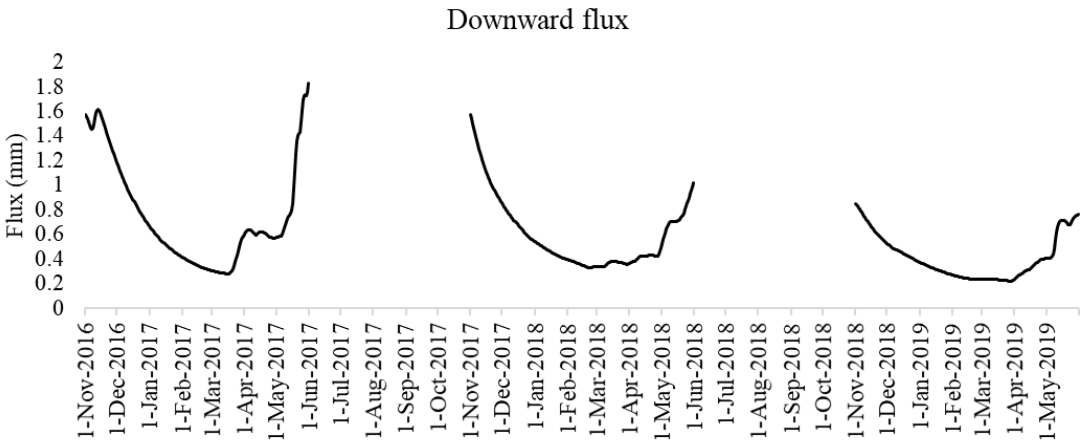


*Figure 23: Daily variation of the downward flux from the soil column of the aquifer region*

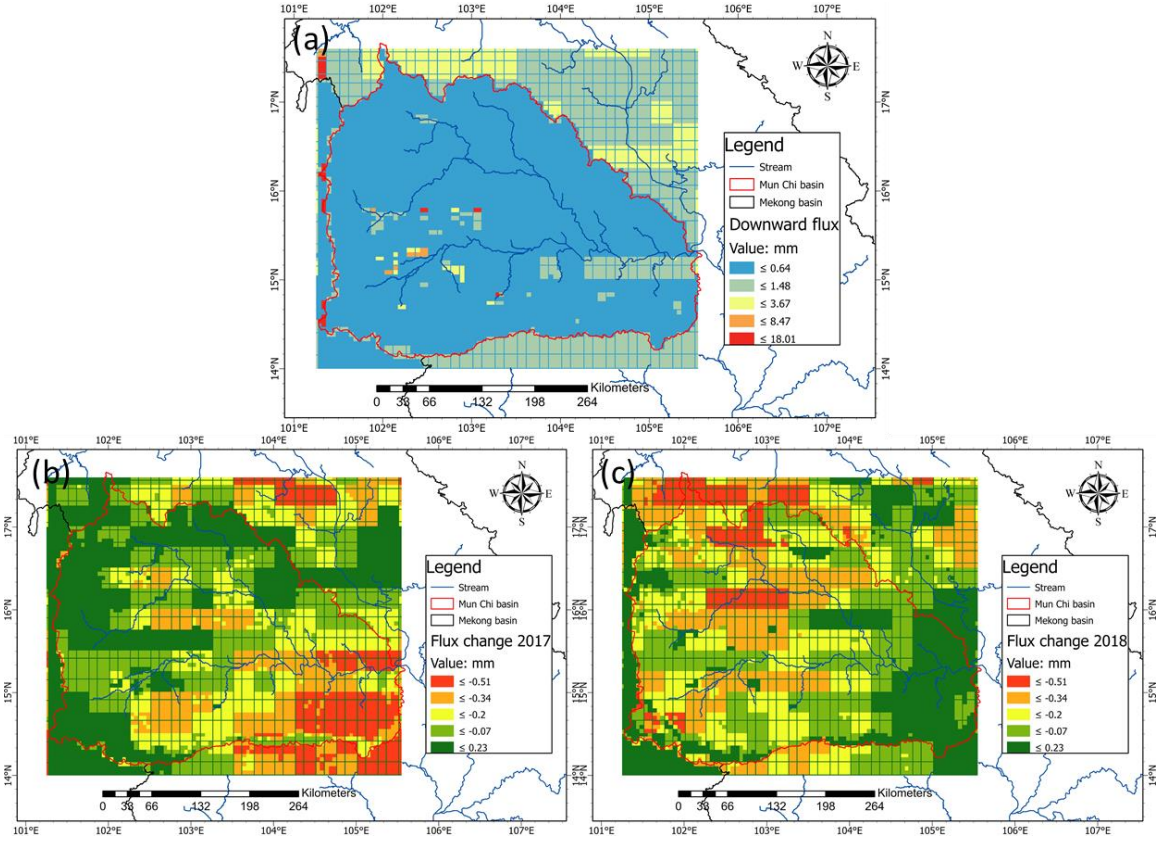


*Figure 24: Spatial distribution of the downward flux in the MunChi basin (a), and (b) change during 201, and (c) 2018*

### 3.4 Conclusion

In this study, the net irrigation water requirement for the MRB was estimated under the impact of climate change. Remote sensing data and GIS techniques proved to be a valuable tool for exploring the groundwater resources in the data scare region of the Mekong river basin. The conclusions of the study are:

- NIWR was estimated for the MRB using the improved VIC model with the irrigation scheme for the observed period classifying the basin into seven subbasins, namely, Upper Mekong, Middle Mekong, Mun Chi, Vietnamese, Siem Bok, Tolne Sap, and Delta. The simulated NIWR for the Mun Chi subbasin for 2007 estimated as 2268 million $m^3$ showed comparable volume to the observed estimates of 2452 million $m^3$ obtained from the AQUASTAT database.
- The total irrigated area of the MRB was estimated as 66,000 $km^2$ with the proportion distributed between the subbasins as 52%, 30%, 12%, and 5% for Delta, Mun Chi, Middle Mekong, Tolne Sap, respectively. The irrigation water requirement for the MRB was calculated as 65,000 million $m^3$ for the observed period (1981-2019). Moreover, the NIWR for the Delta, Middle Mekong, Tolne Sap, Mun Chi, Vietnamese, Siem Bok, and Upper Mekong regions were estimated as 54,000 million $m^3$, 5000 million $m^3$, 3000 million $m^3$, 2500 million $m^3$, 450 million $m^3$, 3.6 million $m^3$, and 1.3 million $m^3$, respectively.
- The climate is generally expected to benefit the MRB with a decrease in the NIWR as 0.25% for the future period as compared to the historic period. Similarly, the projected NIWR will reduce for Delta, Siem Bok, Vietnamese, and Middle Mekong with the value ranging from 0.53% to 0.24%. On the other hand, the Upper Mekong and Mun Chi will face an increase of 5% in the projected NIWR. The seasonal variation of the NIWR is expected to increase during the summer season (March-May) and fall during the monsoon season (July-October).
- A weighted overlay analysis was utilized to explore groundwater potential zones. A total of seven factors were determined and prepared as thematic layers to be integrated and processed in a GIS environment. Based on the AHP, it was found that the drainage density, land cover, slope, and precipitation were the most effective indicators of the subsurface conditions and therefore aided in deciphering groundwater conditions in the

area. A majority portion of the lower MRB showed the moderate potential for the groundwater availability, with areas of Laos and Thailand indicated high groundwater potentiality.

**Reference for Chapter 3**


Adamson, P. T., Rutherfurd, I. D., Peel, M. C., & Conlan, I. A. (2009). The Hydrology of the Mekong River. In *The Mekong* (pp. 53–76). Elsevier. https://doi.org/10.1016/B978-0-12-374026-7.00004-8

Affeltranger, B. (2009a). Mekong Studies at Crossed Glances. In *4th French-MFU Seminar*. Chiang Rai, Thailand. Retrieved from https://www.ggr.ulaval.ca/sites/default/files/documents/Lasserre/Publications/actes_lasserre-affeltranger_irasec-mfu_2009.pdf

Affeltranger, B. (2009b). Sustainability of Environmental Regimes: The Mekong River Commission (pp. 593–601). Springer, Berlin, Heidelberg. https://doi.org/10.1007/978-3-540-68488-6_43

Agriculture and fishing | Open Development Mekong. (2019). Retrieved August 15, 2020, from https://opendevelopmentmekong.net/topics/agriculture-and-fishing/

Akter, A., & Babel, M. S. (2012). Hydrological modeling of the Mun River basin in Thailand. *Journal of Hydrology*, *452–453*, 232–246. https://doi.org/10.1016/J.JHYDROL.2012.05.059

Al-Ruzouq, R., Shanableh, A., Merabtene, T., Siddique, M., Khalil, M. A., Idris, A., & Almulla, E. (2019). Potential groundwater zone mapping based on geo-hydrological considerations and multi-criteria spatial analysis: North UAE. *CATENA*, *173*, 511–524. https://doi.org/10.1016/J.CATENA.2018.10.037

Alaouze, C. (1996). Shadow Prices in Linear Programming Problems. *Papers*.

Ali, Syed A., & Sridhar, V. (2019). Deriving the Reservoir Conditions for Better Water Resource Management Using Satellite-Based Earth Observations in the Lower Mekong River Basin. *Remote Sensing*, *11*(23), 2872. https://doi.org/10.3390/rs11232872

Ali, Syed Azhar, Aadhar, S., Shah, H. L., & Mishra, V. (2018). Projected Increase in Hydropower Production in India under Climate Change. *Scientific Reports*, *8*(1), 12450. https://doi.org/10.1038/s41598-018-30489-4

Aliagha, C. (2004). Environmental Clearinghouse as an Institutional Incentive for Data and Information Sharing and Conflict Reuction in the Mekong River Basin. In *OpenSIUC* (pp. 7–20). Southern Illinois University, Carbondale, Illinois. Retrieved from http://opensiuc.lib.siu.edu/ucowrconfs_2004/2

Allen, R., Pereira, L., Raes, D., & Smith, M. (1998). Crop evapotranspiration-Guidelines for computing crop water requirements-FAO Irrigation and drainage paper 56. *FAO Irrigation and Drainage Paper No. 56.* Retrieved from https://www.researchgate.net/profile/Hawre_Kiani/post/What_is_the_more_effective_way_of_deficit_irrigation/attachment/5af42706b53d2f63c3cafa73/AS%3A624694629777415%401525950214858/download/Allen_FAO1998.pdf

AQUASTAT. (2014). Irrigation water requirement and water withdrawals by country. Retrieved January 11, 2019, from http://www.fao.org/nr/water/aquastat/main/index.stm

Awawdeh, M., Obeidat, M., Al-Mohammad, M., Al-Qudah, K., & Jaradat, R. (2014). Integrated GIS and remote sensing for mapping groundwater potentiality in the Tulul al Ashaqif, Northeast Jordan. *Arabian Journal of Geosciences*, *7*(6), 2377–2392. https://doi.org/10.1007/s12517-013-0964-8

Bastakoti, R. C., Gupta, J., Babel, M. S., & van Dijk, M. P. (2014). Climate risks and

adaptation strategies in the Lower Mekong River basin. *Regional Environmental Change*, *14*(1), 207–219. https://doi.org/10.1007/s10113-013-0485-8

Becker, M., Papa, F., Frappart, F., Alsdorf, D., Calmant, S., da Silva, J. S., et al. (2018). Satellite-based estimates of surface water dynamics in the Congo River Basin. *International Journal of Applied Earth Observation and Geoinformation*, *66*, 196–209. https://doi.org/10.1016/J.JAG.2017.11.015

Birkett, C., Reynolds, C., Beckley, B., & Doorn, B. (2011). From Research to Operations: The USDA Global Reservoir and Lake Monitor. In *Coastal Altimetry* (pp. 19–50). Berlin, Heidelberg: Springer. https://doi.org/10.1007/978-3-642-12796-0_2

Bonnema, M., & Hossain, F. (2017). Inferring reservoir operating patterns across the Mekong Basin using only space observations. *Water Resources Research*, *53*(5), 3791–3810. https://doi.org/10.1002/2016WR019978

Bosch, J. M., & Hewlett, J. D. (1982). *A REVIEW OF CATCHMENT EXPERIMENTS TO DETERMINE THE EFFECT OF VEGETATION CHANGES ON WATER YIELD AND EVAPOTRANSPIRATION*. *Journal of Hydrology* (Vol. 55). Retrieved from http://coweeta.uga.edu/publications/2117.pdf

Boucher, O., Myhre, G., & Myhre, A. (2004). Direct human influence of irrigation on atmospheric water vapour and climate. *Climate Dynamics*, *22*(6–7), 597–603. https://doi.org/10.1007/s00382-004-0402-4

Box, M. J. (1965). A new method of constrained optimization and a comparison with other methods. *The Computer Journal*, *8*(1), 42–52. https://doi.org/10.1093/COMJNL/8.1.42

Brito, M. G., Costa, C. N., Almeida, J. A., Vendas, D., & Verdial, P. H. (2006). Characterization of maximum infiltration areas using GIS tools. *Engineering Geology*, *85*(1–2), 14–18. https://doi.org/10.1016/J.ENGGEO.2005.09.022

Browder, G., & Ortolano, L. (2000). *The Evolution of an International Water Resources Management Regime in the Mekong*. *Source: Natural Resources Journal* (Vol. 40). Retrieved from https://www.jstor.org/stable/pdf/24888536.pdf?refreqid=excelsior%3Af1fd62acc9ba6474184989cb5355f678

Cao, Q., Yu, D., Georgescu, M., Han, Z., & Wu, J. (2015). Impacts of land use and land cover change on regional climate: a case study in the agro-pastoral transitional zone of China. *Environmental Research Letters*, *10*(12), 124025. https://doi.org/10.1088/1748-9326/10/12/124025

Carruthers, I., Rosegrant, M. W., & Seckler, D. (1997). Irrigation and food security in the 21st century. *Irrigation and Drainage Systems*, *11*(2), 83–101. https://doi.org/10.1023/A:1005751232728

Chang, F.-J., Chen, L., & Chang, L.-C. (2005). Optimizing the reservoir operating rule curves by genetic algorithms. *Hydrological Processes*, *19*(11), 2277–2289. https://doi.org/10.1002/hyp.5674

Chapman, A., & Darby, S. (2016). Evaluating sustainable adaptation strategies for vulnerable mega-deltas using system dynamics modelling: Rice agriculture in the Mekong Delta's An Giang Province, Vietnam. *Science of the Total Environment*, *559*, 326–338. https://doi.org/10.1016/j.scitotenv.2016.02.162

Chase, T. N., Pielke Sr, R. A., F Kittel, T. G., Baron, J. S., & Stohlgren, T. J. (1999). *Potential impacts on Colorado Rocky Mountain weather due to land use changes on*

*the adjacent Great Plains*. *JOURNAL OF GEOPHYSICAL RESEARCH* (Vol. 104). https://doi.org/10.1029/1999JD900118

Chen, C.-J., Jayasekera, D. L., & Senarath, S. U. S. (2015). Assessing Uncertainty in Precipitation and Hydrological Modeling in the Mekong. In *World Environmental and Water Resources Congress 2015* (pp. 2510–2519). Reston, VA: American Society of Civil Engineers. https://doi.org/10.1061/9780784479162.246

Claverie, M., Ju, J., Masek, J. G., Dungan, J. L., Vermote, E. F., Roger, J. C., et al. (2018). The Harmonized Landsat and Sentinel-2 surface reflectance data set. *Remote Sensing of Environment*, *219*, 145–161. https://doi.org/10.1016/j.rse.2018.09.002

Cleugh, H. A., Leuning, R., Mu, Q., & Running, S. W. (2007). Regional evaporation estimates from flux tower and MODIS satellite data. *Remote Sensing of Environment*, *106*(3), 285–304. https://doi.org/10.1016/j.rse.2006.07.007

Conway, D., Van Garderen, E. A., Deryng, D., Dorling, S., Krueger, T., Landman, W., et al. (2015, August 21). Climate and southern Africa's water-energy-food nexus. *Nature Climate Change*. Nature Publishing Group. https://doi.org/10.1038/nclimate2735

Cosby, B. J., Hornberger, G. M., Clapp, R. B., & Ginn, T. R. (1984). A Statistical Exploration of the Relationships of Soil Moisture Characteristics to the Physical Properties of Soils. *Water Resources Research*, *20*(6), 682–690. https://doi.org/10.1029/WR020i006p00682

Costa-Cabral, M. C., Richey, J. E., Goteti, G., Lettenmaier, D. P., Feldkötter, C., & Snidvongs, A. (2008a). Landscape structure and use, climate, and water movement in the Mekong River basin. *Hydrological Processes*, *22*(12), 1731–1746. https://doi.org/10.1002/hyp.6740

Costa-Cabral, M. C., Richey, J. E., Goteti, G., Lettenmaier, D. P., Feldkötter, C., & Snidvongs, A. (2008b). Landscape structure and use, climate, and water movement in the Mekong River basin. *Hydrological Processes*, *22*(12), 1731–1746. https://doi.org/10.1002/hyp.6740

Crétaux, J.-F., Jelinski, W., Calmant, S., Kouraev, A., Vuglinski, V., Bergé-Nguyen, M., et al. (2011). SOLS: A lake database to monitor in the Near Real Time water level and storage variations from remote sensing data. *Advances in Space Research*, *47*(9), 1497–1507. https://doi.org/10.1016/J.ASR.2011.01.004

Dar, I. A., Sankar, K., & Dar, M. A. (2010). Remote sensing technology and geographic information system modeling: An integrated approach towards the mapping of groundwater potential zones in Hardrock terrain, Mamundiyar basin. *Journal of Hydrology*, *394*(3), 285–295. https://doi.org/10.1016/j.jhydrol.2010.08.022

Delgado, J. M., Merz, B., & Apel, H. (2012). A climate-flood link for the lower Mekong River. *Hydrology and Earth System Sciences*, *16*(5), 1533–1541. https://doi.org/10.5194/hess-16-1533-2012

Deligios, P. A., Chergia, A. P., Sanna, G., Solinas, S., Todde, G., Narvarte, L., & Ledda, L. (2019). Climate change adaptation and water saving by innovative irrigation management applied on open field globe artichoke. *Science of the Total Environment*, *649*, 461–472. https://doi.org/10.1016/j.scitotenv.2018.08.349

Dinar, A., & Letey, J. (1991). Agricultural water marketing, allocative efficiency, and drainage reduction. *Journal of Environmental Economics and Management*, *20*(3), 210–223. https://doi.org/10.1016/0095-0696(91)90009-8

Dore, John, Xiaogang Yu, and K. Y. L. (2007). China's energy reforms and hydropower expansion in Yunnan. *Democratizing Water Governance in the Mekong Region. Mekong Press*.

Duan, Z., & Bastiaanssen, W. G. M. (2013). Estimating water volume variations in lakes and reservoirs from four operational satellite altimetry databases and satellite imagery data. *Remote Sensing of Environment*, *134*, 403–416. https://doi.org/10.1016/J.RSE.2013.03.010

Eastham, J., Mpelasoka, F., Mainuddin, M., Ticehurst, C., Dyce, P., Hodgson, G., et al. (2008). Mekong River Basin water resources assessment: impacts of climate change. CSIRO: Water for a Healthy Country National Research Flagship. Retrieved from http://www.clw.csiro.au/publications/waterforahealthycountry/2008/wfhc-MekongWaterResourcesAssessment.pdf

Edet, A. E., Okereke, C. S., Teme, S. C., & Esu, E. O. (1998). Application of remote-sensing data to groundwater exploration: A case study of the Cross River State, southeastern Nigeria. *Hydrogeology Journal*, *6*(3), 394–404. https://doi.org/10.1007/s100400050162

Erban, L. E., Gorelick, S. M., & Zebker, H. A. (2014). Groundwater extraction, land subsidence, and sea-level rise in the Mekong Delta, Vietnam. *Environmental Research Letters*, *9*(8), 084010. https://doi.org/10.1088/1748-9326/9/8/084010

Fallah-Mehdipour, E., Bozorg Haddad, O., & Mariño, M. A. (2013). Extraction of Optimal Operation Rules in an Aquifer-Dam System: Genetic Programming Approach. *Journal of Irrigation and Drainage Engineering*, *139*(10), 872–879. https://doi.org/10.1061/(ASCE)IR.1943-4774.0000628

Feng, J.-M., Wang, Y.-L., Ma, Z.-G., & Liu, Y.-H. (2012). Simulating the Regional Impacts of Urbanization and Anthropogenic Heat Release on Climate across China. *Journal of Climate*, *25*(20), 7187–7203. https://doi.org/10.1175/JCLI-D-11-00333.1

Feng, M., Liu, P., Li, Z., Zhang, J., Liu, D., & Xiong, L. (2016). Modeling the nexus across water supply, power generation and environment systems using the system dynamics approach: Hehuang Region, China. *Journal of Hydrology*, *543*, 344–359. https://doi.org/10.1016/j.jhydrol.2016.10.011

Fischer, G., Tubiello, F. N., van Velthuizen, H., & Wiberg, D. A. (2007). Climate change impacts on irrigation water requirements: Effects of mitigation, 1990–2080. *Technological Forecasting and Social Change*, *74*(7), 1083–1107. https://doi.org/10.1016/J.TECHFORE.2006.05.021

Franchini, M., & Pacciani, M. (1991). Comparative analysis of several conceptual rainfall-runoff models. *Journal of Hydrology*, *122*(1–4), 161–219. https://doi.org/10.1016/0022-1694(91)90178-K

Fu, L.-L., & Cazenave, A. (2001). *Satellite altimetry and earth sciences : a handbook of techniques and applications*. Academic.

Ganapuram, S., Kumar, G. T. V., Krishna, I. V. M., Kahya, E., & Demirel, M. C. (2009). Mapping of groundwater potential zones in the Musi basin using remote sensing data and GIS. *Advances in Engineering Software*, *40*(7), 506–518. https://doi.org/10.1016/J.ADVENGSOFT.2008.10.001

Gao, B. (1996). NDWI—A normalized difference water index for remote sensing of vegetation liquid water from space. *Remote Sensing of Environment*, *58*(3), 257–266. https://doi.org/10.1016/S0034-4257(96)00067-3

Gao, H., Birkett, C., & Lettenmaier, D. P. (2012). Global monitoring of large reservoir storage from satellite remote sensing. *Water Resources Research*, *48*(9). https://doi.org/10.1029/2012WR012063

Gerlak, A. K., Lautze, J., & Giordano, M. (2011). Water resources data and information exchange in transboundary water treaties. *International Environmental Agreements: Politics, Law and Economics*, *11*(2), 179–199. https://doi.org/10.1007/s10784-010-9144-4

Gleeson, T., Wada, Y., Bierkens, M. F. P., & van Beek, L. P. H. (2012). Water balance of global aquifers revealed by groundwater footprint. *Nature*, *488*(7410), 197–200. https://doi.org/10.1038/nature11295

Goteti, G., & Lettenmaier, D. P. (2001). *Effects of streamflow regulation and land cover change on the hydrology of the Mekong river basin*. University of Washington. Retrieved from https://www.ce.washington.edu/sites/cee/files/pdfs/research/hydrology/water-resources/WRS169.pdf

Grumbine, R. E., & Xu, J. (2011). Mekong Hydropower Development. *Science*, *332*(6026), 178–179. https://doi.org/10.1126/science.1200990

Guo, H., Bao, A., Liu, T., Ndayisaba, F., He, D., Kurban, A., et al. (2017). Meteorological Drought Analysis in the Lower Mekong Basin Using Satellite-Based Long-Term CHIRPS Product. *Sustainability*, *9*(6), 901. https://doi.org/10.3390/su9060901

Habibi Davijani, M., Banihabib, M. E., Nadjafzadeh Anvar, A., & Hashemi, S. R. (2016). Multi-Objective Optimization Model for the Allocation of Water Resources in Arid Regions Based on the Maximization of Socioeconomic Efficiency. *Water Resources Management*, *30*(3), 927–946. https://doi.org/10.1007/s11269-015-1200-y

Haddeland, I., Skaugen, T., & Lettenmaier, D. P. (2006). Anthropogenic impacts on continental surface water fluxes. *Geophysical Research Letters*, *33*(8), L08406. https://doi.org/10.1029/2006GL026047

Haddeland, I., Lettenmaier, D. P., & Skaugen, T. (2006). Effects of irrigation on the water and energy balances of the Colorado and Mekong river basins. *Journal of Hydrology*, *324*(1–4), 210–223. https://doi.org/10.1016/j.jhydrol.2005.09.028

Hanasaki, N., Kanae, S., & Oki, T. (2006). A reservoir operation scheme for global river routing models. *Journal of Hydrology*, *327*(1–2), 22–41. https://doi.org/10.1016/j.jhydrol.2005.11.011

Hanim, F., & Rahim, A. (2017). *Supply and Demand of Rice in Malaysia: A System Dynamics Approach*. *International Journal of Supply Chain Management* (Vol. 6). Retrieved from http://excelingtech.co.uk/

Hapuarachchi, H. A. P., Takeuchi, K., Zhou, M., Kiem, A. S., Georgievski, M., Magome, J., & Ishidaira, H. (2008). Investigation of the Mekong River basin hydrology for 1980–2000 using the YHyM. *Hydrological Processes*, *22*(9), 1246–1256. https://doi.org/10.1002/hyp.6934

Harbaugh, A. W. (2005). *MODFLOW-2005, The U.S. Geological Survey Modular Ground-Water Model-the Ground-Water Flow Process*. Retrieved from http://water.usgs.gov/software/ground_water.html/.

Heinimann, A., Messerli, P., Schmidt-Vogt, D., & Wiesmann, U. (2007). The Dynamics of Secondary Forest Landscapes in the Lower Mekong Basin. *Mountain Research and Development*, *27*(3), 232–241. https://doi.org/10.1659/mrd.0875

Hempel, S., Frieler, K., Warszawski, L., Schewe, J., & Piontek, F. (2013). A trend-preserving bias correction – the ISI-MIP approach. *Earth System Dynamics*, *4*(2), 219–236. https://doi.org/10.5194/esd-4-219-2013

Henriksen, H. J., Troldborg, L., Højberg, A. L., & Refsgaard, J. C. (2008). Assessment of exploitable groundwater resources of Denmark by use of ensemble resource indicators and a numerical groundwater–surface water model. *Journal of Hydrology*, *348*(1–2), 224–240. https://doi.org/10.1016/J.JHYDROL.2007.09.056

Heywood, I., Corneluis, S., & Carver, S. (2003). An introduction to geographic information systems, 1st Indian Ed. Retrieved from https://scholar.google.com/scholar?hl=en&as_sdt=0%2C47&q=Heywood+I%2C+Corneluis+S%2C+Carver+S+%282003%29+An+introduction+to+geographic+information+systems%2C+1st+Indian+Ed.+Pearson+Education%2C+Delhi&btnG=

Hibbert, A. R. (1983). WATER YIELD IMPROVEMENT POTENTIAL BY VEGETATION MANAGEMENT ON WESTERN RANGELANDS. *Journal of the American Water Resources Association*, *19*(3), 375–381. https://doi.org/10.1111/j.1752-1688.1983.tb04594.x

Hoang, L. P., Lauri, H., Kummu, M., Koponen, J., van Vliet, M. T. H., Supit, I., et al. (2016). Mekong River flow and hydrological extremes under climate change. *Hydrology and Earth System Sciences*, *20*(7), 3027–3041. https://doi.org/10.5194/hess-20-3027-2016

Hoanh, C. T., Guttman, H., Droogers, P., & Aerts, J. (2004). Will we produce sufficient food under climate change?: Mekong Basin (South-east Asia). Retrieved from https://cgspace.cgiar.org/handle/10568/37433

Hoanh, C. T., Jirayoot, K., Lacombe, G., Srinetr, V., Hoanh, C. T., Jirayoot, K., et al. (2010). Impacts of climate change and development on Mekong flow regimes. First assessment - 2009. Retrieved from https://econpapers.repec.org/paper/iwtrerpts/h043262.htm

Hoekema, D. J., & Sridhar, V. (2013a). A System Dynamics Model for Conjunctive Management of Water Resources in the Snake River Basin. *JAWRA Journal of the American Water Resources Association*, *49*(6), 1327–1350. https://doi.org/10.1111/jawr.12092

Hoekema, D. J., & Sridhar, V. (2013b). A System Dynamics Model for Conjunctive Management of Water Resources in the Snake River Basin. *JAWRA Journal of the American Water Resources Association*, *49*(6), 1327–1350. https://doi.org/10.1111/jawr.12092

Homdee, T., Pongput, K., & Kanae, S. (2011). Impacts of Land Cover Changes on Hydrologic Responses: A Case Study of Chi River Basin, Thailand. *Journal of Japan Society of Civil Engineers, Ser. B1 (Hydraulic Engineering)*, *67*(4), I_31-I_36. https://doi.org/10.2208/jscejhe.67.I_31

Hook, J., Novak, S., & Johnston, R. (2003). Social Atlas of the Lower Mekong Basin. In *Mekong River Commission* (pp. 1727–1800). Phnom Penh.

Hossain, F., & Katiyar, N. (2006). Improving flood forecasting in international river basins. *Eos, Transactions American Geophysical Union*, *87*(5), 49. https://doi.org/10.1029/2006EO050001

Huffman, G., Adler, R., Stocker, E., Bolvin, D., & Nelkin, E. (2003). Analysis of TRMM 3-hourly multi-satellite precipitation estimates computed in both real and post-real

time. In *12th Conf. on Satellite Meteorology and Oceanography* (pp. 4–11). Long Beach, CA: Amer. Meteor. Soc., CD-ROM. Retrieved from https://ntrs.nasa.gov/search.jsp?R=20040026654

Huffman, G. J., Adler, R. F., Morrissey, M. M., Bolvin, D. T., Curtis, S., Joyce, R., et al. (2001). Global Precipitation at One-Degree Daily Resolution from Multisatellite Observations. *Journal of Hydrometeorology*, *2*(1), 36–50. https://doi.org/10.1175/1525-7541(2001)002<0036:GPAODD>2.0.CO;2

Intralawan, A., Wood, D., & Frankel, R. (2017). *Economic Evaluation of Hydropower Projects in the Lower Mekong Basin*. Retrieved from http://www.mrcmekong.org/assets/Uploads/Final-report-Mekong-Study-March-2017-8.pdf

Ioslovich, I., & Gutman, P. O. (2001). A model for the global optimization of water prices and usage for the case of spatially distributed sources and consumers. *Mathematics and Computers in Simulation*, *56*(4–5), 347–356. https://doi.org/10.1016/S0378-4754(01)00306-8

Jackson, R. B., Carpenter, S. R., Dahm, C. N., McKnight, D. M., Naiman, R. J., Postel, S. L., & Running, S. W. (2001). WATER IN A CHANGING WORLD. *Ecological Applications*, *11*(4), 1027–1045. https://doi.org/10.1890/1051-0761(2001)011[1027:WIACW]2.0.CO;2@10.1002/(ISSN)1939-5582(CAT)SPECIALCOLLECTION(VI)VIRTUALISSUE

Jain, P. K. (1998). Remote sensing techniques to locate ground water potential zones in upper Urmil River Basin, district Chhatarpur — Central India. *Journal of the Indian Society of Remote Sensing*, *26*(3), 135–147. https://doi.org/10.1007/BF03026671

Jaksa, W. T., & Sridhar, V. (2015). Effect of irrigation in simulating long-term evapotranspiration climatology in a human-dominated river basin system. *Agricultural and Forest Meteorology*, *200*, 109–118. https://doi.org/10.1016/j.agrformet.2014.09.008

Jha, M. K., Chowdhury, A., Chowdary, V. M., & Peiffer, S. (2007). Groundwater management and development by integrated remote sensing and geographic information systems: prospects and constraints. *Water Resources Management*, *21*(2), 427–467. https://doi.org/10.1007/s11269-006-9024-4

Ji, L., Zhang, L., & Wylie, B. (2009). Analysis of Dynamic Thresholds for the Normalized Difference Water Index. *Photogrammetric Engineering & Remote Sensing*, *75*(11), 1307–1317. https://doi.org/10.14358/PERS.75.11.1307

Jin, X., & Sridhar, V. (2010). An integrated model coupling VIC and MODFLOW to study the hydrological prediction at the Snake River Basin. Retrieved from https://www.researchgate.net/profile/Xin_Jin48/publication/267410713_An_integrated_model_coupling_VIC_and_MODFLOW_to_study_the_hydrological_prediction_at_the_Snake_River_Basin/links/55c69e9b08aea2d9bdc548ec/An-integrated-model-coupling-VIC-and-MODFLOW-to-

Jin, Y., Schaaf, C. B., Gao, F., Li, X., Strahler, A. H., Lucht, W., et al. (2003). Consistency of MODIS surface bidirectional reflectance distribution function and albedo retrievals: 1. Algorithm performance. *J. Geophys. Res*, *108*(D5), 4158. https://doi.org/10.1029/2002JD002803

Johnston, R., & Kummu, M. (2012). Water Resource Models in the Mekong Basin: A Review. *Water Resources Management*, *26*(2), 429–455.

https://doi.org/10.1007/s11269-011-9925-8
Kaiser, B., & Roumasset, J. (2002). Valuing indirect ecosystem services: The case of tropical watersheds. *Environment and Development Economics, 7*(4), 701–714. https://doi.org/10.1017/S1355770X02000426
Kalnay, E., Kanamitsu, M., Kistler, R., Collins, W., Deaven, D., Gandin, L., et al. (1996). The NCEP/NCAR 40-Year Reanalysis Project. *Bulletin of the American Meteorological Society*, *77*(3), 437–471. https://doi.org/10.1175/1520-0477(1996)077<0437:TNYRP>2.0.CO;2
Kang, H., & Sridhar, V. (2019). Drought assessment with a surface-groundwater coupled model in the Chesapeake Bay watershed. *Environmental Modelling and Software*, *119*, 379–389. https://doi.org/10.1016/j.envsoft.2019.07.002
Kang, H., Sridhar, V., Mills, B. F., Hession, W. C., & Ogejo, J. A. (2019). Economy-wide climate change impacts on green water droughts based on the hydrologic simulations. *Agricultural Systems*, *171*, 76–88. https://doi.org/10.1016/j.agsy.2019.01.006
Keskinen, M., Kummu, M., Käkönen, M., & Varis, O. (2012). Mekong at the Crossroads: Next Steps for Impact Assessment of Large Dams. *AMBIO*, *41*(3), 319–324. https://doi.org/10.1007/s13280-012-0261-x
Khandelwal, A., Karpatne, A., Wei, Z., Kuang, H., Ghosh, R., Dugan, H., et al. (2019). *GLADD-R: A new Global Lake Dynamics Database for Reservoirs created using machine learning and satellite data GLADD-R: A new Global Lake Dynamics Database for Reservoirs*. Retrieved from http://umnlcc.cs.umn.edu/GlobalReservoirDatabase/
Kiem, A. S., Ishidaira, H., Hapuarachchi, H. P., Zhou, M. C., Hirabayashi, Y., & Takeuchi, K. (2008). Future hydroclimatology of the Mekong River basin simulated using the high-resolution Japan Meteorological Agency (JMA) AGCM. *Hydrological Processes*, *22*(9), 1382–1394. https://doi.org/10.1002/hyp.6947
Kingston, D. G., Thompson, J. R., & Kite, G. (2011). Uncertainty in climate change projections of discharge for the Mekong River Basin. *Hydrology and Earth System Sciences*, *15*(5), 1459–1471. https://doi.org/10.5194/hess-15-1459-2011
Kondolf, G. M., Rubin, Z. K., & Minear, J. T. (2014). Dams on the Mekong: Cumulative sediment starvation. *Water Resources Research*, *50*(6), 5158–5169. https://doi.org/10.1002/2013WR014651
Kondolf, G. Mathias, Schmitt, R. J. P., Carling, P., Darby, S., Arias, M., Bizzi, S., et al. (2018). Changing sediment budget of the Mekong: Cumulative threats and management strategies for a large river basin. *Science of the Total Environment*, *625*, 114–134. https://doi.org/10.1016/j.scitotenv.2017.11.361
Kueppers, L. M., Snyder, M. A., & Sloan, L. C. (2007). Irrigation cooling effect: Regional climate forcing by land-use change. *Geophysical Research Letters*, *34*(3). https://doi.org/10.1029/2006GL028679
Kuhn, A., & Britz, W. (2012). Can hydro-economic river basin models simulate water shadow prices under asymmetric access? *Water Science and Technology*, *66*(4), 879–886. https://doi.org/10.2166/wst.2012.251
Kummu, M., Lu, X. X., Wang, J. J., & Varis, O. (2010). Basin-wide sediment trapping efficiency of emerging reservoirs along the Mekong. *Geomorphology*, *119*(3–4), 181–197. https://doi.org/10.1016/J.GEOMORPH.2010.03.018
Kummu, M, & Sarkkula, J. (2008). Impact of the Mekong River Flow Alteration on the

Tonle Sap Flood Pulse. *AMBIO*, *37*(3), 185–192. https://doi.org/10.1579/0044-7447(2008)37[185:IOTMRF]2.0.CO;2

Kummu, Matti, & Varis, O. (2007). Sediment-related impacts due to upstream reservoir trapping, the Lower Mekong River. *Geomorphology*, *85*(3–4), 275–293. https://doi.org/10.1016/J.GEOMORPH.2006.03.024

Lauri, H., de Moel, H., Ward, P. J., Räsänen, T. A., Keskinen, M., & Kummu, M. (2012). Future changes in Mekong River hydrology: impact of climate change and reservoir operation on discharge. *Hydrology and Earth System Sciences*, *16*(12), 4603–4619. https://doi.org/10.5194/hess-16-4603-2012

Leck, H., Conway, D., Bradshaw, M., & Rees, J. (2015). Tracing the Water-Energy-Food Nexus: Description, Theory and Practice. *Geography Compass*, *9*(8), 445–460. https://doi.org/10.1111/gec3.12222

Li, D., Long, D., Zhao, J., Lu, H., & Hong, Y. (2017). Observed changes in flow regimes in the Mekong River basin. *Journal of Hydrology*, *551*, 217–232. https://doi.org/10.1016/j.jhydrol.2017.05.061

Li, Han, Wei, Y. D., & Korinek, K. (2018). Modelling urban expansion in the transitional Greater Mekong Region. *Urban Studies*, *55*(8), 1729–1748. https://doi.org/10.1177/0042098017700560

Li, Hongyi, Wu, H., Huang, M., & Leung, L. R. (2012). Irrigation & Drainage Systems Engineering Representing Natural and Manmade Drainage Systems in an Earth System Modeling Framework, *1*(2), 1–2. https://doi.org/10.4172/2168-9768.1000e107

Li, W., Qin, Y., Sun, Y., Huang, H., Ling, F., Tian, L., & Ding, Y. (2016). Estimating the relationship between dam water level and surface water area for the Danjiangkou Reservoir using Landsat remote sensing images. *Remote Sensing Letters*, *7*(2), 121–130. https://doi.org/10.1080/2150704X.2015.1117151

Liang, X., Lettenmaier, D. P., Wood, E. F., & Burges, S. J. (1994). A simple hydrologically based model of land surface water and energy fluxes for general circulation models. *Journal of Geophysical Research*, *99*(D7), 14415. https://doi.org/10.1029/94JD00483

Lipscomb, M., Mobarak, A. M., & Barham, T. (2013). Development Effects of Electrification: Evidence from the Topographic Placement of Hydropower Plants in Brazil. *American Economic Journal: Applied Economics*, *5*(2), 200–231. https://doi.org/10.1257/app.5.2.200

Liu, Xingcai, Tang, Q., Voisin, N., & Cui, H. (2016). Projected impacts of climate change on hydropower potential in China. *Hydrology and Earth System Sciences*, *20*(8), 3343–3359. https://doi.org/10.5194/hess-20-3343-2016

Liu, Xiuli, Chen, X., & Wang, S. (2009). Evaluating and predicting shadow prices of water resources in China and its nine major river basins. *Water Resources Management*, *23*(8), 1467–1478. https://doi.org/10.1007/s11269-008-9336-7

Liu, Y., Xiao, J., Ju, W., Xu, K., Zhou, Y., & Zhao, Y. (2016). Recent trends in vegetation greenness in China significantly altered annual evapotranspiration and water yield. *Environmental Research Letters*, *11*(9), 094010. https://doi.org/10.1088/1748-9326/11/9/094010

Lobell, D. B., & Bonfils, C. (2008). The effect of irrigation on regional temperatures: A spatial and temporal analysis of trends in California, 1934-2002. *Journal of Climate*, *21*(10), 2063–2071. https://doi.org/10.1175/2007JCLI1755.1

Lohmann, D., Raschke, E., Nijssen, B., & Lettenmaier, D. P. (1998). Regional scale hydrology: II. Application of the VIC-2L model to the Weser River, Germany. *Hydrological Sciences Journal*, *43*(1), 143–158. https://doi.org/10.1080/02626669809492108

Lohmann, Dag, Nolte-Holube, R., & Raschke, E. (1996). A large-scale horizontal routing model to be coupled to land surface parametrization schemes. *Tellus, Series A: Dynamic Meteorology and Oceanography*. https://doi.org/10.1034/j.1600-0870.1996.t01-3-00009.x

Lyon, S. W., King, K., Polpanich, O., & Lacombe, G. (2017). Assessing hydrologic changes across the Lower Mekong Basin. *Journal of Hydrology: Regional Studies*, *12*, 303–314. https://doi.org/10.1016/J.EJRH.2017.06.007

Ma, L., Wang, H., Qi, C., Zhang, X., & Zhang, H. (2019). Characteristics and Adaptability Assessment of Commonly Used Ecological Flow Methods in Water Storage and Hydropower Projects, the Case of Chinese River Basins. *Water*, *11*(10), 2035. https://doi.org/10.3390/w11102035

Manh, N. Van, Dung, N. V., Hung, N. N., Kummu, M., Merz, B., & Apel, H. (2015). Future sediment dynamics in the Mekong Delta floodplains: Impacts of hydropower development, climate change and sea level rise. *Global and Planetary Change*, *127*, 22–33. https://doi.org/10.1016/J.GLOPLACHA.2015.01.001

Marhaento, H., Booij, M. J., Rientjes, T. H. M., & Hoekstra, A. Y. (2017). Attribution of changes in the water balance of a tropical catchment to land use change using the SWAT model. *Hydrological Processes*, *31*(11), 2029–2040. https://doi.org/10.1002/hyp.11167

Martin, S. M., & Lorenzen, K. (2016). Livelihood Diversification in Rural Laos. *World Development*, *83*, 231–243. https://doi.org/10.1016/J.WORLDDEV.2016.01.018

Mekong River Commission. (2005). *Overview of the Hydrology of the Mekong Basin Mekong River Commission Meeting the Needs, Keeping the Balance*. Retrieved from http://www.mekonginfo.org/assets/midocs/0001968-inland-waters-overview-of-the-hydrology-of-the-mekong-basin.pdf

Mekong River Commission. (2010). Assessment of basin-wide development scenarios–main report. *Mekong River Commission, Vientiane, Lao PDR*.

Merola, R. B., Hien, T. T., Quyen, D. T. T., & Vengosh, A. (2015). Arsenic exposure to drinking water in the Mekong Delta. *Science of The Total Environment*, *511*, 544–552. https://doi.org/10.1016/J.SCITOTENV.2014.12.091

Minderhoud, P. S. J., Coumou, L., Erban, L. E., Middelkoop, H., Stouthamer, E., & Addink, E. A. (2018). The relation between land use and subsidence in the Vietnamese Mekong delta. *Science of The Total Environment*, *634*, 715–726. https://doi.org/10.1016/J.SCITOTENV.2018.03.372

Ming, B., Liu, P., Chang, J., Wang, Y., & Huang, Q. (2017). Deriving Operating Rules of Pumped Water Storage Using Multiobjective Optimization: Case Study of the Han to Wei Interbasin Water Transfer Project, China. *Journal of Water Resources Planning and Management*, *143*(10), 05017012. https://doi.org/10.1061/(ASCE)WR.1943-5452.0000828

Mitchell, T. D., & Jones, P. D. (2005). An improved method of constructing a database of monthly climate observations and associated high-resolution grids. *International Journal of Climatology*, *25*(6), 693–712. https://doi.org/10.1002/joc.1181

Monteith, L. J. (1965). Evaporation and environment, In The state and movement of water in living organisms. *Symp. Soc. Exp. Biol.*, 205–234. Retrieved from https://ci.nii.ac.jp/naid/10007810939/

MRC. (2018). *Irrigation database improvement for the lower Mekong basin*. Retrieved from http://www.mrcmekong.org/publications/

Mu, Q., Heinsch, F. A., Zhao, M., & Running, S. W. (2007). Development of a global evapotranspiration algorithm based on MODIS and global meteorology data. *Remote Sensing of Environment*, *111*(4), 519–536. https://doi.org/10.1016/J.RSE.2007.04.015

Mu, Q., Zhao, M., & Running, S. W. (2011). Improvements to a MODIS global terrestrial evapotranspiration algorithm. *Remote Sensing of Environment*, *115*(8), 1781–1800. https://doi.org/10.1016/J.RSE.2011.02.019

Muala, E., Mohamed, Y. A., Duan, Z., & Van der Zaag, P. (2014). Estimation of Reservoir Discharges from Lake Nasser and Roseires Reservoir in the Nile Basin Using Satellite Altimetry and Imagery Data. *Remote Sensing*, *6*(8), 7522–7545. https://doi.org/10.3390/rs6087522

Myneni, R. ., Hoffman, S., Knyazikhin, Y., Privette, J. ., Glassy, J., Tian, Y., et al. (2002). Global products of vegetation leaf area and fraction absorbed PAR from year one of MODIS data. *Remote Sensing of Environment*, *83*(1), 214–231. https://doi.org/10.1016/S0034-4257(02)00074-3

Narendra, K., Nageswara Rao, K., & Swarna Latha, P. (2013). Integrating remote sensing and GIS for identification of groundwater prospective zones in the Narava basin, Visakhapatnam region, Andhra Pradesh. *Journal of the Geological Society of India*, *81*(2), 248–260. https://doi.org/10.1007/s12594-013-0028-4

Nash, J. E., & Sutcliffe, J. V. (1970). River flow forecasting through conceptual models part I — A discussion of principles. *Journal of Hydrology*, *10*(3), 282–290. https://doi.org/10.1016/0022-1694(70)90255-6

Nesbitt, H., R. Johnston, and M. S. (2004). Mekong River water: will river flows meet future agriculture needs in the Lower Mekong Basin? *Water in Agriculture, Seng, V., Craswell, E., Fukai, S., and Fisher, K.(Eds), Australian Centre of International Agricultural Research Proceedings 116*.

Oikonomidis, D., Dimogianni, S., Kazakis, N., & Voudouris, K. (2015). A GIS/Remote Sensing-based methodology for groundwater potentiality assessment in Tirnavos area, Greece. *Journal of Hydrology*, *525*, 197–208. https://doi.org/10.1016/j.jhydrol.2015.03.056

Olson, K. R., & Morton, L. W. (2018). Tonle Sap Lake and River and confluence with the Mekong River in Cambodia Soil management View project. *Article in Journal of Soil and Water Conservation*, *73*(3), 60A-66A. https://doi.org/10.2489/jswc.73.3.60A

Paper, W. (2009). *GoldSim: Engineering and Environmental Simulation Software for Water Resource Applications*.

Pech, S., & Sunada, K. (2008). Population Growth and Natural-Resources Pressures in the Mekong River Basin. *Ambio*. SpringerRoyal Swedish Academy of Sciences. https://doi.org/10.2307/25547886

Pham, H. T., Marshall, L., Johnson, F., & Sharma, A. (2018). Deriving daily water levels from satellite altimetry and land surface temperature for sparsely gauged catchments: A case study for the Mekong River. *Remote Sensing of Environment*, *212*, 31–46.

https://doi.org/10.1016/j.rse.2018.04.034
Pipitone, C. I., Maltese, A., Dardanelli, G. I., Lo Brutto, M. I., & La Loggia, G. I. (2018). Monitoring Water Surface and Level of a Reservoir Using Different Remote Sensing Approaches and Comparison with Dam Displacements Evaluated via GNSS. *Remote Sensing*, *10*(1), 71. https://doi.org/10.3390/rs10010071
Pittock, J., Dumaresq, D., & Bassi, A. (2016). Modeling the Hydropower–Food Nexus in Large River Basins: A Mekong Case Study. *Water*, *8*(10), 425. https://doi.org/10.3390/w8100425
Plengsaeng, B., Wehn, U., & van der Zaag, P. (2014). Data-sharing bottlenecks in transboundary integrated water resources management: a case study of the Mekong River Commission's procedures for data sharing in the Thai context. *Water International*, *39*(7), 933–951. https://doi.org/10.1080/02508060.2015.981783
Pokhrel, Y., Burbano, M., Roush, J., Kang, H., Sridhar, V., & Hyndman, D. (2018). A Review of the Integrated Effects of Changing Climate, Land Use, and Dams on Mekong River Hydrology. *Water*, *10*(3), 266. https://doi.org/10.3390/w10030266
Quinn, J. D., Reed, P. M., Giuliani, M., Castelletti, A., Oyler, J. W., & Nicholas, R. E. (2018). Exploring How Changing Monsoonal Dynamics and Human Pressures Challenge Multireservoir Management for Flood Protection, Hydropower Production, and Agricultural Water Supply. *Water Resources Research*, *54*(7), 4638–4662. https://doi.org/10.1029/2018WR022743
Rasul, G., & Sharma, B. (2016). The nexus approach to water–energy–food security: an option for adaptation to climate change. *Climate Policy*, *16*(6), 682–702. https://doi.org/10.1080/14693062.2015.1029865
Richter, B., & Thomas, G. (2007). Restoring environmental flows by modifying dam operations. *JSTOR*. Retrieved from https://www.jstor.org/stable/26267852?casa_token=aiozWKMVOdAAAAAA:pnbt3UP1Bk1W1O0fEKoMA6xl41grmqT_XdN7ngBGS43u5Yg6Nn_7lw0OJ4y3T01IQamjIzNU6wXvvmHQ2-oRgMM64_XbHnasRSAGgJ8nQlWeSVcJxGQr
Ringler, C., von Braun, J., & Rosegrant, M. W. (2004). Water Policy Analysis for the Mekong River Basin. *Water International*, *29*(1), 30–42. https://doi.org/10.1080/02508060408691746
Rosegrant, M. W., Ringler, C., McKinney, D. C., Cai, X., Keller, A., & Donoso, G. (2000). Integrated economic-hydrologic water modeling at the basin scale: the Maipo river basin. *Agricultural Economics*, *24*(1), 33–46. https://doi.org/10.1111/j.1574-0862.2000.tb00091.x
Sabo, J. L., Ruhi, A., Holtgrieve, G. W., Elliott, V., Arias, M. E., Ngor, P. B., et al. (2017). Designing river flows to improve food security futures in the Lower Mekong Basin. *Science (New York, N.Y.)*, *358*(6368), eaao1053. https://doi.org/10.1126/science.aao1053
Sacks, W. J., Cook, B. I., Buenning, N., Levis, S., & Helkowski, J. H. (2009). Effects of global irrigation on the near-surface climate. *Climate Dynamics*, *33*(2–3), 159–175. https://doi.org/10.1007/s00382-008-0445-z
Sakamoto, T., Van Nguyen, N., Kotera, A., Ohno, H., Ishitsuka, N., & Yokozawa, M. (2007). Detecting temporal changes in the extent of annual flooding within the Cambodia and the Vietnamese Mekong Delta from MODIS time-series imagery. *Remote Sensing of Environment*, *109*(3), 295–313.

https://doi.org/10.1016/J.RSE.2007.01.011
Salomon, J. G., Schaaf, C. B., Strahler, A. H., Feng Gao, & Yufang Jin. (2006). Validation of the MODIS bidirectional reflectance distribution function and albedo retrievals using combined observations from the aqua and terra platforms. *IEEE Transactions on Geoscience and Remote Sensing*, *44*(6), 1555–1565. https://doi.org/10.1109/TGRS.2006.871564
Schubert, S. D., Suarez, M. J., Pegion, P. J., Koster, R. D., & Bacmeister, J. T. (2004). Causes of Long-Term Drought in the U.S. Great Plains. *Journal of Climate*, *17*(3), 485–503. https://doi.org/10.1175/1520-0442(2004)017<0485:COLDIT>2.0.CO;2
Senanayake, I. P., Dissanayake, D. M. D. O. K., Mayadunna, B. B., & Weerasekera, W. L. (2016). An approach to delineate groundwater recharge potential sites in Ambalantota, Sri Lanka using GIS techniques. *Geoscience Frontiers*, *7*(1), 115–124. https://doi.org/10.1016/j.gsf.2015.03.002
Sener, E., Davraz, A., & Ozcelik, M. (2005). An integration of GIS and remote sensing in groundwater investigations: A case study in Burdur, Turkey. *Hydrogeology Journal*, *13*(5–6), 826–834. https://doi.org/10.1007/s10040-004-0378-5
Shaban, A., Khawlie, M., & Abdallah, C. (2006). Use of remote sensing and GIS to determine recharge potential zones: the case of Occidental Lebanon. *Hydrogeology Journal*, *14*(4), 433–443. https://doi.org/10.1007/s10040-005-0437-6
Sheffield, J., Goteti, G., & Wood, E. F. (2006). Development of a 50-Year High-Resolution Global Dataset of Meteorological Forcings for Land Surface Modeling. *Journal of Climate*, *19*(13), 3088–3111. https://doi.org/10.1175/JCLI3790.1
Shrestha, B., Babel, M. S., Maskey, S., van Griensven, A., Uhlenbrook, S., Green, A., & Akkharath, I. (2013). Impact of climate change on sediment yield in the Mekong River basin: a case study of the Nam Ou basin, Lao PDR. *Hydrology and Earth System Sciences*, *17*(1), 1–20. https://doi.org/10.5194/hess-17-1-2013
Siebert, S., Burke, J., Faures, J. M., Frenken, K., Hoogeveen, J., Döll, P., & Portmann, F. T. (2010). Groundwater use for irrigation – a global inventory. *Hydrology and Earth System Sciences*, *14*(10), 1863–1880. https://doi.org/10.5194/hess-14-1863-2010
Sigvaldson, O. T. (1976). A simulation model for operating a multipurpose multireservoir system. *Water Resources Research*, *12*(2), 263–278. https://doi.org/10.1029/WR012i002p00263
Solomon, S., & Quiel, F. (2006). Groundwater study using remote sensing and geographic information systems (GIS) in the central highlands of Eritrea. *Hydrogeology Journal*, *14*(5), 729–741. https://doi.org/10.1007/s10040-005-0477-y
Son, N. T., Chen, C. F., Chen, C. R., Chang, L. Y., & Minh, V. Q. (2012). Monitoring agricultural drought in the Lower Mekong Basin using MODIS NDVI and land surface temperature data. *International Journal of Applied Earth Observation and Geoinformation*, *18*, 417–427. https://doi.org/10.1016/J.JAG.2012.03.014
Spruce, J., Bolten, J., Srinivasan, R., Lakshmi, V., Spruce, J., Bolten, J., et al. (2018). Developing Land Use Land Cover Maps for the Lower Mekong Basin to Aid Hydrologic Modeling and Basin Planning. *Remote Sensing*, *10*(12), 1910. https://doi.org/10.3390/rs10121910
Spruce, J., Bolten, J., Mohammed, I. N., Srinivasan, R., & Lakshmi, V. (2020). Mapping Land Use Land Cover Change in the Lower Mekong Basin From 1997 to 2010. *Frontiers in Environmental Science*, *8*, 21. https://doi.org/10.3389/fenvs.2020.00021

Sridhar, V. (2013). Tracking the Influence of Irrigation on Land Surface Fluxes and Boundary Layer Climatology. *Journal of Contemporary Water Research & Education*, *152*(1), 79–93. https://doi.org/10.1111/j.1936-704X.2013.03170.x

Sridhar, V., & Anderson, K. A. (2017). Human-induced modifications to land surface fluxes and their implications on water management under past and future climate change conditions. *Agricultural and Forest Meteorology*, *234–235*, 66–79. https://doi.org/10.1016/j.agrformet.2016.12.009

Sridhar, V., Billah, M. M., & Hildreth, J. W. (2018). Coupled Surface and Groundwater Hydrological Modeling in a Changing Climate. *Groundwater*, *56*(4), 618–635. https://doi.org/10.1111/gwat.12610

Sridhar, V., Ali, S. A., & Lakshmi, V. (2019). Assessment and validation of total water storage in the Chesapeake Bay watershed using GRACE. *Journal of Hydrology: Regional Studies*, *24*, 100607. https://doi.org/10.1016/J.EJRH.2019.100607

Sridhar, V., Kang, H., & Ali, S. A. (2019). Human-Induced Alterations to Land Use and Climate and Their Responses for Hydrology and Water Management in the Mekong River Basin. *Water*, *11*(6), 1307. https://doi.org/10.3390/w11061307

Stackhouse, P. W., Gupta, S. K., Cox, S. J., Mikowitz, J. C., Zhang, T., & Chiacchio, M. (2004). 12-year surface radiation budget data se. *GEWEX News*, *14*(4), 10–12.

Stone, R. (2016). Dam-building threatens Mekong fisheries. Retrieved from http://science.sciencemag.org/content/354/6316/1084.summary

Stone, Richard. (2011a). Mayhem on the Mekong. *Science*, *333*(6044), 814–818. https://doi.org/10.1126/science.333.6044.814

Stone, Richard. (2011b, August 12). Mayhem on the Mekong. *Science*. https://doi.org/10.1126/science.333.6044.814

Subba Rao, N. (2006). Groundwater potential index in a crystalline terrain using remote sensing data. *Environmental Geology*, *50*(7), 1067–1076. https://doi.org/10.1007/s00254-006-0280-7

Sun, S., Yan, X., Cui, P., & Feng, J. (2011). A four-step method for optimising the normal water level of reservoirs based on a mathematical programming model--a case study for the Songyuan backwater dam in Jilin Province, China. *International Journal of Environmental Research and Public Health*, *8*(4), 1049–60. https://doi.org/10.3390/ijerph8041049

Tatsumi, K., & Yamashiki, Y. (2015a). Effect of irrigation water withdrawals on water and energy balance in the Mekong River Basin using an improved VIC land surface model with fewer calibration parameters. *Agricultural Water Management*, *159*, 92–106. https://doi.org/10.1016/J.AGWAT.2015.05.011

Tatsumi, K., & Yamashiki, Y. (2015b). Effect of irrigation water withdrawals on water and energy balance in the Mekong River Basin using an improved VIC land surface model with fewer calibration parameters. *Agricultural Water Management*, *159*, 92–106. https://doi.org/10.1016/j.agwat.2015.05.011

Te, N. (2007). *Drought management in the Lower Mekong Basin*. The 3rd Southeast Asia Water Forum, Kuala Lumpur, Malaysia.

Teeuw, R. M. (1995). Groundwater Exploration Using Remote Sensing And A Low-Cost Geographical Information System. *Hydrogeology Journal*, *3*(3), 21–30. https://doi.org/10.1007/s100400050057

Thanh, T. N., Tri, V. P. D., Kim, S., Phuong, T. N., Mong, T. L., & Tuan, P. V. (2020). A

subregional model of system dynamics research on surface water resource assessment for paddy rice production under climate change in the Vietnamese mekong delta. *Climate*, *8*(3). https://doi.org/10.3390/cli8030041

Thiery, W., Visser, A. J., Fischer, E. M., Hauser, M., Hirsch, A. L., Lawrence, D. M., et al. (2020). Warming of hot extremes alleviated by expanding irrigation. *Nature Communications*, *11*(1), 1–7. https://doi.org/10.1038/s41467-019-14075-4

Thilakarathne, M., & Sridhar, V. (2017). Characterization of future drought conditions in the Lower Mekong River Basin. *Weather and Climate Extremes*, *17*, 47–58. https://doi.org/10.1016/J.WACE.2017.07.004

Thu, H. N., & Wehn, U. (2016). Data sharing in international transboundary contexts: The Vietnamese perspective on data sharing in the Lower Mekong Basin. *Journal of Hydrology*, *536*, 351–364. https://doi.org/10.1016/j.jhydrol.2016.02.035

Tran, H., Tran, T., Kervyn, M., Tran, H., Tran, T., & Kervyn, M. (2015). Dynamics of Land Cover/Land Use Changes in the Mekong Delta, 1973–2011: A Remote Sensing Analysis of the Tran Van Thoi District, Ca Mau Province, Vietnam. *Remote Sensing*, *7*(3), 2899–2925. https://doi.org/10.3390/rs70302899

Tsur, Y., Dinar, A., Doukkali, R. M., Roe, T. L., Tsur, Y., Dinar, A., et al. (2004). Irrigation water pricing: policy implications based on international comparison. *Environment and Development Economics*, *9*(6), 735–755.

Västilä, K., Kummu, M., Sangmanee, C., & Chinvanno, S. (2010). Modelling climate change impacts on the flood pulse in the Lower Mekong floodplains. https://doi.org/10.2166/wcc.2010.008

van Vuuren, D. P., Edmonds, J., Kainuma, M., Riahi, K., Thomson, A., Hibbard, K., et al. (2011). The representative concentration pathways: An overview. *Climatic Change*, *109*(1), 5–31. https://doi.org/10.1007/s10584-011-0148-z

Wang, W., Lu, H., Ruby Leung, L., Li, H.-Y., Zhao, J., Tian, F., et al. (2017). Dam Construction in Lancang-Mekong River Basin Could Mitigate Future Flood Risk From Warming-Induced Intensified Rainfall. *Geophysical Research Letters*, *44*(20), 10,378-10,386. https://doi.org/10.1002/2017GL075037

Winemiller, K. O., McIntyre, P. B., Castello, L., Fluet-Chouinard, E., Giarrizzo, T., Nam, S., et al. (2016). Balancing hydropower and biodiversity in the Amazon, Congo, and Mekong. *Science*, *351*(6269), 128–129. https://doi.org/10.1126/science.aac7082

Wood, E. F., Lettenmaier, D. P., & Zartarian, V. G. (1992). A land-surface hydrology parameterization with subgrid variability for general circulation models. *Journal of Geophysical Research*, *97*(D3), 2717. https://doi.org/10.1029/91JD01786

Wu, C. S., Chen, Y., Jeng, M. R., Hwong, J. L., & Lee, K. C. (2004). Evaluating the economic benefit of water resource nourishment by forests. *Taiwan Journal of Forest Science*, *19*(3), 187–197.

Wu, L., Feng, J., & Miao, W. (2018). Simulating the Impacts of Irrigation and Dynamic Vegetation Over the North China Plain on Regional Climate. *Journal of Geophysical Research: Atmospheres*, *123*(15), 8017–8034. https://doi.org/10.1029/2017JD027784

Yang, B., Zhang, Y., Qian, Y., Tang, J., & Liu, D. (2016). Climatic effects of irrigation over the Huang-Huai-Hai Plain in China simulated by the weather research and forecasting model. *Journal of Geophysical Research: Atmospheres*, *121*(5), 2246–2264. https://doi.org/10.1002/2015JD023736

Yang, Y., Zhang, M., Zhu, L., Liu, W., Han, J., & Yang, Y. (2017). Influence of Large

Reservoir Operation on Water-Levels and Flows in Reaches below Dam: Case Study of the Three Gorges Reservoir. *Scientific Reports*, *7*(1), 15640. https://doi.org/10.1038/s41598-017-15677-y

Zargar, A., Sadiq, R., Naser, B., & Khan, F. I. (2011). A review of drought indices. *Environmental Reviews*, *19*(NA), 333–349. https://doi.org/10.1139/a11-013

Zatarain Salazar, J., Reed, P. M., Quinn, J. D., Giuliani, M., & Castelletti, A. (2017). Balancing exploration, uncertainty and computational demands in many objective reservoir optimization. *Advances in Water Resources*, *109*, 196–210. https://doi.org/10.1016/J.ADVWATRES.2017.09.014

Zhao, R., & Chen, S. (2008). Fuzzy pricing for urban water resources: Model construction and application. *Journal of Environmental Management*, *88*(3), 458–466. https://doi.org/10.1016/j.jenvman.2007.03.004

Zhou, T., Haddeland, I., Nijssen, B., & Lettenmaier, D. P. (2016). Human-Induced Changes in the Global Water Cycle (pp. 55–69). American Geophysical Union (AGU). https://doi.org/10.1002/9781118971772.ch4

Zhou, T., Nijssen, B., Gao, H., Lettenmaier, D. P., Zhou, T., Nijssen, B., et al. (2016). The Contribution of Reservoirs to Global Land Surface Water Storage Variations. *Journal of Hydrometeorology*, *17*(1), 309–325. https://doi.org/10.1175/JHM-D-15-0002.1

Ziolkowska, J. R. (2015). Shadow price of water for irrigation-A case of the High Plains. *Agricultural Water Management*, *153*, 20–31. https://doi.org/10.1016/j.agwat.2015.01.024

Ziv, G., Baran, E., Nam, S., Rodriguez-Iturbe, I., & Levin, S. A. (2012). Trading-off fish biodiversity, food security, and hydropower in the Mekong River Basin. *Proceedings of the National Academy of Sciences*, *109*(15), 5609–5614. https://doi.org/10.1073/pnas.1201423109

Ziv, Guy, Baran, E., Nam, S., Rodríguez-Iturbe, I., & Levin, S. A. (2012). Trading-off fish biodiversity, food security, and hydropower in the Mekong River Basin. *Proceedings of the National Academy of Sciences of the United States of America*, *109*(15), 5609–14. https://doi.org/10.1073/pnas.1201423109

# Chapter 4
# Evaluation of the hydropower production for the existing dams considering the water demand for irrigation

**Keywords:** VIC, NIWR, hydropower, Mekong, GCMs, GoldSim

## 4.1 Introduction

The optimal operation of the multi-purpose dams depends on satisfying the water requirement by different sectors, viz. agriculture, domestic needs, industrial demand, and hydropower production. Moreover, the rule curve of the dams provides guidance for the release of the storage water to the downstream regions. Numerous studies have been conducted for the optimization of the operating rule curve of dams and reservoir management via genetic algorithms (Chang et al., 2005; Fallah-Mehdipour et al., 2013) and reservoir models (Hoekema & Sridhar, 2013a; Richter & Thomas, 2007; Sigvaldson, 1976). However, the actual operation of the dams is dependent on the fluctuation of the water demand by different sectors.

The enormous flow of the Mekong river, combined with the strong topographic gradient, projects the MRB as the ideal site for the large-scale hydropower generation. The MRB has the hydropower potential of approximately 53,000 MW in the mainstem Mekong and 35,000 MW in the tributaries (Stone, 2011a). However, with approximately 42 dams in the basin, only a small fraction of the enormous potential has been developed thus far, as its total active reservoir capacity (8.6 $km^3$) accounting to a mere 2% of its mean annual discharge (Kummu et al., 2010). Specifically, an immense amount of the hydropower generation potential remains unharnessed in the LMRB. In order to utilize the untapped hydropower potential of the MRB, 16 dams in the main stem, and more than 110 dams in the tributaries have been planned by the Mekong River Commission with the combined installed capacity of all existing and planned dams exceeding 65,000 MW (Dore, John, Yu, 2007).

The crisis for the water management exaggerates with the increasing population of the MRB. The growth of the population was estimated as 45% between 1980 and 2000, which

is further expected to increase in the next two decades, exerting extensive pressure on the land and water for supplementary food production (Johnston, 2004). Over the past few decades, the conversion of large forest areas into agricultural lands is devoted to rapid population growth, urbanization, and socio-economic development in the countries of the MRB (Sabo et al., 2017). Pokhrel et al. (2018) estimated the conversion of the land use as a 2% increase in the cropland and a 3% decline in the tree coverage. Furthermore, the fulfillment of the growing food demand of the population in the MRB is satisfied by the cultivation of an additional rice crop during the growing season in the basin. The total irrigated area in the basin is approximately 4 million hectares, and irrigated areas are expanding steadily in all four Member Countries (MRC, 2018). The expanding agricultural area and intensification of the crop cycle demand enormous water requirements for the cultivation of crops, competing with the water needs of the hydropower generation. The ideal distribution of the finite available water for irrigation and energy generation purposes is the key to the sustainable management of the MRB. System dynamics is an approach to frame, understand, and discuss the complex behavior of complicated systems over time using stocks, flows, feedback loops, and time delays (Hanim & Rahim, 2017). The system dynamics framework provides an ideal environment to analyze the reservoir operation in fulfilling the water demands of diverse sectors under the influence of dynamic inflows, water demands, and climate impacts. The system dynamics provides the advantage of making intercomparison between the system behavior due to variation of the single parameter while the other information remains rigid, through the generation of different scenarios. Nexus approaches are recognized as an effective way to provide a sustainable solution to the natural resources scarcity accomplished with the challenge of climate change and anthropogenic activities (Conway et al., 2015; Leck et al., 2015; Rasul & Sharma, 2016).

A comprehensive study of the hydropower production of the dams and the effects of climate change is lacking. An investigation of the effect of increased irrigation water demand on the hydropower production of multipurpose dams commissioned for irrigation and hydropower generation in the MRB has not been performed in the context of balancing the water demand between the two sectors. This study aims to explore the water requirement satisfaction by irrigation and electricity sectors for the recent observed period

(2006-2019) and future period (2020-2099) based on the various possibilities of the agricultural expansion in the MRB. The analysis is performed to estimate the electricity generation by the hydropower dams and multipurpose dams along with satisfying the irrigation water demand under the influence of climate change and irrigation variation conditions. Additionally, the irrigation dams are included to estimate the efficiency of the approach in simulating the irrigation diversion. The objectives of the study are to:

- quantify the hydropower potential of the existing dams and the projected hydropower capacities of the basin for the observed and future period.
- investigate the optimal water distribution between the irrigation and hydropower sector in the system dynamics environment under different irrigation expansion and intensification scenarios.

## 4.2 Materials and Methods

### 4.2.1 Study Area

The selection of the dams for the study was done from the 722 dams in China, 101 in Vietnam, 39 in Thailand, 17 in Myanmar, 7 in Lao PDR, and 2 in Cambodia on the basis of the purpose and location (Figure 1). Since the objective of the study considers the agriculture and energy needs, the dams commissioned for irrigation and hydroelectricity generation were chosen for the analysis. Six multipurpose dams, four irrigation dams, and 10 hydropower dams were shortlisted. The details of the dams can be found in Table 1. The multipurpose dams used for the analysis, namely, Sirindhorn, Ubol Ratana, Nam Pung, Lam Takhong, and Lam Phra Phloeng were constructed in Thailand before 1972. The irrigation dams include Lam Pao, Upper Mun, Lam Nang Rong, and Lam Sae are also located in Thailand. Out of 10 hydropower dams, Nam Ngum, Xeset1, Theun-Hinboun, Houay-Ho, Nam Leuk, and Nam Mang3 are located in Laos PDR, while Huai Kum, Xiaowan, Ochum, and Yaly are situated in Thailand, China, Cambodia, and Vietnam, respectively. The annual energy generation of the hydropower dams varies from 1 GWh to 18990 GWh, while the range for the multipurpose dams was 15GWh-400GWh. The distribution of the irrigated area in the MRB was extracted from the 2004 irrigation map provided by the Mekong River Commission (MRC).

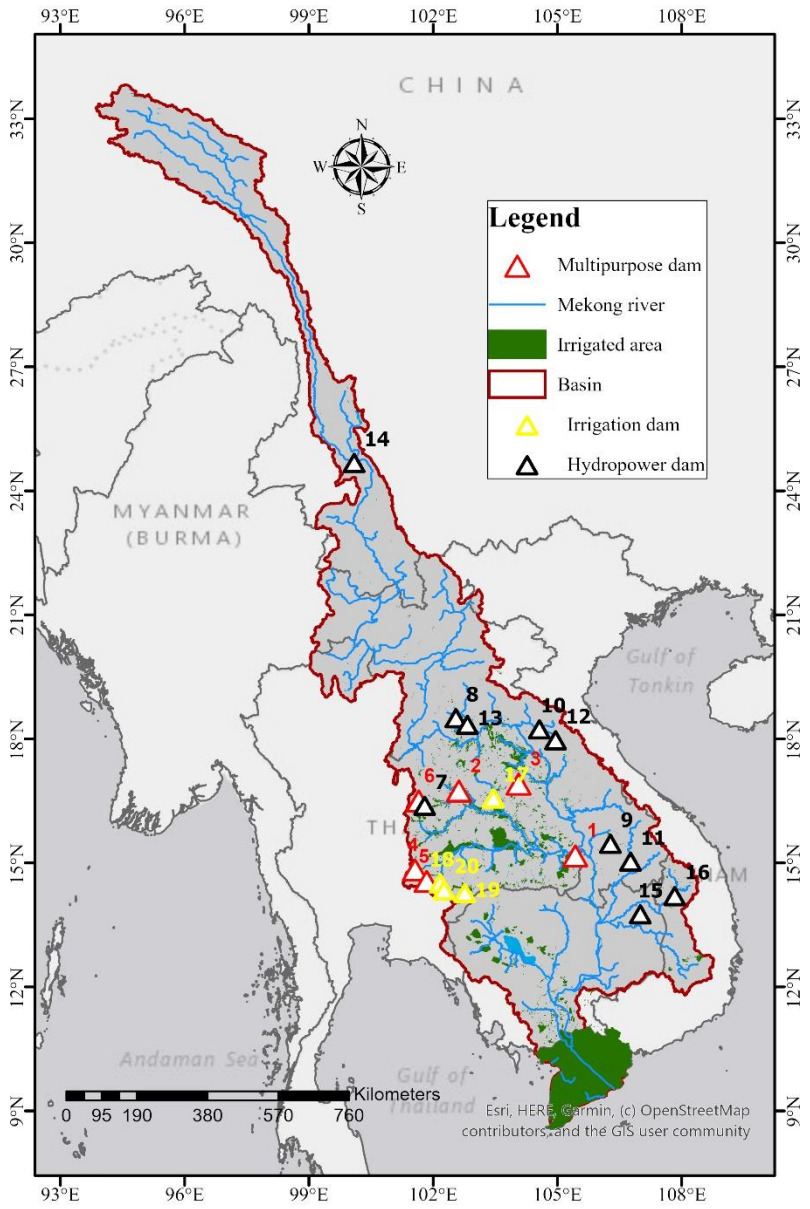


*Figure 1: Location map of the Mekong River basin along with the river's mainstream and irrigated area (2004). The geographical location of the dams considered in this study categorized as multipurpose dams (red triangle), hydropower dams (black triangle), and irrigation dams (yellow triangle).*

*Table 1: List of the dams considered in the study*

| S. No | Name of dam | Country | Purpose | Completed /operational since | Dam height (m) | Reservoir capacity (million $m^3$) | Reservoir area ($km^2$) | Installed Capacity (MW) | Annual Generation (GWh) |
|---|---|---|---|---|---|---|---|---|---|
| 1 | Sirindhorn | Thailand | M | 1971 | 42 | 1966 | 288 | 36 | 90 |

| | | | | | | | | | |
|---|---|---|---|---|---|---|---|---|---|
| 2 | Ubol Ratana | Thailand | M | 1966 | 32 | 2859 | 41 | 25.2 | 57 |
| 3 | Nam Pung | Thailand | M | 1965 | 40 | 165 | 2.165 | 6.3 | 15 |
| 4 | Lam Takhong | Thailand | M | 1969 | 40.3 | 310 | 3.7 | 500 | 400 |
| 5 | Lam Phra Phloeng | Thailand | M | 1970 | 50 | 110 | 1.31 | 6.5 | 15 |
| 6 | Chulabhorn | Thailand | M | 1972 | 70 | 188 | 31 | 40 | 59 |
| 7 | Huai Kum | Thailand | HP | 1982 | 36 | 22.8 | 1.8 | 1.2 | 2 |
| 8 | Nam Ngum | Laos PDR | HP | 1985 | 75 | 4700 | 370 | 155 | 865 |
| 9 | Xeset 1 | Laos PDR | HP | 1991 | 18 | 30 | 0.1 | 45 | 154.3 |
| 10 | Theun-Hinboun | Laos PDR | HP | 1998 | 27 | 20 | NA | 220 | 1645 |
| 11 | Houay-Ho | Laos PDR | HP | 1998 | 80 | 3530 | 37 | 152.1 | 450 |
| 12 | Nam Leuk | Laos PDR | HP | 2000 | 51.5 | 185 | NA | 60 | 215 |
| 13 | Nam Mang 3 | Laos PDR | HP | 2004 | 22 | 49.43 | 10.2 | 40 | 150 |
| 14 | Xiaowan | China | HP | 2010 | 292 | 15043 | 190 | 4200 | 18990 |
| 15 | Ochum | Cambodia | HP | 1993 | 10 | 1 | NA | 1 | 51 |
| 16 | Yaly | Viet Nam | HP | 2002 | 69 | 1037 | 64.5 | 720 | 3658.6 |
| 17 | Lam Pao | Thailand | IR | 1969 | 33 | 1430 | 240 | NA | NA |
| 18 | Upper Mun | Thailand | IR | 1980 | 32.7 | 141 | 1.275 | NA | NA |
| 19 | Lam Nang Rong | Thailand | IR | 1982 | 23 | 150 | 11.6 | NA | NA |
| 20 | Lam Sae | Thailand | IR | 1998 | 29.5 | 275 | 2.95 | NA | NA |

### 4.2.2 Data

*Storage:*

The daily time series of the observed total storage of the 10 reservoirs situated in Thailand were obtained from the reservoir database (http://app.rid.go.th:88/reservoir/) from 2006 to 2019. The monthly time series were generated for the reservoirs from the daily variation of the reservoir storage. The variation of the total storage of the reservoirs was used for the validation of the simulated storage results obtained through the developed methodology.

The rule curves for the reservoirs were derived by taking the ensemble mean of the monthly variation of the total storage. Figures 2a and 2b show the derived rule curve of the multipurpose dams and irrigation dams, respectively, located in Thailand. The fluctuation of the total storage of the multipurpose and irrigation reservoirs followed the monsoon season, resulting in the shrinkage of the reservoir before the onset of the monsoon (May) and swelling at the end of the season (November). On the contrary, there was decreasing storage from November to April as discharges were regulated with higher outflows. Furthermore, the change in the variation of the storage of the reservoirs is negative for May-October and positive for November-April with respect to the mean annual storage. Though the seasonal variation of the reservoir storage followed a similar pattern, the magnitude of the storage varies considerably between the reservoirs. The volume of the water storage in the reservoir reaches 2000 million $m^3$ for the Ubol Ratana, and 1700 million $m^3$ for Sirindhorn, while the accumulated storage volume was less than 240 million $m^3$ for the remaining multipurpose dams. The monthly range of the rule curve of the reservoirs was primarily governed by the magnitude of the inflow. The low reservoir storage during the dry period helps to accommodate the high inflows during the monsoon period, which was discharged throughout the year to provide stability during the low-flow periods. Apart from the inflow from the catchment, water diversion for irrigation purposes, especially during the growing and sowing period (January-April), causes substantial lowering of the reservoir storage. The monthly fluctuation in the storage volume was smooth for the reservoirs with large storage capacities such as Sirindhorn and Ubol Ratana, while the small storage capacity reservoirs face competing water demand for irrigation purposes leading to the abrupt changes in storage during the summer season. On the other hand, the maximum storage volume of the irrigation reservoirs was hosted by Lam Pao with 1200 million $m^3$ volume, while the storage capacity of the other irrigation reservoirs was less than 200 million $m^3$. The monthly variation of the irrigation reservoir storage was smooth as the water was diverted from the reservoir only for irrigation purposes without consideration for the electricity generation.

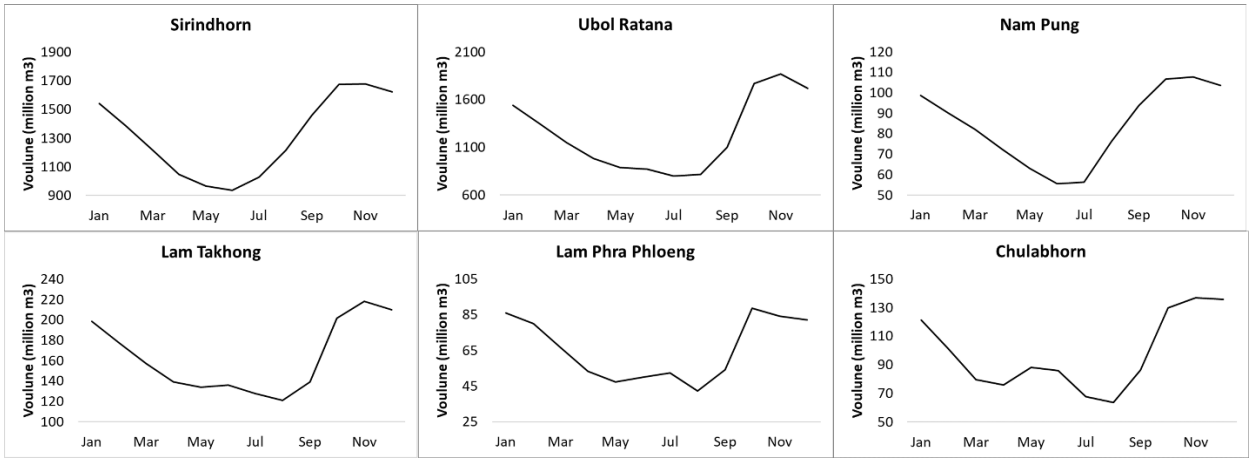


*Figure 2(a): The rule curve of the multipurpose dams derived using the monthly variation of the total storage from 2006 to 2019.*

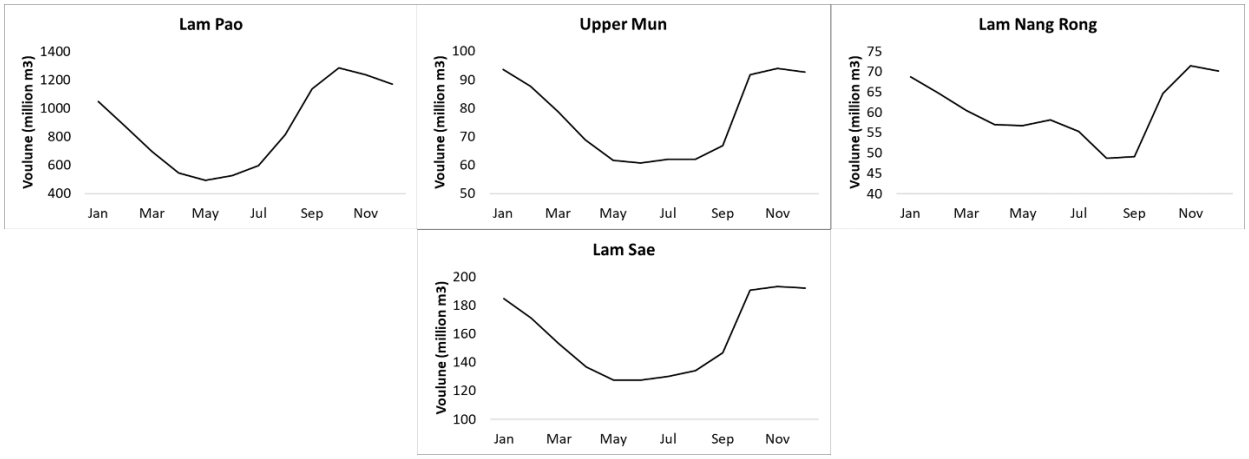


*Figure 2(b): The rule curve of the irrigation dams derived using the monthly variation of the total storage from 2006 to 2019.*

*Surface Area:*

The rule curve of the reservoirs situated outside Thailand was derived using the change in the surface area of the reservoirs. The surface area of the 8 multipurpose reservoirs was obtained from the Global Lake Dynamics Database for Reservoirs (GLADD-R) available at http://umnlcc.cs.umn.edu/GlobalReservoirDatabase/. Khandelwal et al. (2019) used the machine learning and satellite data for the visualization and surface area time series of 1882 reservoirs between 1 and 100 $km^2$ in size. The period of surface variation information was from 2001 to 2015, however, the available data varied for each reservoir. Figure 3 shows the surface area variation of the eight hydropower dams, namely Huai Kum, Xeset1, Theun-Hinboun, Houay-Ho, Nam Leuk, Nam Mang3, Ochum, and Yaly at monthly

timesteps. The duration and time record of the surface area varied broadly between the hydropower reservoirs with the longest information for Huai Kum and Houay-Ho The surface area of the Theun-Hinboun and Nam Leuk, and shortest record for Theun-Hinboun and Nam Leuk. The surface area of the reservoir was the largest for Theun-Hinboun and Nam Leuk with the range from 50 $km^2$ to 120 $km^2$. However, the maximum surface area of the Yaly, Houay-Ho, Nam Mang3, Huai Kum, Ochum, and Xeset1 was observed as 70 $km^2$, 30 $km^2$, 12 $km^2$, 2.5 $km^2$, 1.5 $km^2$, and 0.15 $km^2$, respectively. The reservoir with surface area variation record of more than ten years showed some seasonality in the area change, however, the seasonal variation was not consistent over the years. The surface area variation of the two dams, namely, Nam Ngum and Xiaowan was obtained using the LandSat8 and Sentinel2 reflectance imageries.

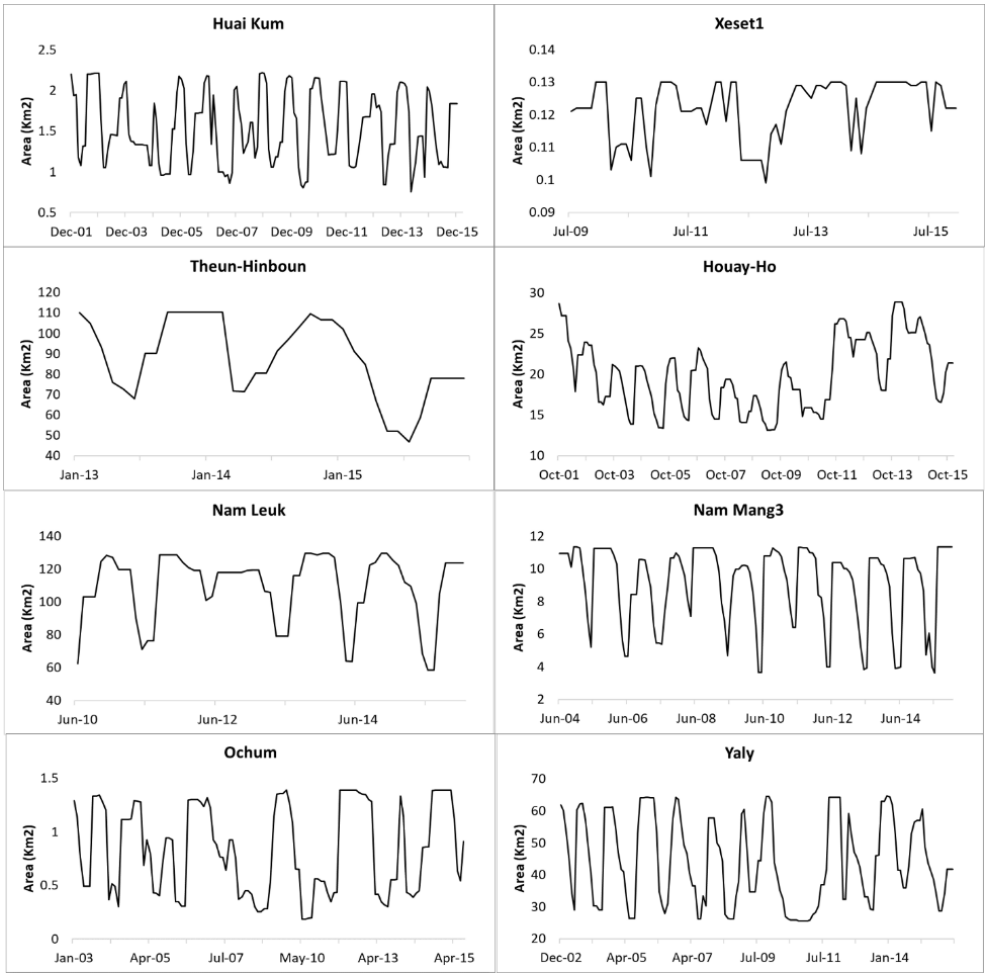


*Figure 3: The surface area variation of the eight hydropower dams at monthly timesteps obtained from [http://umnlcc.cs.umn.edu/GlobalReservoirDatabase/](http://umnlcc.cs.umn.edu/GlobalReservoirDatabase/).*

*Derived Rule curve:*

The rule curve of the reservoirs with the available surface area fluctuation was derived using the time series of the surface area variation. Although the duration and time record of the surface area varied broadly between the reservoirs, Huai Kum, Houay-Ho, Nam Mang3, Ochum, ad Yaly can be grouped together as the record was available for more than ten years. As the rule curve was derived by generating the seasonal cycle of the surface variation over different years, the common timeline for all the reservoir was not emphasized assuming the behavior remains similar over time. Firstly, the seasonal variation of the surface area of the reservoir was developed using the ensemble mean on the monthly series of the surface area. The seasonal change in the total storage was assumed to be similar to the seasonal fluctuations in the surface area of the reservoirs. The rule curve of the reservoirs was finally developed using the maximum storage capacity of the reservoirs. Figure 4 shows the rule curve of the 10 hydropower reservoirs developed using the monthly surface area variations. The characteristics of the rule of the 10 hydropower reservoirs were similar to the rule curve of the multipurpose and irrigation reservoirs, with the minimum storage before the onset of the monsoon (May) and maximum storage at the end of the season (November). As observed in the hydropower and irrigation reservoirs, the hydropower reservoir's rule curve was not confined by the diversion for the irrigation water demand, resulting in the smooth curve defining the seasonal variation. During the onset of the monsoon, the storage of the reservoir falls by 50% of the maximum storage capacity. As the rule curve was derived directly from the surface area variation, the jagged character of the rule curve of Xeset1 can be due to the abrupt surface area fluctuation during the short span of five years.

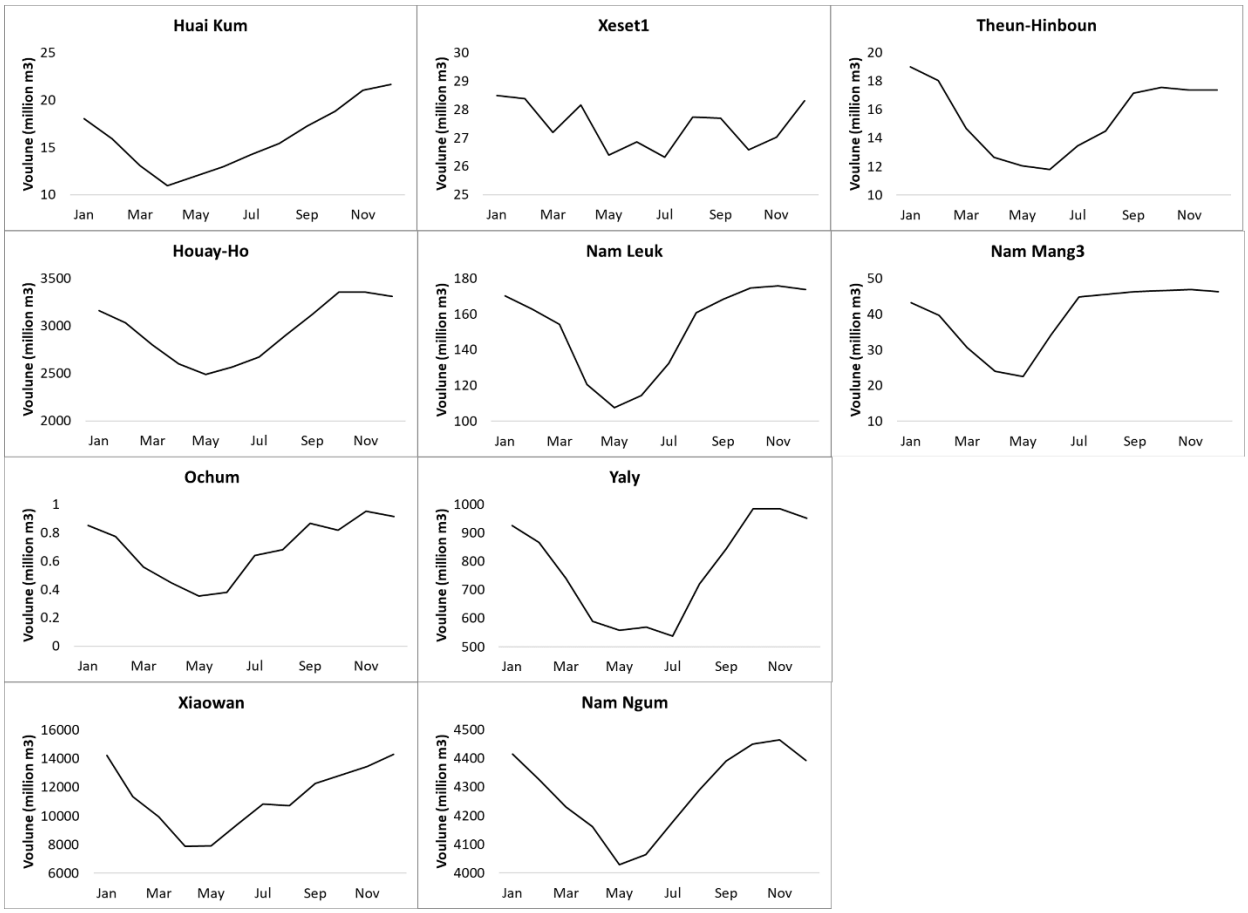


*Figure 4: The rule curve of the hydropower dams derived using the monthly variation of the surface area of the reservoirs.*

### 4.2.3 Hydrological and routing model

The Variable Infiltration Capacity (VIC) model was used for the estimation of the inflow to the dam locations for the observed and future climate. The VIC is a semi-distributed physically-based hydrological model that solves water and energy balance for each grid (here, 0.05º spatial resolution) separately at a daily time step (Liang et al., 1994). The meteorological parameters for the execution of the model include precipitation, minimum, and maximum temperature and wind speed from the Global Meteorological Forcing Dataset (GMFD), Climate Hazards Group InfraRed Precipitation with Station (CHIRPS) and Climate Prediction Center (CPC) gridded dataset available at 0.25º spatial and daily temporal resolution (Sheffield et al., 2006). The dataset was statistically downscaled to 0.05º spatial resolution. The vegetation texture containing the land cover type, leaf area index, and albedo was developed using Advanced Very High-Resolution Radiometer (AVHRR) at a 1 km spatial resolution. The soil class from the United States Department

of Agriculture (USDA) classification and pedo-transfer functions (Cosby et al., 1984) applied to Harmonized World Soil Database (HWSD) were combined to extract soil parameters. The VIC model takes into consideration the vegetation variability within a grid cell, as the fractional value of the grid covered by the particular vegetation class. Also, the VIC model has three soil layers; the rainfall is responded quickly by the top two layers with diffusion from the middle to the top layer, and the bottom layer corresponds to baseflow calculated using the Arno model formulation (Franchini & Pacciani, 1991). The total ET is calculated based on the Penman-Monteith approach and the infiltration of water into the soil layer is defined by the variable infiltration curve (Wood et al., 1992).

The routing model developed by Lohmann et al. (1998; 1996) was used for the estimation of the streamflow at the desired location by routing the fluxes of each grid generated by the VIC model. The routing scheme explicitly routed the surface and subsurface flow within a grid using a unit hydrograph that contributed to a channel network where the node of the channel network represented each grid-cell of the VIC model. The unit hydrograph governed the distribution of travel time within the grid cell and implicitly assimilated the travel time across hill slope and tributaries that connected the hill slopes and main channel (Hongyi Li et al., 2012).

### 4.2.4 Net Irrigation Water Requirement (NIWR)

An improved VIC model including the irrigation scheme developed by Haddeland et al. (2006) was used to simulate daily water abstraction for irrigation purposes. The irrigated area of the MRB was derived from the Mekong River Commission (MRC) database for the year 2004 and was used for the estimation of crop fraction in the grids for irrigation scheme implementation. The main objective of the irrigation scheme is to augment root zone soil moisture and the removal of vegetation stress caused by limited soil moisture availability. The irrigation process is designed to initiate when soil moisture of the top layer falls below the level at which transpiration is limited. The modified VIC model allows for irrigation water use based on the predicted soil moisture content for agricultural grid cells at every computational step. Specifically, when the soil moisture drops below the wilting point, irrigation is represented in the model as additional precipitation until the soil moisture reaches field capacity. The additional precipitation continues on a daily basis until soil

moisture reaches field capacity (Zhou, Nijssen, et al., 2016). Based on water availability, Haddeland et al. (2006) introduced two modules for the extraction of the water i.e. free-irrigation, where unlimited water availability was assumed, and limited-irrigation, where the withdrawal was constrained by the amount available as runoff or from river channels and dams. The free-irrigation module of the irrigation scheme was used in this study. The NIWR was estimated as (Allen et al., 1998):

$$NIWR = \frac{\sum_{i=1}^{N}\left[\sum_{t=1}^{T}\left(k_{c_t} \text{ x } ET_{o_t} - P_{eff_t}\right) \text{x } S_i\right] \text{x } A_{paddy}}{S} \quad (1)$$

where NIWR is the annual net irrigation requirement ($m^3$), i is the number of given crops, N is the total number of given crops, t is the growth stage and T is the final growth stage, $k_c$ is the crop coefficient, which varies for each crop and growth stage, $ET_o$ is the reference evapotranspiration rate (mm), $P_{eff}$ is effective precipitation (mm), $S_i$ is the area cultivated with crop i (ha), $A_{paddy}$ is the area under paddy irrigation (ha), and S is the net cultivable area. Crop characteristics were obtained from the AQUASTAT database of the Food and Agriculture Organization. The reference crop evapotranspiration was for each grid cell was estimated based on the Penman-Monteith method (Monteith, 1965). The value of the leaf area index throughout the growing season was determined based on the crop coefficients and heights specified by FAO. Figure 4(a) shows the value of the crop coefficient during the different stages of growth.

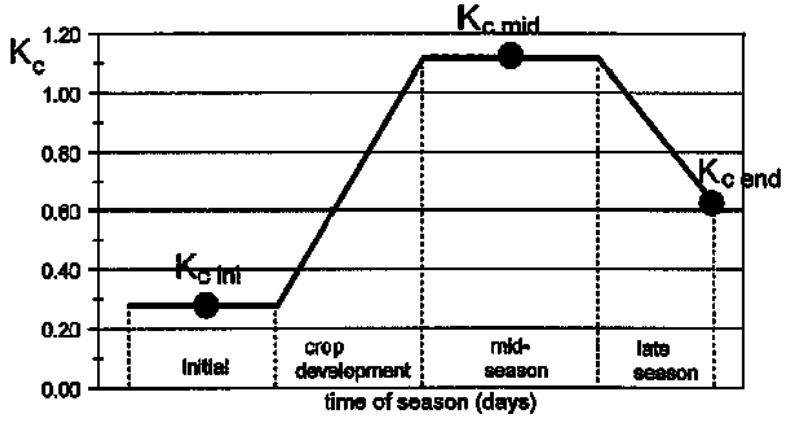


Figure 4 (a): Crop coefficient curve obtained from the Food and Agriculture Organization (source: http://www.fao.org/3/x0490e/x0490e0b.htm)

### 4.2.5 Hydropower potential

The hydropower potential of the multipurpose and hydropower reservoirs was estimated based on monthly release using generic regulation rules as described in Hanasaki *et al.* (2006). The maximum hydropower generation from the dam based on the current hydroelectric facilities such as Installed Hydropower Capacity (IHC), storage capacity, and dam height is termed as developed hydropower potential (DHP, Xingcai Liu et al., 2016). The monthly release $R_m$ ($m^3/s$) from a reservoir was estimated as the case of no irrigation demands in Hanasaki *et al.* (2006) :

$$R_m = \left(\frac{c}{0.5}\right)^2 k_y i_a + \left\{1 - \left(\frac{c}{0.5}\right)^2\right\} i_m \quad (2)$$

where $i_m$ is monthly inflow ($m^3/s$), $i_a$ is mean annual inflow ($m^3/s$), $k_y = S_{beg}/\alpha C$, and $c=F_cC/I_a$. $S_{beg}$ is the reservoir storage at the beginning of a year ($m^3$), C is the maximum storage capacity of the reservoir ($m^3$), $I_a$ is the mean total annual inflow ($m^3/yr$), α is an empirical coefficient (0.85 in this study, as suggested by Hanasaki *et al.* (2006) based on sensitivity analysis), which influences inter-annual variation in releases. The shortcoming of using the $c=C/I_a$ as defined by Hanasaki *et al.* (2006) was the inability of the approach to introducing monthly variation in the storage of the reservoirs of high capacity and low inflow magnitudes. For, most of the reservoirs, the original c value was more than 0.5 causing the reservoirs to release outflow at a constant rate throughout the year (Table 2). The modification in the equation was done by introducing the parameter $F_c$ to better simulate the storage variation of the reservoirs, which is based on the ratio of C and $I_a$. The equation of the $F_c$ is developed by comparing the simulated storage variation and the observed data for the 10 reservoirs with $R^2$ value as 0.8674:

$$F_c = 0.1862\ (C/I_a)^3 - 0.7496\ (C/I_a)^2 + 0.4909\ (C/I_a) + 0.7054 \quad (3)$$

Table 2 shows the value of $F_c$ and α for each reservoir for the estimation of monthly release. Moreover, equation 3 emphasized the annual inflow of the reservoir to govern the storage variation, although the characteristics of equation 2 remained the same. As the annual inflow to the reservoir was affected by climate change and variability, the modified equation enhanced the sensitivity of the reservoir towards climate change, anthropogenic activities, and non-stationarity. The variation in the storage of the reservoirs is governed

by the inflow from the upstream catchment area and outflow from the reservoir to meet the purpose of the dams (hydropower generation, irrigation, and other water demands). For the multipurpose and irrigation dams, the water requirement for the irrigation purpose was estimated using the NIWR simulated by the VIC model. The irrigation demand from the reservoir was estimated by aggregating the NIWR for the grids downstream of the reservoirs. The outflow from the reservoir used for the estimation of the hydropower generation was calculated by deducting the irrigation water supply from the monthly release ($R_m$):

$$O_m = R_m - \sum_{Days} \sum_{Grids} NIWR \times S_r \quad (4)$$

where NIWR ($m^3$) is the daily water requirement of the girds integrated over the number of grids downstream of the reservoirs falling within the commanding area, and $S_r$ is the spatial resolution of the grids (here, 0.05 deg). The streamflow simulated by the VIC model was fed to a reservoir as inflow and the other parameters of the dam to estimate the monthly release using the equation (2). Two conditions were enforced while using the method:

(a) The minimum monthly release was set as 10% of the monthly inflow to the reservoir as the environmental flow requirement to support downstream ecosystem, and

(b) As mentioned in Liu *et al.* (Xingcai Liu et al., 2016), a minimum of 10% of the total capacity of reservoirs is maintained.

The monthly storage of the reservoir was calculated using the monthly inflow and monthly release, which was compared with the observed reservoir storage to ensure that storage follows the rule curve of each reservoir. The developed hydropower (HP, kW) potential of a reservoir was then estimated based on the monthly release:

$$HP = \min(O_m \times h \times g, IHC) \quad (5)$$

where the hydraulic head (h) was assumed to be linearly related to the reservoir storage, h =S/A, where S is the mean reservoir storage during the estimation time step, and A is the reservoir area. Also, A=C/H, where H is the height of the dam, which is also the maximum of h. The annual energy generation was estimated by accumulating the HP developed over each month of the specific year.

*Table 2: Value of the Fc and α for each reservoir for the calculation of monthly release $R_m$ using equation 2.*

| S.No. | Name of dam | Reservoir capacity (million m3) | Average inflow | C/I | Fact_c | Alpha |
|---|---|---|---|---|---|---|
| 1 | Sirindhorn | 1966 | 59.32 | 1.05 | 0.45 | 0.8 |
| 2 | Ubol Ratana | 2859 | 87.08 | 0.00 | 0.7 | 0.8 |
| 3 | Nam Pung | 165 | 3.77 | 1.39 | 0.5 | 0.8 |
| 4 | Lam Takhong | 310 | 9.86 | 1.00 | 0.8 | 0.8 |
| 5 | Lam Phra Phloeng | 110 | 5.31 | 0.66 | 0.75 | 0.8 |
| 6 | Chulabhorn | 188 | 5.41 | 1.10 | 0.8 | 0.8 |
| 7 | Huai Kum | 22.8 | 5.9 | 0.12 | 0.10 | 0.85 |
| 8 | Nam Ngum | 7010 | 459.73 | 0.48 | 0.55 | 0.85 |
| 9 | Xeset 1 | 30 | 26.09 | 0.04 | 0.72 | 0.85 |
| 10 | Theun-Hinboun | 20 | 299.21 | 0.00 | 10.00 | 0.85 |
| 11 | Houay-Ho | 3530 | 8.06 | 13.89 | 0.05 | 0.85 |
| 12 | Nam Leuk | 185 | 184.4 | 0.03 | 1.50 | 0.85 |
| 13 | Nam Mang 3 | 49.43 | 1.31 | 1.20 | 0.20 | 0.85 |
| 14 | Xiaowan | 15043 | 958.24 | 0.50 | 0.79 | 0.85 |
| 15 | Ochum | 1 | 2.08 | 0.02 | 0.71 | 0.85 |
| 16 | Yaly | 1037 | 283.07 | 0.12 | 0.75 | 0.85 |
| 17 | Lam Pao | 1430 | 57.88 | 0.78 | 0.7 | 0.8 |
| 18 | Upper Mun | 141 | 3.24 | 1.38 | 0.45 | 0.8 |
| 19 | Lam Nang Rong | 150 | 1.89 | 2.52 | 0.14 | 0.4 |
| 20 | Lam Sae | 275 | 6.97 | 1.25 | 0.45 | 0.8 |

### 4.2.6 General Circulation models

Four global circulation models (GCM) from two Representative Concentration Pathways (RCPs) 4.5 and 8.5 were used for future meteorological parameters in this analysis and they are GFDL-ESM2M, IPSL-CM5A-LR, MIROC-ESM-CHEM, and NorESM1-M. The selection of the climate models was based on the collection of the distribution of wet/dry and cold/hot climate conditions defined using the precipitation and temperature change for five future periods between 2006 and 2099. The meteorological parameters of the GCMs were bias-corrected and statistically downscaled to 0.25-degree resolution using the Intersectoral Impact Model Intercomparison Project (ISI-MIP) approach (Hempel et al., 2013). Since the future period temperature was higher for all the GCMs relative to the historic period, the cool climate scenario was not analyzed.

### 4.2.7 GoldSim

GoldSim is a powerful and flexible Windows-based system dynamics tool to support the management and decision-making of complex systems by carrying out probabilistic simulations (Paper, 2009). The framework and methodology provided by system simulation help to integrate different components and considerations of the realistic system to explicitly represent the interrelationships and feedback mechanisms and uncertainties about the conditions. The GoldSim simulation environment is a highly graphical and completely object-oriented visual spreadsheet allowing readily evaluation of the system over time and future behavior. GoldSim uses Monte Carlo simulation to propagate uncertainty in processes and parameters defined by the probability distribution and disruptive events throughout the model. Dynamic optimization and scenario analysis capabilities of GoldSim provides the mechanism to support the decision making under transforming conditions based on the available information.

A GoldSim model for the simulation of outflow and hydroelectric generation through the optimal distribution of the water between irrigation and energy sectors from multipurpose and irrigation reservoirs under climate change and irrigation intensification scenarios was developed. The primary forcing data were monthly simulated inflow to the reservoir, NIWR of the downstream irrigated area, and rule curve of the dams. VIC model and Lohmann et al. (1998; 1996) routing scheme was used for the estimation of the inflow to the dam locations for the observed and future climate using the GMFD dataset and four climate models. NIWR was estimated using an improved VIC model including the irrigation scheme developed by Haddeland et al. (2006). The rule curve and depth-storage relationship for the reservoirs were developed using the daily time series of the observed total storage obtained from the reservoir database (http://app.rid.go.th:88/reservoir/) and remote sensing approach.

The model was comprised of different components, called containers, each representing a reservoir. The monthly inflow, NIWR, and storage variation of the reservoirs were defined using the ‘TimeSeries’ input element, whereas the relationship between the storage and depth was defined using the ‘Lookup Table’ element. The equations governing the operation and production of the reservoirs such as water balance equation, energy

generation equation, storage simulation, and ecological flow conditions were defined using the 'Expression' function element. The feedback and interaction between the different members of the model were established by creating a link between the elements.

The optimization of the water distribution between the demand from the different sectors was performed in the model using the Box complex method by defining the objective function and objective variables (Box, 1965). The dynamic optimization of the model was achieved by utilizing the submodel feature of GoldSim and defining the current values of the variables at each time step using the interface between the submodel and outer variables. The objective function for the optimization of reservoir operation was expressed as:

$$\text{Objective Function} = \text{Outflow} + \text{Irrigation\_Supply} \quad (6)$$

where Outflow was the volume of outflow from the reservoir contributing to the energy generation, and Irrigation_Supply is the volume of water supplied to the irrigation sector. The optimization was carried out against the optimization variable, here, Irrigation_Supply with the upper limit as NIWR demand volume and lower limit as 80% of the NIWR demand volume.

The scenario analysis of the hypothetical conditions of intensification of the irrigated area was performed using the scenario manager by varying the scenario data. The variables defining the increase in the irrigated area and the number of crop cycles per year were used as the scenario data to create six scenarios.

### 4.2.8 Irrigated area and scenarios

The amount of water use for the crop is influenced by land use and dependent on the irrigated area. The estimates of the irrigated area for the MRB were inferred from the MRC database for the year 2004 (MRC, 2018), which was further assured by the country-wise irrigation area data from AQUASTAT (2014). The total irrigated area was estimated as 2,110,000 hectares in Myanmar (2004), 61,897,940 hectares in China (2005), 900,000 hectares in Cambodia (2006), 310,000 hectares in Lao PDR (2005), 6,414,880 hectares in Thailand (2007), and 4,585,500 hectares in Vietnam (2005). Although the area equipped

for irrigation in the member countries considers both groundwater and surface water for the water requirement, the proportion of the groundwater supply is negligible. The spatial variation of the irrigated area in the MRB was better exposed by the data obtained at the province level from AQUASTAT (2014).

The net irrigation water requirement (NIWR) is the amount of free available water that is essential for sustained agricultural production and stable food supply. The annual NIWR is directly correlated with the evapotranspiration, therefore, the monthly variation of the NIWR was derived as the function of evapotranspiration (from the modified VIC model with the irrigation scheme) and crop calendar for Thailand (from MRC). Thailand region cultivates rice crop twice a year with sowing period from May to August (January to early March), growing period during September (by the end of April), and harvesting period from October to January (till the end of June) for the first (second) crop cycle. The water is required mainly during the sowing and growth stages (90% of total requirement), while is nominally needed during the harvesting period.

The investigation of the response of the six multipurpose and four irrigation dams under different conditions of agriculture expansion was explored by the development of six scenarios corresponding to 5% and 10% increase in irrigated area by incorporating two-crop cycles or three-crop cycles per year (Table 3). The sowing period for the proposed third crop cycle was October to January, while the growing and harvesting period was February to May. The reference scenario (Scenario1) corresponds to the present condition, viz, two-crop cycles per year, and the irrigated area commissioned for the dams.

*Table 3: Details of the scenarios considered to account for the increase in the water demand by the irrigation sector based on the variation of the irrigation area and number of crop cycles per year*

| S. No. | Scenario | Percentage increase in the irrigation area | Number of crop cycles per year |
|---|---|---|---|
| Scenario1 | 0% increase with 2 cycles (Reference) | 0% | 2 cycles |
| Scenario2 | 5% increase with 2 cycles | 5% | 2 cycles |
| Scenario3 | 10% increase with 2 cycles | 10% | 2 cycles |
| Scenario4 | 0% increase with 3 cycles | 0% | 3 cycles |
| Scenario5 | 5% increase with 3 cycles | 5% | 3 cycles |

| | | | |
|---|---|---|---|
| Scenario6 | 10% increase with 3 cycles | 10% | 3 cycles |

### 4.3 Results and Discussions

#### 4.3.1 Climate Change

The spatial variation of the precipitation is remarkable, following east-to-west gradient, with the mean annual rainfall of 3,000 mm for uplands in the Lao PDR and Cambodia and 1000 to 1600 mm in northeast Thailand in the LMB, whereas in UMB, the Tibetan Plateau receives 600 mm and mountains of Yunnan gets 1700 mm mean annual rainfall. On the other hand, the variation of the temperature and elevation follows a north-to-south gradient. The temperature during the warmest months (March and April) fluctuates between 30 $^{o}$C and 38 $^{o}$C, with November to February marked with the coolest temperature, while the winter temperate at higher elevations of the Lao PDR is around 15 $^{o}$C. Figure A1 shows the spatial variation of the precipitation and temperature in the Mekong River basin. Compared with the historic period of 1950-2005 with mean daily precipitation average of 4.16 mm/day, a modest increase in precipitation was expected in the future between 2006 and 2099 and these increases were 4.26 mm/day for RCP 4.5 and 4.25 mm/day for RCP 8.5. NorESM1-M showed the highest increase in precipitation under RCP 4.5 and RCP 8.5 in the basin, whereas GFDL-ESM2M projected a decline in precipitation. Increase in monthly precipitation for all the months except February to May under RCP 4.5 and RCP 8.5. Mean Annual precipitation for the historic period is 1520 mm, while for the future period is 1551 mm and 1548 mm under RCP 4.5 and RCP 8.5, respectively. The mean annual temperature for the historic period was 22.2 °C, while for the future period it was estimated to be about 23.9 °C and 24.7 °C under RCP 4.5 and RCP 8.5, respectively. The average increase in monthly temperature of 1.8 °C and 2.6 °C were projected between now and the end of the century for RCP 4.5 and RCP 8.5, respectively. The highest increase is predicted for April month.

#### 4.3.2 Flow duration curve

VIC model was used for the simulation of the inflow to the reservoirs using the observed and future climate conditions. The calibration and evaluation of the VIC model were performed using the monthly discharge data from the seven gauging stations distributed

across the basin and 10 reservoirs commissioned for irrigation and/or hydropower generation. The parameter used for the calibration of the model were variable infiltration curve parameter ($b_i$), the depth of the second and third soil layers (D, 0.1m – 1.5m), a fraction of maximum velocity of baseflow where non-linear baseflow begins ($D_s$), and a fraction of maximum soil moisture where non-linear baseflow occurs ($W_s$) with the allowable range as 0.1-0.5, 0.1-1.5, 0-0.4, and 0.5-1.0, respectively. The performance of the VIC model was estimated by calculating the NSE and r values between the monthly simulated and observed streamflow for the calibration and evaluation periods (Table 4). The VIC model was able to precisely simulate the observed streamflow with the NSE value of more than 0.74, and a correlation coefficient of more than 0.91 at gage stations during the calibration and evaluation periods. While the NSE and r values for the inflow at the dam locations were more than 0.5 and 0.71, respectively for the calibration and evaluation periods. The decline in the NSE and r values for the dams as compared to the gage station was partly due to low streamflow magnitudes.

*Table 4: List of the stations used for the calibration and evaluation of the Variable Infiltration Capacity (VIC) model, Nash-Sutcliffe model efficiency coefficient (NSE) and coefficient of correlation (r) values between the observed and simulated streamflow*

| S.No. | Station | | Calibration | | | Evaluation | | |
|---|---|---|---|---|---|---|---|---|
| | Type | Name | Period | NSE | r | Period | NSE | r |
| 1 | Gauge | Chiang Saen | 1986-1991 | 0.84 | 0.94 | 1992-1997 | 0.84 | 0.94 |
| 2 | Gauge | Luang Prabang | 1986-1991 | 0.74 | 0.94 | 1992-1997 | 0.74 | 0.94 |
| 3 | Gauge | Nakhon Phanom | 1986-1991 | 0.80 | 0.91 | 1992-1995 | 0.80 | 0.91 |
| 4 | Gauge | Vientiane | 1986-1991 | 0.77 | 0.94 | 1992-1996 | 0.77 | 0.94 |
| 5 | Gauge | Mukdahan | 1986-1991 | 0.86 | 0.94 | 1992-1995 | 0.86 | 0.94 |
| 6 | Gauge | Pakse | 1986-1991 | 0.84 | 0.94 | 1992-1998 | 0.84 | 0.94 |
| 7 | Gauge | Kratie | 1986-1991 | 0.85 | 0.92 | 1992-1998 | 0.85 | 0.92 |
| 8 | Dam | NamPung | 2004-2010 | 0.6 | 0.78 | 2011-2016 | 0.6 | 0.78 |
| 9 | Dam | UbolRatana | 2006-2011 | 0.63 | 0.89 | 2012-2016 | 0.63 | 0.89 |
| 10 | Dam | Chulabhorn | 2006-2011 | 0.76 | 0.88 | 2012-2016 | 0.76 | 0.88 |
| 11 | Dam | LamPao | 2004-2010 | 0.62 | 0.89 | 2011-2016 | 0.62 | 0.89 |
| 12 | Dam | LamTakhong | 2004-2010 | 0.58 | 0.77 | 2011-2016 | 0.58 | 0.77 |
| 13 | Dam | LamPhraPloeng | 2004-2010 | 0.50 | 0.71 | 2011-2016 | 0.50 | 0.71 |
| 14 | Dam | UpperMun | 2004-2010 | 0.66 | 0.82 | 2011-2016 | 0.66 | 0.82 |
| 15 | Dam | LamSae | 2006-2011 | 0.64 | 0.83 | 2012-2016 | 0.64 | 0.83 |
| 16 | Dam | LamNangRong | 2004-2010 | 0.72 | 0.89 | 2011-2016 | 0.72 | 0.89 |

| | | | | | | | | |
|---|---|---|---|---|---|---|---|---|
| 17 | Dam | Sirindhorn | 2004-2010 | 0.83 | 0.91 | 2011-2016 | 0.83 | 0.91 |

Flow duration curves (FDC) describing the relationship between the probability of exceedance of time and flow magnitude were used for the estimation of DHP for the observed and future period. The flow duration curves were developed by the VIC simulated inflow at the dam locations for observed (1981-2019), historic (1951-80) and future period (2020-2099) using the ensemble mean from the four climate models under RCP 4.5 and RCP 8.5. Figure 5 (a) shows the flow duration curve and change in the flow for the future period for the six multipurpose dams. The high flow events were marginally suppressed during the observed period as compared to the historic duration. The 10% exceedance flow value ($Q_{10}$) for the multipurpose dams varies from 140 $m^3$/sec (Sirindhorn) to 8 $m^3$/sec (Nam Pung). As compared to the historic period, the average reduction in the $Q_{10}$ values for the observed period was 40%. However, the $Q_{50}$ values were highest for Ubol Ratana (23 $m^3$/sec) and Sirindhorn (18 $m^3$/sec), while other multipurpose dams had an average value of 2.6 $m^3$/sec. For the future period, the change in the FDC for the flows with exceedance value less than 20% was positive while the flows more than $Q_{20}$ were negative under RCP 4.5 and RCP 8.5 as compared to the historic period. The future is projected to have high magnitude flood events as compared to the historic period under both RCP 4.5 and RCP 8.5. The magnitude of the flows under RCP 8.5 is projected to be marginally less than the flows under RCP 4.5. But the average flow for all the multipurpose reservoirs is expected to be equal or less than the $Q_{50}$ value of the historic period with an average decrease of 2.5% and 5.2% under RCP 4.5 and RCP 8.5, respectively. Also, the $Q_{95}$ flow values are projected to increase for Ubol Ratana, Lam Takhong, Lam Phra Phloeng, and Chulabhorn.

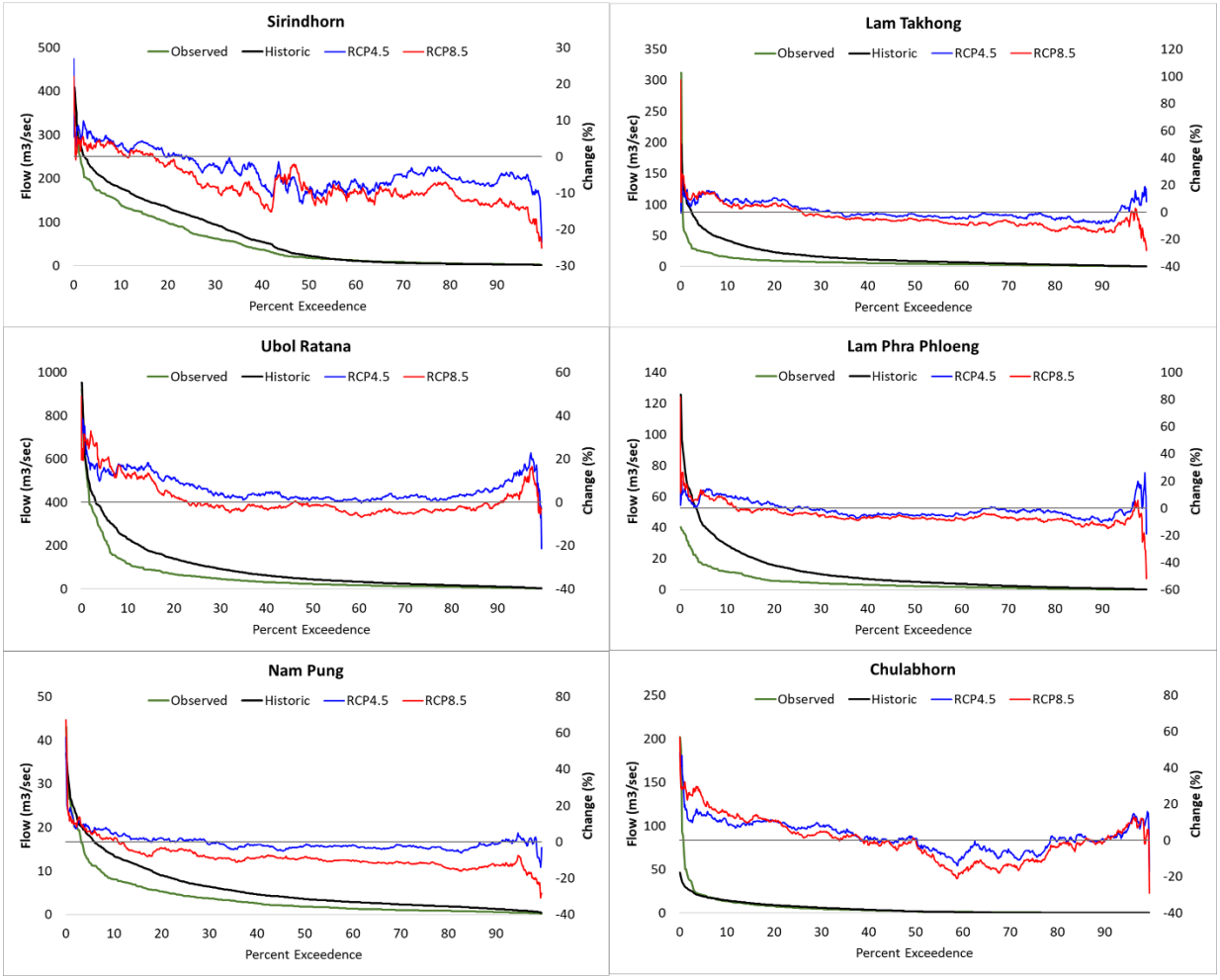


*Figure 5(a): Flow duration curve for the observed (1981-2019) and historic (1951-1980) period for the multipurpose dams. The change in the future flow duration curve (2020-2099) under RCP 4.5 and RCP 8.5 with respect to the historic flow.*

Figure 5 (b) shows the FDC for the historic, observed periods and projected change in the flows for the future period under RCP 4.5 and RCP 8.5 for the four irrigation dams. The FDC shows similar behavior of the inflows to the irrigation as multipurpose dams. The $Q_{10}$ value was highest for the Lam Pao reservoir (112 $m^3$/sec), while for other irrigation dams the value was less than 15 $m^3$/sec. Also, Lam Pao showed the highest average value ($Q_{50}$) of 20 $m^3$/sec, on the other hand, the value was less than 5 $m^3$/sec for the remaining three reservoirs. The project inflow for the future period showed an increase in the values with the probability of exceedance less than 30% of the time ($Q_{30}$) under RCP 4.5 and RCP 8.5.

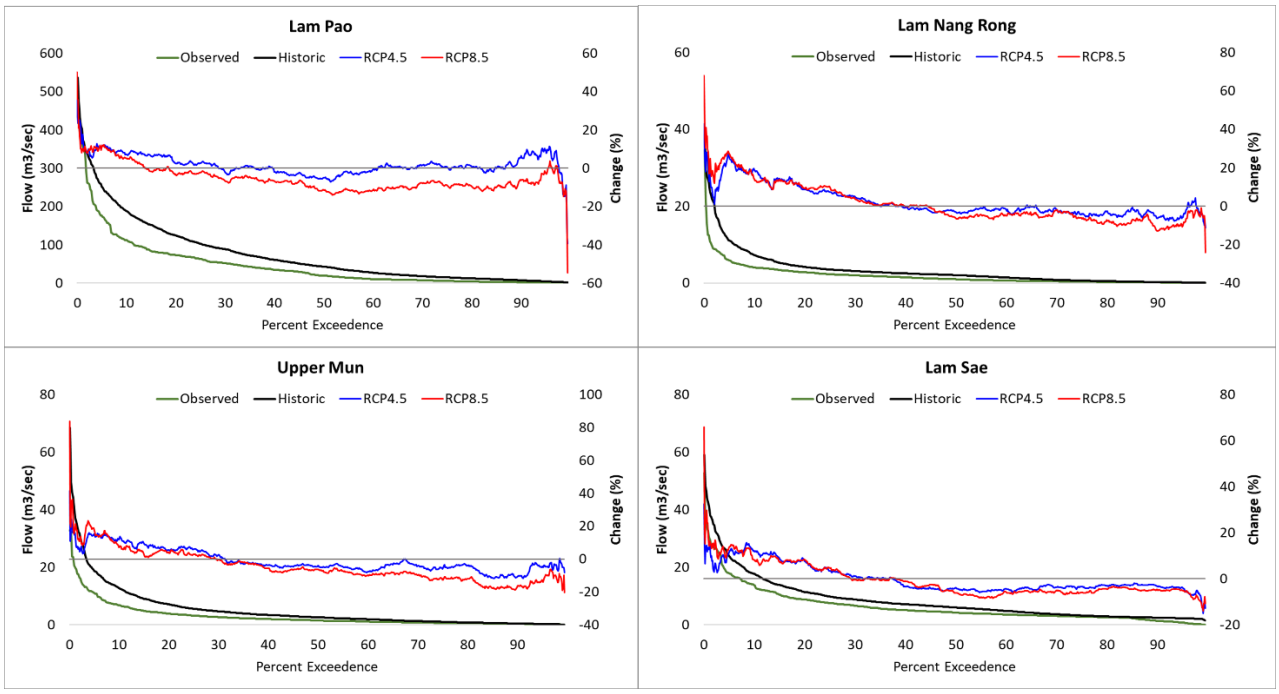


*Figure 5(b): Flow duration curve for the observed (1981-2019) and historic (1951-1980) period for the irrigation dams. The change in the future flow duration curve (2020-2099) under RCP 4.5 and RCP 8.5 with respect to the historic flow.*

The FDC for the hydropower dams showed high flow for the Xiaowan, Nam Ngum, Theun-Hinboun, Yaly and Nam Leuk reservoirs with Q10 values as 2300 $m^3$/sec, 1000 $m^3$/sec, and 720 $m^3$/sec, 550 $m^3$/sec, and 435 $m^3$/sec, respectively and Q50 values as 650 $m^3$/sec, 315 $m^3$/sec, and 175 $m^3$/sec, 160 $m^3$/sec, and 100 $m^3$/sec, respectively (Figure 5(c)). On the other hand, the remaining hydropower dams showed low flow with $Q_{10}$ varying between 3 $m^3$/sec to 60 $m^3$/sec with an average value of 20 $m^3$/sec. However, the average inflow for the low-flow hydropower dams during the historic period was estimated as 4 $m^3$/sec.

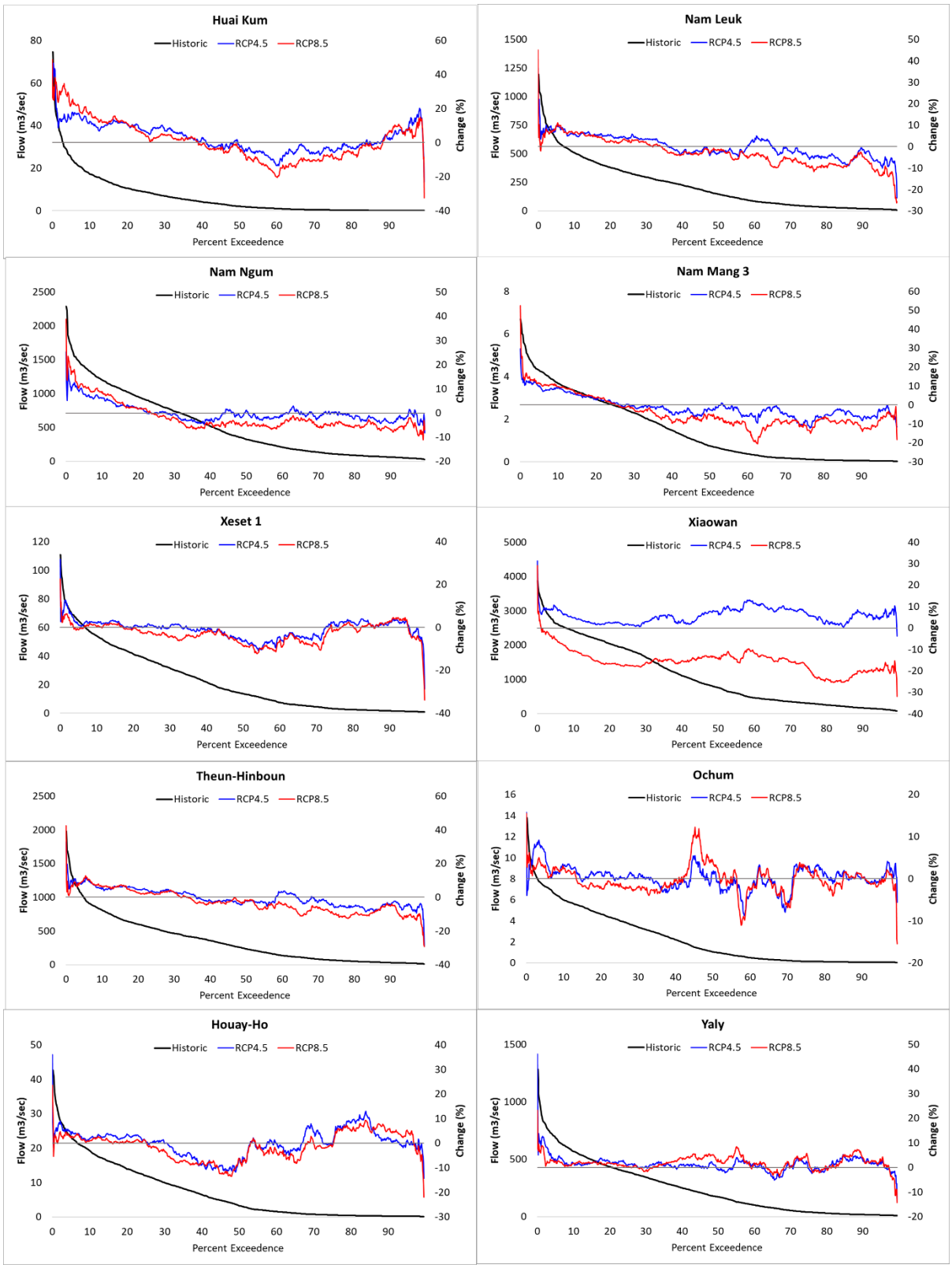


*Figure 5(c): Flow duration curve for the historic (1951-1980) period for the hydropower dams. The change in the future flow duration curve (2020-2099) under RCP 4.5 and RCP 8.5 with respect to the historic flow.*

The impact of climate change on the inflow to the hydropower reservoirs shows an increase in the magnitude of the high flow, while the inflow flow value is projected to decrease. The effect on each dam is specific to the catchment area of the reservoir. The contrasting difference in the climate effect for Xiaowan under RCP 4.5 and RCP 8.5 can be attributed to the difference in the precipitation for the catchment of the reservoir. The decrease in the average flow is projected to be three-fold under RCP 8.5 as compared to RCP 4.5 for all the hydropower dams accounting 1.4% and 3.6% under RCP 4.5 and RCP 8.5, respectively as compared to the historic flow.

### 4.3.3 Comparison of storage and outflow

The performance of the approach in simulating the dam operation was determined by comparing the monthly simulated storage variation and outflow from the multipurpose and irrigation reservoirs with the observed data from 2006 to 2019. Mathematically, the capability was accessed by the calculation of the Nash-Sutcliffe model efficiency coefficient (NSE, Nash & Sutcliffe, 1970), coefficient of correlation (r) and relative root mean square error (RRMSE) between the simulated and observed storage, while r value was estimated for the outflow (Table 5). Figure 6(a) shows the comparison between the monthly observed and simulated storage variation and the outflow from the multipurpose dams. The variation in the monthly observed storage of the reservoirs was precisely followed by the simulated storage with NSE values more than 0.6 for Ubol Ratana and Nam Pung, while the value for other multipurpose reservoirs was 0.33. Also, the r-value for the monthly storage comparison was more than 0.7 for all the multipurpose reservoirs, except Lam Phra Phloeng.

*Table 5: The accuracy of the simulated storage variation and outflow from the multipurpose and irrigation dams estimated by the calculation of Nash-Sutcliffe model efficiency coefficient (NSE), coefficient of correlation (r), and relative root mean square error (RRMSE) between the observed and simulated values from 2006 to 2019.*

| S.No. | Dam | Purpose | Storage | | | Outflow |
|---|---|---|---|---|---|---|
| | | | NSE | r | RRMSE | r |
| 1 | Ubol Ratna | Multipurpose | 0.64 | 0.87 | 27.23 | 0.53 |
| 2 | Sirindhorn | Multipurpose | 0.33 | 0.74 | 20.17 | 0.63 |
| 3 | Nam Pung | Multipurpose | 0.63 | 0.88 | 23.05 | 0.37 |
| 4 | Lam Takhong | Multipurpose | 0.35 | 0.71 | 32.29 | 0.26 |
| 5 | Lam Phra Phloeng | Multipurpose | 0.33 | 0.60 | 37.46 | 0.41 |
| 6 | Chulabhorn | Multipurpose | 0.33 | 0.79 | 34.27 | 0.31 |

| | | | | | | |
|---|---|---|---|---|---|---|
| 7 | Lam Pao | Irrigation | 0.56 | 0.78 | 30.41 | 0.64 |
| 8 | Upper Mun | Irrigation | 0.57 | 0.77 | 25.65 | 0.47 |
| 9 | Lam Rang Rong | Irrigation | 0.42 | 0.72 | 22.97 | 0.78 |
| 10 | Lam Sae | Irrigation | 0.54 | 0.75 | 24.76 | 0.16 |

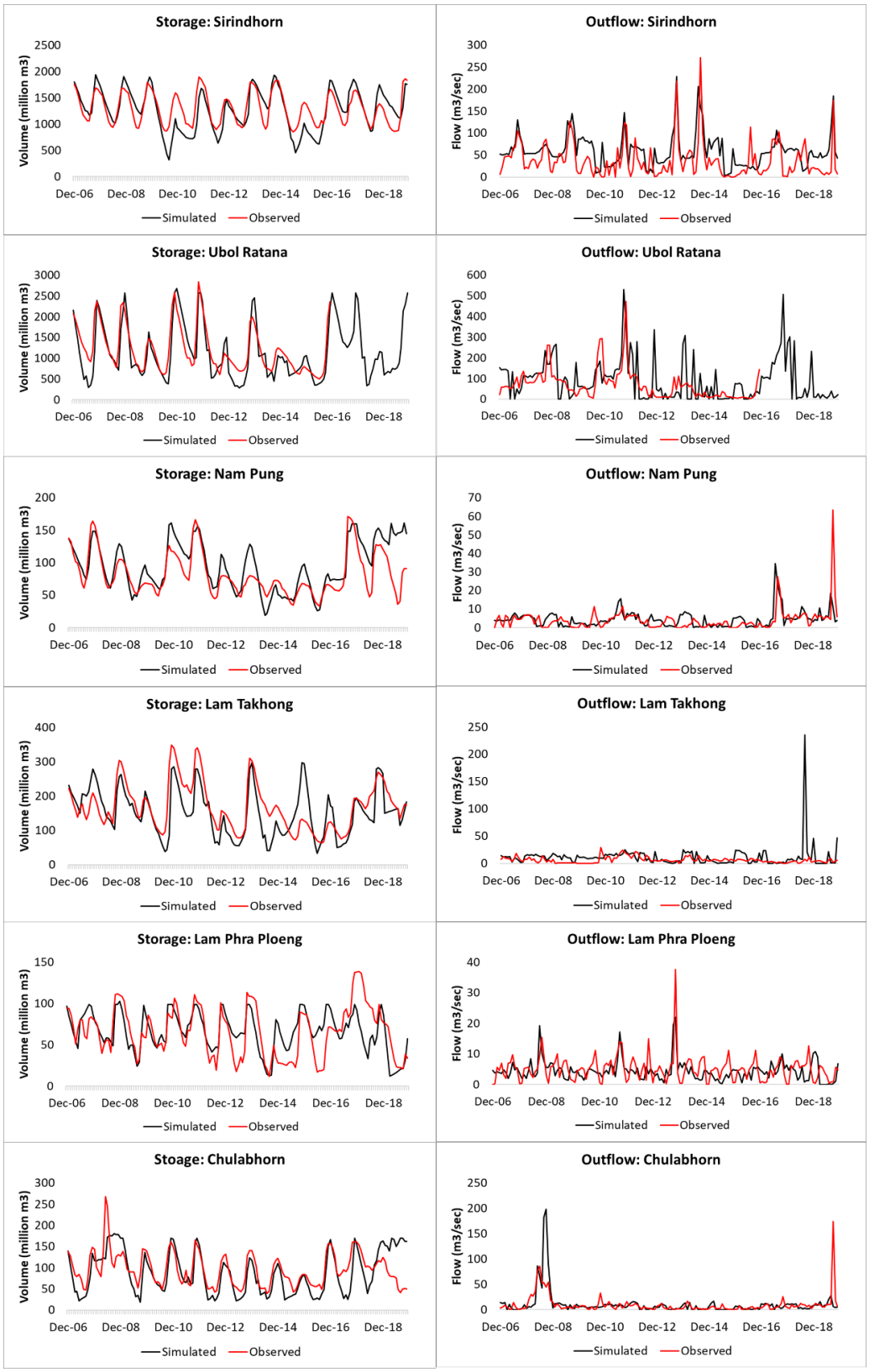


*Figure 6(a): Evaluation of the approach with the comparisons of the simulated and observed streamflow and outflow from the six multipurpose dams from 2006 to 2019*


*Figure 6(b): Evaluation of the approach with the comparisons of the simulated and observed streamflow and outflow from the four irrigation dams from 2006 to 2019*

The estimated error for the simulated storage variation in the observed storage varied from 20% (Sirindhorn) to 37% (Lam Phra Phloeng) for the multipurpose reservoirs. On the other hand, the observed outflow from the reservoirs showed high fluctuation between the months due to the high-frequency operation of the gates of the dam to fulfill high varying demand as evident from the monthly NIWR simulated using the VIC model. The simulated outflow takes into consideration the ecological flow requirement and irrigation water demand from the reservoir for each month, however other miscellaneous demands such as reservoirs such as municipal water demand, industrial demand were assumed to be

negligible. As a result, the average simulated outflow from the reservoirs was marginally higher than the observed monthly outflow with an effect of the accuracy of the outflow estimates. The r-value between the observed and simulated monthly outflow from the multipurpose reservoirs ranged between 0.26 to 0.63. The low r-value for Lam Takhong was due to the limitation of this approach in simulating the extremely high outflow (10 times the average outflow) that occurred during the flood event in 2018 in Thailand.

Figure 6 (b) shows the comparison of the monthly simulated storage and outflow with the observed data from 2006 to 2019 for the four irrigation reservoirs. The efficacy of the approach to simulate the operation of the irrigation reservoirs was exhibited with the NSE values more than 0.54 (except Lam Nang Rong with NSE value equal to 0.42) and r value more than 0.72. The RRMSE for the storage simulation was confined within 30% with respect to the observed monthly storage. The approach performed better in simulating the outflow for the irrigation reservoir with r-value up to 0.78 as compared to the multipurpose reservoirs. The outflow simulation for the Lam Sae reservoir was not able to harmonize with the high fluctuating observed outflow as the water supply for irrigation from Lam Sae was steady over the period.

The monthly storage variation for the 10 hydropower reservoirs was simulated from 2006 to 2019 using the VIC simulated inflow (Figure 6(c)). The comparison of the simulated storage and outflow with the observed data was not performed due to the absence of the observed data, however, the simulated storage variation exhibits a similar pattern shown by the rule curve derived from the surface area variation of the reservoirs. The storage of the reservoirs was highest after the monsoon season (October -November), which gradually decreases to the minimum storage before the onset of the monsoon (April-May). The storage variation was governed by the inflow to the reservoirs, as a result, there exists a discrepancy between the magnitude of the simulated storage and rule. The range of the storage variation was dependent on the storage capacity, inflow, and ecological flow demand from the reservoirs. Similar characteristics were shown by the simulated outflow from the hydropower reservoirs with high outflow during the monsoon season and low flows during the dry season. However, as compared to the inflow, the outflow was suppressed during the monsoon season to facilitate the impoundment of inflow to increase the reservoir storage and the outflow was more than inflow during the dry season. The

monthly simulated outflow for the reservoirs was dependent on the storage variation, inflow, and ecological flow requirement to the downstream region (Figure 6(d)). The monthly release value is the governing factor for the estimation of the DHP of the hydropower dams.

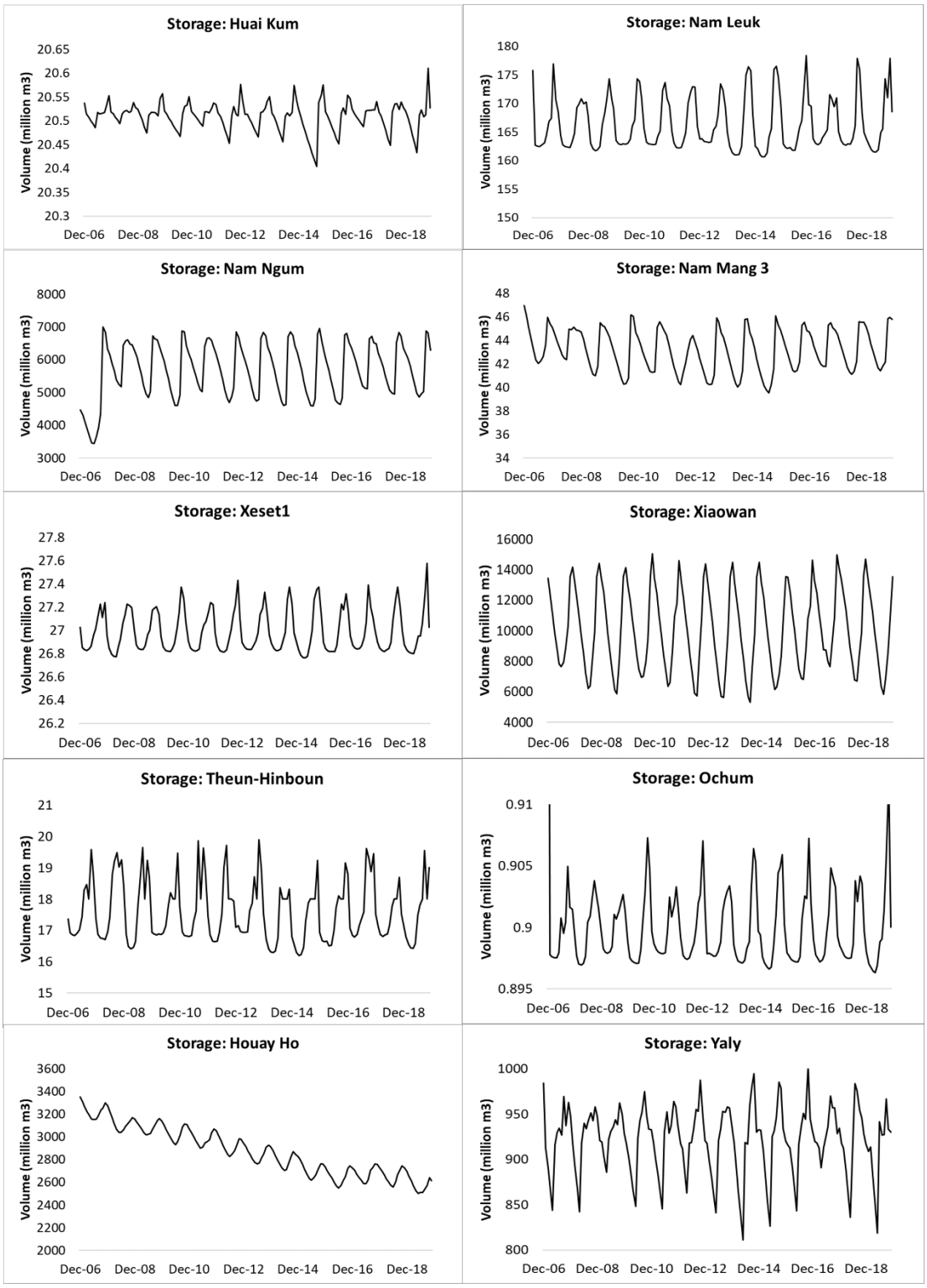


*Figure 6(c): The monthly simulated storage variation of the 10 hydropower dams from 2006 to 2019.*

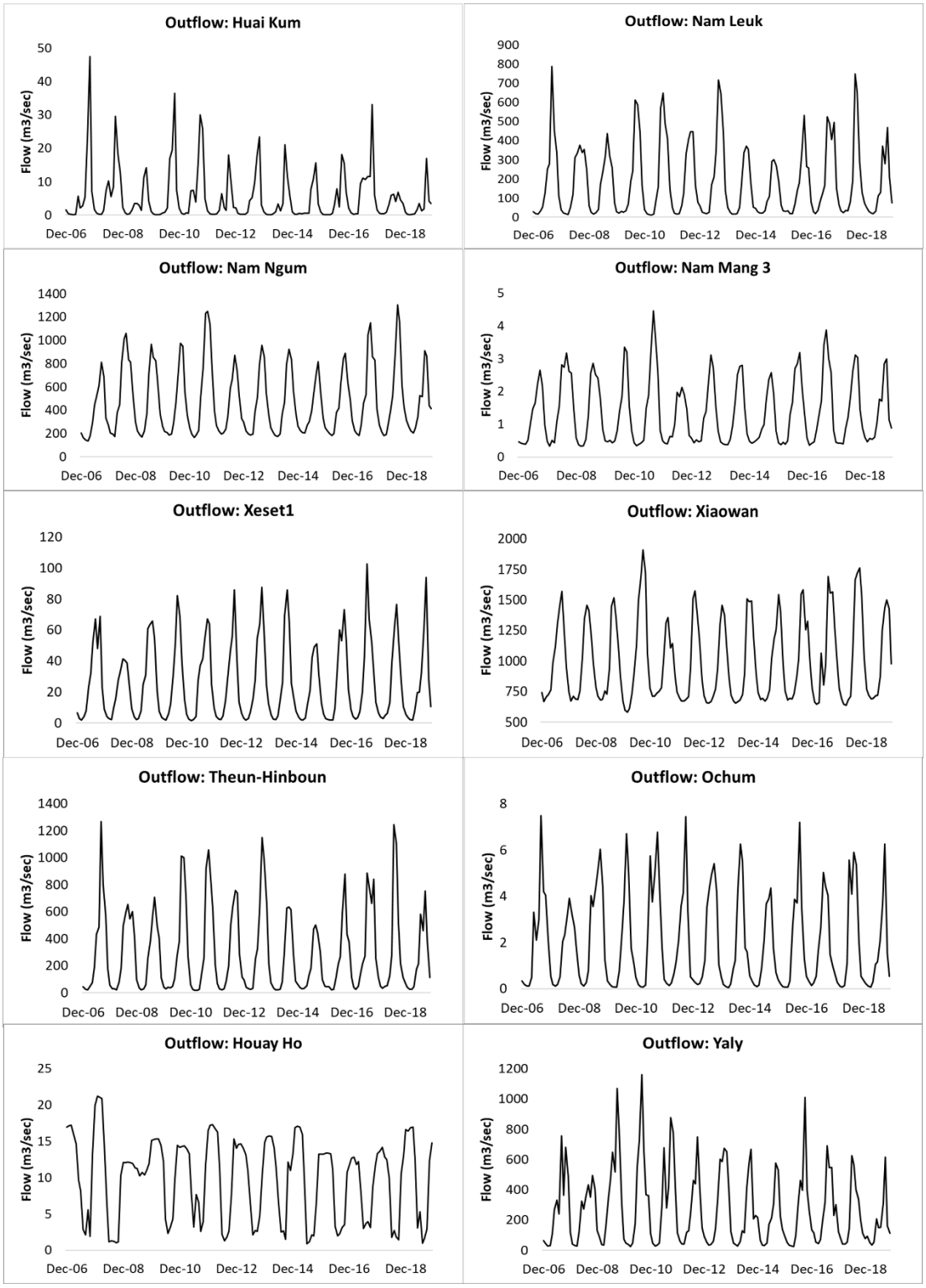


*Figure 6(d): The monthly simulated outflow from the 10 hydropower dams from 2006 to 2019.*

### 4.3.4 Hydropower generation

The hydropower production was dependent on the inflow to the dams and storage variation of the reservoirs governing the rule curve. However, irrigation water supply also plays a dominant role in the hydropower estimates of the multipurpose dams. Figure 7(a) shows the annual energy generation and percentage of irrigation water demand fulfilled by the six multipurpose dams for the observed period from 2007 to 2019. The irrigation water demand from the dam was estimated by accumulating the NIWR of the downstream area within the proximity of the reservoir. The commanding area (Here it is also called as contributing area) of the water supply for irrigation was governed by the total storage capacity of the reservoirs. The Sirindhorn, Ubol Ratana, Nam Pung, Lam Takhong, Lam Phra Phloeng, and Chulabhorn supplied water to an approximate irrigated area of 280 $km^2$, 1420 $km^2$, 70 $km^2$, 490 $km^2$, 440 $km^2$, and 640 $km^2$, respectively.

As the reservoir operation was confined by the ecological flow to support the ecosystem downstream of the reservoir and minimum water storage of the reservoir to be maintained as 10% of the storage capacity, the water supplied for irrigation fluctuates over the monthly time scale. The annual energy generation of the reservoir was estimated by accumulating the monthly hydropower production for the observed period. The average energy production of the Sirindhorn dam was estimated as 136 GWh with the irrigation supply satisfying the 96.6% of the water demand as compared to the observed value of 90 GWh. Similarly, the Ubol Ratana was able to produce the 89 GWh of annual energy and supply 90% of the irrigation water requirement. The annual energy production of the Nam Pung, Lam Phra Phloeng, and Chulabhorn was slightly lower than the targeted value with 10 GWh, 12.23 GWh, and 33 GWh, respectively, along with the water supply satisfaction more than 85%. While the annual energy production of the Lam Takhong dam was confined to 80 GWh due to low inflow to the dam, however, more than 95% of the irrigation water demand was satisfied. The inconsistency between the simulated and observed annual energy production of the hydropower dams can be attributed to the efficiency of the dam operation and the number of turbines. On average, the multipurpose dams were able to generate 86% of the desired annual energy and satisfy more than 90% of the irrigation water demand. The catchment behavior in response to the meteorological changes was reflected in the variation of the annual energy generation and irrigation water

supply. The energy production and irrigation supply were observed to the minimum during 2015 due to low inflows to the dams caused by the decreased precipitation.


*Figure 7(a): The annual energy generation (GWh) and the percentage of the irrigation water demand met by the multipurpose reservoirs from 2007 to 2019.*

Figure 7(b) shows the annual variation of the percentage water demand for irrigation supplied by the four irrigation dams during 2007-2019. Lam Pao was designated to supply water to approximately 1500 $km^2$ of the irrigated land, whereas the command area of the water supply for Upper Mun, Lam Nang Rong, and Lam Sae reservoir was defined as 240 $km^2$, 95 $km^2$, and 205 $km^2$, respectively. The reservoir mechanism for the water allocation from the irrigation dams was straightforward as the water withdrawal for the energy generation was relaxed. Lam Pao and Lam Sae supplied more than 91% of the water demand for irrigation, whereas 88.5% of the water demand was met by Lam Nang Rong. The lowest water supply satisfaction was exhibited by Upper Mun accounting 82.4%

caused due to low water availability during 2015 with the supply percentage as 36%. The fluctuating NIWR combined with the varying inflow to the dams influence the performance of the dam in maintaining the constant satisfaction level. The overall efficiency of the irrigation dams was estimated to be 90% in satisfying the irrigation water demand.

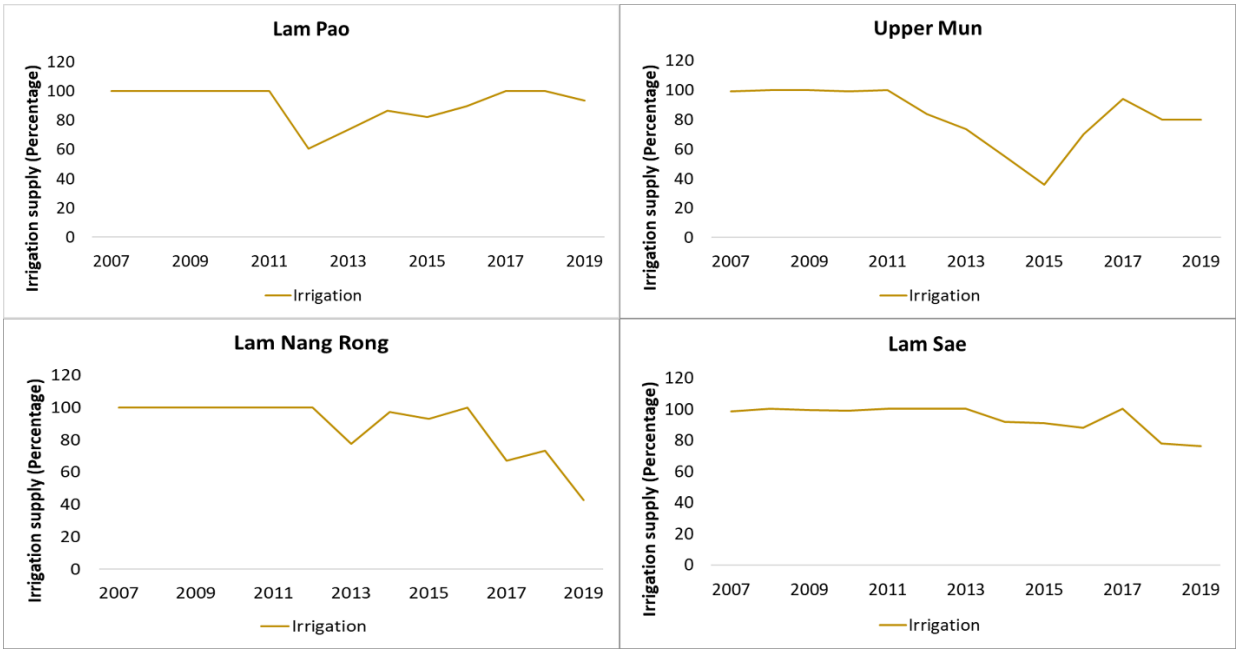


*Figure 7(b): The percentage of the irrigation water demand met by the irrigation reservoirs from 2007 to 2019.*

The hydropower production of the dams commissioned for energy generation was dependent on the reservoir storage and meteorological conditions of the catchment that contributed the inflow to the dams. The annual energy generation of the 10 hydropower dams is shown in figure 7(c) for the observed period. As compared to the multipurpose dams, the energy production of the hydropower dams was more consistent as the abrupt water supply for the irrigation purpose was eradicated. Xiaowan was the highest energy-producing dam as it was located on the main stem of the Mekong River with an average inflow of 960 $m^3$/sec. On the other hand, the lowest energy production was estimated for the Nam Mang3 with an average value of 2.3 GWh. The average annual energy production of the Huai Kum, Nam Ngum, Nam Leuk, and Xiaowan satisfied the required annual production with values 5.8 GWh, 1230 GWh, 337 GWh, and 16900 GWh, respectively. While the remaining dams showed suppressed energy production accounting 36.7 GWh, 609 GWh, 55 GWh, 2.3 GWh, 1.5 GWh, and 1460 GWh for Xeset1, Theun-Hinboun,

Houay-Ho, Nam Mang3, Ochum, and Yaly. The reduced energy production of the dams can be majorly attributed to the catchment response to the meteorological conditions along with the efficiency of the dam operation and quantity of the turbines. The effect of the low flow during 2015 was reflected in the energy production of the hydropower dams. The combined efficiency of the hydropower dams was estimated as the production of 80% of the annual energy target.

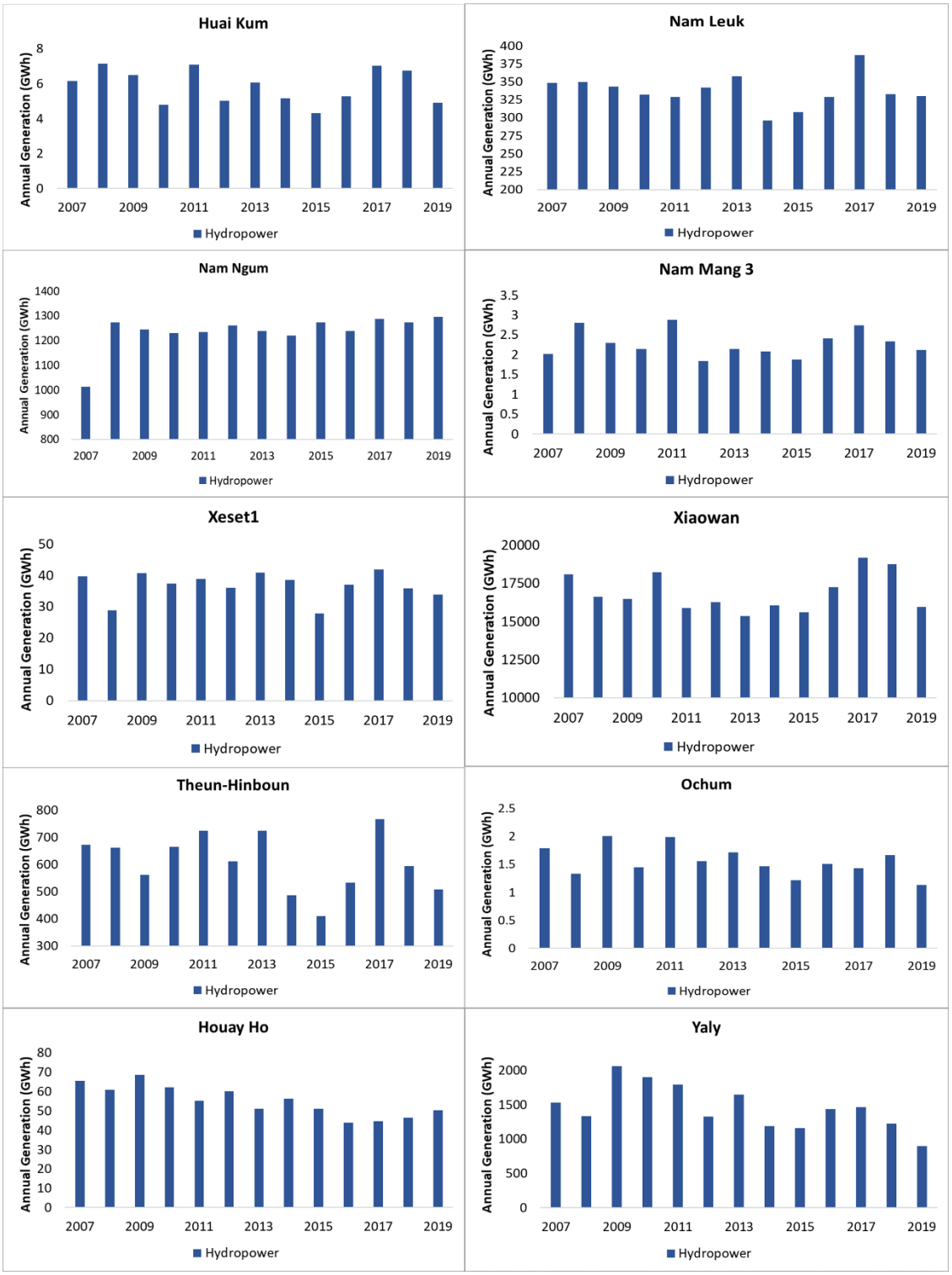


*Figure 7(c): The annual energy generation (GWh) by the hydropower reservoirs from 2007 to 2019.*

### 4.3.5 Hydropower potential under climate change

The effect of climate change will be reflected in the operation of the reservoir through the variation in the streamflow and the net irrigation water demand. Figure 8(a) shows the annual energy generation (GWh) and the percentage of the irrigation water demand met by the multipurpose reservoirs from 1950 to 2099 under the influence of climate change under RCP 4.5 and RCP 8.5. Climate change is expected to have positive feedback on the energy potential and irrigation water supply from the multipurpose dams in the Mekong river basin. The increase in the energy potential of the Ubol Ratana, Lam Takhong, and Chulabhorn is expected to be more than 11% in the future as compared to the historic period. While the change in the energy potential of the NamPung, Sirindhorn and Lam Phra Phloeng is projected as +1.55%, -0.36%, and -0.15%, respectively, under RCP 4.5, however, the decrease is expected to be 3.65%, 3.42%, and 4.87%, respectively, under RCP 8.5 during the period 2021-2099. The irrigation supply from the multipurpose is forecasted to marginally be affected by climate change with the increase of 1.31%, 0.03%, 0.46% for Ubol Ratana, Nam Pung, and Lam Takhong, respectively for the future period with respect to the historic period. The decrease in the future irrigation water demand satisfaction from the Sirindhorn and Lam Phra Phloeng is anticipated as -0.38%, and -3.07%, respectively. On the other hand, under the RCP 8.5 scenario, the water supply for the irrigation purpose is expected to be worse than the RCP 4.5 with an average decrease of 1.87% for all the multipurpose reservoirs except Chulabhorn. The Chulabhorn catchment response to climate change will enable the reservoir to satisfy 1.5% more water demand of the irrigation sector in the future as compared to the historic period. Overall, the water supply from the multipurpose dams will be able to meet more than 85% of the water demand under RCP 4.5 and RCP 8.5.

Figure 8(b) shows the percentage of the irrigation water demand met by the irrigation reservoirs from 1950 to 2099 under the influence of climate change under RCP 4.5 and RCP 8.5. Climate change under RCP 4.5 will marginally affect the water diversion from the irrigation reservoirs in the future. Specifically, the projected decrease of 0.04%, 0.93%, and 0.54% in satisfying the irrigation water demand is expected for Lam Pao, Upper Mun, and Lam Nang Rong, respectively. While Lam Sae is anticipated to experience an increase in meeting the water demand from 98.9% to 99.1% for the period 2021-2099 under RCP

4.5 as compared to the historic period. However, the irrigation supply efficiency is projected to suffer an average decrease of 1.45% in meeting the water demand under RCP 8.5 with the highest decrease of 2.8% for Upper Mun and the least decrease of 0.04% for the Lam Sae reservoir. But the reservoirs are expected to satisfactorily fulfill more than 86% of the future water demand from the irrigation sector. Based on the projected production of seven hydropower projects, Thailand is expected to experience 6.3% and 4.3% increase in hydropower generation under RCP 4.5 and RCP 8.5, respectively. A similar change in the hydropower generation is projected for Cambodia and Vietnam based on the single dam analysis accounting 1.9% (1.6%), and 2.5% (3.1%) increase under RCP 4.5 (RCP 8.5). While the Xiowan dam in China will experience a change of +2.7% and -18.9% in the hydropower generation for the future period under RCP 4.5 and RCP 8.5. On the other hand, Laos PDR will suffer from the marginal reduction in the energy generation accounting 0.1% and 0.9% under RCP 4.5 and RCP 8.5, respectively. Since all the ten irrigation supply reservoirs are located in Thailand, the irrigation met efficacy is projected to decline by 0.2% and 1.3% under RCP 4.5 and RCP 8.5, respectively, even though meeting more than 90% of the irrigation water demand.

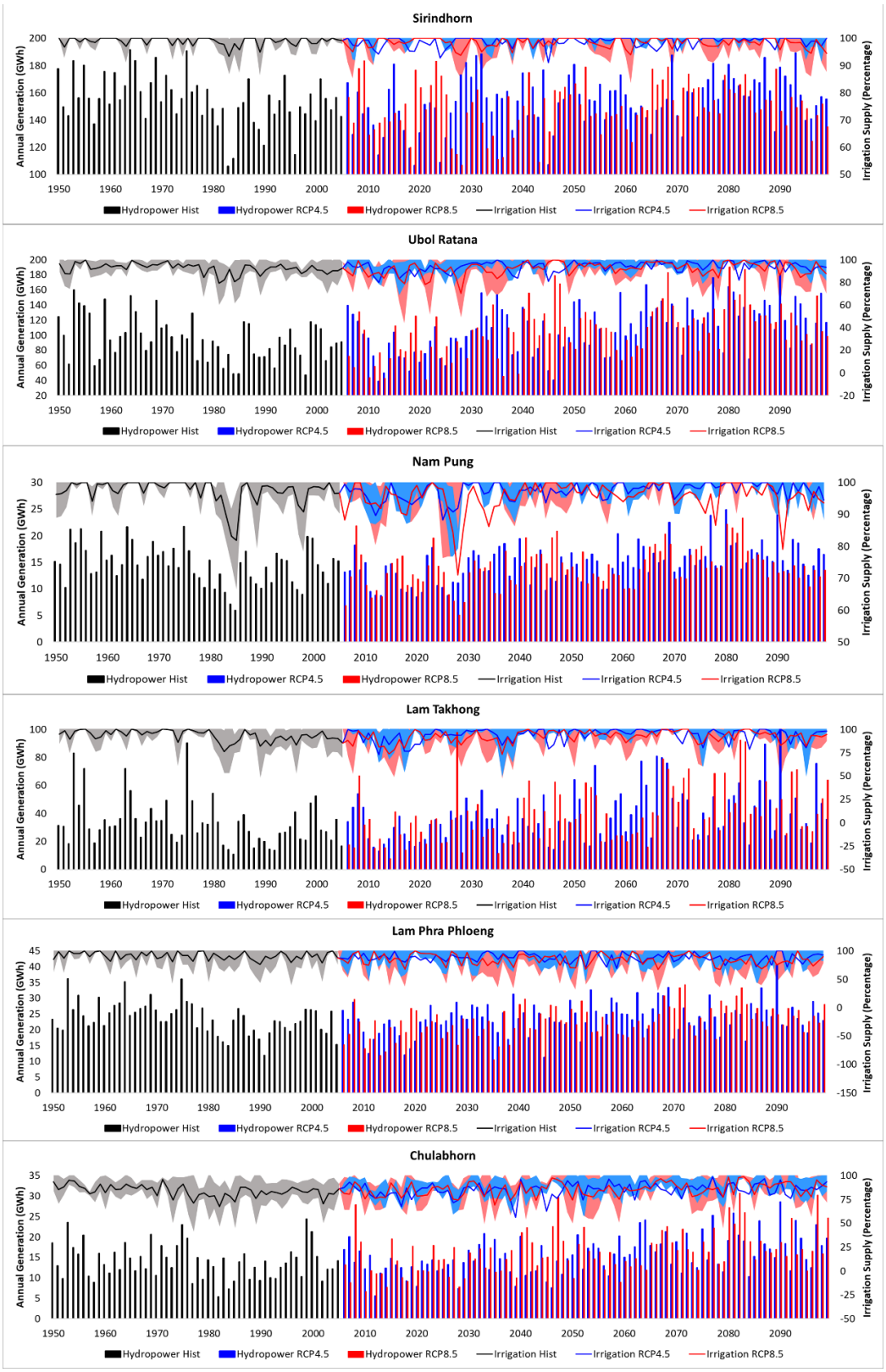


*Figure 8(a): The annual energy generation (GWh) and the percentage of the irrigation water demand met by the multipurpose reservoirs from 1950 to 2099 under the influence of climate change under RCP 4.5 and RCP 8.5.*

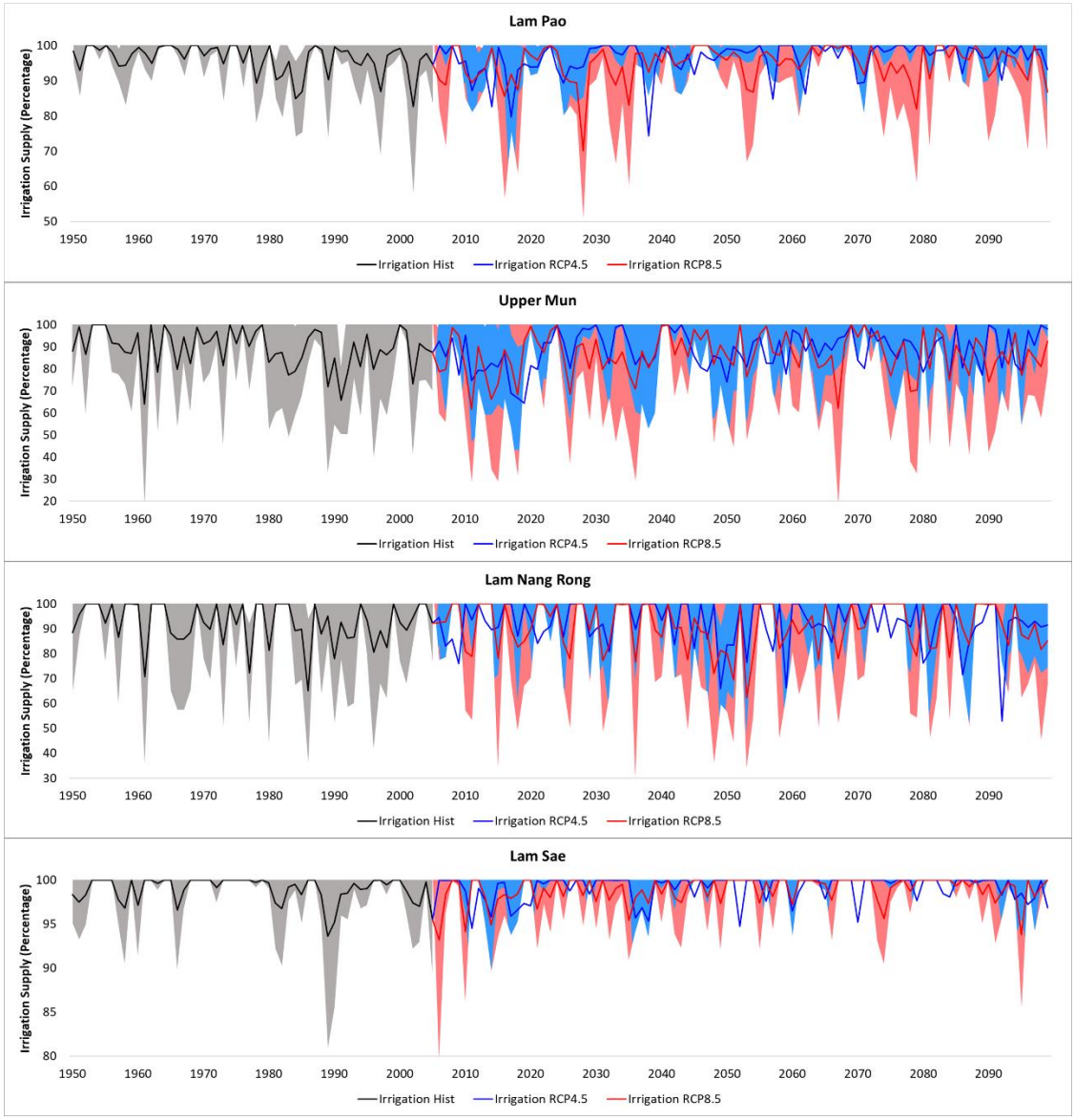


*Figure 8(b): The percentage of the irrigation water demand met by the irrigation reservoirs from 1950 to 2099 under the influence of climate change under RCP 4.5 and RCP 8.5.*

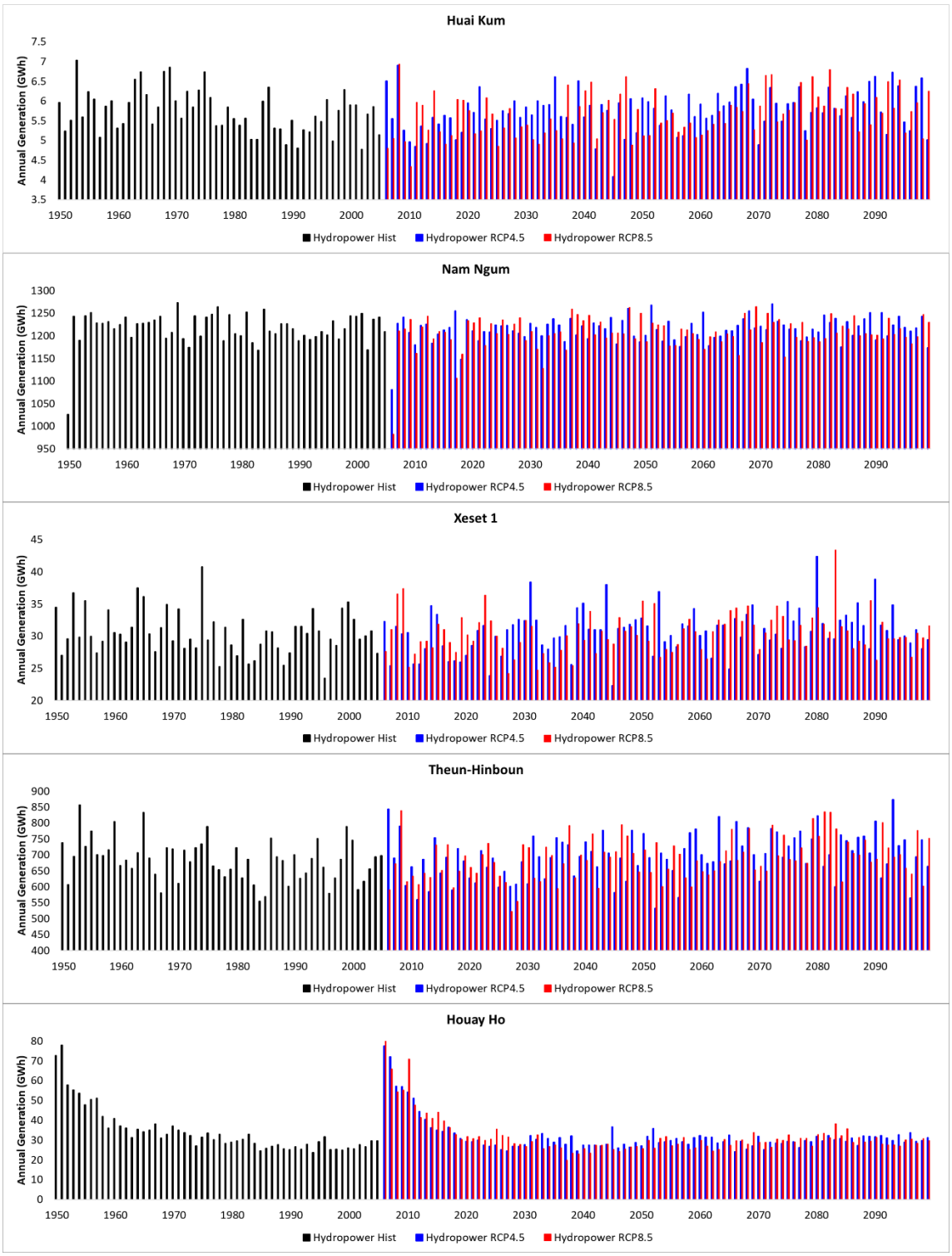


*Figure 8(c): The annual energy generation (GWh) by the hydropower reservoirs from 1950 to 2099 under the influence of climate change under RCP 4.5 and RCP 8.5.*

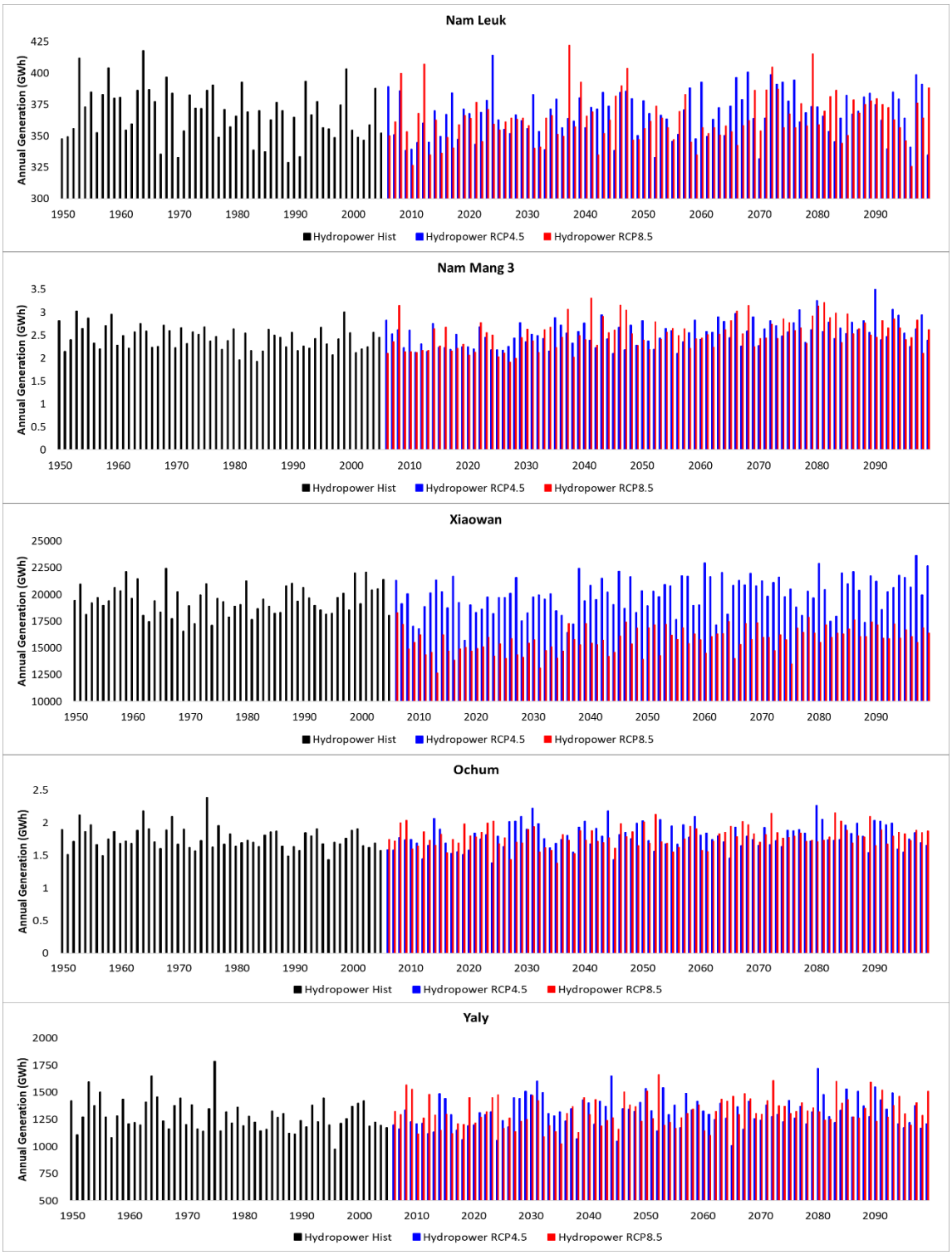


*Figure 8(d): The annual energy generation (GWh) by the hydropower reservoirs from 1950 to 2099 under the influence of climate change under RCP 4.5 and RCP 8.5.*

The annual energy generation (GWh) by the hydropower reservoirs from 1950 to 2099 under the influence of climate change under RCP 4.5 and RCP 8.5 is shown in Figure 8(c) and 8(d). The response of the climate change on the hydropower potential of the dams is specific to the catchment behavior of the reservoirs. The climate change is expected beneficial for the Theun-Hinboun, Nam Mang3, Ochum and Yaly with the increase of 1.86%, 4.08%, 1.92%, and 2.5%, respectively, in the energy potential for the future period under RCP 4.5, however, the increase will be marginally suppressed to the value 0.74%, 3.7%, 1.63%, and 3.13%, respectively under RCP 8.5. Contradictorily, the Nam Ngum, Houay-Ho, and Nam Leuk are anticipated to suffer a decrease of 0.17%, 6.97%, and 0.28%, respectively, in the future energy potential under RCP 4.5, which will further fall to 0.85%, 7.62%, and 1.18%, respectively under RCP 8.5. On the other hand, remaining dams were expected to behave differently under RCP 4.5 and RCP 8.5 future climate scenarios. The projected annual energy potential of the Huai Kum, Xeset1, and Xiaowan is anticipated to increase by 0.38%, 0.59%, and 2.7%, respectively, in future under RCP 4.5 as compared to the historic period, while the energy potential is expected to reduce by 1.43%, 0.48%, and 19%, respectively, under RCP 8.5.

### 4.3.6 Hydropower potential under varying water demand

The energy generation of the multipurpose dams and the efficacy of the irrigation dams are driven by the inflow to the reservoirs and NIWR based irrigation water demands. The inflow and NIWR estimates are primarily governed by the meteorological conditions of the catchment and irrigation supply area. The anthropogenic impact on the performance of the multipurpose and irrigation dams was evaluated by assuming the increase in the irrigated area and the introduction of additional crop cycle to ensure the food security of the region. Figure 9(a) shows the change in the irrigation water supply and energy production of the multipurpose dams under different scenarios for the observed period (2006-2020) and future period (2021-2099) under RCP 4.5 and RCP 8.5 relative to the reference scenario (0% increase in irrigated area and 2 crop cycles per year) for observed period. During the observed period, the influence of the increase in the irrigated area (5% and 10%) resulted in the marginal increase in the irrigated water supply (0.17%) above 90% at the cost of energy generation (-1.5%). Moreover, the inclusion of the third crop

cycle in a year caused a reduction in the irrigation water supply as well as energy generation of the multipurpose dams. The decrease in the irrigation water supply was insignificant (-0.15%), but the energy generation is reduced by more than 10%. In addition, the increase in the irrigated area with 3 crop cycles per year further reduced the energy generation of the dams. On the other hand, the irrigation dams were able to supply the full demand of the irrigation water under all the scenarios of irrigation expansion under observed climate as the constraint of the water allocation for the energy generation was relaxed (Figure 9(b)). Figure 10 shows the annual change in the irrigation water supply and energy generation for the multipurpose dams for the observed period for different scenarios with respect to the reference scenario. The irrigation water supply was marginally impacted by the increased food production throughout the observed period, but the energy generation was reduced for every year under all the scenarios. The energy generation was considerably reduced during 2015 due to low inflow to the reservoir caused by the minimal precipitation. On the other hand, 2008 was the least affected year due to the availability of the abundant water supply for the irrigation and energy sector, although the energy generation by the dams was reduced as compared to the reference scenario.

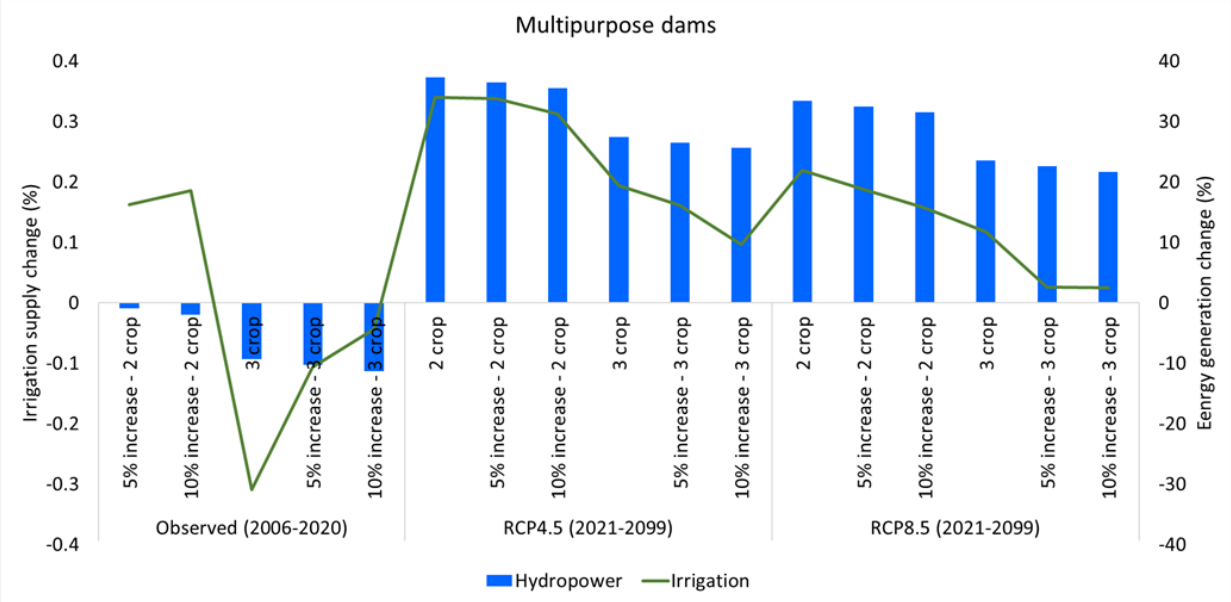


*Figure 9(a): Change in the irrigation supply and energy generation under different scenarios of irrigated area expansion and number of crop cycle per year under observed climate and future period under RCP 4.5 and RCP 8.5 for multipurpose dams in the Mekong River Basin*

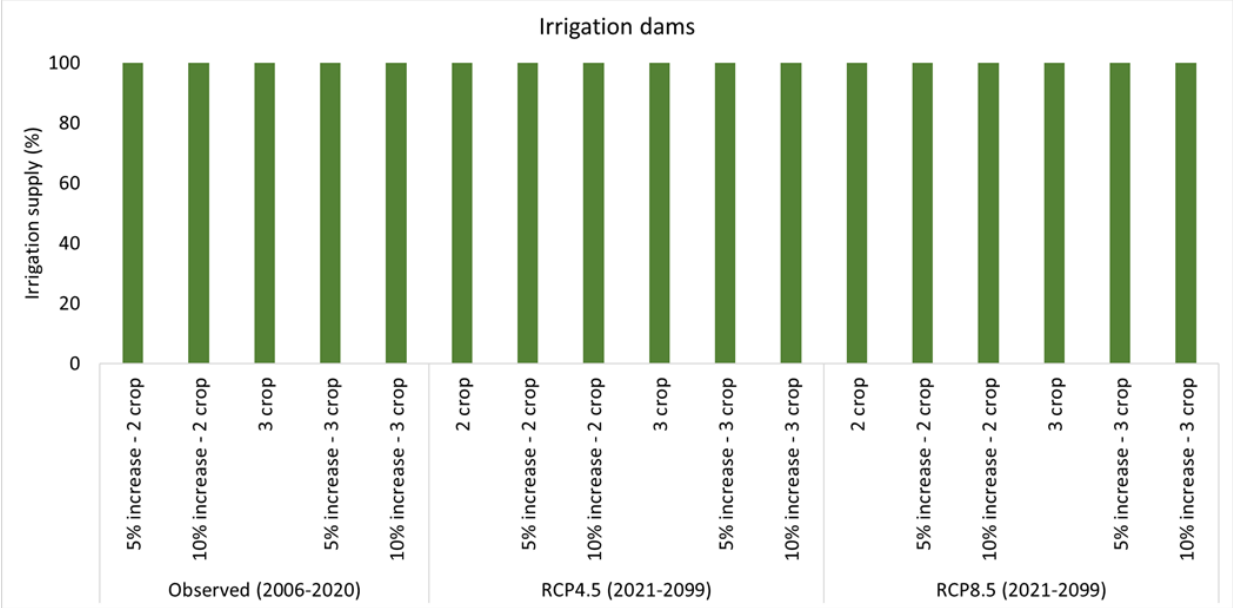


*Figure 9(b): Irrigation supply under different scenarios of irrigated area expansion and number of crop cycle per year under observed climate and future period under RCP 4.5 and RCP 8.5 for irrigation dams in the Mekong River Basin*

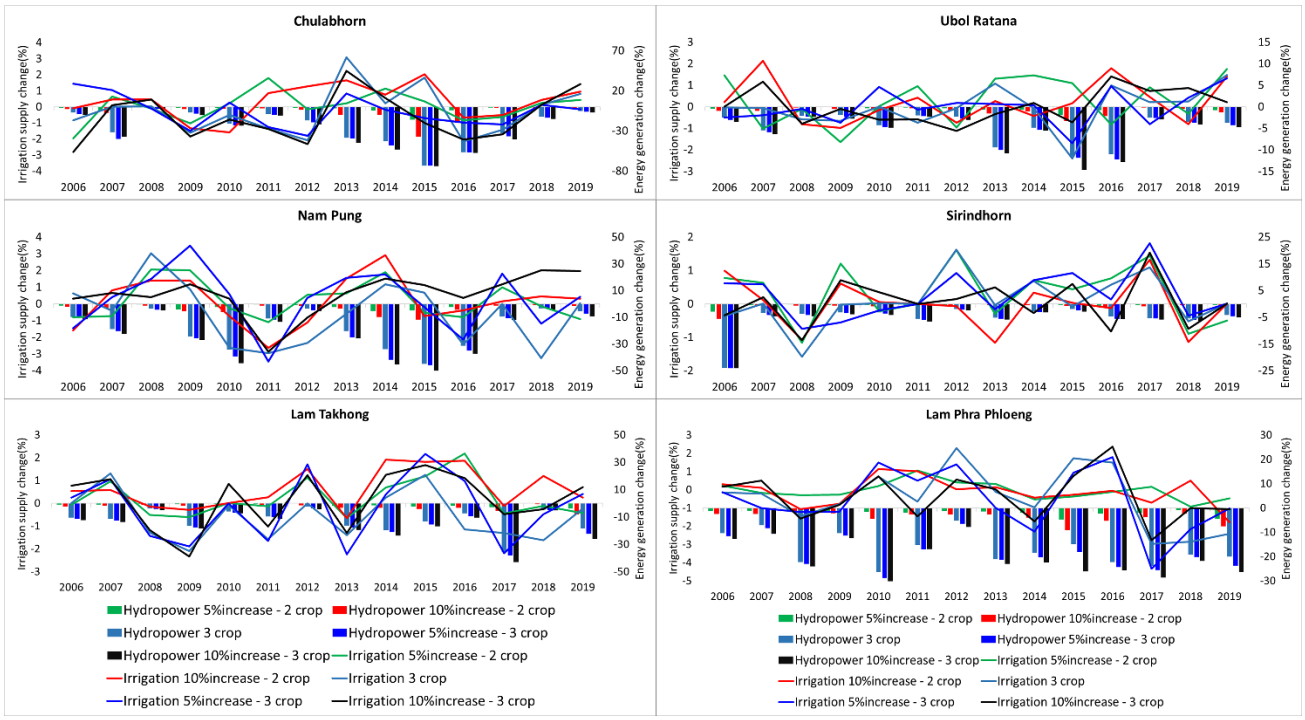


*Figure 10: Annual change in the irrigation supply and energy generation under different scenarios of irrigated area expansion and the number of crop cycles per year under observed climate for multipurpose dams in the Mekong River Basin.*

The seasonal variation of the change in the irrigation water supply and energy generation shows the efficacy of the multipurpose dams in meeting the water demand by the irrigation and energy sectors during the monsoon season (June-October) (Figure 11). Under the increase in the irrigated area scenarios, the decrease in the energy generated during the monsoon period was -1.5%, whereas the reduction was -2.8% during the non-monsoon period. Also, the irrigation water supply met more than 90.2% of the water demand from the irrigation sector. However, with the introduction of the additional crop cycle, the energy generation and irrigation water supply were significantly affected during the sowing months (November-January). For the 3-crop cycle per year scenarios, the reduction in the energy generated during the monsoon period was -2.8%, however, the decrease was more than 38% for the sowing period of the third crop cycle. Similarly, the irrigation water supply was 90.29% of the demand during the monsoon season but the water supply was marginally decreased to 89.86% during November-January.

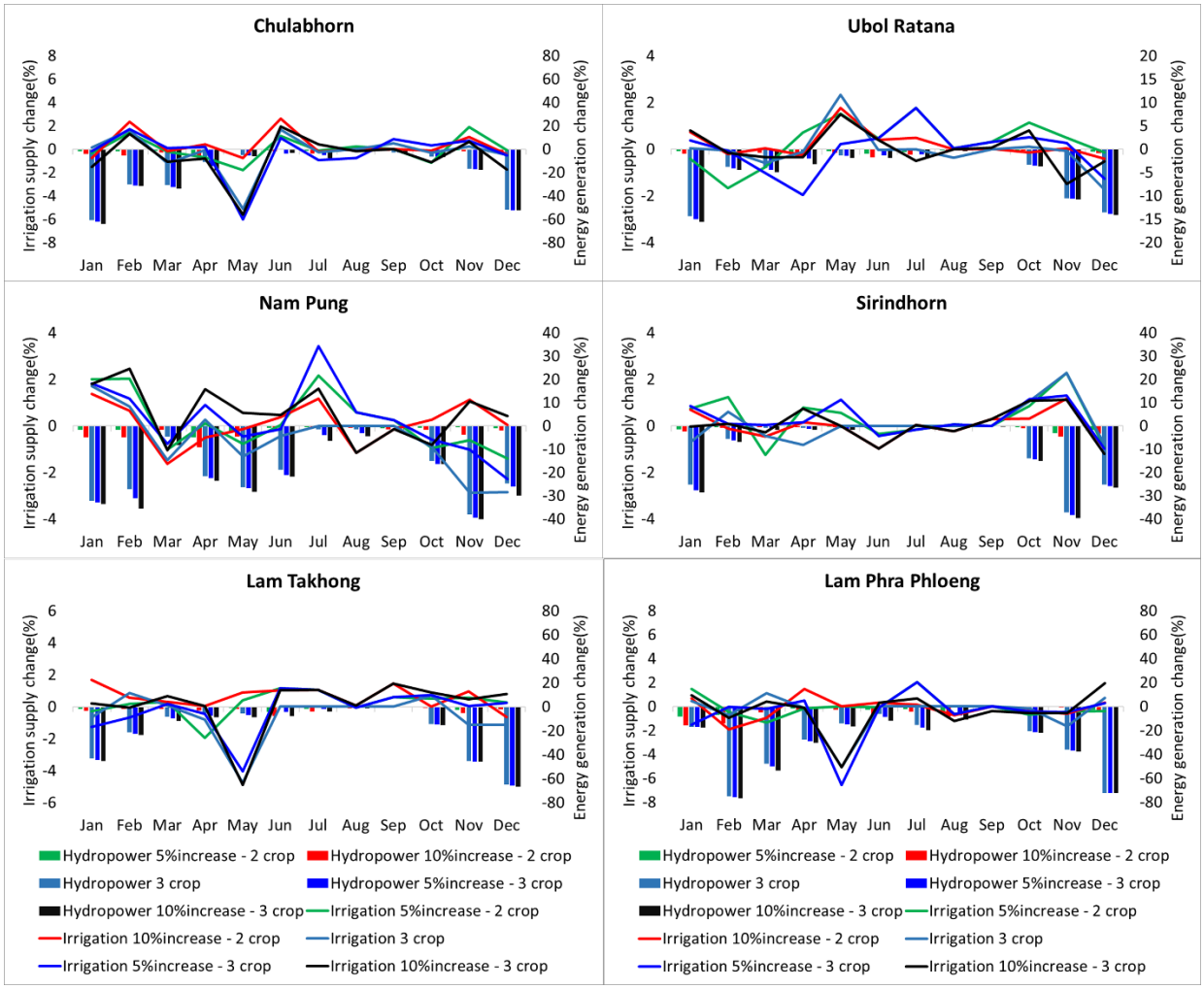

*Figure 11: Seasonal change in the irrigation supply and energy generation under different scenarios of irrigated area expansion and number of crop cycle per year under observed climate for multipurpose dams in the Mekong River Basin*

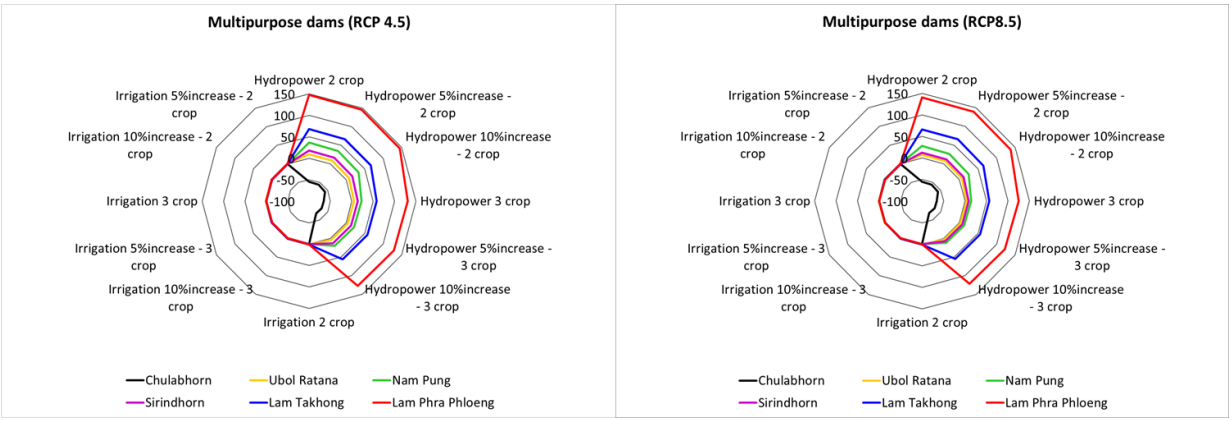


*Figure 12: Impact of climate change on the irrigation supply and energy generation under different scenarios of irrigated area expansion and number of crop cycle per year under RCP 4.5 and RCP 8.5 for multipurpose dams in the Mekong River Basin (with reference scenario)*

The combined effect of climate change and anthropogenic activities were analyzed by executing the scenarios of irrigation expansion with the inflow and NIWR estimated using the climate model under RCP 4.5 and RCP 8.5. Climate change had a favorable influence on the irrigation water supply and energy potential of the multipurpose dams. Figure 9(a) shows the change in the irrigation water supply and energy potential of the multipurpose dams for the future period (2021-2099). The increase in the energy potential was more than 37% and 33% under RCP 4.5 and RCP 8.5, respectively. Also, the water supply to the irrigation fields increased by 0.34% and 0.22% under RCP 4.5 and RCP 8.5, respectively. Moreover, the expansion of the irrigated area and additional crop cycle had a similar influence was shown during the observed period. But the climate effect overshadowed the anthropogenic effect of irrigation expansion with the increase in energy potential approximately 27% and 23% for the 3 crop cycle scenarios under RCP 4.5 and RCP 8.5 respectively. A similar effect on the irrigation water supply was projected for the future period for the multipurpose dams. The irrigation dams were able to perfectly operate under the influence of climate change with the supply satisfying the 100% demand from the irrigation sector (Figure 9(b)). The enhanced performance of the dam operation can be attributed to the projected increased precipitation by the climate models resulting in the escalated inflow to the reservoirs.

Figure 12 shows the combined impact of climate change and anthropogenic activities on the operation of the multipurpose dams. Chulabhorn was negatively impacted by climate change with the decrease in energy potential more than 54% for 2 crop cycles and 66% for 3 crop cycles, in addition to an average reduction of 0.25% in the irrigation water supply. On the other hand, the energy potential for Lam Phra Phloeng is expected to double for the future period under the irrigation expansion. The average increase in the energy potential of the remaining dams was 28% under RCP 4.5 and 23% under RCP 8.5. The irrigation sector is marginally affected by climate change with the assured supply of more than 88% of the irrigation water demand under all the scenarios.

### 4.4 Conclusion

The major findings of the study were:

- The flow duration curve developed using the VIC simulated inflows to the reservoirs for observed and future periods shows an increase in the projected magnitude of the high flow ($Q_{10}$) accounting 7.8% under RCP 4.5 and 6% under RCP 8.5 as compare to the historic period. While the magnitude of the average flow ($Q_{50}$) and low flow ($Q_{90}$) are projected to decrease by 2.3% (4.9%) and 1.6 % (6.1), respectively, for the future period under RCP 4.5 (RCP 8.5) as compared to the historic period. The inflow to the reservoirs under RCP 4.5 is projected to be higher than the conditions under RCP 8.5.
- The developed approach is the refinement over the Hanasaki et al. (2006) for the better simulation of the storage variation and outflow from the reservoirs. The high-resolution VIC model (0.05 deg spatial resolution) was employed for the estimation of the inflows and NIWR for the reservoirs. The simulated storage was able to precisely capture the observed variation in the storage and outflows. The high-resolution VIC model helped in accurately simulating the inflow to the dams located in close proximity, which otherwise would have fallen under the same grid locations. Also, the NIWR simulation at $0.05^{o}$ spatial resolution contributed towards the precise allocation of the irrigation grid cell to the dams in defining the commanding area and avoid the repetition of the irrigation area assignment. The modification in the Hanasaki et at (2005) approach in simulating the outflow from the reservoir assisted in introducing the seasonality in the storage variation of the large reservoir with low inflows.

- Under the observed conditions, the multipurpose reservoirs were able to generate the desired annual energy along with satisfying more than 80% of the irrigation water demand. The annual energy generation and the irrigation water supply were least during 2015 due to low inflows to the reservoirs. Similarly, the irrigation reservoirs also satisfied more than 80% of the water demand for the irrigation purpose and hydropower reservoirs generated the required energy during the observed period.
- Climate change will enhance the hydropower potential of the multipurpose dams with an average increase of 7.3% and 5.3% in the energy generation in the future under RCP 4.5 and RCP 8.5, respectively. But the irrigation water supply will suffer a decrease of 1.3% in fulfilling the future water demand as compared to the historic period. While the efficacy of the irrigation dams in meeting the irrigation water demand is expected to fall by 1%, however meeting more than 93% of the irrigation water demand. The hydropower dams are expected to continue producing the same energy volume in the future under RCP 4.5 as during the historic period, but the energy potential will reduce by 2% under RCP 8.5.
- Based on the projected production of seven hydropower projects, Thailand is expected to experience 6.3% and 4.3% increase in hydropower generation under RCP 4.5 and RCP 8.5, respectively. A similar change in the hydropower generation is projected for Cambodia and Vietnam based on the single dam analysis accounting 1.9% (1.6%), and 2.5% (3.1%) increase under RCP 4.5 (RCP 8.5). While the Xiowan dam in China will experience a change of +2.7% and -18.9% in the hydropower generation for the future period under RCP 4.5 and RCP 8.5. On the other hand, Laos PDR will suffer from the marginal reduction in the energy generation accounting 0.1% and 0.9% under RCP 4.5 and RCP 8.5, respectively. Since all the ten irrigation supply reservoirs are located in Thailand, the irrigation met efficacy is projected to decline by 0.2% and 1.3% under RCP 4.5 and RCP 8.5, respectively, even though meeting more than 90% of the irrigation water demand.
- The increase in the irrigated area reduces the energy generation of the multipurpose dams by 1.5% (5.4 GWh), however, the addition of a crop cycle lowers the energy generation by more than 10% (36 GWh). The dam operation during the monsoon period executes the required performance but the November-January period shows more than

a 38% reduction in energy generation. Climate change positively influences the dam operation with an increase in the energy potential of 31% under RCP 4.5 and 27% under RCP 8.5. The irrigation sector is marginally affected by climate change and anthropogenic activities as the multipurpose dams will be able to fulfill 88% of the water demand for irrigation and irrigation dams will completely satisfy the water needs for irrigation purposes for the future period.

**Reference for Chapter 4**


Allen, R., Pereira, L., Raes, D., & Smith, M. (1998). Crop evapotranspiration-Guidelines for computing crop water requirements-FAO Irrigation and drainage paper 56. *FAO Irrigation and Drainage Paper No. 56.* Retrieved from https://www.researchgate.net/profile/Hawre_Kiani/post/What_is_the_more_effective_way_of_deficit_irrigation/attachment/5af42706b53d2f63c3cafa73/AS%3A624694629777415%401525950214858/download/Allen_FAO1998.pdf

AQUASTAT. (2014). Irrigation water requirement and water withdrawals by country. Retrieved January 11, 2019, from http://www.fao.org/nr/water/aquastat/main/index.stm

Box, M. J. (1965). A new method of constrained optimization and a comparison with other methods. *The Computer Journal*, *8*(1), 42–52. https://doi.org/10.1093/COMJNL/8.1.42

Chang, F.-J., Chen, L., & Chang, L.-C. (2005). Optimizing the reservoir operating rule curves by genetic algorithms. *Hydrological Processes*, *19*(11), 2277–2289. https://doi.org/10.1002/hyp.5674

Conway, D., Van Garderen, E. A., Deryng, D., Dorling, S., Krueger, T., Landman, W., et al. (2015, August 21). Climate and southern Africa's water-energy-food nexus. *Nature Climate Change*. Nature Publishing Group. https://doi.org/10.1038/nclimate2735

Cosby, B. J., Hornberger, G. M., Clapp, R. B., & Ginn, T. R. (1984). A Statistical Exploration of the Relationships of Soil Moisture Characteristics to the Physical Properties of Soils. *Water Resources Research*, *20*(6), 682–690. https://doi.org/10.1029/WR020i006p00682

Dore, John, Xiaogang Yu, and K. Y. L. (2007). China's energy reforms and hydropower expansion in Yunnan. *Democratizing Water Governance in the Mekong Region. Mekong Press*.

Fallah-Mehdipour, E., Bozorg Haddad, O., & Mariño, M. A. (2013). Extraction of Optimal Operation Rules in an Aquifer-Dam System: Genetic Programming Approach. *Journal of Irrigation and Drainage Engineering*, *139*(10), 872–879. https://doi.org/10.1061/(ASCE)IR.1943-4774.0000628

Franchini, M., & Pacciani, M. (1991). Comparative analysis of several conceptual rainfall-runoff models. *Journal of Hydrology*, *122*(1–4), 161–219. https://doi.org/10.1016/0022-1694(91)90178-K

Haddeland, I., Lettenmaier, D. P., & Skaugen, T. (2006). Effects of irrigation on the water and energy balances of the Colorado and Mekong river basins. *Journal of Hydrology*, *324*(1–4), 210–223. https://doi.org/10.1016/j.jhydrol.2005.09.028

Hanasaki, N., Kanae, S., & Oki, T. (2006). A reservoir operation scheme for global river routing models. *Journal of Hydrology*, *327*(1–2), 22–41. https://doi.org/10.1016/j.jhydrol.2005.11.011

Hanim, F., & Rahim, A. (2017). *Supply and Demand of Rice in Malaysia: A System Dynamics Approach*. *International Journal of Supply Chain Management* (Vol. 6). Retrieved from http://excelingtech.co.uk/

Hempel, S., Frieler, K., Warszawski, L., Schewe, J., & Piontek, F. (2013). A trend-preserving bias correction – the ISI-MIP approach. *Earth System Dynamics*, *4*(2), 219–236. https://doi.org/10.5194/esd-4-219-2013

Hoekema, D. J., & Sridhar, V. (2013). A System Dynamics Model for Conjunctive Management of Water Resources in the Snake River Basin. *JAWRA Journal of the American Water Resources Association*, *49*(6), 1327–1350. https://doi.org/10.1111/jawr.12092

Khandelwal, A., Karpatne, A., Wei, Z., Kuang, H., Ghosh, R., Dugan, H., et al. (2019). *GLADD-R: A new Global Lake Dynamics Database for Reservoirs created using machine learning and satellite data GLADD-R: A new Global Lake Dynamics Database for Reservoirs*. Retrieved from http://umnlcc.cs.umn.edu/GlobalReservoirDatabase/

Kummu, M., Lu, X. X., Wang, J. J., & Varis, O. (2010). Basin-wide sediment trapping efficiency of emerging reservoirs along the Mekong. *Geomorphology*, *119*(3–4), 181–197. https://doi.org/10.1016/J.GEOMORPH.2010.03.018

Leck, H., Conway, D., Bradshaw, M., & Rees, J. (2015). Tracing the Water-Energy-Food Nexus: Description, Theory and Practice. *Geography Compass*, *9*(8), 445–460. https://doi.org/10.1111/gec3.12222

Li, H., Wu, H., Huang, M., & Leung, L. R. (2012). Irrigation & Drainage Systems Engineering Representing Natural and Manmade Drainage Systems in an Earth System Modeling Framework, *1*(2), 1–2. https://doi.org/10.4172/2168-9768.1000e107

Liang, X., Lettenmaier, D. P., Wood, E. F., & Burges, S. J. (1994). A simple hydrologically based model of land surface water and energy fluxes for general circulation models. *Journal of Geophysical Research*, *99*(D7), 14415. https://doi.org/10.1029/94JD00483

Liu, X., Tang, Q., Voisin, N., & Cui, H. (2016). Projected impacts of climate change on hydropower potential in China. *Hydrology and Earth System Sciences*, *20*(8), 3343–3359. https://doi.org/10.5194/hess-20-3343-2016

Lohmann, D., Raschke, E., Nijssen, B., & Lettenmaier, D. P. (1998). Regional scale hydrology: II. Application of the VIC-2L model to the Weser River, Germany. *Hydrological Sciences Journal*, *43*(1), 143–158. https://doi.org/10.1080/02626669809492108

Lohmann, Dag, Nolte-Holube, R., & Raschke, E. (1996). A large-scale horizontal routing model to be coupled to land surface parametrization schemes. *Tellus, Series A: Dynamic Meteorology and Oceanography*. https://doi.org/10.1034/j.1600-0870.1996.t01-3-00009.x

Monteith, L. J. (1965). Evaporation and environment, In The state and movement of water

in living organisms. *Symp. Soc. Exp. Biol.*, 205–234. Retrieved from https://ci.nii.ac.jp/naid/10007810939/

MRC. (2018). *Irrigation database improvement for the lower Mekong basin*. Retrieved from http://www.mrcmekong.org/publications/

Nash, J. E., & Sutcliffe, J. V. (1970). River flow forecasting through conceptual models part I — A discussion of principles. *Journal of Hydrology*, *10*(3), 282–290. https://doi.org/10.1016/0022-1694(70)90255-6

Nesbitt, H., R. Johnston, and M. S. (2004). Mekong River water: will river flows meet future agriculture needs in the Lower Mekong Basin? *Water in Agriculture, Seng, V., Craswell, E., Fukai, S., and Fisher, K.(Eds), Australian Centre of International Agricultural Research Proceedings 116*.

Paper, W. (2009). *GoldSim: Engineering and Environmental Simulation Software for Water Resource Applications*.

Pokhrel, Y., Burbano, M., Roush, J., Kang, H., Sridhar, V., & Hyndman, D. (2018). A Review of the Integrated Effects of Changing Climate, Land Use, and Dams on Mekong River Hydrology. *Water*, *10*(3), 266. https://doi.org/10.3390/w10030266

Rasul, G., & Sharma, B. (2016). The nexus approach to water–energy–food security: an option for adaptation to climate change. *Climate Policy*, *16*(6), 682–702. https://doi.org/10.1080/14693062.2015.1029865

Richter, B., & Thomas, G. (2007). Restoring environmental flows by modifying dam operations. *JSTOR*. Retrieved from https://www.jstor.org/stable/26267852?casa_token=aiozWKMVOdAAAAAA:pnbt3UP1Bk1W1O0fEKoMA6xl41grmqT_XdN7ngBGS43u5Yg6Nn_7lw0OJ4y3T01IQamjIzNU6wXvvmHQ2-oRgMM64_XbHnasRSAGgJ8nQlWeSVcJxGQr

Sabo, J. L., Ruhi, A., Holtgrieve, G. W., Elliott, V., Arias, M. E., Ngor, P. B., et al. (2017). Designing river flows to improve food security futures in the Lower Mekong Basin. *Science (New York, N.Y.)*, *358*(6368), eaao1053. https://doi.org/10.1126/science.aao1053

Sheffield, J., Goteti, G., & Wood, E. F. (2006). Development of a 50-Year High-Resolution Global Dataset of Meteorological Forcings for Land Surface Modeling. *Journal of Climate*, *19*(13), 3088–3111. https://doi.org/10.1175/JCLI3790.1

Sigvaldson, O. T. (1976). A simulation model for operating a multipurpose multireservoir system. *Water Resources Research*, *12*(2), 263–278. https://doi.org/10.1029/WR012i002p00263

Stone, R. (2011). Mayhem on the Mekong. *Science*, *333*(6044), 814–818. https://doi.org/10.1126/science.333.6044.814

Wood, E. F., Lettenmaier, D. P., & Zartarian, V. G. (1992). A land-surface hydrology parameterization with subgrid variability for general circulation models. *Journal of Geophysical Research*, *97*(D3), 2717. https://doi.org/10.1029/91JD01786

Zhou, T., Nijssen, B., Gao, H., Lettenmaier, D. P., Zhou, T., Nijssen, B., et al. (2016). The

Contribution of Reservoirs to Global Land Surface Water Storage Variations. *Journal of Hydrometeorology*, *17*(1), 309–325. https://doi.org/10.1175/JHM-D-15-0002.1

# Chapter 5
# Development of a dynamics model for the sustainable optimization of water allocation to the irrigation, domestic, hydropower generation and ecological sectors

**Keywords:** GoldSim, optimization, hydropower, irrigation water, GCMs, shadow price

## 5.1 Introduction

The complexity of sustainable management of the water resources in the basin involves multiple factors, including water supply from surface runoff and groundwater aquifers, and the water demands of the domestic, industrial, agricultural, and energy generation sectors. External factors affecting the system include precipitation and temperature variation due to climate change, growing population, and land transformation. Even during unfavorable conditions, a minimal volume of water needs to be supplied for domestic and irrigation purposes to support the growing population. The management of the MRB is complex as the region poses a challenging multiobjective control problem as the basin has suffered from various climate extremes and anthropogenic changes in land cover (Pokhrel et al., 2018; Sridhar, et al., 2019), resulting in low flows and high flows during drought and flood events, respectively. However, reservoir storage plays an important role in moderating the effect of drought and flood through the basin's capacity to store and discharge surplus water (Yang et al., 2017). However, an optimal distribution of water resources to meet the demand from various sectors and the prediction of inflows in the mainstem, as well as tributaries, would be required for sustainable management of the basin considering the dynamics in the water demand and water availability. To study such a system, researchers generally use a system dynamics approach, which has been applied to several basins (Hoekema & Sridhar, 2013b; Quinn et al., 2018; Salazar et al., 2017).

Various sectors, such as irrigation, domestic, industrial, energy, and environment, have been studied in isolation to evaluate water supply scenarios under the influence of climate and population change in MRB (Homdee et al., 2011; Sridhar, et al., 2019; Stone, 2011b; Västilä et al., 2010; Ziv et al., 2012). The integration of the different sectors for the management of the water resources has been done in the basins of Columbia, the United

States, India, Australia, and China. Hoekema & Sridhar (2013b) developed the Snake River Planning Model (SRPM) in the system dynamic framework by accounting the interaction between the surface and groundwater systems for the water supply through the feedback loop involving climate change effects and management scenarios. The water supply, power generation, and environment (WPE) nexus was modeled for China's Hehuang region, part of the Yellow River basin located in Qinghai Province, using the system dynamics approach (Feng et al., 2016). The convolution process was defined using the nonlinear equation describing the storage, water supply, energy generation, population biomass, and environmental awareness. The system dynamic approach has been used in the MRB for evaluating sustainable adaptation strategies for vulnerable mega-deltas rice agriculture in Vietnam. The dynamics of the rice-sediment system including delays, feedbacks, and tipping points suggested triple-cropping strategy being beneficial only for wealthier groups (Chapman & Darby, 2016). Similarly, the significantly impacted regions of the Vietnamese Mekong Delta for rice production was determined using the system dynamics approach involving the climate change, and water consumption by domestic, industrial, and agricultural sectors. The factors incorporated in the model included water consumption, rainfall-evapotranspiration difference, and salinity intrusion under climate scenarios RCP 4.5 and RCP 8.5 (Thanh et al., 2020). Pittock et al. (2016) assessed the hydropower-food supply nexus in the MRB using an influence model for estimating the consequences of altering variables on the basin system. The approach was developed to assist national and sub-national policymakers for taking decisions across energy, water, and food systems. However, an integrated approach studying all these constantly changing sectors in conjunction, using methods from system dynamics, has not been fully explored in the MRB.

Studies that emphasize the economic aspects to quantify the profit and loss under the changing conditions can help stakeholders and sector managers. Apart from providing direct benefits, such as fulfilling food and water requirement, energy demand and monetary profits, the societal and externalities advantages generated by the agents play an important role, for example, job opportunities, infrastructure development, and human development index(Dinar & Letey, 1991; Davijani et al., 2016; Lipscomb et al., 2013; Sun et al., 2011).

A shadow price is an estimated price for something that is not normally priced in the market or sold in the market. The shadow price of a constraint, in linear programming problems, is the difference between the optimized value and the value of the objective function, evaluated at the optional basis, when the right-hand side (RHS) of a constraint is increased by one unit (Alaouze, 1996). Conceptually, the shadow price of water can also be viewed as the difference between the given water rate for irrigation and the actual economic value of water as a natural resource (Ziolkowska, 2015). Some studies have been conducted to estimate the shadow prices of different kinds of water resources. Ioslovich and Gutman (2001) calculated water shadow prices for different users (urban, agricultural, and other secondary users) for the case of spatially distributed sources and consumers. Wu et al. (2004) estimated the economic value of water resources nourishment by the average shadow price of water for Taiwan's forest ecosystem. The value of the water saved from the conservation of trees was also valued by using shadow prices obtained from an optimizing model, without resorting to survey methods (Kaiser & Roumasset, 2002). Nevertheless, it was also said that, in practice, it is almost impossible to obtain water shadow price by solving a linear programming problem (Zhao & Chen, 2008).

The evaluation of the shadow prices of the water resources in China and its nine major river basins and prediction till 2020 was carried out by Liu et al. (2009) combining the input-output analysis method with the linear programming method. Also, the shadow price technique was used to detect the underpriced water for irrigation in the United States High Plains (Ziolkowska, 2015). Rosegrant et al. (2000) developed the integrated economic-hydrologic modeling framework that accounts for the interactions between water allocation, farmer input choice, agricultural productivity, non-agricultural water demand, and resource degradation in order to estimate the social and economic gains from improvement in the allocation and efficiency of water use for the application to the Maipo river basin in Chile. The shadow price technique has been used in simulating the economic value of the hydropower generation using hydro-economic river basin models under asymmetric access. Kuhn and Britz (2012) proposed a new solution format for Hydro-economic river basin models (HERBMs), based on the format of the mixed complementarity problem (MCP), where modified shadow price relations express spatial

externalities resulting from asymmetric access to water use. One of the most important applications of the shadow price is the policy formation based on the international comparison, specifically for the transboundary rivers (Tsur et al., 2004).

Ringler et al. (2004) describe the water policy analysis for the Mekong River basin containing the methodology for the economic assessment of the water supply to agriculture, energy generation, domestic, industrial, and fisheries purposes. To establish a relationship between crop yield and water, the crop yield-water stress relationship, which has been developed by the FAO following extensive field experiments over a wide range of crops, can be utilized (Doorenbos & Pruitt, 1977; Doorenbos & Kassam, 1979). The function is dependent on the actual yield, maximum yield, seasonal actual evapotranspiration, seasonal potential evapotranspiration, and seasonal crop yield response coefficient. The function for net profits from irrigated agriculture can be specified by irrigation demand site using crop area, crop price, cost of fertilizer, machinery, labor, and irrigation. The net benefit can be calculated as water use benefits minus water supply cost. The profit can be determined as the function of monthly water withdrawal, and water supply cost. In-stream water uses are of particular importance in the MRB. Profit from power production can be calculated as power production multiplied by the difference between the power selling price and power production cost for each hydropower station. Due to the unequal distribution of supply and demand—the low-cost hydropower potential is located in Laos, Myanmar, and Yunnan Province, China, whereas the main markets are Thailand, increasingly Vietnam, and the more distant markets of Malaysia and Singapore— the Greater Mekong Sub-region (including all six riparian countries) has substantial potential for power trade (Crousillat, 1998).

The system dynamics approach used in the MRB was performed at a regional scale. Therefore, a dynamic model is required to encompass the whole MRB through the assessment of the dams in the basin. Previous chapters specify the characteristics of the water (streamflow), food (net irrigation water requirement), and energy (hydropower) of the MRB with the projected change in the future. The system dynamics framework provides the platform to link all the segments of the nexus for the comprehensive analysis

of MRB. To understand and provide a sustainable solution, the dynamics of the MRB impacted by climate change and human activities, the food-energy-water nexus of the region was analyzed using the system dynamics approach. The integration of the water resources was achieved by assembling various dams located throughout the basin into the system. The dams commissioned to fulfill the water demands of the food, energy, domestic, industrial, and environmental sectors are the lifeline of the regional areas. The model incorporates a complex assessment of the reservoir operations including the cascading effects of the upstream dams, function during extreme events, population growth, and climate change. The derivation of the forcing parameters to the model, such as inflow to reservoir, irrigation water requirement, and climate impact was done using the high-resolution VIC model with a dense routing network. The shock caused by the extremely high/low inflow volume to the reservoir and economic analysis to understand the sector and regions of benefit was further analyzed. This study aims to develop a dynamic model for the sustainable optimization of water allocation to the irrigation, domestic, hydropower generation, and ecological sectors, thereby taking into account the effects of climate and land use and land cover change and satisfying the multiple criteria through feedback loops in the MRB. The objectives of the study are to:

- develop a model in the system dynamic platform accounting for domestic demand, irrigation requirement, dam operation, and ecological flows to investigate future conditions using projected population and GCM datasets.
- assess the stress of the system against extreme events.
- evaluate the value of a unit of water for each agent using a shadow pricing technique.
- analyze trade-offs between different agents to maximize profit considering the societal benefits and obligations.

## 5.2 Materials and Methods

### 5.2.1 Study Area

The Mekong is a transboundary river in Southeast Asia, ranking 7th in Asia and 12th globally in terms of river length. The river originates in southeastern Qinghai province in China and flows through Tibetan Plateau, and Yunnan province to empty into the South China Sea at the Mekong Delta in Vietnam. It courses through China, Myanmar, Laos,

Thailand, Cambodia, and Vietnam, covering a total length of approximately 4800 km and draining an area of nearly 765,000 $km^2$. The selection of the dams for the study was done from the 722 dams in China, 101 in Vietnam, 39 in Thailand, 17 in Myanmar, 7 in Lao PDR, and 2 in Cambodia on the basis of the purpose and location (Figure 1). Since the objective of the study considers sustainable management of the agriculture and energy sectors along with other water demands, the dams commissioned for irrigation and hydroelectricity generation were chosen for the analysis. 31 dams commissioned for irrigation and hydropower purpose were shortlisted. The details of the dams can be found in Table 1.

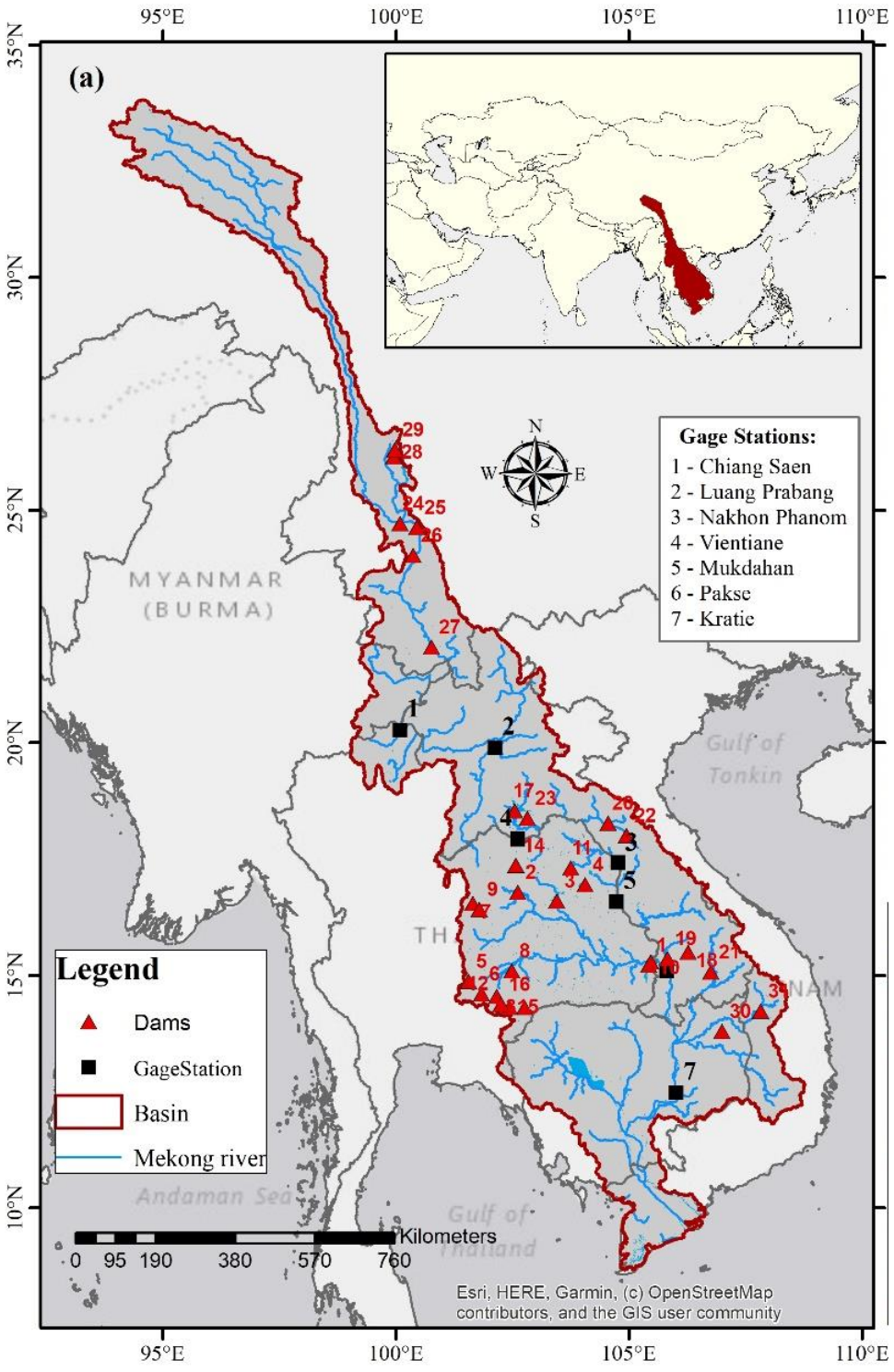


*Figure 1: Location map of the Mekong River basin along with the river's mainstream with gauge stations used for streamflow validation (black square) and the dams considered in this study (red triangle).*

*Table 1: List of the dams considered in this study*

| S. No. | Name of dam | Country | Completed / operational since | Dam height (m) | Capacity (million $m^3$) | Reservoir area ($km^2$) | Function | | | | Flood ($m^3$/sec) | Low flow ($m^3$/sec) |
|---|---|---|---|---|---|---|---|---|---|---|---|---|
| | | | | | | | Irrigation | Hydropower | Municipal Supply | Industrial Supply | | |
| 1 | Sirindhorn | Thailand | 1971 | 42 | 1966 | 288 | x | x | x | x | 178.19 | 3.15 |
| 2 | Ubol Ratana | Thailand | 1966 | 32 | 2.559 | 41 | x | x | x | x | 233.27 | 11.13 |
| 3 | Lam Pao | Thailand | 1969 | 33 | 1430 | 240 | x | | x | x | 188.93 | 7.40 |
| 4 | Nam Pung | Thailand | 1965 | 40 | 165 | 2.165 | x | x | x | x | 13.77 | 1.32 |
| 5 | Lam Takhong | Thailand | 1969 | 40.3 | 310 | 3.7 | x | x | x | x | 42.52 | 1.75 |
| 6 | Lam Phra Phloeng | Thailand | 1970 | 50 | 110 | 1.31 | x | x | x | x | 28.97 | 0.93 |
| 7 | Chulabhorn | Thailand | 1972 | 70 | 188 | 31 | x | x | x | x | 14.37 | 0.09 |
| 8 | Lam Chang Han | Thailand | 1992 | 18 | 26 | 4.8 | x | x | x | x | 2.89 | 0.18 |
| 9 | Huai Kum | Thailand | 1982 | 36 | 22.8 | 1.8 | | x | x | x | 17.30 | 0.12 |
| 10 | Pakmun | Thailand | 1994 | 17 | 114.3 | 1.7 | | x | x | x | 2925.86 | 165.05 |
| 11 | Nam Un | Thailand | 1973 | 29.5 | 520 | 8.5 | x | | x | x | 66.24 | 2.32 |
| 12 | Upper Mun | Thailand | 1980 | 32.7 | 141 | 1.275 | x | | x | x | 12.84 | 0.47 |
| 13 | Lam Nang Rong | Thailand | 1982 | 23 | 150 | 11.6 | x | | x | x | 7.30 | 0.29 |
| 14 | Huai Luang | Thailand | 1984 | 12.5 | 113 | 3.2 | x | | x | x | 33.89 | 3.00 |
| 15 | Lam Plai Mas | Thailand | 1988 | 32 | 98 | 1.04 | x | | x | x | 3.01 | 0.14 |
| 16 | Lam Sae | Thailand | 1998 | 29.5 | 275 | 2.95 | x | | x | x | 17.77 | 2.49 |
| 17 | Nam Ngum | Laos PDR | 1985 | 75 | 4700 | 370 | | x | | | 1206.63 | 64.34 |
| 18 | Xeset 1 | Laos PDR | 1991 | 18 | 30 | 0.1 | | x | | | 54.17 | 1.67 |
| 19 | Selabam | Laos PDR | 1993 | 3.7 | 30 | | | x | | | 556.89 | 33.80 |
| 20 | Theun-Hinboun | Laos PDR | 1998 | 27 | 20 | | | x | | | 814.08 | 30.78 |
| 21 | Houay-Ho | Laos PDR | 1998 | 80 | 3530 | 37 | | x | | | 19.27 | 0.23 |
| 22 | Nam Leuk | Laos PDR | 2000 | 51.5 | 185 | | | x | | | 510.26 | 19.45 |
| 23 | Nam Mang 3 | Laos PDR | 2004 | 22 | 49.43 | 10.2 | | x | | | 3.68 | 0.05 |
| 24 | Xiaowan | China | 2010 | 292 | 15043 | 190 | | x | | | 2424.09 | 168.94 |

| | | | | | | | | | | | | |
|---|---|---|---|---|---|---|---|---|---|---|---|---|
| 25 | Manwan | China | 1995 | 132 | 662 | | | x | | | 2449.02 | 177.63 |
| 26 | Dachaoshan | China | 2004 | 111 | 933 | | | x | | | 2577.19 | 216.15 |
| 27 | Jinghong | China | 2008 | 108 | 1233 | 510 | | x | | | 3682.35 | 363.08 |
| 28 | Cibihe | China | | | 93.22 | 7.9 | x | | | | 35.70 | 2.27 |
| 29 | Haixihai | China | | | 61.854 | 4 | x | | | | 9.89 | 0.51 |
| 30 | Ochum | Cambodia | 1993 | 10 | 1 | | | x | | | 6.00 | 0.07 |
| 31 | Yaly | Viet Nam | 2002 | 69 | 1037 | 64.5 | | x | x | x | 567.74 | 17.71 |

### 5.2.2 Data and models

*Water quantity:* The water available from the various catchments of the different countries for the utilization for the irrigation, hydropower, municipal, domestic and industrial purposes was primarily derived from the heterogeneous precipitation occurring over the catchment. The water balance and energy balance equations were used for the conversion of precipitation to available water. The Variable Infiltration Capacity (VIC) is a semi-distributed physically-based hydrological model that solves water and energy balance for each grid separately at a daily time step (Liang et al., 1994). The meteorological parameters for the execution of the model include precipitation, minimum, and maximum temperature and wind speed at daily temporal resolution. The VIC model takes into consideration the vegetation variability within a grid cell, as the fractional value of the grid covered by the particular vegetation class. Also, the VIC model has three soil layers; the rainfall is responded quickly by the top two layers with diffusion from the middle to the top layer, and the bottom layer corresponds to baseflow calculated using the Arno model formulation (Franchini & Pacciani, 1991). The total ET is calculated based on the Penman-Monteith approach and considered as the sum of evaporation from bare soil and canopy, and transpiration from vegetation features. Since VIC is a one-dimensional hydrologic model, the exchange of the fluxes is considered only vertically, i.e. the interaction between the adjacent grids is assumed to be negligible. Therefore, the water can enter the grid cell from the atmosphere but the lateral movement in the subsurface layer is considered negligible. The infiltration of water into the soil layer is defined by the variable infiltration curve (Wood et al., 1992), which is a non-linear function of the fractional saturated area. The VIC model provides only the fluxes for each grid at a daily temporal resolution based on the forcing parameters, therefore to extract the accumulated effect at the particular location,

a separate routing scheme developed by Lohmann et al. (1998; 1996) can be employed on the fluxes simulated by VIC model.

*Irrigation water requirement:* The net irrigation water requirement (NIWR) is the amount of free available water that is essential for the sustained agricultural production of the stable food supply. The NIWR was estimated as (Allen et al., 1998):

$$NIWR = \frac{\sum_{i=1}^{N}\left[\sum_{t=1}^{T}\left(k_{c_t} \text{ x } ET_{o_t} - P_{eff_t}\right) \text{x } S_i\right] \text{x } A_{paddy}}{S} \quad (1)$$

where NIWR is the annual net irrigation requirement ($m^3$), i is the number of given crops, N is the total number of given crops, t is the growth stage and T is the final growth stage, $k_c$ is the crop coefficient, which varies for each crop and growth stage, $ET_o$ is the reference evapotranspiration rate (mm), $P_{eff}$ is effective precipitation (mm), $S_i$ is the area cultivated with crop i (ha), $A_{paddy}$ is the area under paddy irrigation (ha), and S is the net cultivable area. The annual NIWR is directly correlated with the evapotranspiration. Thailand region cultivates rice crop twice a year with sowing period from May to August (January to early March), growing period during September (by the end of April), and harvesting period from October to January (till the end of June) for the first (second) crop cycle. The water is required mainly during the sowing and growth stages (90% of total requirement), while it is nominally needed during the harvesting period.

*Hydropower generation:* The hydropower generation from a dam was estimated as follows:

$$HP = n\eta\rho qgh \quad (2)$$

where: n is the number of turbines; η is the dimensionless efficiency of the turbine; ρ is the density of water (1000 $kg/m^3$); q is the volumetric flow rate ($m^3$/sec); g is the acceleration due to gravity (9.81 $m/sec^2$); h is the height between inlet and outlet (m).

*Municipal and Industrial water requirement:* The total water demand from the dam was derived using the population data of the province of dam location from the Social atlas of the lower Mekong basin developed by MRC (Hook et al., 2003). The per capita water

demand for Thailand is 350 $m^3$/person/year, Laos PDR is 280 $m^3$/person/year, Cambodia is 150 $m^3$/person/year, Vietnam is 550 $m^3$/person/year, and China is 250 $m^3$/person/year. Out of the total water demand derived by multiplying the water rate and population, the municipal and industrial water demand was estimated at 5% and 1% of the total volume. The water supply for municipal and industrial purposes is considered only for the dams which are located in the provinces with a population of more than 750,000. If more than one dams are located in a province, the water demand was proportioned based on the storage capacity of the dams. The future projection of population growth from 2021 to 2099 was derived from the Social atlas of the lower Mekong basin with a range between 0.5% to 3.5% increase per year.

*Table 2: List of the dams considered for supplying the municipal and industrial water demand*

| S.No. | Name of dam | Country | Province | Population (in thousand) | Population growth (%/year) |
|---|---|---|---|---|---|
| 1 | Sirindhorn | Thailand | Ubon Ratchathani | 1500 | 0.5 |
| 2 | Ubol Ratana | Thailand | Khon Kaen | 1500 | 0.5 |
| 3 | Lam Pao | Thailand | Kalasin | 875 | 0.5 |
| 4 | Nam Pung | Thailand | Mukdahan | 750 | 1.5 |
| 5 | Lam Takhong | Thailand | Nakhon Ratchasima | 2500 | 0.5 |
| 6 | Lam Phra Phloeng | Thailand | Nakhon Ratchasima | 2500 | 0.5 |
| 7 | Chulabhorn | Thailand | Chaiyaphum | 1500 | 0.5 |
| 8 | Lam Chang Han | Thailand | Nakhon Ratchasima | 2500 | 0.5 |
| 9 | Huai Kum | Thailand | Chaiyaphum | 1500 | 0.5 |
| 10 | Pakmun | Thailand | Ubon Ratchathari | 1500 | 0.5 |
| 11 | Nam Un | Thailand | Sakon Nakhon | 1500 | 0.5 |
| 12 | Upper Mun | Thailand | Nakhon Ratchasima | 2500 | 0.5 |
| 13 | Lam Nang Rong | Thailand | Buriram | 1500 | 0.5 |
| 14 | Huai Luang | Thailand | Udon Thani | 1500 | 0.5 |
| 15 | Lam Plai Mas | Thailand | Nakhon Ratchasima | 2500 | 0.5 |
| 16 | Lam Sae | Thailand | Nakhon Ratchasima | 2500 | 0.5 |
| 17 | Yaly | Vietnam | Gia Lai | 875 | 3.5 |

### 5.2.3 GoldSim

GoldSim is a powerful and flexible Windows-based system dynamics tool to support the management and decision-making of complex systems by carrying out probabilistic simulations (Paper, 2009). The framework and methodology provided by system

simulation help to integrate different components and considerations of the realistic system to explicitly represent the interrelationships and feedback mechanisms and uncertainties about the conditions. The GoldSim simulation environment is a highly graphical and completely object-oriented visual spreadsheet allowing readily evaluation of the system over time and future behavior. GoldSim uses Monte Carlo simulation to propagate uncertainty in processes and parameters defined by the probability distribution and disruptive events throughout the model. Dynamic optimization and scenario analysis capabilities of GoldSim provides the mechanism to support the decision making under transforming conditions based on the available information.

A GoldSim model for the simulation of outflow and hydroelectric generation through the optimal distribution of the water between irrigation and energy sectors from multipurpose and irrigation reservoirs under climate change and irrigation intensification scenarios was developed. The primary forcing data were monthly simulated inflow to the reservoir, NIWR of the downstream irrigated area, and rule curve of the dams. VIC model and Lohmann et al. (1998; 1996) routing scheme was used for the estimation of the inflow to the dam locations for the observed and future climate using the GMFD dataset and four climate models. NIWR was estimated using an improved VIC model including the irrigation scheme developed by Haddeland et al. (2006). The rule curve and depth-storage relationship for the reservoirs were developed using the daily time series of the observed total storage obtained from the reservoir database (http://app.rid.go.th:88/reservoir/) and remote sensing approach (Syed A. Ali & Sridhar, 2019).

The model is comprised of different components, called containers, each representing a reservoir. The monthly inflow, NIWR, and storage variation of the reservoirs were defined using the 'TimeSeries' input element, whereas the relationship between the storage and depth was defined using the 'Lookup Table' element. The equations governing the operation and production of the reservoirs such as water balance equation, energy generation equation, storage simulation, and ecological flow conditions were defined using the 'Expression' function element. The feedback and interaction between the different members of the model were established by creating a link between the elements and the cascading effects of the dams were replicated by linking the outflow of the upstream dam with the inflow of the downstream dam.

Figure 1(a,b) shows the setup of the 7 multipurpose, 9 irrigation, and 15 hydropower dams of the MRB in system dynamics environment at the approximate geographical location. The setup incorporates the cascading effects of the dams shown as the connecting arrow from the upstream dam to the downstream dam. The operation of dams comprised of the three layers; layer 1 shows the input and output from the dams; layer 2 shows the details of the dam operation, and layer 3 shows the optimization of the water allocation for different purposes (Figure 1 (c-e)). Layer 1 included the inflow to the reservoir along with the upstream dam outflow for cascading reservoirs, water demand for irrigation, municipal, and industrial purposes, and storage-depth relationship as the input. On the other hand, the output from the dam included outflow, energy generation, percentage of demand met of irrigation, municipal and industrial sectors. Layer 2 contained the storage change between the time step for water availability estimates, extreme events thresholds (flood and low flow conditions), the examination of the conditions for the reservoir operation based on extreme events and storage status, an optimization scheme. Layer 3 was the detailed elaboration of the optimization scheme for the available water allocation based on the water demand from the irrigation, municipal and industrial sectors and maximizing the energy production of the dam considering the ecological flow requirement of the downstream region.

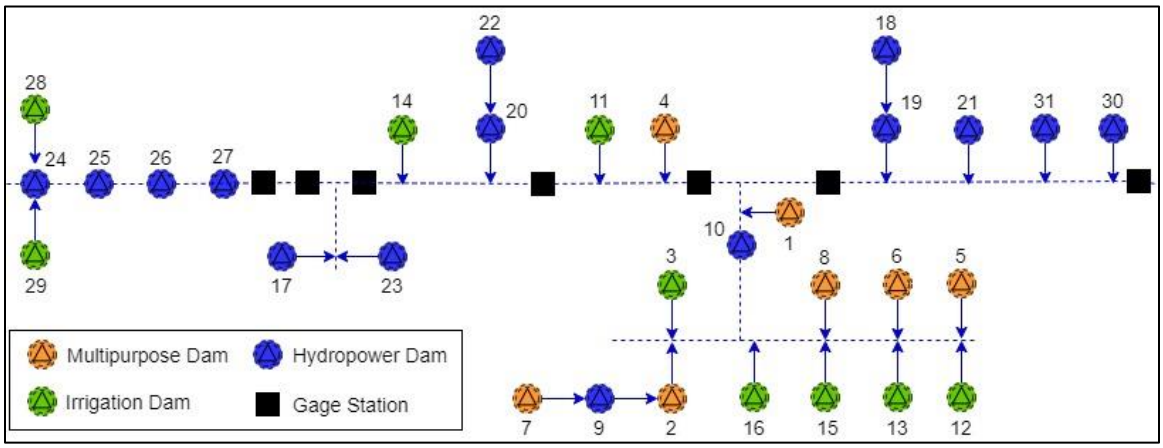


*Figure 1(a): Layout of the multipurpose, irrigation and hydropower dams in the Mekong river basin*

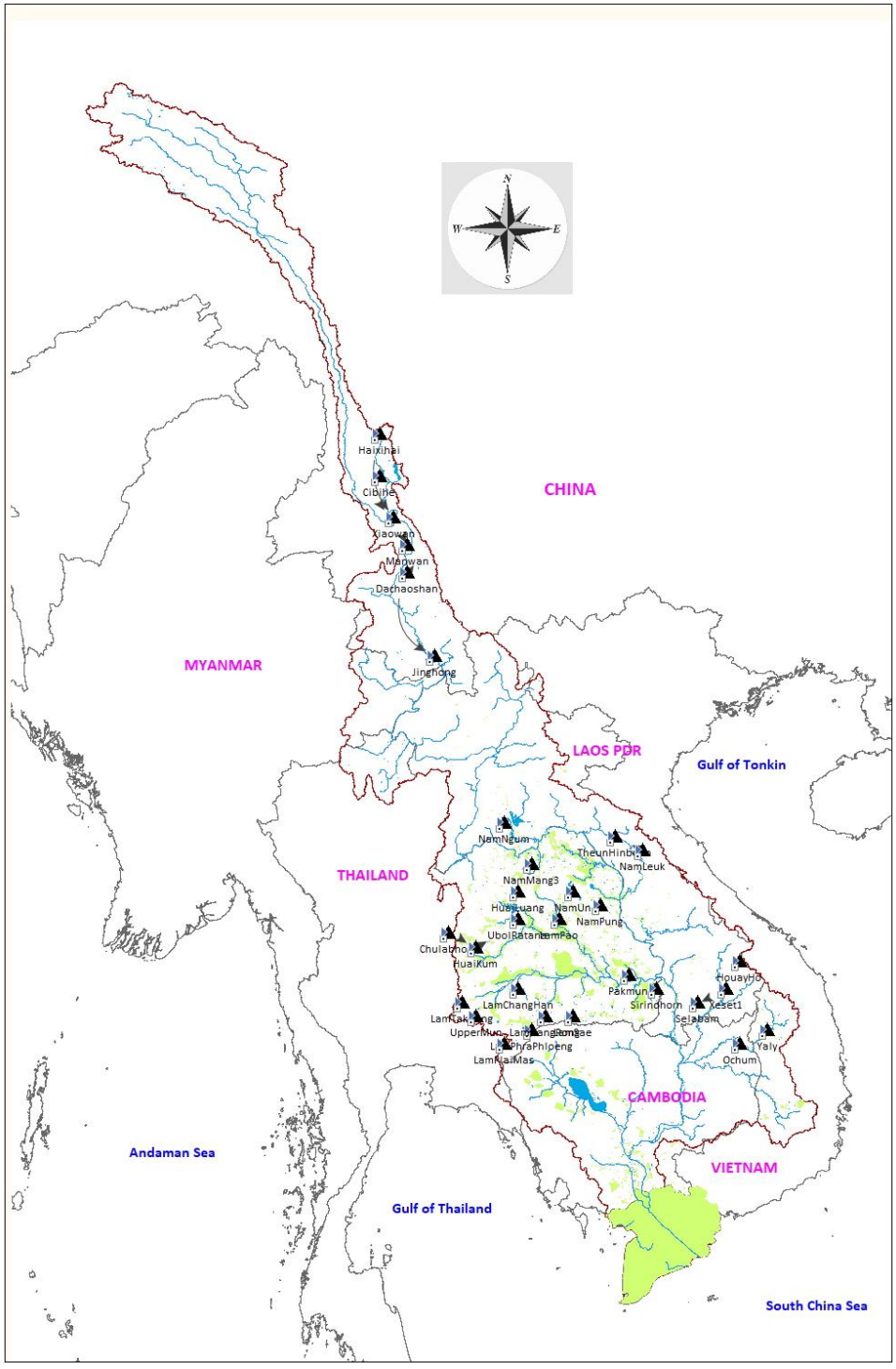


*Figure 1(b): Schematic of the multipurpose, irrigation and hydropower dams in the Mekong river basin*

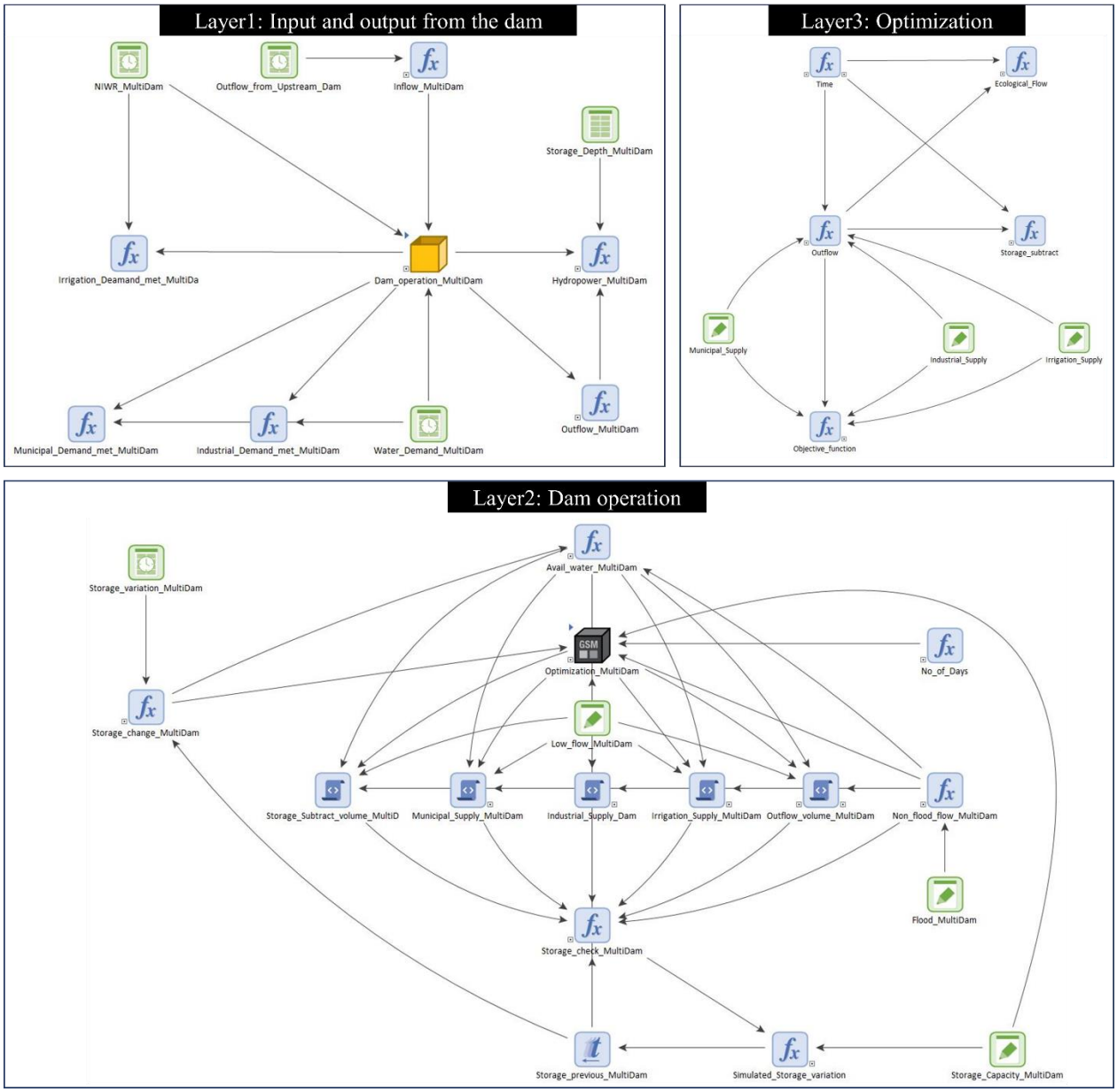


*Figure 1(c): System dynamics setup of a multipurpose dam in GoldSim showing the input-output (layer 1), dam operation (layer 2), and optimization scheme (layer 3).*

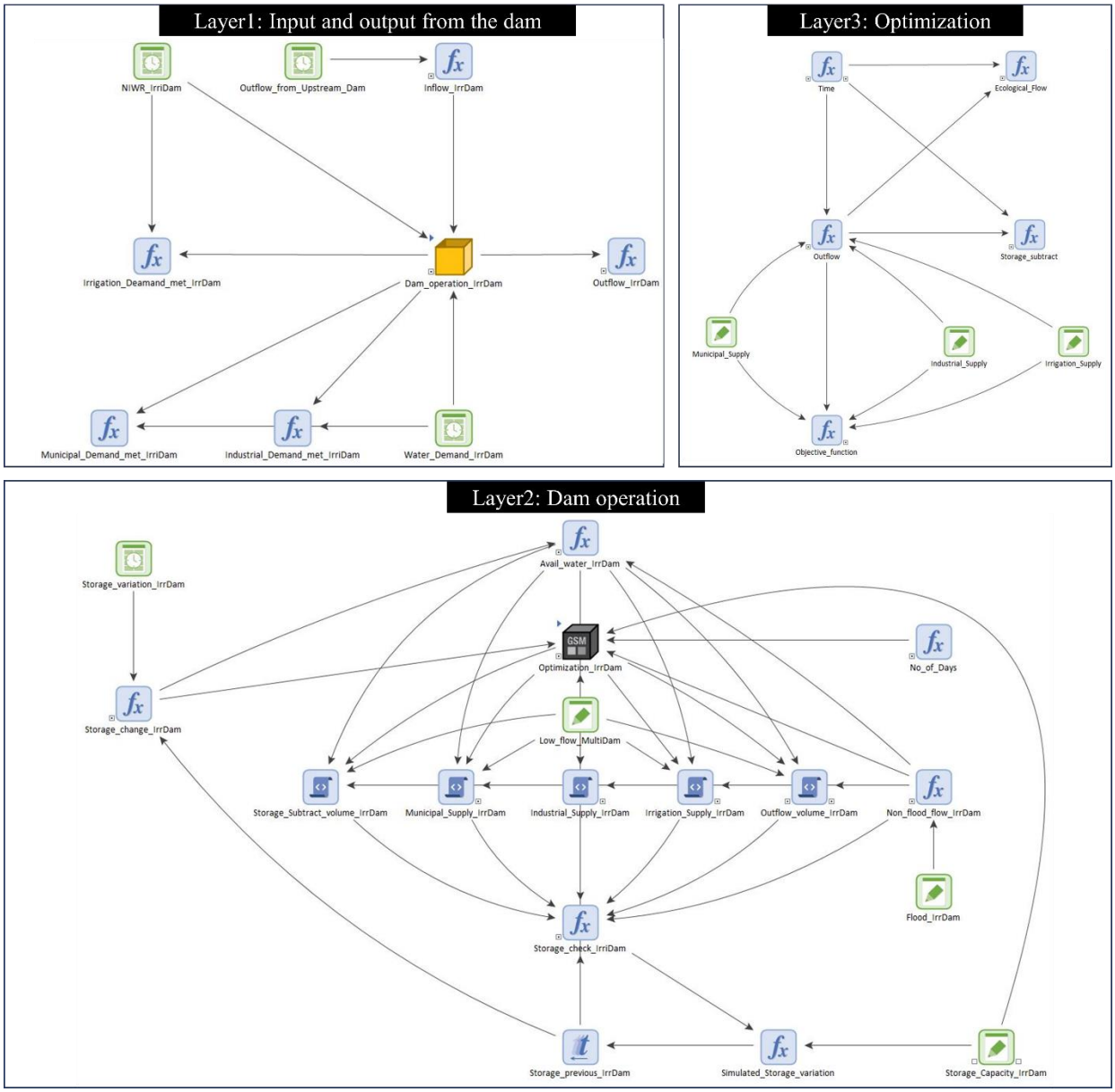


*Figure 1(d): System dynamics setup of an irrigation dam in GoldSim showing the input-output (layer 1), dam operation (layer 2), and optimization scheme (layer 3).*

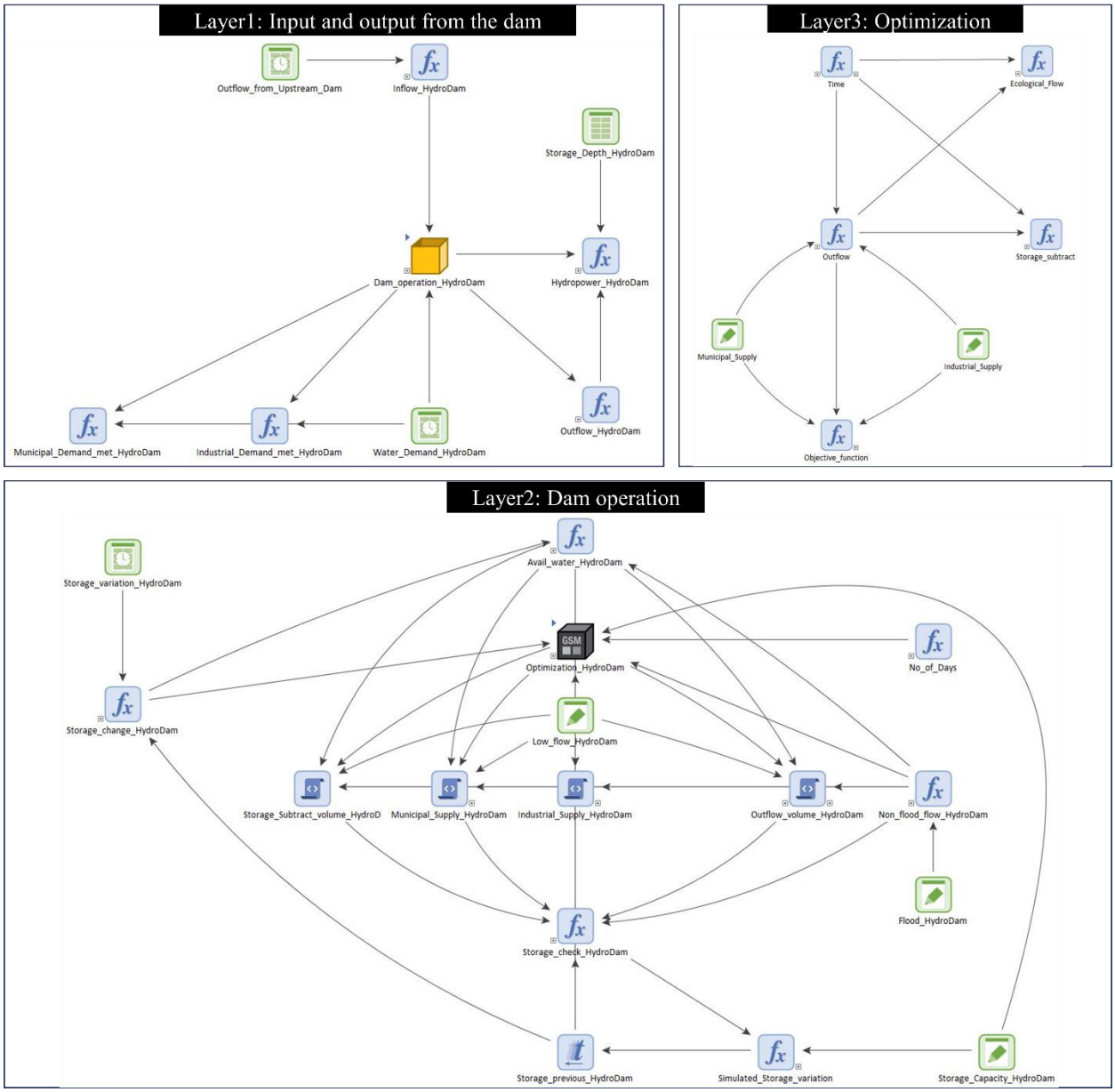


*Figure 1(e): System dynamics setup of a hydropower dam in GoldSim showing the input-output (layer 1), dam operation (layer 2), and optimization scheme (layer 3).*

### 5.2.4 Optimization

The optimization of the water distribution between the demand from the different sectors was performed in the model using the Box complex method by defining the objective function and objective variables (Box, 1965). The dynamic optimization of the model was achieved by utilizing the submodel feature of GoldSim and defining the current values of the variables at each time step using the interface between the submodel and outer

variables. The objective functions and associated constraints for the optimization of the reservoir's operation in the Mekong River basin were expressed as follows:

Variables:

The following variables are involved in the model of the optimization of the reservoir

i. $Q^h$: turbined flow;
ii. $Q^I$: irrigation flow;
iii. $Q^m$: municipal flow;
iv. $Q^{Ind}$: industrial flow;
v. $S$ : volume stored in the reservoir;
vi. $S^{max}$: maximal operational volume of the reservoir (95% of the storage capacity of the reservoir);
vii. $S^{min}$: minimal operational volume of the reservoir (10% of the storage capacity of the reservoir);
viii. $h$: height of the reservoir elevation, as a function of the stored volume;
ix. $ID$ : irrigation demand;
x. $MD$ : municipal demand;
xi. $IndD$ : industrial demand;
xii. $Q^F$: water inflow into the reservoir;
xiii. $I$: inflow contribution from the catchment area;
xiv. η: efficiency of the turbine;
xv. $Q_{ecological}^{D,min}$: minimum downstream flow for sustaining the ecosystem (10% of the inflow).

Here, $Q^h, Q^I, Q^m, Q^{Ind}$ are the decision variables.

Objectives:

To rationally and effectively use the water resources of a reservoir, a multi-objective optimization model was required that considers both water diversion and power generation objectives for reservoirs with water diversion and power generation tasks (Ming et al., 2017). The amount of water for water diversion and power generation was dynamically

determined by the water level for each period, and also affects the water level of the reservoir in turn. Once the inflow to the reservoir was known, the amount of available water was determined through the water balance equation. In terms of the hydroelectric power station, the increase of the outflow resulted in a higher energy generation. In contrast, the water diversion for irrigation lowered the energy production of the dam. Similarly, the water supply for each sector decreased the demand fulfillment of other sectors. Thus, the objective functions have obvious conflict. These three objective functions were combined into a single equation as follows:

Maximize the water distribution between the water demanding sectors based on the purpose of the dam:

$$maximize\ f_{objective} = Q^h + Q^I + Q^m + Q^{Ind} \tag{3}$$

The annual energy generation from the reservoir was estimated as:

$$Energy_{hydropower} = \sum_{Jan}^{Dec} Q_t^h \times h \times g \times \eta \tag{4}$$

Constraints:

The above objective functions of the model on reservoir optimization operation are subject to the following constraints:

A. Water balance constraint:

$$S_{t+1} - S_t = (Q_t^F - Q_t^h - Q_t^I - Q_t^m - Q_t^{Ind})\Delta t \tag{5}$$

If the reservoir is the first one on a river, the inflow is determined by nature. If not, the total volume coming from the upstream reservoir must be added to the incremental volume - that of water from other tributaries, added between the two reservoirs:

$$Q_t^F = \sum_{k=1,k\in U}^{N} (Q_{t,k}^h + I_t) \tag{6}$$

Here U is the set of upstream reservoirs.

B. Storage of the reservoir constraint:

$$S^{min} \leq S_t \leq S^{max} \quad (7)$$

C. Irrigation supply constraint:

$$0.8 \times ID \leq Q_t^I \leq ID \quad (8)$$

D. Municipal supply constraint:

$$0.8 \times MD \leq Q_t^m \leq MD \quad (9)$$

E. Industrial supply constraint:

$$0.8 \times IndD \leq Q_t^{Ind} \leq IndD \quad (10)$$

F. Ecological demand constraint:

$$Q_{ecological}^{D,min} \leq Q_t^h \quad (11)$$

G. Nonnegative constraints:

All values above are positive.

The optimization setup for the multipurpose, irrigation, and hydropower dams in the MRB is shown as layer 3 in Figure 1(b-d). The current analysis gives equal weightage to each sectors.

### 5.2.5 Reservoir operation

The operation of the reservoir was basically based on following the rule curve with water balance between the inflow and outflow from the reservoir including the water demand from different sectors. The water supply to irrigation, municipal, industrial, energy, and ecological sectors are primarily governed by the inflow to the reservoir apart from dynamic demands from the sectors. Two conditions were maintained for the release of outflow from the reservoirs:

(a)The minimum monthly release was set as 10% of the monthly inflow to the reservoir, and

(b) As mentioned in Liu *et al.* (Xingcai Liu et al., 2016), a minimum of 10% of the total capacity of reservoirs is maintained.

The operation of the reservoir was altered during different inflow conditions, i.e. extremely high and low inflow. The flood and low-inflow magnitude were estimated as the $10^{th}$ percentile and $90^{th}$ percentile of the flow duration curve developed using the inflow from 1950 to 2005. Specifically, the water supply to the different sectors was modified under the following three conditions to facilitate the safety of the dam:

(a) When inflow is less than the low-inflow magnitude, no water was supplied to any sector in order to accumulate water to enhance the storage of the reservoir.

(b) When inflow is more than the flood magnitude, the volume of water above the flood magnitude was spilled from the emergency spillway and the remaining volume was used for reservoir operation.

(c) When inflow is not sufficient to meet the desired rule curve volume, water was only supplied to the environmental sector and the remaining volume of water was stored in the reservoir.

### 5.2.6 Extreme events

The extreme events experienced by the system were defined based on the inflow magnitude to the reservoirs**.** Very high inflow of magnitude more than $10^{th}$ percentile flow value (flood events) and very low inflow of magnitude less than $90^{th}$ percentile flow value (low-flow events) causes disruption of the operation of the system in supplying water to various sectors (Table 1). However, the system recovers to the normal operation after the termination of the extreme events. The stress in the system caused by the onset of singular or series of extreme events were defined by the impact and duration of the events. The impact of the extreme events was estimated as the deficit volume during the low flow event and surface volume during the flood events with respect to the long-term historic inflow volume. The stress index of the system for the extreme events for each reservoir was defined as:

$$Stress\ Index_{Flood} = \max\left(\sum \frac{Volume_{Flood} - Volume_{Average\ flow}}{Volume_{Average\ flow}} dt\right) \quad (12)$$

$$Stress\ Index_{Low\ flow} = \max\left(\sum \frac{Volume_{Average\ flow} - Volume_{Low\ flow}}{Volume_{Average\ flow}} dt\right) \quad (13)$$

In other words, the stress index indicates the maximum stress survived by the system due to the occurrence of extreme events. In order to make a comparison between different reservoirs with contrasting average, flood, and low flow values, the stress index was classified into four classes (Table 3).

*Table 3: Classification of the Stress index of the different reservoir against the extreme events*

| Class | Stress Index: Flood | | Stress Index: Low flow | |
|---|---|---|---|---|
| | Min | Max | Min | Max |
| Low | 2.90 | 5.99 | 1.50 | 1.99 |
| Medium | 6.00 | 8.99 | 2.00 | 2.49 |
| High | 9.00 | 13.99 | 3.00 | 3.99 |
| Very high | 14.00 | 19.99 | 4.00 | 5.49 |

### 5.2.7 Economic model

The shadow price is a proxy value of a good or service where no market price for the good exists. The shadow price is not the mean retail price of the finished good, however, it provides a method for making the management decision. Generally, the linear programming model for the shadow price estimation can be represented as follows (Xiuli Liu et al., 2009):

$$\max (a_{v1}X_1 + a_{v2}X_2) \text{ for each country or project} \quad (14)$$

subject to:

$$AX + Y = X \quad (15)$$

$$X^l \leq X \leq X^h \quad (16)$$

$$a_{w1}X_1 + a_{w2}X_2 = w \quad (17)$$

$$Y \geq Y^l \quad (18)$$

where: subscript *1* indicates irrigation sector; subscript *2* indicates hydropower sector; *X* is a column vector of total output; $a_{v1}$ is the value-added coefficient of irrigation sector, $a_{v2}$ is the value-added coefficient of hydropower sector, *A* is the direct input coefficient matrix; *Y* is a column vector of final demand; $a_{w1}$ is the water used the coefficient of irrigation sector; $a_{w2}$ is the water used the coefficient of hydropower sector; *w* is the total volume of water that can be used in a period; $X^l$ and $X^h$ are the lower and upper bounds of X.

Irrigation and hydropower shadow price for each country can be evaluated by solving the linear programming model. Specifically, the shadow price can be estimated as the ratio of the revenue generated from the sector and the quantity of water supplied. The shadow price of irrigation water can be estimated using the following equation employed by Ziolkowska (2015):

$$P_{wi} = \frac{Y_i \times P_i - (Q_{Ki} \times P_{Ki} + Q_{Hi} \times P_{Hi} + Q_{Li} \times P_{Li})}{Q_{Wi}} \quad (19)$$

where: $P_{Wi}$ is the shadow price of water; $Q_{Wi}$ is the amount of water applied for the crop production; $Y_i$ is the quantity of crop output; $P_i$ is the price received for the crop; $Q_{Ki}$ is the quantity of capital input; $P_{Ki}$ is the price of capital input; $Q_{Hi}$ is the quantity of human labor input; $P_{Hi}$ is the price of human labor; $Q_{Li}$ is the area of land applied to produce the crop; $P_{Li}$ is the price of land used.

Similarly, the shadow price of the hydropower production can be estimated as follows:

$$P_{Wh} = \frac{n\eta\rho qgh \times P_h}{Q_{Wh}} \quad (20)$$

where: n is the number of turbines; η is the dimensionless efficiency of the turbine; ρ is the density of water; q is the volumetric flow rate; g is the acceleration due to gravity; h is the height between inlet and outlet; $P_h$ is the price of the electricity; $Q_{Wh}$ is the amount of water applied for the hydropower production.

However, the approach estimates the shadow price of water for each country or projected based on the average conditions existing over time, diluting the conflict between the different sectors for obtaining the limited available water. To qualitatively infer the information, the concept of obtaining an additional unit of water to enhance the production of individual sectors was used. Another definition of the shadow price was the improvement in the total value or service generated by the factor constrained activity by gaining access to one additional unit of the limiting factor with all the other variables are kept constant. Here, the limiting factor was the volume of water. Based on the above equations, the production of the hydropower sector, the irrigation sector was dependent on the volume of water supplied to the sector. Similarly, the yield of the municipal and

industrial sectors was governed by the volume of the water supplied for the purpose. In other words, both the objective and constraint functions can be expressed in terms of the volume of water, so, the shadow price was a function of the fraction of the volume of water supplied and the volume of water required to increase the production. Hence, the shadow price was dependent on the percentage of the demand met by the available water volume supplied to the sector. Inversely, the shadow price of the water was higher for the sector with the least percentage of the demand met and vice-versa. The requirement of an additional unit of water was more crucial for the sector with the least production (or the percentage of demand met) and willing to pay a higher price to obtain the last unit. On the other hand, the sector with 100% of the demand met was not requiring any more water, hence the shadow price was not bonded by constraints . Similarly, to understand the cruciality of the water requirement of an additional unit, six classes of the shadow price were defined (Table 4). Very low shadow price means the sector was willing to pay a small amount of money to obtain the last unit of water and vice-versa.

*Table 4: Classification of the Shadow price classes based on the percentage of demand met by the energy, irrigation, municipal and industrial sectors.*

| **Shadow price class** | **Percentage of demand met** |
|---|---|
| No binding constraints | >100 % |
| Very low | 100 % to 81 % |
| Low | 80 % to 61 % |
| High | 60 % to 41 % |
| Very high | 40 % to 21 % |
| Extremely high | <20 % |

### 5.3 Results and Discussion

#### 5.3.1 Comparison of storage and outflow

Monthly storage and outflow from the reservoir simulated through the reservoir operation considering the rule curve and water demand from the energy, irrigation, municipal, industrial and ecological sectors were compared with the observed data from 2006 to 2019. Figure 2(a) and 2(b) shows the comparison of the monthly simulated and observed storage and outflow from 2006 to 2019 for six multipurpose and four irrigation reservoirs, respectively. Mathematically, the Nash-Sutcliffe model efficiency coefficient (NSE, Nash

& Sutcliffe, 1970), coefficient of correlation (r) and relative root mean square error (RRMSE) between the simulated and observed storage, and r value between the simulated and observed outflow was estimated to access the efficacy of the system dynamics model (Table 5). As the reservoir operation was primarily driven with the objective of replicating the rule curve, the simulated storage closely follows the observed storage variation. The NSE value between the monthly simulated and observed storage for the multipurpose and irrigation dams varied from 0.68 to 0.99, while the r value ranged between 0.83 and 0.99. All the 10 dams considered for the evaluation of the approach are located on the tributaries in the Thailand region and situated on the most upstream are of the tributaries without any cascading effect, except Ubol Ratana. The cascading effect of HuaiKum on the operation of Ubol Ratana was negligible as the inflow contribution to Ubol Ratana from the outflow of HuaiKum contributed less than 10%, while the remaining inflow was collected from the catchment downstream of HuaiKum. Moreover, the cascading effect of the upstream reservoir was reflected in the outflow of the reservoir and water diversion to various sectors. The evaluation of the approach was performed for the optimized system under normal conditions. In other words, the normal condition was defined based on the inflow to the reservoir such that the inflow is between the $10^{th}$ and $90^{th}$ percentile of the historic flow, i.e., no extreme events. As the reservoir operation was designed to fluctuate the reservoir storage between the 10% and 95% of the storage capacity, the rule curve was considered to be same for the future period assuming the height of the dam will not be increased in future to enhance the storage capacity of the reservoir.

Besides, the estimated error for the simulated storage variation relative to the observed storage varied from 2.7% (Sirindhorn) to 26.3% (Lam Pao) under the observed climate. The high precision of the Sirindhorn dam was due to the rhythmic variation of the reservoir storage with minimal fluctuation between the different years for the observed period. The operation of the reservoirs under varying inflow volume and dynamic demands from the irrigation, municipal, and industrial along with considering the dam safety caused the high fluctuation in the outflow from the reservoir. The r value between the monthly observed and simulated outflow from the reservoirs reaches up to 0.26. The low r value for the dams was also caused by the sudden increase in the observed outflow during 2018 for Nam Pung, Chulabhorn and Lam Nang Rong, which was not captured by the systems model, however,

the storage variation reaches the minimum value during the period for the dams. On average, the simulated outflow from the multipurpose was slightly higher than the observed values as the objective was to maximize the energy generation and fulfill ecological water demands primarily due to the availability of the water. As the objective of the optimization involves the water demand from irrigation, municipal, industrial, and energy sector with no preference order, the water supply for the sectors was equally considered. However, the water diversion for irrigation, municipal, and industrial sector was constrained by the upper limit of the water demand, but the outflow from the reservoir was not bound by the upper limit. So, the available water after considering the rule curve and water demand from the irrigation, municipal, and industrial sector, was discharged to the downstream region for the operation of downstream dams.

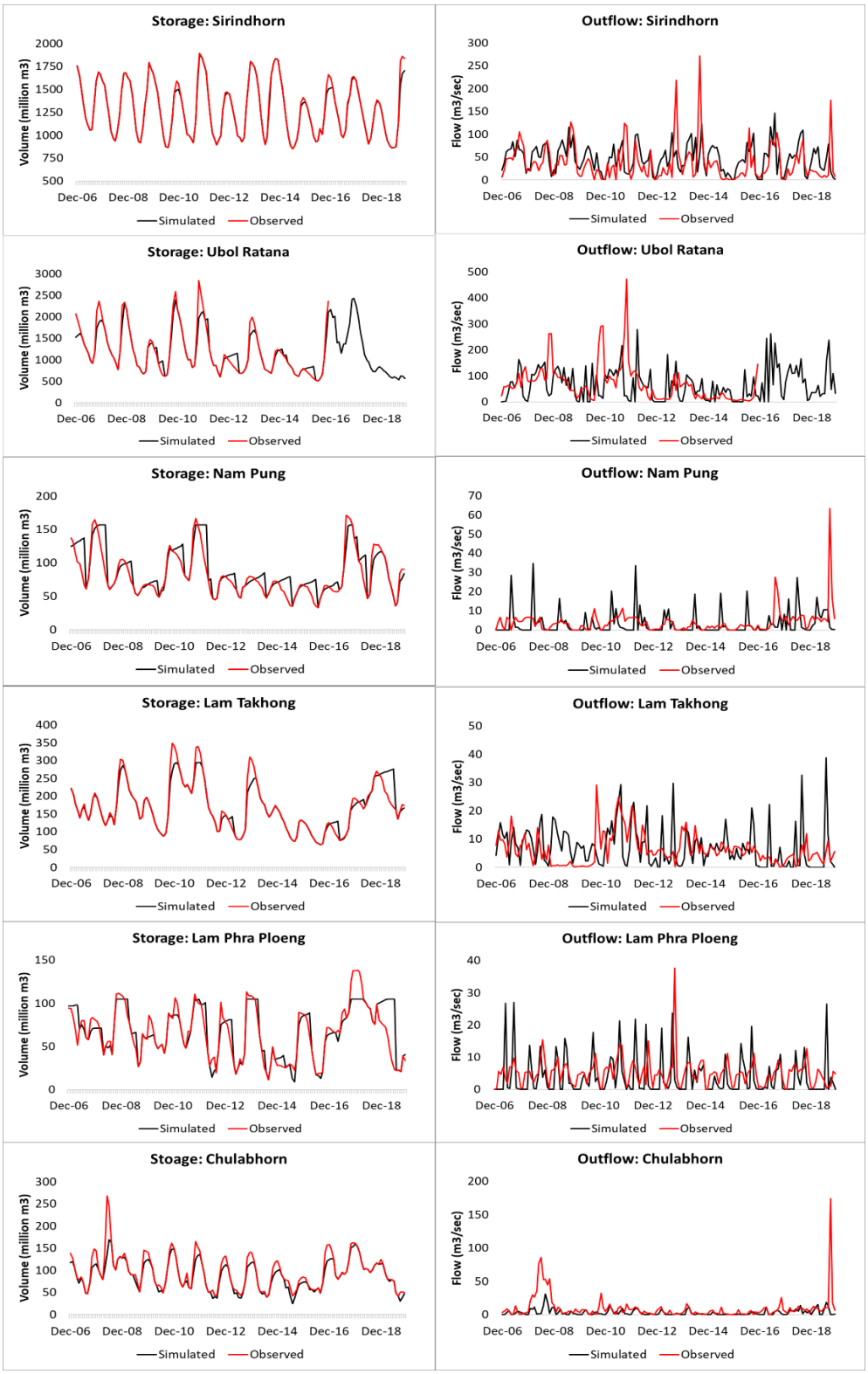


*Figure 2(a): Evaluation of the approach with the comparisons of the simulated and observed streamflow and outflow from the six multipurpose dams from 2006 to 2019*

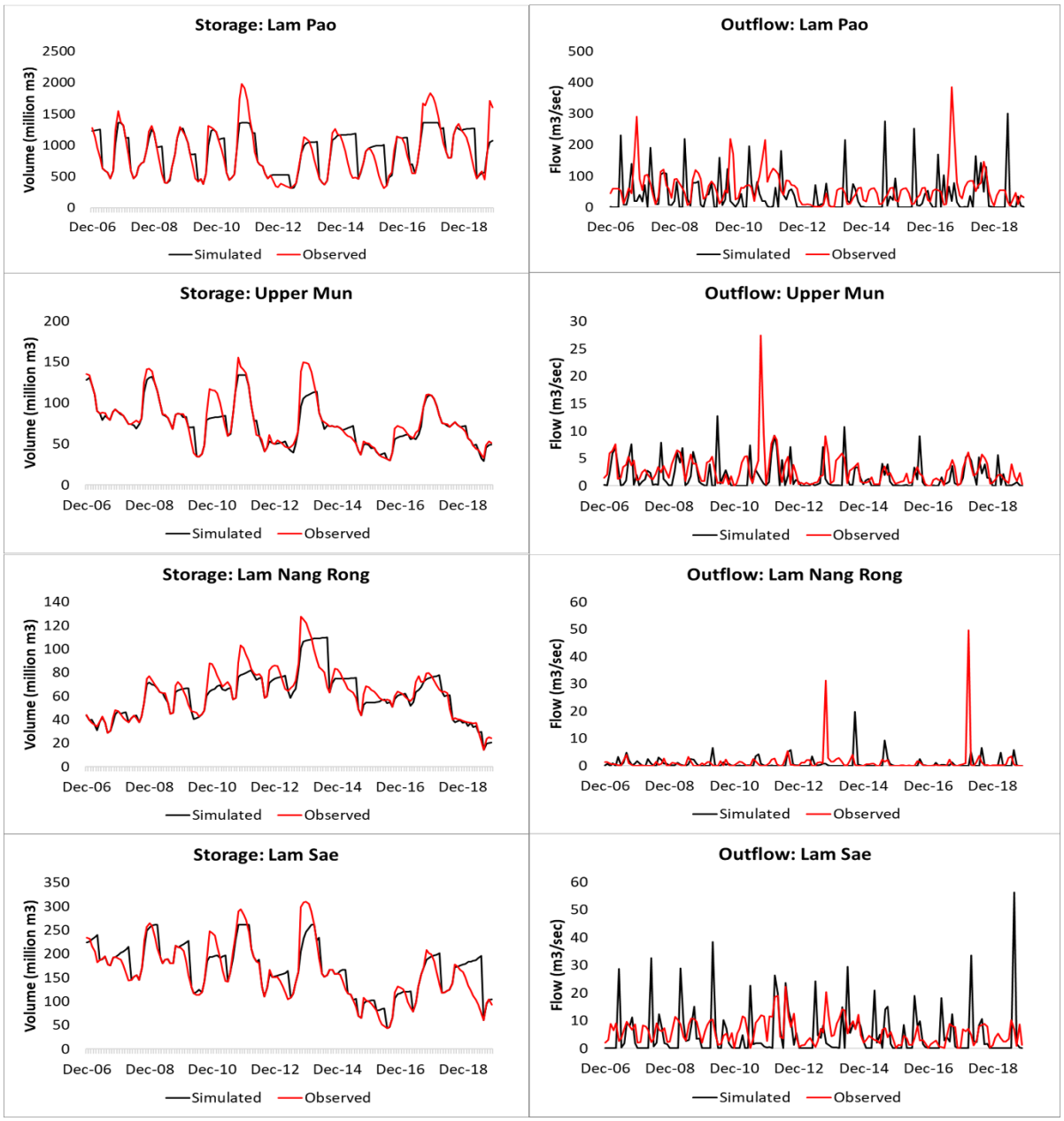


*Figure 2(b): Evaluation of the approach with the comparisons of the simulated and observed streamflow and outflow from the four irrigation dams from 2006 to 2019*

*Table 5: Comparison of the monthly simulated and observed storage variation of the reservoir and outflow from the reservoir from 2006 to 2019.*

| S.No. | Dam | Purpose | Storage | | | Outflow |
|---|---|---|---|---|---|---|
| | | | NSE | r | RRMSE | r |
| 1 | Ubol Ratana | Multipurpose | 0.90 | 0.96 | 14.26 | 0.09 |
| 2 | Sirindhorn | Multipurpose | 0.99 | 0.99 | 2.76 | 0.39 |
| 3 | Nam Pung | Multipurpose | 0.68 | 0.86 | 22.48 | 0.05 |
| 4 | Lam Takhong | Multipurpose | 0.89 | 0.95 | 13.00 | 0.26 |
| 5 | Lam Phra Phloeng | Multipurpose | 0.72 | 0.85 | 24.39 | 0.24 |
| 6 | Chulabhorn | Multipurpose | 0.81 | 0.93 | 17.67 | 0.23 |
| 7 | Lam Pao | Irrigation | 0.67 | 0.83 | 26.35 | 0.03 |
| 8 | Upper Mun | Irrigation | 0.88 | 0.95 | 13.67 | 0.27 |
| 9 | Lam Rang Rong | Irrigation | 0.81 | 0.91 | 14.45 | 0.03 |
| 10 | Lam Sae | Irrigation | 0.77 | 0.88 | 17.64 | 0.19 |

### 5.3.2 Optimization of water allocation between different sectors

The distribution of the available water from the reservoir was dependent on the demand volume of water from each sector. Moreover, the optimization of the supply of the water was crucial for the reservoir commissioned for various purposes as each sector competing for the same resource and affecting the other. In this study, the ecological demand for the downstream area was always considered, except during the extremely low flow events, the water allocation was primarily optimized between irrigation, energy, municipal and industrial sectors. The ecological demand was considered as 10% of the inflow to the reservoir. The minimum water required to support the ecosystem of the region was assumed as the 10% of the nature streamflow in tributaries and mainstem which remains uninterrupted by the dam operation. Although the 'Technical Guide for Environmental Impact Assessment of River Ecological Flow, Cold Water, and Fish passage Facilities for Water Conservation Construction Projects (Trial) EIA Letter (2006) No.4' specifies the minimum ecological flow as 10% of the average annual natural runoff, to incorporate the seasonality of the river, the ecological flow was considered as 10% of the monthly natural flow (Ma et al., 2019). Figure 3(a) shows the annual and seasonal variation of energy generation (GWh), percentage of demand met of irrigation, municipal and industrial sector from multipurpose dams during the observed period (2006-2019). The operation of the multipurpose dams was more complicated as the water was supplied to the hydropower,

irrigation, municipal and industrial sectors. The reservoirs with large storage capacity such as Sirindhorn and Ubol Ratana was able to cope with the high demands from the various sectors with satisfactory supply levels. During the observed period, the average annual hydropower energy produced by the Sirindhorn was accounted as 130GWh, which was a 44% surplus of the desired energy production, while the supply to the other sectors was able to fulfill more than 80% demand of the irrigation, municipal and industrial sector. Similarly, the annual energy production of the Ubol Ratana was more than twice the desired energy generation with a value of 132GWh per year, along with satisfying more than 60% of the water demand from other sectors.

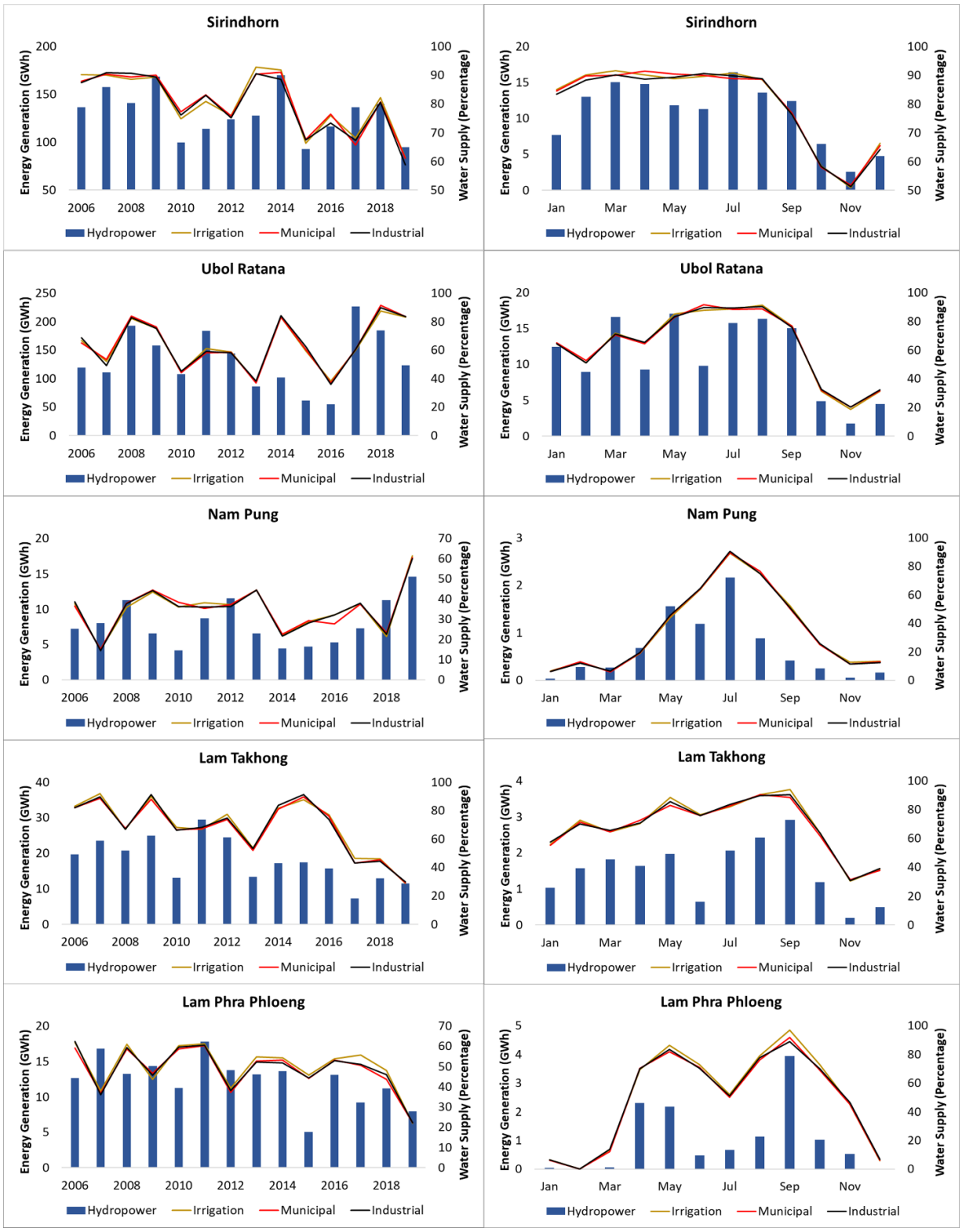


*Figure 3(a): Annual and seasonal variation of energy generation (GWh), percentage of demand met of irrigation, municipal and industrial sector from multipurpose dams for the observed period (2006-2019)*

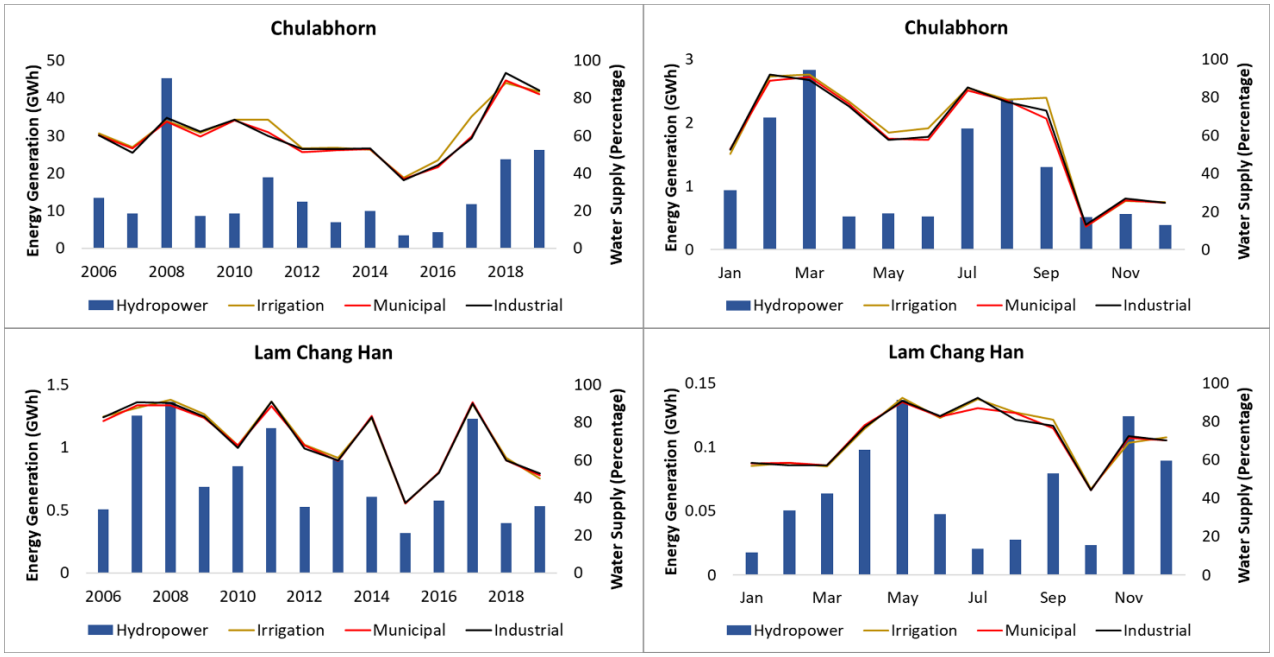


*Figure 3(a): Annual and seasonal variation of energy generation (GWh), percentage of demand met of irrigation, municipal and industrial sector from multipurpose dams for the observed period (2006-2019)*

On the other hand, the remaining multipurpose dams were not able to completely satisfy the water demand from all the sectors during the observed period due to the low storage capacity of the reservoirs. The multiple reservoirs with a storage capacity of more than 2000 million $m^3$ were able to fulfill the water requirement of all the demanding sectors, viz., irrigation, energy, municipal, industrial, and environment. The average annual energy production of the Nam Pung was 8 GWh, Lam Takhong dam was 18 GWh, Lam Phra Phloeng was 12.5 GWh, and Chulabhorn was 14.5 GWh which accounts for 53%, 45%, 82%, and 25% of the desired energy production from the dams, respectively. The fraction of the water demand met of the irrigation, municipal and industrial sectors were similar for the multipurpose dams with values 35%, 69%, 50%, and 62% for Nam Pung, Lam Takhong, Lam Phra Phloeng, and Chulabhorn, respectively. The Lam Chang Han was able to satisfy more than 71% of the water demand from the irrigation, municipal and industrial sectors as the energy production of the dam was minimal with an average annual energy generation of 0.8 GWh. The interannual energy generation and degree of water demand fulfillment of the various sectors from the multipurpose dams were observed from 2006 to 2019 but 2015 was distinct with the lowest energy generation and water supply from all

the multipurpose dams due to reduced inflow caused by the dry meteorological precipitation conditions in the basin. The seasonal variation of the energy generation and water supply follows the monsoon season with higher fulfillment during July-October. The elevated inflow to the reservoir during the monsoon season derived the higher energy production, while the irrigation water demand was less during the period which assists towards satisfying a higher proportion of the demand and supply to the municipal and industrial sectors. On the other hand, the higher irrigation water demand before the onset of the monsoon due to the elevated temperature limited the hydropower energy generation. The energy generation and water demand were least after the monsoon, specifically October-December, as the inflow water stored in the reservoir was gradually released to facilitate the water supply during the other months of the year.

The allocation of the available water from the irrigation reservoirs was straightforward as compared to the multipurpose dams since the water supply from the energy sector was relaxed, declining the complexity in the water allocation. The irrigation reservoirs were obliged to supply water to irrigation, municipal, and industrial sectors, moreover, two reservoirs located in China was commissioned only for the irrigation purpose due to location of the dams encompassing small region in the basin (Figure 3b). The water supply to the irrigation sector was prioritized over the municipal and industrial demands. However, the difference in the meeting the demands varied marginally between the different sectors. Lam Pao and Nam Un reservoirs supplied 54% and 19%, respectively, of the total water demand from the various sectors. The water supply to the irrigation sector was 70%, 56%, 53%, and 47.6% from the Upper Mun, Lam Nang Rong, Lam Plai Mas, and Lam Sae, respectively. On the other hand, the water supply for the municipal and industrial sectors was compromised due to the scarcity of the water that accounted 63%, 38%, 48%, and 45% of the demand from the Upper Mun, Lam Nang Rong, Lam Plai Mas, and Lam Sae, respectively. The efficiency of the Huai Luang reservoir was excellent during the observer period supplying more than 90% of the water demand from the irrigation, municipal, and industrial sectors. As the Cibihe and Haixihai were bound to supply water only the irrigation sector, the percentage of demand met accounted for 86.3% and 72.6%, respectively. The interannual variation of the water supply to the various sectors from the irrigation dams was similar in behavior as that of the multipurpose dams. The efficiency of

the reservoirs in meeting the demands of the irrigation, municipal and industrial sectors was suppressed during 2014-2015 due to low inflow to the reservoirs. The seasonal variation of meeting the water demands followed the monsoon season as the inflow was elevated due to high precipitation in the basin and the reduced irrigation water demands improved the water supply to municipal and industrial sectors. The criteria of meeting the demand for irrigation was less during January-April the storage in the reservoir was less and the demand was high due to increasing temperatures and other climatic factors causing increased evapotranspiration from the irrigated fields.

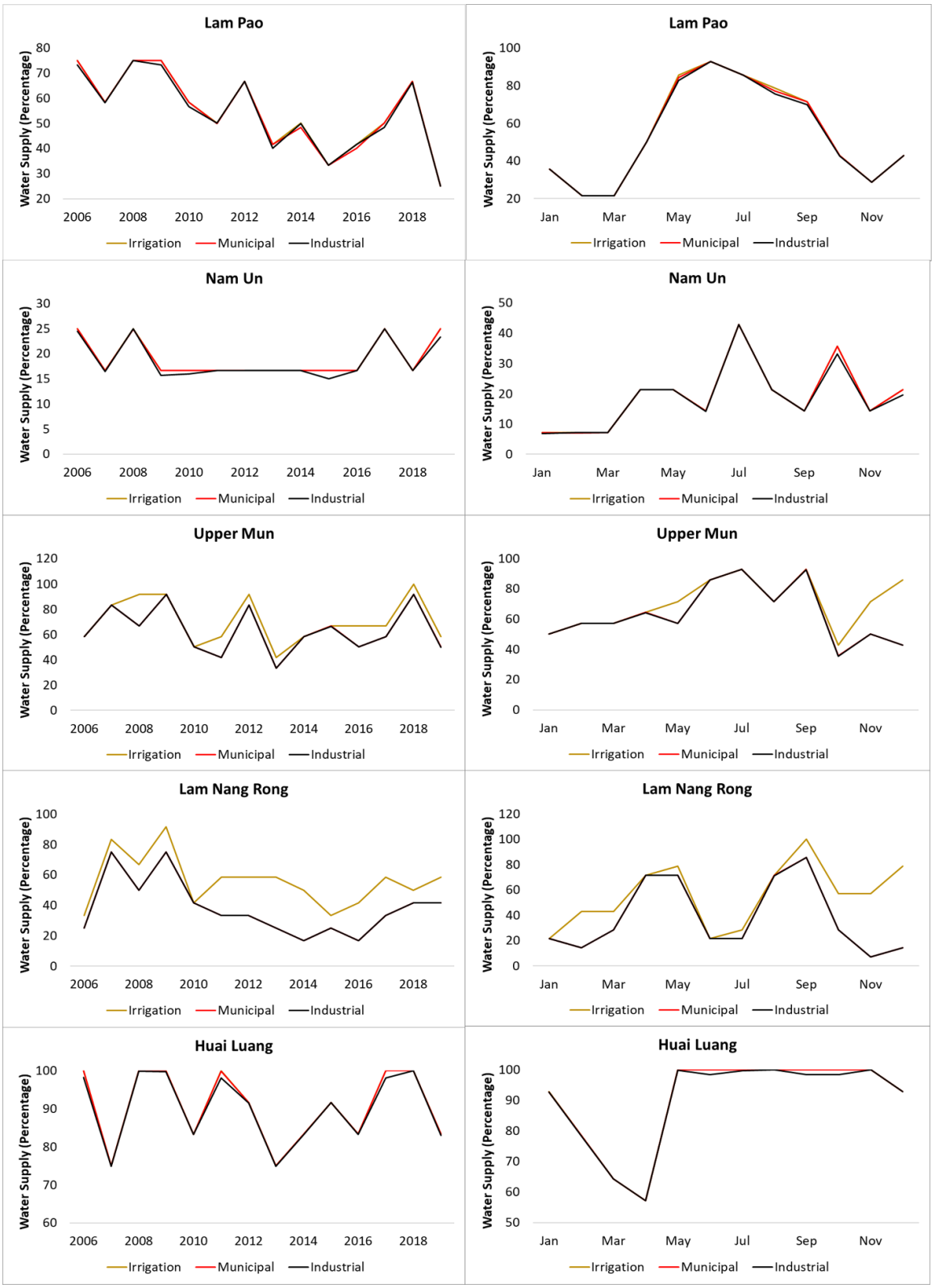


*Figure 3(b): Annual and seasonal variation of percentage of demand met of irrigation, municipal and industrial sector from irrigation dams for the observed period (2006-2019)*

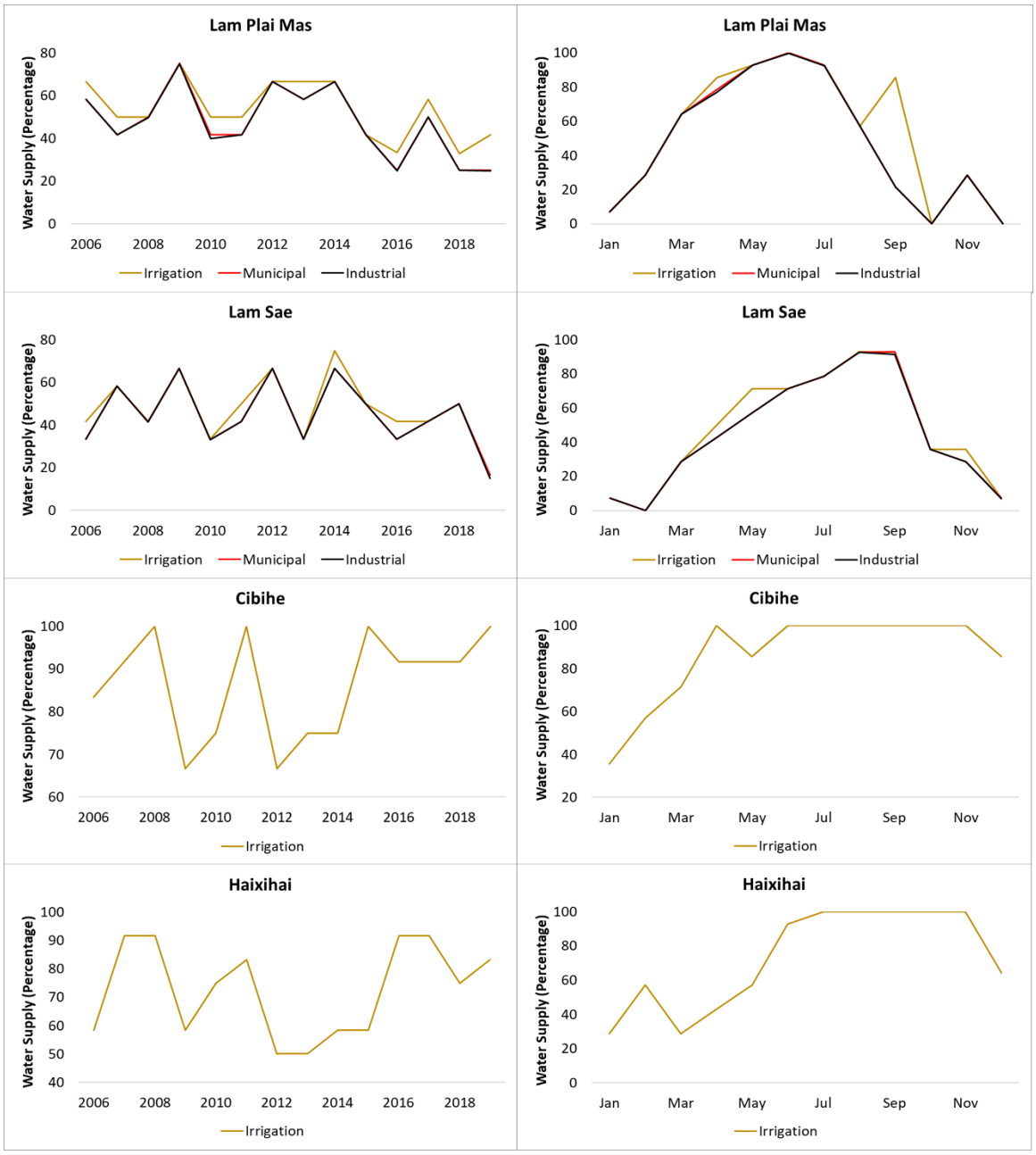


*Figure 3(b): Annual and seasonal variation of percentage of demand met of irrigation, municipal and industrial sector from irrigation dams for the observed period (2006-2019)*

Figure 3(c) shows the annual and seasonal variation of energy generation (GWh), percentage of demand met of municipal and industrial sector from hydropower dams for the observed period (2006-2019). The hydropower reservoirs were mainly commissioned for the generation of electricity using the hydropower energy of the river inflow, however, municipal and industrial water demand was supplied from Huai Kum, Pakmun and Yaly.

The average annual hydropower energy generation from the dams varied from 1 GWh to 15000 GWh. The energy generation of the hydropower dams located in China was highest amongst all the dams in the basin as the dams are located on the mainstem of the Mekong River. During the observed period, the average annual energy production of Xiaowan, Manwan, Dachaoshan, and Jinghong was estimated as 15023 GWh, 6933 GWh, 6407 GWh, and 9472 GWh, respectively. The energy generation of the Xiaowan and Manwan during the observed period comprised 80% and 90%, respectively, of the desired energy generation. On the other hand, Dachaoshan and Jinghong produced 8% and 21%, respectively, surplus hydropower energy during the observed period. In addition, the hydropower energy production of the dams located in the Thailand region was more than twice the desired estimated with values 11 GWh and 800 GWh for Huai Kum and Pakmun, respectively.

Most of the dams located in the Laos PDR were not able to produce the required energy, however, the generation was 28 GWh, 453 GWh, 31 GWh, and 1.5 GWh from Xeset1, Theun-Hinboun, Houay-Ho, and Nam Mang3, respectively. Contradictory, Nam Ngum, Selabam, and Nam Leuk satisfied the energy demand with an annual generation of 2317 GWh, 46 GWh, and 536 GWh, respectively. Ochum dam in Cambodia produced annual energy of 1 GWh, while the Yaly dam in Vietnam generated more than 890 GWh energy. The municipal and industrial water demand was highly satisfied with the reservoirs by meeting 90% of the water demand from the Huai Kum and Yaly, and 75% from the Pakmun dam. As observed in the multipurpose and irrigation dams, the interannual variation in the energy production was not significant, however, the period 2014-2015 was observed to produce less energy and water demand to the municipal and industrial sectors due to low precipitation in the basin. As the competition for the available water between the different sectors was relaxed, the seasonal variation of the energy generation precisely followed the monsoon variation in the region with higher production during July-October as compared to other months of the year. Moreover, some of the dams located in the china region, such as Manwan, Dachoashan, Jinghong, and Xiaowan, observed a marginal increase in the energy production during January-March due to the outflow from the upstream dams reflecting the cascading effect of the dams.

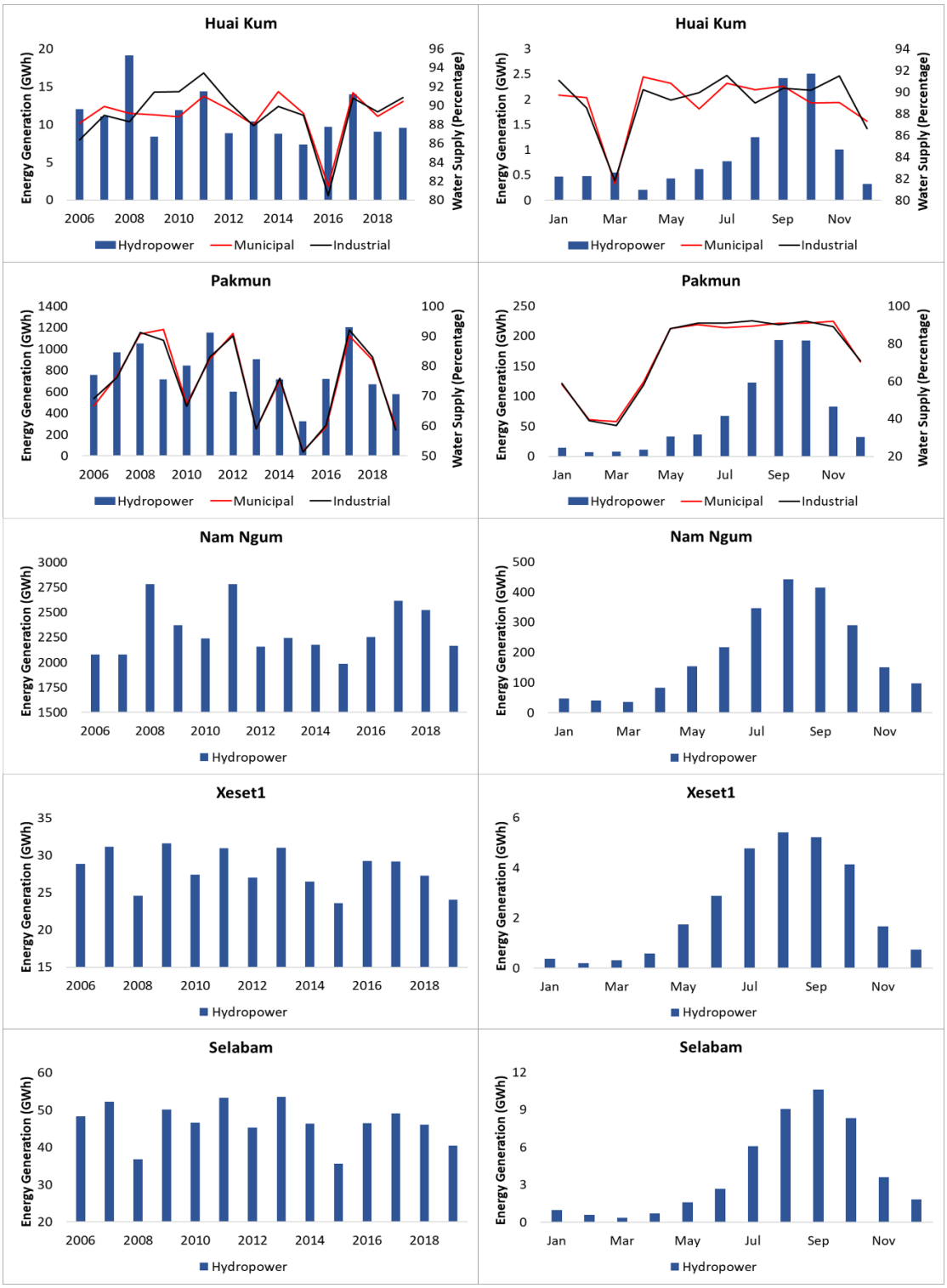


*Figure 3(c): Annual and seasonal variation of energy generation (GWh), percentage of demand met of municipal and industrial sector from hydropower dams for the observed period (2006-2019)*

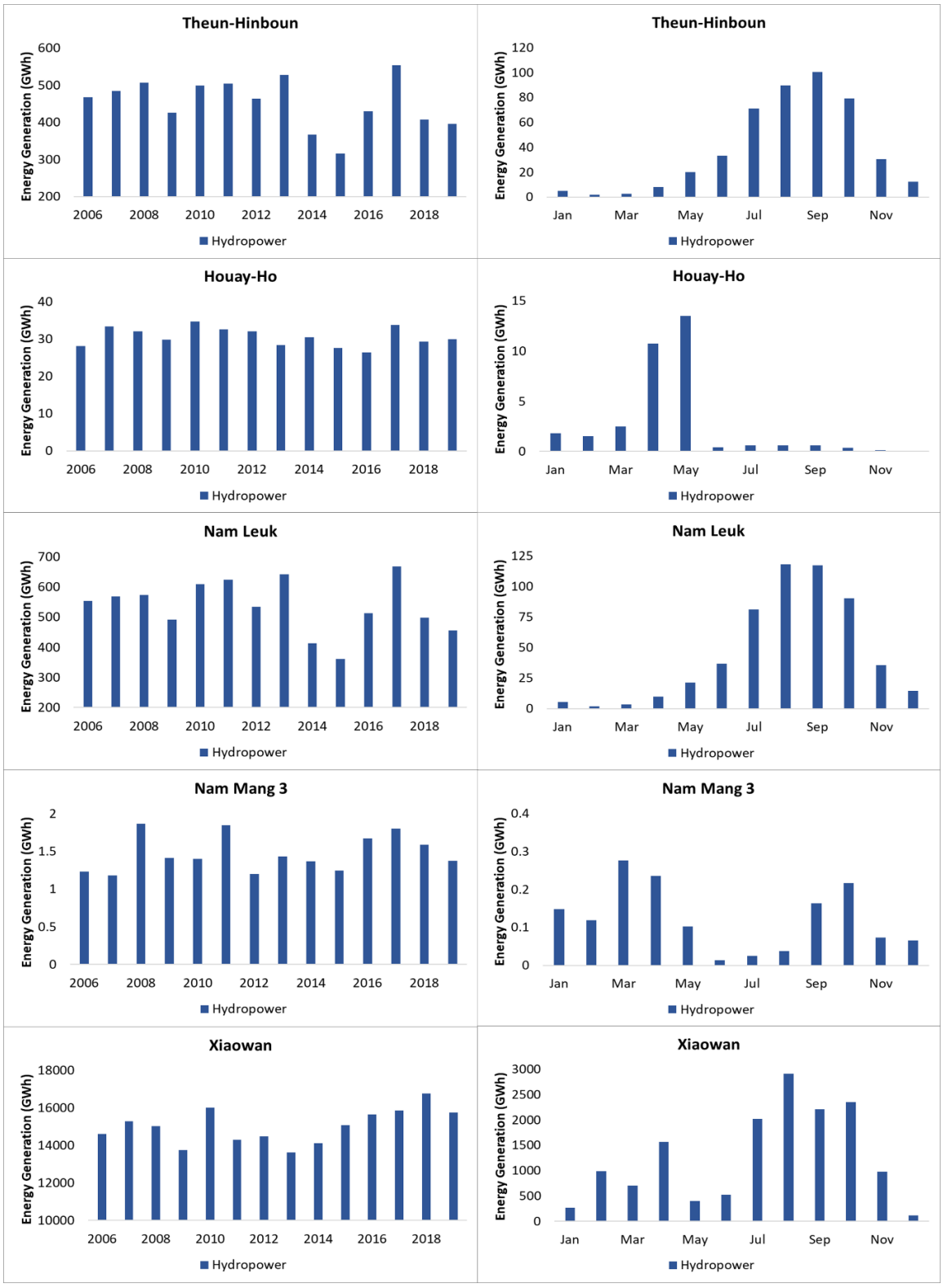


*Figure 3(c) continued*

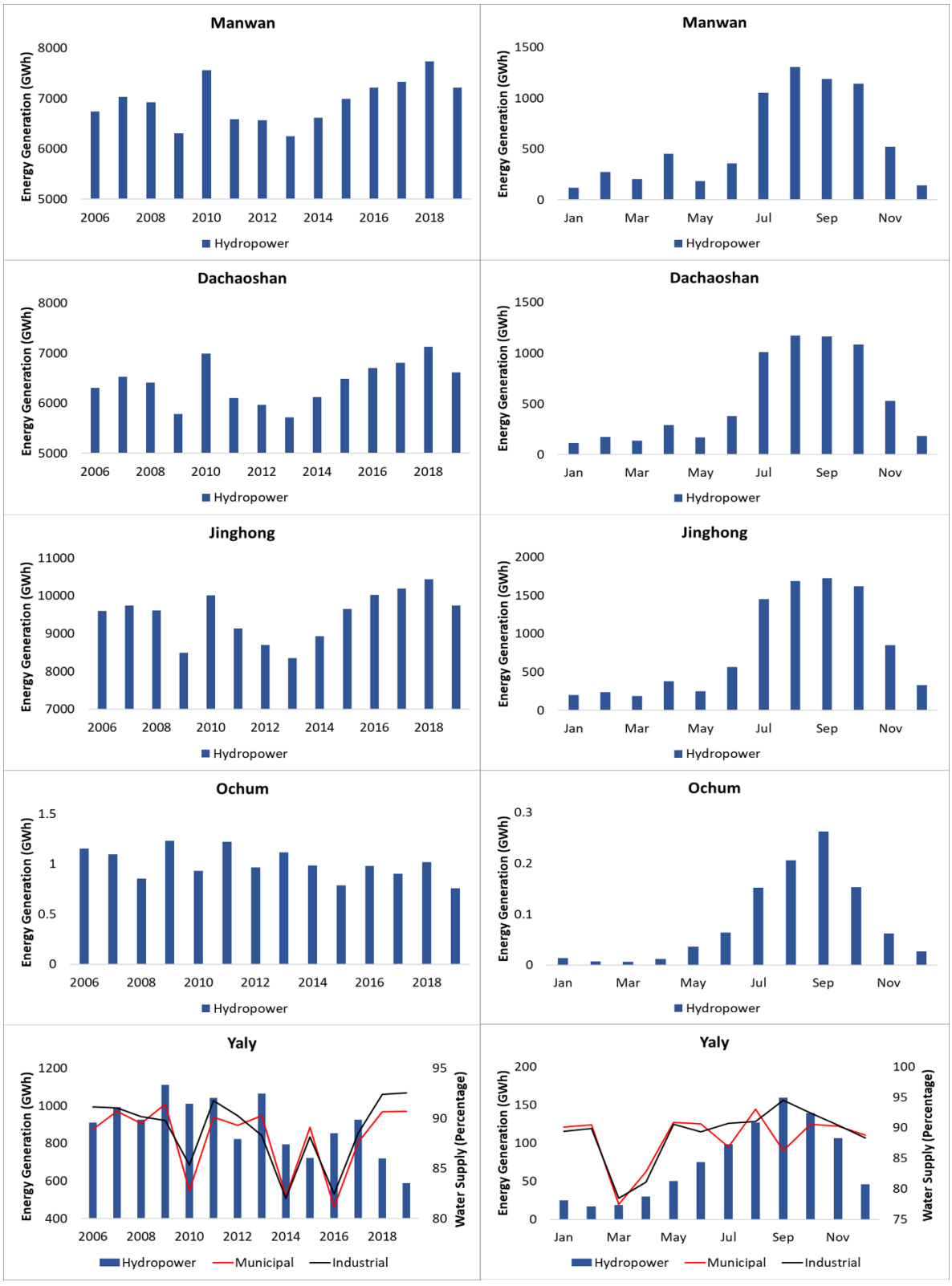


*Figure 3(c) continued*

### 5.3.3 Climate change

The impact of climate change on the operation of the reservoirs was reflected in the ability to fulfill the demands from the energy, irrigation, municipal and industrial sectors. The effects of the projected climate change were primarily governed by the inflow to the reservoirs under RCP 4.5 and RCP 8.5. The increase in the projected precipitation during the future period until 2099 enhanced the water availability to the reservoir to meet the demand from various sectors. Figure A1 shows the spatial variation of the precipitation and temperature in the Mekong River basin. The percentage change in the inflow ranges from +25% to +1.2% under RCP 4.5, while the change under RCP 8.5 is projected as -28.5% to -74.7%. However, the dams located in Thailand will experience a higher increase in the inflow under RCP 4.5 (12.9%), at the same time, Thailand dams will suffer the lowest decrease (55.6%) under extreme temperature conditions (RCP 8.5). Similar flow variations will be experienced by China dams with the average reduction in inflow as 52.4% under RCP 8.5, but the increase in the inflow will be averaged as 6% as compared to the historic inflows. Dams in Laos PDR, Cambodia, and Vietnam are projected to experience similar flow conditions under climate change with an average increase in inflows as 3.7% under RCP 4.5 and decrease as 31.7% under RCP 8.5. However, the elevated inflow due increase in the precipitation under RCP 4.5 is projected to be 10% more than the conditions under RCP 8.5. Simultaneously, the demands from the irrigation sector are also projected to increase on account of anticipated ascent in the evapotranspiration resulting from the temperature rise. Also, the water demand from the municipal and industrial sectors are forecasted to increase accounting for the urbanization and population growth of the developing regions of the Mekong river basin.

Figure 4(a) shows the projected monthly change in the energy generation (GWh), percentage of demand met of irrigation, municipal, and industrial sector from multipurpose dams due to climate change from 2021 to 2099 under RCP 4.5 and RCP 8.5 using four climate models. The hydropower energy generation of the multipurpose dams is projected to increase during the future period. Lam Phra Phloeng is projected to experience the highest increase in the energy generation with an increase of 80% under RCP 4.5 and 72% under RCP 8.5, followed by Lam Takhong with an increase of 56% under RCP 4.5 and 51% under RCP 8.5. Moreover, Sirindhorn, Ubol Ratana, Nam Pung, and Lam Chang are

projected to enhance the energy generation with an increase of 11% under RCP 4.5 and 10% under RCP 8.5. On the other hand, Chulabhorn is projected to produce 10% less energy during the future period under RCP 4.5 as compared to the observed energy production, and the decrease in the energy generation is forecasted as 15% under RCP 8.5. The efficiency of the reservoir in meeting the demands of the irrigation, municipal, and industrial sectors is also expected to enhance due to more availability of water in the future. The percentage of demand met by the supply from the reservoir will be similar for irrigation, municipal and industrial sectors. Nam Pung is projected to fulfill 32% more demand from the various sector under RCP45 as compared to the observed water supply. A similar increase in the water supply is expected from Lam Phra Phloeng with an increase of 21.4% under RCP45 and 19.6% under RCP 8.5. The marginal increase in the percentage of demand met from the Ubol Ratana, Lam Takhong, and Lam Chang Han in projected for the future period with a value of less than 10%. The demand met from the Sirindhorn and Chulabhorn is projected to decrease by 11% under RCP 4.5 and RCP 8.5 as compared to the observed period. The seasonal variation of the change in energy generation and water supply to the various sectors shows the marginal increase in energy generation while meeting water demand during the monsoon period. Moreover, the increase in demand after the monsoon season (November-December) is expected to be more than 20%, indicating the shift in the efficiency of the reservoirs in meeting the demands of the various sectors. Also, a shortage of water supply from the reservoir is expected to higher during February-April due to the projected rise in net irrigation water requirement.

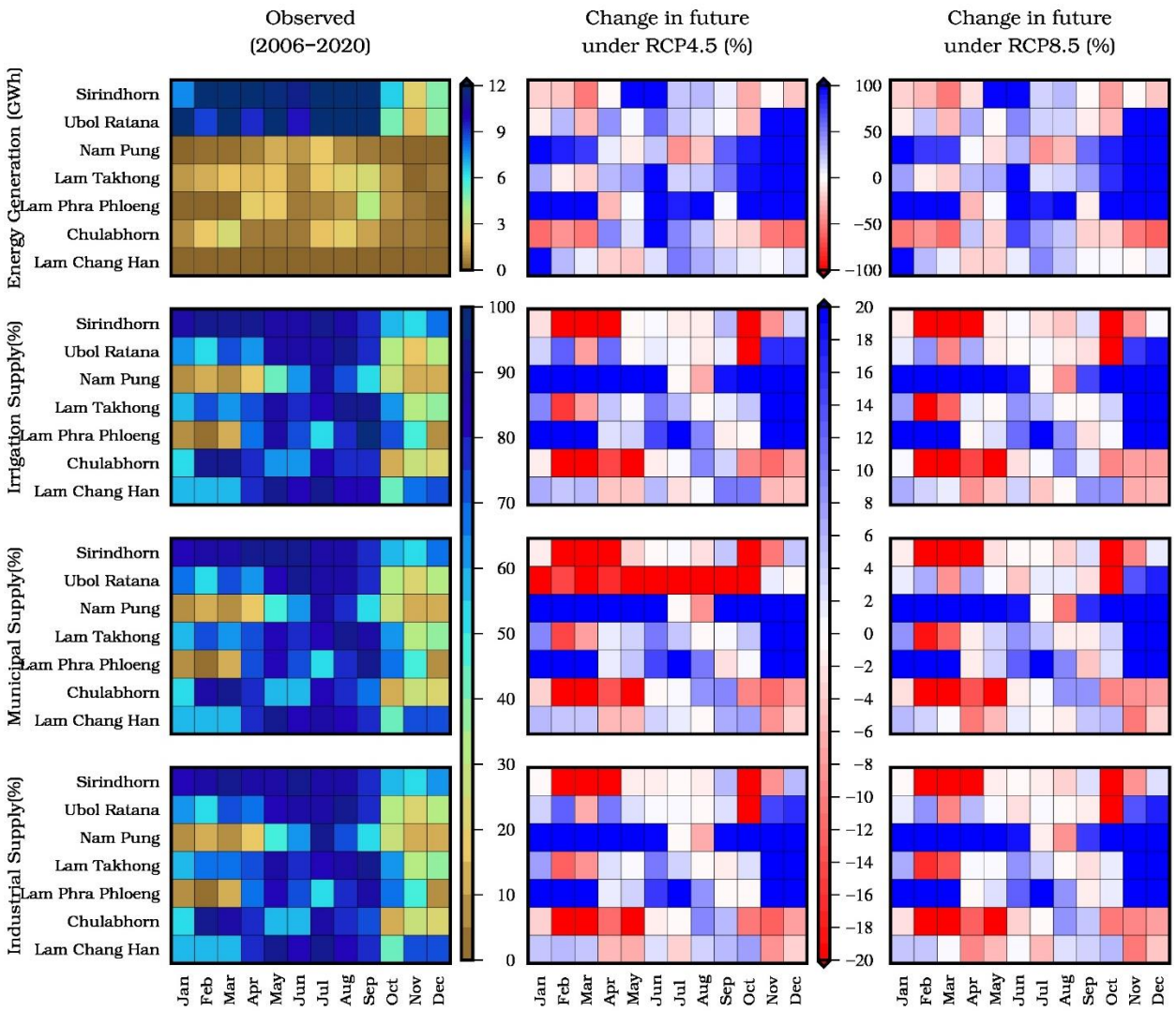


*Figure 4(a): Projected change in the energy generation (GWh), percentage of demand met from irrigation, municipal, and industrial sector from multipurpose dams due to climate change under RCP 4.5 and RCP 8.5 using four climate models from 2021-2099*

Climate change is expected to have a beneficial influence on the operation of the irrigation reservoirs commissioned for water supply to irrigation, municipal and industrial sectors of the basin. Figure 4(b) shows the projected monthly change in the percentage of demand met of irrigation, municipal, and industrial sectors from irrigation dams due to climate change from 2021 to 2099 under RCP 4.5 and RCP 8.5 using four climate models. All the irrigation reservoirs, except Huai Luang and Lam Plai Mas, are projected to meet the demand from the various sectors under RCP 4.5 and RCP 8.5. Lam Pao, Lam Nang Rong, and Lam Sae are projected to enhance the water demand fulfillment by more than 20%

from the irrigation, municipal and industrial sectors. Moreover, the increase in the demand fulfillment of various sectors from the Nam Un, and Upper Mun reservoir is forecasted to be less than 10%. On the other hand, Huai Luang and Lam Plai Mas are expected to meet less demand in the future period as compared to the demand met during the observed period. Cibihe and Haixihai are expected to fulfill more than 85% of the irrigation water demand as the reservoirs are commissioned only for the irrigation purpose. The variation of the degree of demand fulfillment for the future period is expected to be negative during February-April due to the projected increase in the irrigation water demand, while other months are expected to show a positive or marginal increase in the performance of the reservoirs to meet the demands. The monthly variation of the municipal and industrial demand met is similar to the irrigation supply as the major consumer of the water is the irrigation sector and drives the water supply for the other sectors.

Figure 4(c) shows the projected monthly change in the energy generation (GWh), percentage of demand met for municipal, and industrial sector from hydropower dams due to climate change from 2021 to 2099 under RCP 4.5 and RCP 8.5 using four climate models. The performance of the hydropower dams in the basin was appreciable as the water allocation to different sectors was relaxed. The annual energy generation of the Pakmun dam is expected to increase by more than 20% in the future as compared to energy production during the observed period. The projected increase in energy generation from Nam Ngum, Selabam, Theun-Hinboun, Nam Leuk, Nam Mang3, Ochum, and Dachaoshan dams were confined to less than 15%. However, the energy production of the Xeset1, Hoay-Ho, and Yaly dams are expected to decrease due to south-eastern Laos PDR and Cambodia regions are projected with the reduction in the flow. While Huai Kum is projected to keep producing the same energy quantity under RCP 4.5 as generated during the observed period, but the energy generation is expected to fall under RCP 8.5. The hydropower dams located in China are expected to show drastically contrasting behavior under different climate scenarios, i.e., RCP 4.5 and RCP 8.5. The annual energy generation of Xiaowan, Manwan, Dachaoshan, and Jinghong dams are forecasted to increase by 9% under RCP 4.5, however, the energy generated is expected to decrease by more than 15% under RCP 8.5 as compared to the observed period. The water demand fulfillment of the municipal and industrial sectors from the Yaly is also expected to decrease from 88% to

82% in the future. The monthly variation of the energy generation shows the favorable conditions during the monsoon season causing an increase in energy generation during July-October, however, some dams are expected to encounter decrease during February-April.

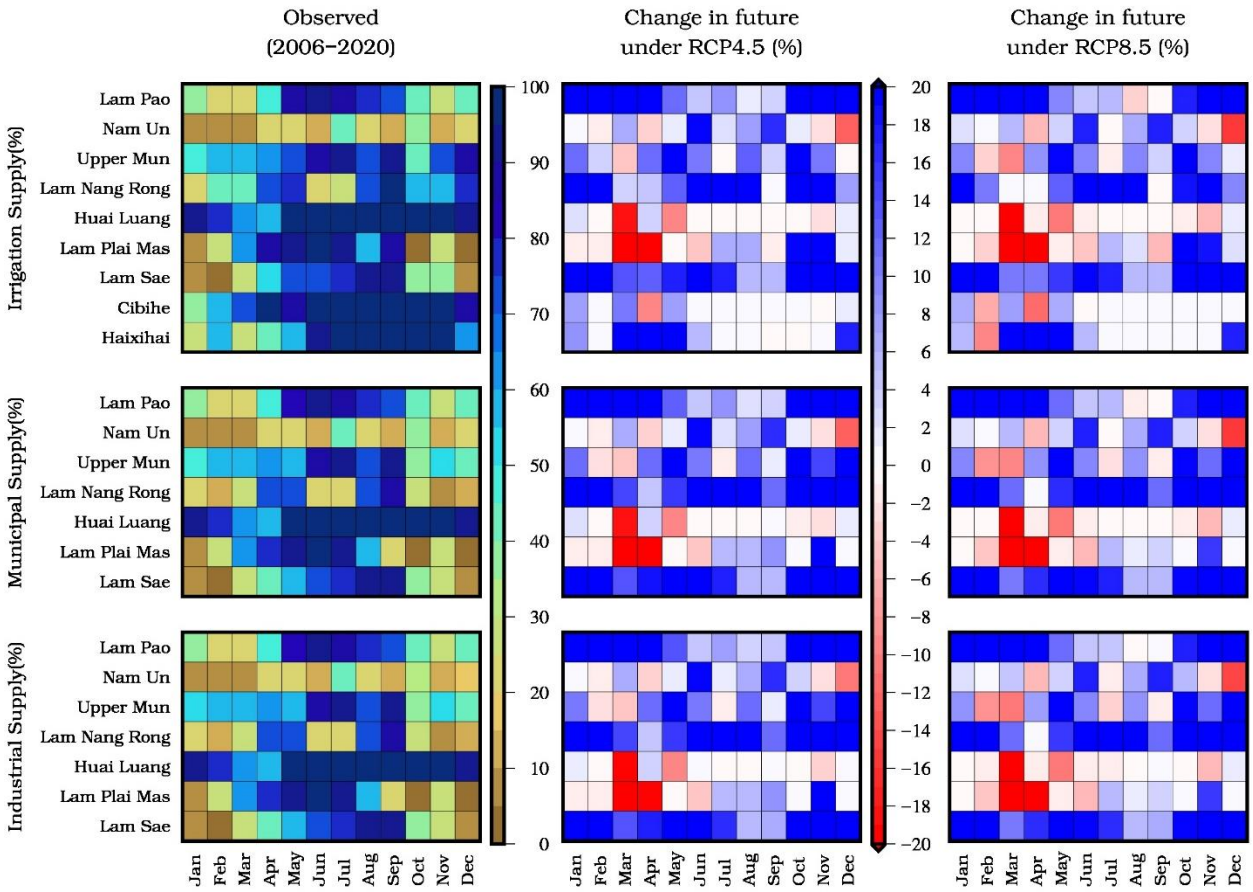


*Figure 4(b): Projected change in the percentage of demand met from irrigation, municipal, and industrial sector from irrigation dams due to climate change under RCP 4.5 and RCP 8.5 using four climate models from 2021-2099*

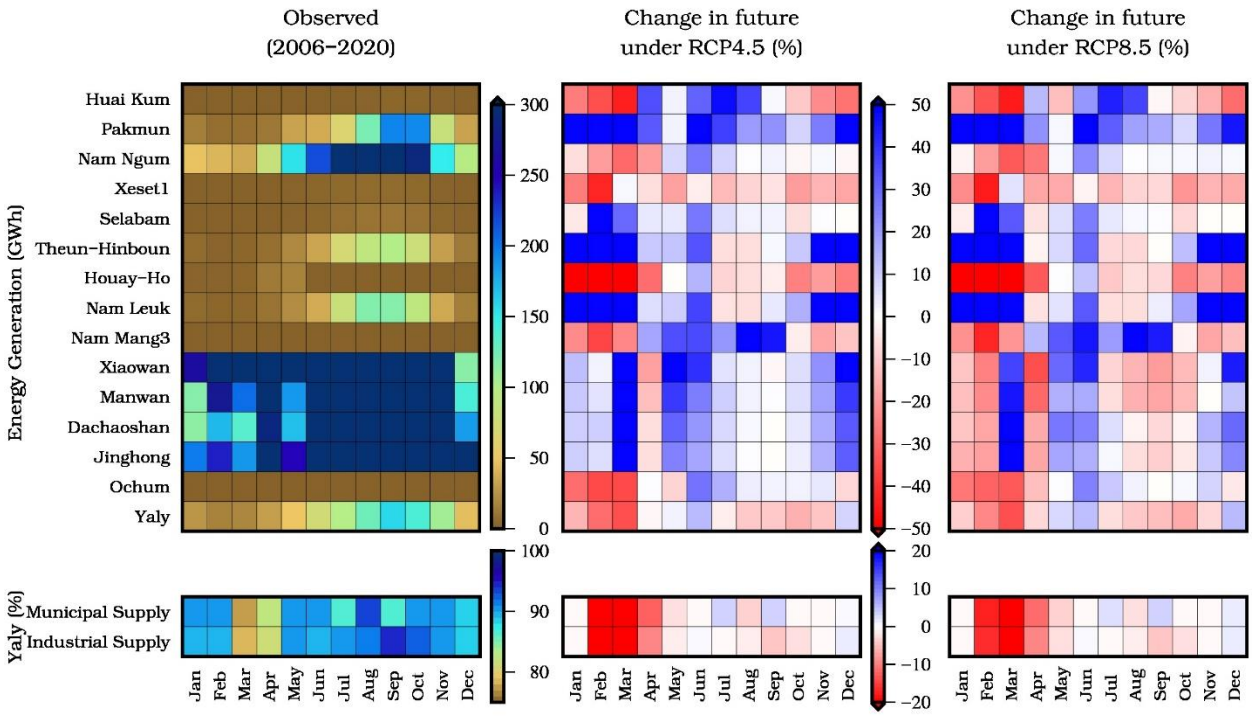


*Figure 4(c): Projected change in the energy generation (GWh), percentage of demand met from municipal, and industrial sector from hydropower dams due to climate change under RCP 4.5 and RCP 8.5 using four climate models from 2021-2099*

### 5.3.4 Extreme events stress

The stress index of the reservoir shows the biggest and persistent disturbance endured by the system while remaining functional during the historic and future periods. The disturbance faced by the system can be perceived as the stress introduced due to the occurrence of the extreme events and evaluated as the impact caused the event and the continuity of the occurrence. The impact was calculated as the fraction of the surplus volume during the flood event or deficit volume during the low flow event with the long-term average volume as the reference. A higher stress index value indicates that the particular dam has survived a bigger disturbance caused by the occurrence of a single or continuous series of extreme events. Figure 5 shows the stress index of the multipurpose, irrigation, and hydropower dams for flood and low flow events during the historic and future period under RCP 4.5 and RCP 8.5 using four climate models from 2051-2099. The stress index value ranges from 2.9 to 20 for flood and 1.5 to 5.5 for low flow events. The large range of the stress index for the flood event was due to the absence of the upper limit

for the flood volume, however, the minimum value for the low flow was confined by zero value.

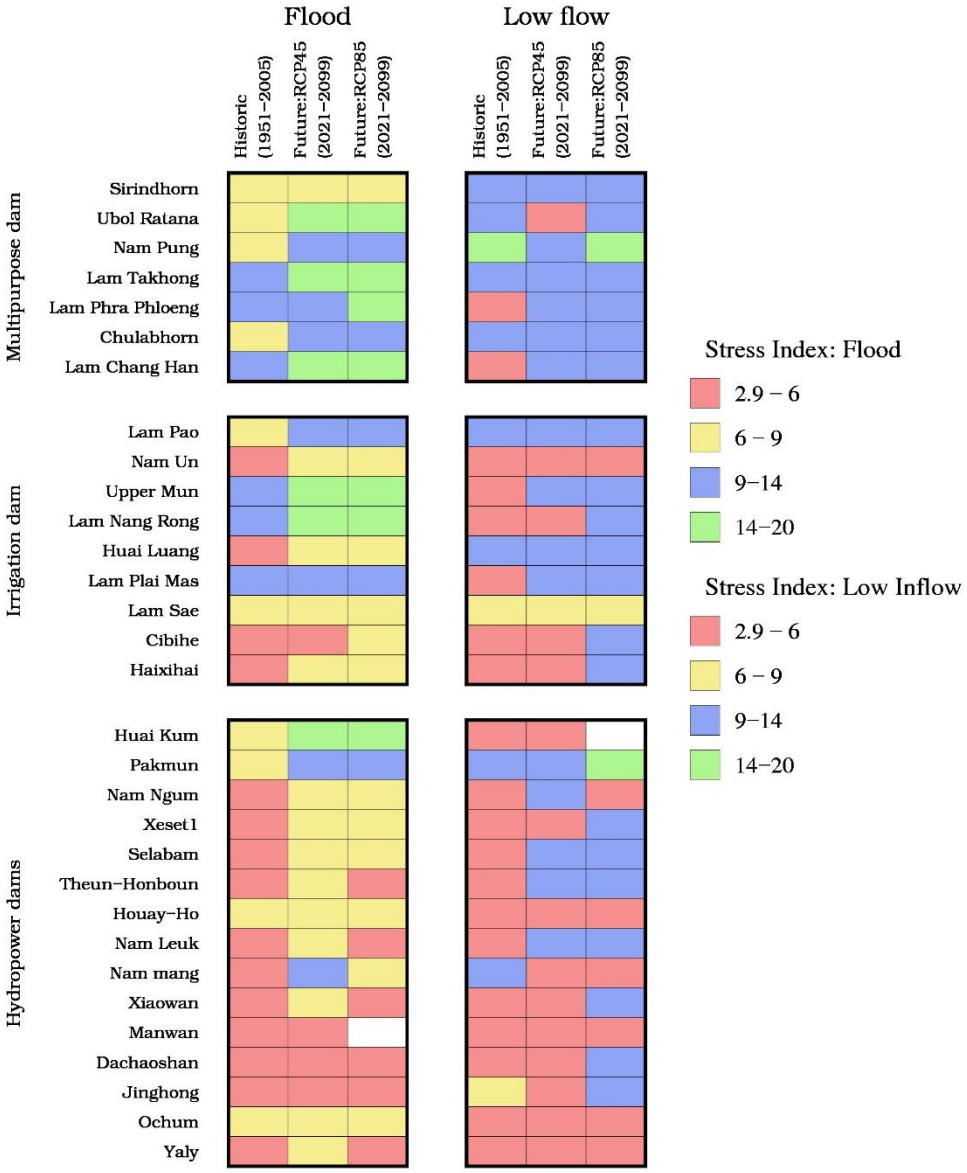


*Figure 5: Stress index of the multipurpose, irrigation and hydropower dams for flood and low flow events during the historic and future period under RCP 4.5 and RCP 8.5 using four climate models from 2051-2099*

During the historic period, most of the multipurpose reservoirs were classified as medium and high class based on the stress index value as the reservoir was operational with the survival of moderate flood events. On the other hand, the reservoirs were categorized into high and very high class based on the low flow events, except Lam Phra Phloeng and Lam Chang Han in the low class. All the reservoirs were projected to experience severe stress

with a high magnitude flood in the future. As the flood-based stress index is projected to increase, the class of the multipurpose reservoirs was shifted from medium to high or high to very high under RCP 4.5 and RCP 8.5. But the low flow stress class of the reservoir is projected to be marginally affected by climate change. Similarly, the irrigation reservoirs were classified as low and medium stress class as the historic flood was of less magnitude, except Upper Mun, Lam Nang Rong, and Lam Plai Mas. Moreover, the irrigation reservoirs experienced minimal disruption of the operation due to low inflow events and classified as low stress class, except Lam Pao, Huai Luang, and Lam Sae. As projected for the multipurpose dams, the impact of climate change is expected for the flood related stress classes with the transition of the class to the higher values for all the reservoirs except Lam Plai Mas. In contrast to the multipurpose dams, the low flow events in the future are projected to interrupt the reservoir operations, causing the upgradation of the stress class from low to high, especially under the RCP 8.5 scenario. Most of the hydropower dams experienced minor stress due to flood and low flow events during the historic period and falls under the low-stress class of flood and low flow events. For the future period, the stress index of the hydropower is projected to increase for both the flood and low flow events. The stress class of the hydropower dams for the flood events is expected to change from low to medium for the future period under RCP 4.5, while the leap in the low flow stress class is projected from low to high under RCP 8.5 due to dry conditions in the basin.

### 5.3.5 Shadow price

The shadow price of the water for energy, irrigation, municipal, and industrial sectors was estimated based on the fraction of the water demand met by the reservoirs for the future period. The available water from the reservoir was allocated to various sectors to fulfill the monthly water demand. But the non-availability of the required amounts of water resulted in the partial meeting the demand volumes. Hence, to enhance the productivity of a particular sector, the water can be purchased from other reservoirs or regions based on their water availability. The price for obtaining the water was dependent on the urgency of meeting the demands, especially where the demand met fraction was very low. Table 6 shows the shadow price of water for generating electricity or meeting water demand for irrigation, municipal, and industrial sectors in the future period. About 10 out of 22

hydropower commissioned dams including the multipurpose dams were projected to have ‘no binding constrains’ shadow price as the annual energy generation was found to be surplus. Also, 5 dams, namely, Sirindhorn, Ubol Ratana, Lam Phra Phloeng, Huai Kum, and Pak were located in Thailand, while Selabam and Nam Leuk were in Laos PDR and Dachaoshan and Jinghong were in China. On the other hand, the energy sector of Xeset1, Houay-Ho, and Nam Mang3 will have to pay an extremely high price for obtaining the last unit of water for producing electricity. Similarly, the shadow price of water for energy production will be very high for Chulabhorn in Thailand, Theun-Hinboun in Laos PDR, Ochum in Cambodia, and Yaly in Vietnam due to low projected energy generation in future. However, the efficacy of the Lam Chang Han, Xiaowan, and, Manwan dam in producing hydropower energy requires a fractional water volume at a very low price to meet the required demand. The shadow price of the water for the irrigation sector is expected to be low or very low for most of the dams commissioned for water irrigation water diversions. But Chulabhorn, Nam Un, and Lam Plai Mas will have to pay a high price for obtaining an additional unit of water to meet the net irrigation water demand as only 50% of the demand will be met by the dams. While the two irrigation dams in China, Cibihe and Haixihai, and Huai Luang in Thailand will barely require the water at a very low price to fulfill the water demand in the future. The remaining 10 out of 16 dams for irrigation purposes will have a low shadow price for food production in the future. Similar behavior as the irrigation sector is expected from the municipal and industrial sectors with most of the dams willing to pay a low or very low price to obtain an additional unit of water in the future to fulfill water demands. The region supplied by Chulabhorn, Nam Un, and Lam Plai Mas for the municipal and industrial purposes will have to bear a high price for water. The projected water demand met for these reservoirs will be less than 50% due to climate change and anthropogenic activities. While the shadow price of water to meet the demands of the municipal and industrial sectors will be low for the remaining 10 dams.

*Table 6: The shadow price of the water for energy, irrigation, municipal, and industrial sectors for the 31 dams in the Mekong River Basin*

| | Energy sector | | | Irrigation sector | | Municipal sector | | Industrial sector | |
|---|---|---|---|---|---|---|---|---|---|
| | **GWh** | **Demand met (%)** | **Shadow price** | **Demand met (%)** | **Shadow price** | **Demand met (%)** | **Shadow price** | **Demand met (%)** | **Shadow price** |
| **Multipurpose Dams** | | | | | | | | | |
| Sirindhorn | 144.2 | 160.2 | No binding | 68.6 | Low | 68.5 | Low | 68.6 | Low |
| Ubol Ratana | 149.9 | 262.9 | No binding | 65.2 | Low | 52.4 | High | 65.2 | Low |
| Nam Pung | 8.9 | 59.1 | High | 65.3 | Low | 65.4 | Low | 65.4 | Low |
| Lam Takhong | 27.6 | 6.9 | Extremely high | 74.1 | Low | 73.0 | Low | 72.9 | Low |
| Lam Phra Phloeng | 21.7 | 144.9 | No binding | 70.5 | Low | 69.0 | Low | 69.1 | Low |
| Chulabhorn | 12.7 | 21.5 | Very high | 50.6 | High | 49.1 | High | 49.1 | High |
| Lam Chang Han | 0.8 | 81.7 | Very low | 73.1 | Low | 71.6 | Low | 71.5 | Low |
| **Irrigation Dams** | | | | | | | | | |
| Lam Pao | | | | 75.7 | Low | 75.6 | Low | 75.0 | Low |
| Nam Un | | | | 22.0 | Very high | 21.9 | Very high | 21.7 | Very high |
| Upper Mun | | | | 78.1 | Low | 72.7 | Low | 72.4 | Low |
| Lam Nang Rong | | | | 76.7 | Low | 64.6 | Low | 64.5 | Low |
| Huai Luang | | | | 87.6 | Very low | 87.5 | Very low | 87.0 | Very low |
| Lam Plai Mas | | | | 52.5 | High | 45.6 | High | 45.4 | High |
| Lam Sae | | | | 75.1 | Low | 74.3 | Low | 73.9 | Low |
| Cibihe (Zibihe) | | | | 87.2 | Very low | | | | |
| Haixihai | | | | 84.0 | Very low | | | | |
| **Hydropower Dams** | | | | | | | | | |
| Huai Kum | 11.0 | 549.2 | No binding | | | | | | |
| Pakmun | 983.4 | 339.1 | No binding | | | | | | |
| Nam Ngum | 2379.7 | 275.1 | No binding | | | | | | |
| Xeset 1 | 24.7 | 16.0 | Extremely high | | | | | | |
| Selabam | 47.2 | 188.8 | No binding | | | | | | |
| Theun-Hinboun | 509.9 | 31.0 | Very high | | | | | | |
| Houay-Ho | 28.9 | 6.4 | Extremely high | | | | | | |
| Nam Leuk | 608.8 | 283.2 | No binding | | | | | | |

| | | | | | | | | | |
|---|---|---|---|---|---|---|---|---|---|
| Nam Mang 3 | 1.5 | 9.9 | Extremely high | | | | | | |
| Xiaowan | 14958.6 | 78.8 | Low | | | | | | |
| Manwan | 6946.3 | 89.2 | Very low | | | | | | |
| Dachaoshan | 6786.3 | 114.4 | No binding | | | | | | |
| Jinghong | 9829.5 | 125.1 | No binding | | | | | | |
| Ochum | 1.0 | 20.4 | Very high | | | | | | |
| Yaly | 825.2 | 22.6 | Very high | | | 82.9 | Very Low | 82.9 | Very Low |

The performance of the dams in meeting the demands and shadow price varied considerably between the reservoirs, but Chulabhorn, Lam Plai Mas, Nam Un, Xeset1, Houay-Ho, and Nam Mang3 will be the most suffering reservoirs with all the sectors dependent on these dams will have to pay a high price for fulfilling the demands. Although the shadow price of water for energy, irrigation, the municipal and industrial sectors was specific to the dams, the assessment at the country level was performed by grouping the dams based on the geographical locations. Table 7 shows the shadow price of the water for the member countries in the MRB to meet water demands for energy, irrigation, municipal and industrial sectors. The comparison of the shadow price over all the sectors was not attained as the distribution of the multipurpose, irrigation, and hydropower dams were not uniform over the basin. Also, the purpose of the dams confined the evaluation of the shadow price to the particular sectors, but the shadow price of water for the energy sector was determined for all the member countries in the basin. Thailand and Laos PDR are expected to be the most beneficial countries as the shadow price will not be bonded by constranits for the energy sector. Also, the irrigation, municipal, and industrial sectors will have to bear a low price for fulfilling the water requirements. Moreover, China will be able to satisfy the full water demand of the energy and irrigation sectors by paying a very low price for obtaining the last unit of available water. On the other hand, the energy sector of Cambodia and Vietnam will be struggling to meet the demand and will have to pay a large amount of money for obtaining additional water units, but the effect will be minimal for municipal and industrial sectors of Vietnam. But the shadow price for Cambodia and Vietnam was estimated based on one dam for each country, so the inclusion of more dams will provide more reliable economic analysis. The overall assessment of the shadow price

shows that the dam operation in Thailand, Laos PDR, and China will be sufficient to meet the water demands of the energy, irrigation, municipal, and industrial sectors. Cambodia and Vietnam will be dependent on other countries for meeting the water demand of the energy sector, otherwise other forms of energy production such as solar and thermal will have to be explored.

*Table 7: The shadow price of the water for energy, irrigation, municipal, and industrial sectors for the member countries in the Mekong River Basin*

| Country | Energy sector | | | Irrigation sector | | Municipal sector | | Industrial sector | |
|---|---|---|---|---|---|---|---|---|---|
| | GWh | Demand met (%) | Shadow price | Demand met (%) | Shadow price | Demand met (%) | Shadow price | Demand met (%) | Shadow price |
| Thailand | 1360.0 | 146.4 | No binding | 66.8 | Low | 63.7 | Low | 64.4 | Low |
| Laos PDR | 3600.8 | 106.9 | No binding | | | | | | |
| China | 38520.7 | 95.0 | Very low | 85.6 | Very low | | | | |
| Cambodia | 1.0 | 20.4 | Very high | | | | | | |
| Viet Nam | 825.2 | 22.6 | Very high | | | 82.9 | Very low | 82.9 | Very low |

### 5.3.6 Groundwater effect

The impact of the groundwater contribution to the streamflow was translated in fulfilling the water requirement of the different sectors by changing the inflow to the reservoirs. The streamflow during the non-monsoon season was increase by 60% due to the interaction of the surface and sub-surface water, accounting 80 $m^3$/sec. In order to simulate the condition continuously, the monsoon inflow was also increased by 80 $m^3$/sec. Figure 6 shows the change in the demand fulfillment of the energy, municipal, and industrial sectors from the Pakmun dam during observed period (2006-2019) due to contribution of the groundwater to the streamflow. The groundwater contributes towards a uniform increase in the energy generation by the Pakmun dam at annual and seasonal scale. The average increase in the energy generation was 18.7% for the observed period with the more than 100% increase during January-April. Similarly, the increase in the demand fulfillment of the municipal and industrial sector was 14.3% and 15.3%, respectively. The municipal and industrial demand fulfillment showed similar trend. The increase in the municipal and industrial supply ensured the demand satisfaction of 80% for each month in the observed period. The

highest increase in the municipal and industrial demand fulfillment is expected for December-April with value 20%-50%.

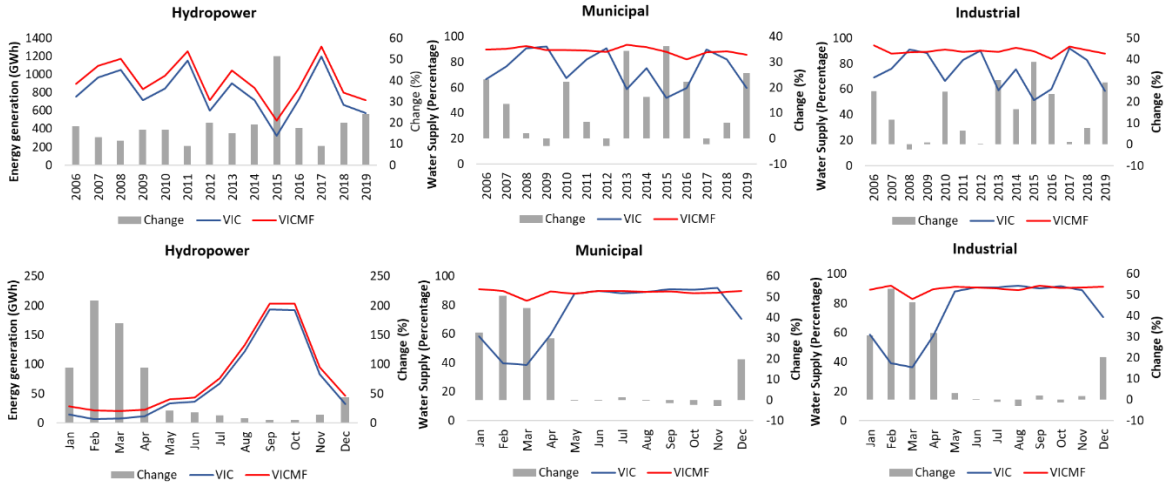


*Figure 6: Change in the demand fulfillment of the hydropower, municipal, and industrial sector from Pakmun dam due to groundwater contribution*

### 5.4 Conclusion

In this study, the system dynamics model comprising of more than 30 dams in the Mekong river basin was developed to simulate the operation of reservoirs in satisfying the water demand from the energy, irrigation, municipal, industrial, and ecological sectors. The model comprised of the multipurpose, irrigation, and hydropower dams incorporating the cascading effect of the upstream dams and feedback efforts. The operation of the reservoirs was optimized to meet the water demand of various sectors. The effect of the extreme events (flood and low flow) on reservoirs was included to analyze the stress resistance by the system. The major findings of the investigations are summarized below:

- The system dynamic model of the Mekong river basin was able to accurately simulate the operation of the multipurpose, hydropower, and irrigation reservoir with the Nash-Sutcliffe model efficiency coefficient (NSE) more than 0.6 and coefficient of correlation (r) more than 0.8 between the simulated and observed monthly storage. The model incorporates the cascading effect of the upstream dams, projected irrigation water demand in the future, and population growth under the influence of climate change.

- The multipurpose dams produced an annual energy generation of 316 GWh accounting 97% of the demand and satisfied more than 60% of the water demand from the irrigation, municipal, and industrial sectors during 2006-2019. Sirindhorn and Ubol Ratana dams are able to perform better than other reservoirs in generating surplus hydropower energy due to large storage capacity. Similar efficiency was observed for the irrigation supplying more than 60% of the irrigation water demand and 50% of the demand from municipal and industrial sectors. The hydropower dams produced 35% more energy than the desired quantity accounting for an annual generation of 2863 GWh while satisfying more than 80% of the water demand of the municipal and industrial sectors.
- Climate change has a positive influence on the performance of the multipurpose dams with an enhancement of 24% and 20% in the energy generation during 2021-2009 under RCP 4.5 and RCP 8.5, respectively, as compared to the observed period. In addition, the increase in the water demand met for the other sectors is projected to be 6% and 4% under RCP 4.5 and RCP 8.5, respectively. Likewise, the irrigation dams are expected to have improved demand met with an increase of 10% for the irrigation demand and 12% for the municipal and industrial water demands. The energy generation of the hydropower dams are forecasted to increase by 4% in the future under RCP 4.5 as compared to the observed period, however, the RCP 8.5 scenario will cause the dams to suffer a marginal decrease of 0.4%.
- The stress index shows the ability of the reservoirs to survive large disturbances in the system while remaining functional during the occurrence of flood and low flow events. The reservoirs were classified into four classes based on the stress index value defining the intensity of the flood and low flow events survived by the system. Most of the multipurpose dams are projected to shift from the medium or high class to medium or very high-stress class for the flood events in the future, on the other hand, the stress class for the low flow events remained as high for the observed and future period. However, the irrigation reservoirs fell under the low or high flood stress class and expected to move to medium or very high classes, while the low flow stress class to shift from low to high in the future. On the other hand, the flood stress class for the hydropower dams is expected to remain as low in the future under RCP 8.5 or change

to medium under RCP 4.5, while the shift is from low to high class for low flow stress under RCP 8.5 or remain as low under RCP 4.5.

- The shadow price of the water for energy, irrigation, municipal and industrial sectors was evaluated based on the percentage of the demand fulfillment by the reservoirs for the future period. At least, 10 out of 22 hydropower commissioned dams including the multipurpose dams are projected to have 'no binding constraints' shadow price as the annual energy generation will be surplus, while the shadow price will be extremely high for four dams. The shadow price is projected to be low or very low for the irrigation, municipal and industrial sectors. Chulabhorn, Lam Plai Mas, Nam Un, Xeset1, Houay-Ho, and Nam Mang3 will be the most suffering reservoirs with all the sectors dependent on these dams will have to pay a high price for fulfilling the demands. The overall assessment of the shadow price shows that the dam operation in Thailand, Laos PDR, and China will be sufficient to meet the water demands of the energy, irrigation, municipal, and industrial sectors. But the energy sector of Cambodia and the Vietnam region will have to pay a high price for obtaining additional units of water for generating electricity.

**Reference for Chapter 5**


Adamson, P. T., Rutherfurd, I. D., Peel, M. C., & Conlan, I. A. (2009). The Hydrology of the Mekong River. In *The Mekong* (pp. 53–76). Elsevier. https://doi.org/10.1016/B978-0-12-374026-7.00004-8

Affeltranger, B. (2009a). Mekong Studies at Crossed Glances. In *4th French-MFU Seminar*. Chiang Rai, Thailand. Retrieved from https://www.ggr.ulaval.ca/sites/default/files/documents/Lasserre/Publications/actes_lasserre-affeltranger_irasec-mfu_2009.pdf

Affeltranger, B. (2009b). Sustainability of Environmental Regimes: The Mekong River Commission (pp. 593–601). Springer, Berlin, Heidelberg. https://doi.org/10.1007/978-3-540-68488-6_43

Agriculture and fishing | Open Development Mekong. (2019). Retrieved August 15, 2020, from https://opendevelopmentmekong.net/topics/agriculture-and-fishing/

Akter, A., & Babel, M. S. (2012). Hydrological modeling of the Mun River basin in Thailand. *Journal of Hydrology*, *452–453*, 232–246. https://doi.org/10.1016/J.JHYDROL.2012.05.059

Al-Ruzouq, R., Shanableh, A., Merabtene, T., Siddique, M., Khalil, M. A., Idris, A., & Almulla, E. (2019). Potential groundwater zone mapping based on geo-hydrological considerations and multi-criteria spatial analysis: North UAE. *CATENA*, *173*, 511–524. https://doi.org/10.1016/J.CATENA.2018.10.037

Alaouze, C. (1996). Shadow Prices in Linear Programming Problems. *Papers*.

Ali, Syed A., & Sridhar, V. (2019). Deriving the Reservoir Conditions for Better Water Resource Management Using Satellite-Based Earth Observations in the Lower Mekong River Basin. *Remote Sensing*, *11*(23), 2872. https://doi.org/10.3390/rs11232872

Ali, Syed Azhar, Aadhar, S., Shah, H. L., & Mishra, V. (2018). Projected Increase in Hydropower Production in India under Climate Change. *Scientific Reports*, *8*(1), 12450. https://doi.org/10.1038/s41598-018-30489-4

Aliagha, C. (2004). Environmental Clearinghouse as an Institutional Incentive for Data and Information Sharing and Conflict Reuction in the Mekong River Basin. In *OpenSIUC* (pp. 7–20). Southern Illinois University, Carbondale, Illinois. Retrieved from http://opensiuc.lib.siu.edu/ucowrconfs_2004/2

Allen, R., Pereira, L., Raes, D., & Smith, M. (1998). Crop evapotranspiration-Guidelines for computing crop water requirements-FAO Irrigation and drainage paper 56. *FAO Irrigation and Drainage Paper No. 56.* Retrieved from https://www.researchgate.net/profile/Hawre_Kiani/post/What_is_the_more_effective_way_of_deficit_irrigation/attachment/5af42706b53d2f63c3cafa73/AS%3A624694629777415%401525950214858/download/Allen_FAO1998.pdf

AQUASTAT. (2014). Irrigation water requirement and water withdrawals by country. Retrieved January 11, 2019, from http://www.fao.org/nr/water/aquastat/main/index.stm

Awawdeh, M., Obeidat, M., Al-Mohammad, M., Al-Qudah, K., & Jaradat, R. (2014). Integrated GIS and remote sensing for mapping groundwater potentiality in the Tulul al Ashaqif, Northeast Jordan. *Arabian Journal of Geosciences*, *7*(6), 2377–2392. https://doi.org/10.1007/s12517-013-0964-8

Bastakoti, R. C., Gupta, J., Babel, M. S., & van Dijk, M. P. (2014). Climate risks and

adaptation strategies in the Lower Mekong River basin. *Regional Environmental Change*, *14*(1), 207–219. https://doi.org/10.1007/s10113-013-0485-8

Becker, M., Papa, F., Frappart, F., Alsdorf, D., Calmant, S., da Silva, J. S., et al. (2018). Satellite-based estimates of surface water dynamics in the Congo River Basin. *International Journal of Applied Earth Observation and Geoinformation*, *66*, 196–209. https://doi.org/10.1016/J.JAG.2017.11.015

Birkett, C., Reynolds, C., Beckley, B., & Doorn, B. (2011). From Research to Operations: The USDA Global Reservoir and Lake Monitor. In *Coastal Altimetry* (pp. 19–50). Berlin, Heidelberg: Springer. https://doi.org/10.1007/978-3-642-12796-0_2

Bonnema, M., & Hossain, F. (2017). Inferring reservoir operating patterns across the Mekong Basin using only space observations. *Water Resources Research*, *53*(5), 3791–3810. https://doi.org/10.1002/2016WR019978

Bosch, J. M., & Hewlett, J. D. (1982). *A REVIEW OF CATCHMENT EXPERIMENTS TO DETERMINE THE EFFECT OF VEGETATION CHANGES ON WATER YIELD AND EVAPOTRANSPIRATION*. *Journal of Hydrology* (Vol. 55). Retrieved from http://coweeta.uga.edu/publications/2117.pdf

Boucher, O., Myhre, G., & Myhre, A. (2004). Direct human influence of irrigation on atmospheric water vapour and climate. *Climate Dynamics*, *22*(6–7), 597–603. https://doi.org/10.1007/s00382-004-0402-4

Box, M. J. (1965). A new method of constrained optimization and a comparison with other methods. *The Computer Journal*, *8*(1), 42–52. https://doi.org/10.1093/COMJNL/8.1.42

Brito, M. G., Costa, C. N., Almeida, J. A., Vendas, D., & Verdial, P. H. (2006). Characterization of maximum infiltration areas using GIS tools. *Engineering Geology*, *85*(1–2), 14–18. https://doi.org/10.1016/J.ENGGEO.2005.09.022

Browder, G., & Ortolano, L. (2000). *The Evolution of an International Water Resources Management Regime in the Mekong*. *Source: Natural Resources Journal* (Vol. 40). Retrieved from https://www.jstor.org/stable/pdf/24888536.pdf?refreqid=excelsior%3Af1fd62acc9ba6474184989cb5355f678

Cao, Q., Yu, D., Georgescu, M., Han, Z., & Wu, J. (2015). Impacts of land use and land cover change on regional climate: a case study in the agro-pastoral transitional zone of China. *Environmental Research Letters*, *10*(12), 124025. https://doi.org/10.1088/1748-9326/10/12/124025

Carruthers, I., Rosegrant, M. W., & Seckler, D. (1997). Irrigation and food security in the 21st century. *Irrigation and Drainage Systems*, *11*(2), 83–101. https://doi.org/10.1023/A:1005751232728

Chang, F.-J., Chen, L., & Chang, L.-C. (2005). Optimizing the reservoir operating rule curves by genetic algorithms. *Hydrological Processes*, *19*(11), 2277–2289. https://doi.org/10.1002/hyp.5674

Chapman, A., & Darby, S. (2016). Evaluating sustainable adaptation strategies for vulnerable mega-deltas using system dynamics modelling: Rice agriculture in the Mekong Delta's An Giang Province, Vietnam. *Science of the Total Environment*, *559*, 326–338. https://doi.org/10.1016/j.scitotenv.2016.02.162

Chase, T. N., Pielke Sr, R. A., F Kittel, T. G., Baron, J. S., & Stohlgren, T. J. (1999). *Potential impacts on Colorado Rocky Mountain weather due to land use changes on*

*the adjacent Great Plains*. *JOURNAL OF GEOPHYSICAL RESEARCH* (Vol. 104). https://doi.org/10.1029/1999JD900118

Chen, C.-J., Jayasekera, D. L., & Senarath, S. U. S. (2015). Assessing Uncertainty in Precipitation and Hydrological Modeling in the Mekong. In *World Environmental and Water Resources Congress 2015* (pp. 2510–2519). Reston, VA: American Society of Civil Engineers. https://doi.org/10.1061/9780784479162.246

Claverie, M., Ju, J., Masek, J. G., Dungan, J. L., Vermote, E. F., Roger, J. C., et al. (2018). The Harmonized Landsat and Sentinel-2 surface reflectance data set. *Remote Sensing of Environment*, *219*, 145–161. https://doi.org/10.1016/j.rse.2018.09.002

Cleugh, H. A., Leuning, R., Mu, Q., & Running, S. W. (2007). Regional evaporation estimates from flux tower and MODIS satellite data. *Remote Sensing of Environment*, *106*(3), 285–304. https://doi.org/10.1016/j.rse.2006.07.007

Conway, D., Van Garderen, E. A., Deryng, D., Dorling, S., Krueger, T., Landman, W., et al. (2015, August 21). Climate and southern Africa's water-energy-food nexus. *Nature Climate Change*. Nature Publishing Group. https://doi.org/10.1038/nclimate2735

Cosby, B. J., Hornberger, G. M., Clapp, R. B., & Ginn, T. R. (1984). A Statistical Exploration of the Relationships of Soil Moisture Characteristics to the Physical Properties of Soils. *Water Resources Research*, *20*(6), 682–690. https://doi.org/10.1029/WR020i006p00682

Costa-Cabral, M. C., Richey, J. E., Goteti, G., Lettenmaier, D. P., Feldkötter, C., & Snidvongs, A. (2008a). Landscape structure and use, climate, and water movement in the Mekong River basin. *Hydrological Processes*, *22*(12), 1731–1746. https://doi.org/10.1002/hyp.6740

Costa-Cabral, M. C., Richey, J. E., Goteti, G., Lettenmaier, D. P., Feldkötter, C., & Snidvongs, A. (2008b). Landscape structure and use, climate, and water movement in the Mekong River basin. *Hydrological Processes*, *22*(12), 1731–1746. https://doi.org/10.1002/hyp.6740

Crétaux, J.-F., Jelinski, W., Calmant, S., Kouraev, A., Vuglinski, V., Bergé-Nguyen, M., et al. (2011). SOLS: A lake database to monitor in the Near Real Time water level and storage variations from remote sensing data. *Advances in Space Research*, *47*(9), 1497–1507. https://doi.org/10.1016/J.ASR.2011.01.004

Dar, I. A., Sankar, K., & Dar, M. A. (2010). Remote sensing technology and geographic information system modeling: An integrated approach towards the mapping of groundwater potential zones in Hardrock terrain, Mamundiyar basin. *Journal of Hydrology*, *394*(3), 285–295. https://doi.org/10.1016/j.jhydrol.2010.08.022

Delgado, J. M., Merz, B., & Apel, H. (2012). A climate-flood link for the lower Mekong River. *Hydrology and Earth System Sciences*, *16*(5), 1533–1541. https://doi.org/10.5194/hess-16-1533-2012

Deligios, P. A., Chergia, A. P., Sanna, G., Solinas, S., Todde, G., Narvarte, L., & Ledda, L. (2019). Climate change adaptation and water saving by innovative irrigation management applied on open field globe artichoke. *Science of the Total Environment*, *649*, 461–472. https://doi.org/10.1016/j.scitotenv.2018.08.349

Dinar, A., & Letey, J. (1991). Agricultural water marketing, allocative efficiency, and drainage reduction. *Journal of Environmental Economics and Management*, *20*(3), 210–223. https://doi.org/10.1016/0095-0696(91)90009-8

Dore, John, Xiaogang Yu, and K. Y. L. (2007). China's energy reforms and hydropower expansion in Yunnan. *Democratizing Water Governance in the Mekong Region. Mekong Press*.

Duan, Z., & Bastiaanssen, W. G. M. (2013). Estimating water volume variations in lakes and reservoirs from four operational satellite altimetry databases and satellite imagery data. *Remote Sensing of Environment*, *134*, 403–416. https://doi.org/10.1016/J.RSE.2013.03.010

Eastham, J., Mpelasoka, F., Mainuddin, M., Ticehurst, C., Dyce, P., Hodgson, G., et al. (2008). Mekong River Basin water resources assessment: impacts of climate change. CSIRO: Water for a Healthy Country National Research Flagship. Retrieved from http://www.clw.csiro.au/publications/waterforahealthycountry/2008/wfhc-MekongWaterResourcesAssessment.pdf

Edet, A. E., Okereke, C. S., Teme, S. C., & Esu, E. O. (1998). Application of remote-sensing data to groundwater exploration: A case study of the Cross River State, southeastern Nigeria. *Hydrogeology Journal*, *6*(3), 394–404. https://doi.org/10.1007/s100400050162

Erban, L. E., Gorelick, S. M., & Zebker, H. A. (2014). Groundwater extraction, land subsidence, and sea-level rise in the Mekong Delta, Vietnam. *Environmental Research Letters*, *9*(8), 084010. https://doi.org/10.1088/1748-9326/9/8/084010

Fallah-Mehdipour, E., Bozorg Haddad, O., & Mariño, M. A. (2013). Extraction of Optimal Operation Rules in an Aquifer-Dam System: Genetic Programming Approach. *Journal of Irrigation and Drainage Engineering*, *139*(10), 872–879. https://doi.org/10.1061/(ASCE)IR.1943-4774.0000628

Feng, J.-M., Wang, Y.-L., Ma, Z.-G., & Liu, Y.-H. (2012). Simulating the Regional Impacts of Urbanization and Anthropogenic Heat Release on Climate across China. *Journal of Climate*, *25*(20), 7187–7203. https://doi.org/10.1175/JCLI-D-11-00333.1

Feng, M., Liu, P., Li, Z., Zhang, J., Liu, D., & Xiong, L. (2016). Modeling the nexus across water supply, power generation and environment systems using the system dynamics approach: Hehuang Region, China. *Journal of Hydrology*, *543*, 344–359. https://doi.org/10.1016/j.jhydrol.2016.10.011

Fischer, G., Tubiello, F. N., van Velthuizen, H., & Wiberg, D. A. (2007). Climate change impacts on irrigation water requirements: Effects of mitigation, 1990–2080. *Technological Forecasting and Social Change*, *74*(7), 1083–1107. https://doi.org/10.1016/J.TECHFORE.2006.05.021

Franchini, M., & Pacciani, M. (1991). Comparative analysis of several conceptual rainfall-runoff models. *Journal of Hydrology*, *122*(1–4), 161–219. https://doi.org/10.1016/0022-1694(91)90178-K

Fu, L.-L., & Cazenave, A. (2001). *Satellite altimetry and earth sciences : a handbook of techniques and applications*. Academic.

Ganapuram, S., Kumar, G. T. V., Krishna, I. V. M., Kahya, E., & Demirel, M. C. (2009). Mapping of groundwater potential zones in the Musi basin using remote sensing data and GIS. *Advances in Engineering Software*, *40*(7), 506–518. https://doi.org/10.1016/J.ADVENGSOFT.2008.10.001

Gao, B. (1996). NDWI—A normalized difference water index for remote sensing of vegetation liquid water from space. *Remote Sensing of Environment*, *58*(3), 257–266. https://doi.org/10.1016/S0034-4257(96)00067-3

Gao, H., Birkett, C., & Lettenmaier, D. P. (2012). Global monitoring of large reservoir storage from satellite remote sensing. *Water Resources Research*, *48*(9). https://doi.org/10.1029/2012WR012063

Gerlak, A. K., Lautze, J., & Giordano, M. (2011). Water resources data and information exchange in transboundary water treaties. *International Environmental Agreements: Politics, Law and Economics*, *11*(2), 179–199. https://doi.org/10.1007/s10784-010-9144-4

Gleeson, T., Wada, Y., Bierkens, M. F. P., & van Beek, L. P. H. (2012). Water balance of global aquifers revealed by groundwater footprint. *Nature*, *488*(7410), 197–200. https://doi.org/10.1038/nature11295

Goteti, G., & Lettenmaier, D. P. (2001). *Effects of streamflow regulation and land cover change on the hydrology of the Mekong river basin*. University of Washington. Retrieved from https://www.ce.washington.edu/sites/cee/files/pdfs/research/hydrology/water-resources/WRS169.pdf

Grumbine, R. E., & Xu, J. (2011). Mekong Hydropower Development. *Science*, *332*(6026), 178–179. https://doi.org/10.1126/science.1200990

Guo, H., Bao, A., Liu, T., Ndayisaba, F., He, D., Kurban, A., et al. (2017). Meteorological Drought Analysis in the Lower Mekong Basin Using Satellite-Based Long-Term CHIRPS Product. *Sustainability*, *9*(6), 901. https://doi.org/10.3390/su9060901

Habibi Davijani, M., Banihabib, M. E., Nadjafzadeh Anvar, A., & Hashemi, S. R. (2016). Multi-Objective Optimization Model for the Allocation of Water Resources in Arid Regions Based on the Maximization of Socioeconomic Efficiency. *Water Resources Management*, *30*(3), 927–946. https://doi.org/10.1007/s11269-015-1200-y

Haddeland, I., Skaugen, T., & Lettenmaier, D. P. (2006). Anthropogenic impacts on continental surface water fluxes. *Geophysical Research Letters*, *33*(8), L08406. https://doi.org/10.1029/2006GL026047

Haddeland, I., Lettenmaier, D. P., & Skaugen, T. (2006). Effects of irrigation on the water and energy balances of the Colorado and Mekong river basins. *Journal of Hydrology*, *324*(1–4), 210–223. https://doi.org/10.1016/j.jhydrol.2005.09.028

Hanasaki, N., Kanae, S., & Oki, T. (2006). A reservoir operation scheme for global river routing models. *Journal of Hydrology*, *327*(1–2), 22–41. https://doi.org/10.1016/j.jhydrol.2005.11.011

Hanim, F., & Rahim, A. (2017). *Supply and Demand of Rice in Malaysia: A System Dynamics Approach*. *International Journal of Supply Chain Management* (Vol. 6). Retrieved from http://excelingtech.co.uk/

Hapuarachchi, H. A. P., Takeuchi, K., Zhou, M., Kiem, A. S., Georgievski, M., Magome, J., & Ishidaira, H. (2008). Investigation of the Mekong River basin hydrology for 1980–2000 using the YHyM. *Hydrological Processes*, *22*(9), 1246–1256. https://doi.org/10.1002/hyp.6934

Harbaugh, A. W. (2005). *MODFLOW-2005, The U.S. Geological Survey Modular Ground-Water Model-the Ground-Water Flow Process*. Retrieved from http://water.usgs.gov/software/ground_water.html/.

Heinimann, A., Messerli, P., Schmidt-Vogt, D., & Wiesmann, U. (2007). The Dynamics of Secondary Forest Landscapes in the Lower Mekong Basin. *Mountain Research and Development*, *27*(3), 232–241. https://doi.org/10.1659/mrd.0875

Hempel, S., Frieler, K., Warszawski, L., Schewe, J., & Piontek, F. (2013). A trend-preserving bias correction – the ISI-MIP approach. *Earth System Dynamics*, *4*(2), 219–236. https://doi.org/10.5194/esd-4-219-2013

Henriksen, H. J., Troldborg, L., Højberg, A. L., & Refsgaard, J. C. (2008). Assessment of exploitable groundwater resources of Denmark by use of ensemble resource indicators and a numerical groundwater–surface water model. *Journal of Hydrology*, *348*(1–2), 224–240. https://doi.org/10.1016/J.JHYDROL.2007.09.056

Heywood, I., Corneluis, S., & Carver, S. (2003). An introduction to geographic information systems, 1st Indian Ed. Retrieved from https://scholar.google.com/scholar?hl=en&as_sdt=0%2C47&q=Heywood+I%2C+Corneluis+S%2C+Carver+S+%282003%29+An+introduction+to+geographic+information+systems%2C+1st+Indian+Ed.+Pearson+Education%2C+Delhi&btnG=

Hibbert, A. R. (1983). WATER YIELD IMPROVEMENT POTENTIAL BY VEGETATION MANAGEMENT ON WESTERN RANGELANDS. *Journal of the American Water Resources Association*, *19*(3), 375–381. https://doi.org/10.1111/j.1752-1688.1983.tb04594.x

Hoang, L. P., Lauri, H., Kummu, M., Koponen, J., van Vliet, M. T. H., Supit, I., et al. (2016). Mekong River flow and hydrological extremes under climate change. *Hydrology and Earth System Sciences*, *20*(7), 3027–3041. https://doi.org/10.5194/hess-20-3027-2016

Hoanh, C. T., Guttman, H., Droogers, P., & Aerts, J. (2004). Will we produce sufficient food under climate change?: Mekong Basin (South-east Asia). Retrieved from https://cgspace.cgiar.org/handle/10568/37433

Hoanh, C. T., Jirayoot, K., Lacombe, G., Srinetr, V., Hoanh, C. T., Jirayoot, K., et al. (2010). Impacts of climate change and development on Mekong flow regimes. First assessment - 2009. Retrieved from https://econpapers.repec.org/paper/iwtrerpts/h043262.htm

Hoekema, D. J., & Sridhar, V. (2013a). A System Dynamics Model for Conjunctive Management of Water Resources in the Snake River Basin. *JAWRA Journal of the American Water Resources Association*, *49*(6), 1327–1350. https://doi.org/10.1111/jawr.12092

Hoekema, D. J., & Sridhar, V. (2013b). A System Dynamics Model for Conjunctive Management of Water Resources in the Snake River Basin. *JAWRA Journal of the American Water Resources Association*, *49*(6), 1327–1350. https://doi.org/10.1111/jawr.12092

Homdee, T., Pongput, K., & Kanae, S. (2011). Impacts of Land Cover Changes on Hydrologic Responses: A Case Study of Chi River Basin, Thailand. *Journal of Japan Society of Civil Engineers, Ser. B1 (Hydraulic Engineering)*, *67*(4), I_31-I_36. https://doi.org/10.2208/jscejhe.67.I_31

Hook, J., Novak, S., & Johnston, R. (2003). Social Atlas of the Lower Mekong Basin. In *Mekong River Commission* (pp. 1727–1800). Phnom Penh.

Hossain, F., & Katiyar, N. (2006). Improving flood forecasting in international river basins. *Eos, Transactions American Geophysical Union*, *87*(5), 49. https://doi.org/10.1029/2006EO050001

Huffman, G., Adler, R., Stocker, E., Bolvin, D., & Nelkin, E. (2003). Analysis of TRMM 3-hourly multi-satellite precipitation estimates computed in both real and post-real

time. In *12th Conf. on Satellite Meteorology and Oceanography* (pp. 4–11). Long Beach, CA: Amer. Meteor. Soc., CD-ROM. Retrieved from https://ntrs.nasa.gov/search.jsp?R=20040026654

Huffman, G. J., Adler, R. F., Morrissey, M. M., Bolvin, D. T., Curtis, S., Joyce, R., et al. (2001). Global Precipitation at One-Degree Daily Resolution from Multisatellite Observations. *Journal of Hydrometeorology*, *2*(1), 36–50. https://doi.org/10.1175/1525-7541(2001)002<0036:GPAODD>2.0.CO;2

Intralawan, A., Wood, D., & Frankel, R. (2017). *Economic Evaluation of Hydropower Projects in the Lower Mekong Basin*. Retrieved from http://www.mrcmekong.org/assets/Uploads/Final-report-Mekong-Study-March-2017-8.pdf

Ioslovich, I., & Gutman, P. O. (2001). A model for the global optimization of water prices and usage for the case of spatially distributed sources and consumers. *Mathematics and Computers in Simulation*, *56*(4–5), 347–356. https://doi.org/10.1016/S0378-4754(01)00306-8

Jackson, R. B., Carpenter, S. R., Dahm, C. N., McKnight, D. M., Naiman, R. J., Postel, S. L., & Running, S. W. (2001). WATER IN A CHANGING WORLD. *Ecological Applications*, *11*(4), 1027–1045. https://doi.org/10.1890/1051-0761(2001)011[1027:WIACW]2.0.CO;2@10.1002/(ISSN)1939-5582(CAT)SPECIALCOLLECTION(VI)VIRTUALISSUE

Jain, P. K. (1998). Remote sensing techniques to locate ground water potential zones in upper Urmil River Basin, district Chhatarpur — Central India. *Journal of the Indian Society of Remote Sensing*, *26*(3), 135–147. https://doi.org/10.1007/BF03026671

Jaksa, W. T., & Sridhar, V. (2015). Effect of irrigation in simulating long-term evapotranspiration climatology in a human-dominated river basin system. *Agricultural and Forest Meteorology*, *200*, 109–118. https://doi.org/10.1016/j.agrformet.2014.09.008

Jha, M. K., Chowdhury, A., Chowdary, V. M., & Peiffer, S. (2007). Groundwater management and development by integrated remote sensing and geographic information systems: prospects and constraints. *Water Resources Management*, *21*(2), 427–467. https://doi.org/10.1007/s11269-006-9024-4

Ji, L., Zhang, L., & Wylie, B. (2009). Analysis of Dynamic Thresholds for the Normalized Difference Water Index. *Photogrammetric Engineering & Remote Sensing*, *75*(11), 1307–1317. https://doi.org/10.14358/PERS.75.11.1307

Jin, X., & Sridhar, V. (2010). An integrated model coupling VIC and MODFLOW to study the hydrological prediction at the Snake River Basin. Retrieved from https://www.researchgate.net/profile/Xin_Jin48/publication/267410713_An_integrated_model_coupling_VIC_and_MODFLOW_to_study_the_hydrological_prediction_at_the_Snake_River_Basin/links/55c69e9b08aea2d9bdc548ec/An-integrated-model-coupling-VIC-and-MODFLOW-to-

Jin, Y., Schaaf, C. B., Gao, F., Li, X., Strahler, A. H., Lucht, W., et al. (2003). Consistency of MODIS surface bidirectional reflectance distribution function and albedo retrievals: 1. Algorithm performance. *J. Geophys. Res*, *108*(D5), 4158. https://doi.org/10.1029/2002JD002803

Johnston, R., & Kummu, M. (2012). Water Resource Models in the Mekong Basin: A Review. *Water Resources Management*, *26*(2), 429–455.

https://doi.org/10.1007/s11269-011-9925-8
Kaiser, B., & Roumasset, J. (2002). Valuing indirect ecosystem services: The case of tropical watersheds. *Environment and Development Economics, 7*(4), 701–714. https://doi.org/10.1017/S1355770X02000426
Kalnay, E., Kanamitsu, M., Kistler, R., Collins, W., Deaven, D., Gandin, L., et al. (1996). The NCEP/NCAR 40-Year Reanalysis Project. *Bulletin of the American Meteorological Society*, *77*(3), 437–471. https://doi.org/10.1175/1520-0477(1996)077<0437:TNYRP>2.0.CO;2
Kang, H., & Sridhar, V. (2019). Drought assessment with a surface-groundwater coupled model in the Chesapeake Bay watershed. *Environmental Modelling and Software*, *119*, 379–389. https://doi.org/10.1016/j.envsoft.2019.07.002
Kang, H., Sridhar, V., Mills, B. F., Hession, W. C., & Ogejo, J. A. (2019). Economy-wide climate change impacts on green water droughts based on the hydrologic simulations. *Agricultural Systems*, *171*, 76–88. https://doi.org/10.1016/j.agsy.2019.01.006
Keskinen, M., Kummu, M., Käkönen, M., & Varis, O. (2012). Mekong at the Crossroads: Next Steps for Impact Assessment of Large Dams. *AMBIO*, *41*(3), 319–324. https://doi.org/10.1007/s13280-012-0261-x
Khandelwal, A., Karpatne, A., Wei, Z., Kuang, H., Ghosh, R., Dugan, H., et al. (2019). *GLADD-R: A new Global Lake Dynamics Database for Reservoirs created using machine learning and satellite data GLADD-R: A new Global Lake Dynamics Database for Reservoirs*. Retrieved from http://umnlcc.cs.umn.edu/GlobalReservoirDatabase/
Kiem, A. S., Ishidaira, H., Hapuarachchi, H. P., Zhou, M. C., Hirabayashi, Y., & Takeuchi, K. (2008). Future hydroclimatology of the Mekong River basin simulated using the high-resolution Japan Meteorological Agency (JMA) AGCM. *Hydrological Processes*, *22*(9), 1382–1394. https://doi.org/10.1002/hyp.6947
Kingston, D. G., Thompson, J. R., & Kite, G. (2011). Uncertainty in climate change projections of discharge for the Mekong River Basin. *Hydrology and Earth System Sciences*, *15*(5), 1459–1471. https://doi.org/10.5194/hess-15-1459-2011
Kondolf, G. M., Rubin, Z. K., & Minear, J. T. (2014). Dams on the Mekong: Cumulative sediment starvation. *Water Resources Research*, *50*(6), 5158–5169. https://doi.org/10.1002/2013WR014651
Kondolf, G. Mathias, Schmitt, R. J. P., Carling, P., Darby, S., Arias, M., Bizzi, S., et al. (2018). Changing sediment budget of the Mekong: Cumulative threats and management strategies for a large river basin. *Science of the Total Environment*, *625*, 114–134. https://doi.org/10.1016/j.scitotenv.2017.11.361
Kueppers, L. M., Snyder, M. A., & Sloan, L. C. (2007). Irrigation cooling effect: Regional climate forcing by land-use change. *Geophysical Research Letters*, *34*(3). https://doi.org/10.1029/2006GL028679
Kuhn, A., & Britz, W. (2012). Can hydro-economic river basin models simulate water shadow prices under asymmetric access? *Water Science and Technology*, *66*(4), 879–886. https://doi.org/10.2166/wst.2012.251
Kummu, M., Lu, X. X., Wang, J. J., & Varis, O. (2010). Basin-wide sediment trapping efficiency of emerging reservoirs along the Mekong. *Geomorphology*, *119*(3–4), 181–197. https://doi.org/10.1016/J.GEOMORPH.2010.03.018
Kummu, M, & Sarkkula, J. (2008). Impact of the Mekong River Flow Alteration on the

Tonle Sap Flood Pulse. *AMBIO*, *37*(3), 185–192. https://doi.org/10.1579/0044-7447(2008)37[185:IOTMRF]2.0.CO;2

Kummu, Matti, & Varis, O. (2007). Sediment-related impacts due to upstream reservoir trapping, the Lower Mekong River. *Geomorphology*, *85*(3–4), 275–293. https://doi.org/10.1016/J.GEOMORPH.2006.03.024

Lauri, H., de Moel, H., Ward, P. J., Räsänen, T. A., Keskinen, M., & Kummu, M. (2012). Future changes in Mekong River hydrology: impact of climate change and reservoir operation on discharge. *Hydrology and Earth System Sciences*, *16*(12), 4603–4619. https://doi.org/10.5194/hess-16-4603-2012

Leck, H., Conway, D., Bradshaw, M., & Rees, J. (2015). Tracing the Water-Energy-Food Nexus: Description, Theory and Practice. *Geography Compass*, *9*(8), 445–460. https://doi.org/10.1111/gec3.12222

Li, D., Long, D., Zhao, J., Lu, H., & Hong, Y. (2017). Observed changes in flow regimes in the Mekong River basin. *Journal of Hydrology*, *551*, 217–232. https://doi.org/10.1016/j.jhydrol.2017.05.061

Li, Han, Wei, Y. D., & Korinek, K. (2018). Modelling urban expansion in the transitional Greater Mekong Region. *Urban Studies*, *55*(8), 1729–1748. https://doi.org/10.1177/0042098017700560

Li, Hongyi, Wu, H., Huang, M., & Leung, L. R. (2012). Irrigation & Drainage Systems Engineering Representing Natural and Manmade Drainage Systems in an Earth System Modeling Framework, *1*(2), 1–2. https://doi.org/10.4172/2168-9768.1000e107

Li, W., Qin, Y., Sun, Y., Huang, H., Ling, F., Tian, L., & Ding, Y. (2016). Estimating the relationship between dam water level and surface water area for the Danjiangkou Reservoir using Landsat remote sensing images. *Remote Sensing Letters*, *7*(2), 121–130. https://doi.org/10.1080/2150704X.2015.1117151

Liang, X., Lettenmaier, D. P., Wood, E. F., & Burges, S. J. (1994). A simple hydrologically based model of land surface water and energy fluxes for general circulation models. *Journal of Geophysical Research*, *99*(D7), 14415. https://doi.org/10.1029/94JD00483

Lipscomb, M., Mobarak, A. M., & Barham, T. (2013). Development Effects of Electrification: Evidence from the Topographic Placement of Hydropower Plants in Brazil. *American Economic Journal: Applied Economics*, *5*(2), 200–231. https://doi.org/10.1257/app.5.2.200

Liu, Xingcai, Tang, Q., Voisin, N., & Cui, H. (2016). Projected impacts of climate change on hydropower potential in China. *Hydrology and Earth System Sciences*, *20*(8), 3343–3359. https://doi.org/10.5194/hess-20-3343-2016

Liu, Xiuli, Chen, X., & Wang, S. (2009). Evaluating and predicting shadow prices of water resources in China and its nine major river basins. *Water Resources Management*, *23*(8), 1467–1478. https://doi.org/10.1007/s11269-008-9336-7

Liu, Y., Xiao, J., Ju, W., Xu, K., Zhou, Y., & Zhao, Y. (2016). Recent trends in vegetation greenness in China significantly altered annual evapotranspiration and water yield. *Environmental Research Letters*, *11*(9), 094010. https://doi.org/10.1088/1748-9326/11/9/094010

Lobell, D. B., & Bonfils, C. (2008). The effect of irrigation on regional temperatures: A spatial and temporal analysis of trends in California, 1934-2002. *Journal of Climate*, *21*(10), 2063–2071. https://doi.org/10.1175/2007JCLI1755.1

Lohmann, D., Raschke, E., Nijssen, B., & Lettenmaier, D. P. (1998). Regional scale hydrology: II. Application of the VIC-2L model to the Weser River, Germany. *Hydrological Sciences Journal*, *43*(1), 143–158. https://doi.org/10.1080/02626669809492108

Lohmann, Dag, Nolte-Holube, R., & Raschke, E. (1996). A large-scale horizontal routing model to be coupled to land surface parametrization schemes. *Tellus, Series A: Dynamic Meteorology and Oceanography*. https://doi.org/10.1034/j.1600-0870.1996.t01-3-00009.x

Lyon, S. W., King, K., Polpanich, O., & Lacombe, G. (2017). Assessing hydrologic changes across the Lower Mekong Basin. *Journal of Hydrology: Regional Studies*, *12*, 303–314. https://doi.org/10.1016/J.EJRH.2017.06.007

Ma, L., Wang, H., Qi, C., Zhang, X., & Zhang, H. (2019). Characteristics and Adaptability Assessment of Commonly Used Ecological Flow Methods in Water Storage and Hydropower Projects, the Case of Chinese River Basins. *Water*, *11*(10), 2035. https://doi.org/10.3390/w11102035

Manh, N. Van, Dung, N. V., Hung, N. N., Kummu, M., Merz, B., & Apel, H. (2015). Future sediment dynamics in the Mekong Delta floodplains: Impacts of hydropower development, climate change and sea level rise. *Global and Planetary Change*, *127*, 22–33. https://doi.org/10.1016/J.GLOPLACHA.2015.01.001

Marhaento, H., Booij, M. J., Rientjes, T. H. M., & Hoekstra, A. Y. (2017). Attribution of changes in the water balance of a tropical catchment to land use change using the SWAT model. *Hydrological Processes*, *31*(11), 2029–2040. https://doi.org/10.1002/hyp.11167

Martin, S. M., & Lorenzen, K. (2016). Livelihood Diversification in Rural Laos. *World Development*, *83*, 231–243. https://doi.org/10.1016/J.WORLDDEV.2016.01.018

Mekong River Commission. (2005). *Overview of the Hydrology of the Mekong Basin Mekong River Commission Meeting the Needs, Keeping the Balance*. Retrieved from http://www.mekonginfo.org/assets/midocs/0001968-inland-waters-overview-of-the-hydrology-of-the-mekong-basin.pdf

Mekong River Commission. (2010). Assessment of basin-wide development scenarios–main report. *Mekong River Commission, Vientiane, Lao PDR*.

Merola, R. B., Hien, T. T., Quyen, D. T. T., & Vengosh, A. (2015). Arsenic exposure to drinking water in the Mekong Delta. *Science of The Total Environment*, *511*, 544–552. https://doi.org/10.1016/J.SCITOTENV.2014.12.091

Minderhoud, P. S. J., Coumou, L., Erban, L. E., Middelkoop, H., Stouthamer, E., & Addink, E. A. (2018). The relation between land use and subsidence in the Vietnamese Mekong delta. *Science of The Total Environment*, *634*, 715–726. https://doi.org/10.1016/J.SCITOTENV.2018.03.372

Ming, B., Liu, P., Chang, J., Wang, Y., & Huang, Q. (2017). Deriving Operating Rules of Pumped Water Storage Using Multiobjective Optimization: Case Study of the Han to Wei Interbasin Water Transfer Project, China. *Journal of Water Resources Planning and Management*, *143*(10), 05017012. https://doi.org/10.1061/(ASCE)WR.1943-5452.0000828

Mitchell, T. D., & Jones, P. D. (2005). An improved method of constructing a database of monthly climate observations and associated high-resolution grids. *International Journal of Climatology*, *25*(6), 693–712. https://doi.org/10.1002/joc.1181

Monteith, L. J. (1965). Evaporation and environment, In The state and movement of water in living organisms. *Symp. Soc. Exp. Biol.*, 205–234. Retrieved from https://ci.nii.ac.jp/naid/10007810939/

MRC. (2018). *Irrigation database improvement for the lower Mekong basin*. Retrieved from http://www.mrcmekong.org/publications/

Mu, Q., Heinsch, F. A., Zhao, M., & Running, S. W. (2007). Development of a global evapotranspiration algorithm based on MODIS and global meteorology data. *Remote Sensing of Environment*, *111*(4), 519–536. https://doi.org/10.1016/J.RSE.2007.04.015

Mu, Q., Zhao, M., & Running, S. W. (2011). Improvements to a MODIS global terrestrial evapotranspiration algorithm. *Remote Sensing of Environment*, *115*(8), 1781–1800. https://doi.org/10.1016/J.RSE.2011.02.019

Muala, E., Mohamed, Y. A., Duan, Z., & Van der Zaag, P. (2014). Estimation of Reservoir Discharges from Lake Nasser and Roseires Reservoir in the Nile Basin Using Satellite Altimetry and Imagery Data. *Remote Sensing*, *6*(8), 7522–7545. https://doi.org/10.3390/rs6087522

Myneni, R. ., Hoffman, S., Knyazikhin, Y., Privette, J. ., Glassy, J., Tian, Y., et al. (2002). Global products of vegetation leaf area and fraction absorbed PAR from year one of MODIS data. *Remote Sensing of Environment*, *83*(1), 214–231. https://doi.org/10.1016/S0034-4257(02)00074-3

Narendra, K., Nageswara Rao, K., & Swarna Latha, P. (2013). Integrating remote sensing and GIS for identification of groundwater prospective zones in the Narava basin, Visakhapatnam region, Andhra Pradesh. *Journal of the Geological Society of India*, *81*(2), 248–260. https://doi.org/10.1007/s12594-013-0028-4

Nash, J. E., & Sutcliffe, J. V. (1970). River flow forecasting through conceptual models part I — A discussion of principles. *Journal of Hydrology*, *10*(3), 282–290. https://doi.org/10.1016/0022-1694(70)90255-6

Nesbitt, H., R. Johnston, and M. S. (2004). Mekong River water: will river flows meet future agriculture needs in the Lower Mekong Basin? *Water in Agriculture, Seng, V., Craswell, E., Fukai, S., and Fisher, K.(Eds), Australian Centre of International Agricultural Research Proceedings 116*.

Oikonomidis, D., Dimogianni, S., Kazakis, N., & Voudouris, K. (2015). A GIS/Remote Sensing-based methodology for groundwater potentiality assessment in Tirnavos area, Greece. *Journal of Hydrology*, *525*, 197–208. https://doi.org/10.1016/j.jhydrol.2015.03.056

Olson, K. R., & Morton, L. W. (2018). Tonle Sap Lake and River and confluence with the Mekong River in Cambodia Soil management View project. *Article in Journal of Soil and Water Conservation*, *73*(3), 60A-66A. https://doi.org/10.2489/jswc.73.3.60A

Paper, W. (2009). *GoldSim: Engineering and Environmental Simulation Software for Water Resource Applications*.

Pech, S., & Sunada, K. (2008). Population Growth and Natural-Resources Pressures in the Mekong River Basin. *Ambio*. SpringerRoyal Swedish Academy of Sciences. https://doi.org/10.2307/25547886

Pham, H. T., Marshall, L., Johnson, F., & Sharma, A. (2018). Deriving daily water levels from satellite altimetry and land surface temperature for sparsely gauged catchments: A case study for the Mekong River. *Remote Sensing of Environment*, *212*, 31–46.

https://doi.org/10.1016/j.rse.2018.04.034
Pipitone, C. I., Maltese, A., Dardanelli, G. I., Lo Brutto, M. I., & La Loggia, G. I. (2018). Monitoring Water Surface and Level of a Reservoir Using Different Remote Sensing Approaches and Comparison with Dam Displacements Evaluated via GNSS. *Remote Sensing*, *10*(1), 71. https://doi.org/10.3390/rs10010071
Pittock, J., Dumaresq, D., & Bassi, A. (2016). Modeling the Hydropower–Food Nexus in Large River Basins: A Mekong Case Study. *Water*, *8*(10), 425. https://doi.org/10.3390/w8100425
Plengsaeng, B., Wehn, U., & van der Zaag, P. (2014). Data-sharing bottlenecks in transboundary integrated water resources management: a case study of the Mekong River Commission's procedures for data sharing in the Thai context. *Water International*, *39*(7), 933–951. https://doi.org/10.1080/02508060.2015.981783
Pokhrel, Y., Burbano, M., Roush, J., Kang, H., Sridhar, V., & Hyndman, D. (2018). A Review of the Integrated Effects of Changing Climate, Land Use, and Dams on Mekong River Hydrology. *Water*, *10*(3), 266. https://doi.org/10.3390/w10030266
Quinn, J. D., Reed, P. M., Giuliani, M., Castelletti, A., Oyler, J. W., & Nicholas, R. E. (2018). Exploring How Changing Monsoonal Dynamics and Human Pressures Challenge Multireservoir Management for Flood Protection, Hydropower Production, and Agricultural Water Supply. *Water Resources Research*, *54*(7), 4638–4662. https://doi.org/10.1029/2018WR022743
Rasul, G., & Sharma, B. (2016). The nexus approach to water–energy–food security: an option for adaptation to climate change. *Climate Policy*, *16*(6), 682–702. https://doi.org/10.1080/14693062.2015.1029865
Richter, B., & Thomas, G. (2007). Restoring environmental flows by modifying dam operations. *JSTOR*. Retrieved from https://www.jstor.org/stable/26267852?casa_token=aiozWKMVOdAAAAAA:pnbt3UP1Bk1W1O0fEKoMA6xl41grmqT_XdN7ngBGS43u5Yg6Nn_7lw0OJ4y3T01IQamjIzNU6wXvvmHQ2-oRgMM64_XbHnasRSAGgJ8nQlWeSVcJxGQr
Ringler, C., von Braun, J., & Rosegrant, M. W. (2004). Water Policy Analysis for the Mekong River Basin. *Water International*, *29*(1), 30–42. https://doi.org/10.1080/02508060408691746
Rosegrant, M. W., Ringler, C., McKinney, D. C., Cai, X., Keller, A., & Donoso, G. (2000). Integrated economic-hydrologic water modeling at the basin scale: the Maipo river basin. *Agricultural Economics*, *24*(1), 33–46. https://doi.org/10.1111/j.1574-0862.2000.tb00091.x
Sabo, J. L., Ruhi, A., Holtgrieve, G. W., Elliott, V., Arias, M. E., Ngor, P. B., et al. (2017). Designing river flows to improve food security futures in the Lower Mekong Basin. *Science (New York, N.Y.)*, *358*(6368), eaao1053. https://doi.org/10.1126/science.aao1053
Sacks, W. J., Cook, B. I., Buenning, N., Levis, S., & Helkowski, J. H. (2009). Effects of global irrigation on the near-surface climate. *Climate Dynamics*, *33*(2–3), 159–175. https://doi.org/10.1007/s00382-008-0445-z
Sakamoto, T., Van Nguyen, N., Kotera, A., Ohno, H., Ishitsuka, N., & Yokozawa, M. (2007). Detecting temporal changes in the extent of annual flooding within the Cambodia and the Vietnamese Mekong Delta from MODIS time-series imagery. *Remote Sensing of Environment*, *109*(3), 295–313.

https://doi.org/10.1016/J.RSE.2007.01.011
Salomon, J. G., Schaaf, C. B., Strahler, A. H., Feng Gao, & Yufang Jin. (2006). Validation of the MODIS bidirectional reflectance distribution function and albedo retrievals using combined observations from the aqua and terra platforms. *IEEE Transactions on Geoscience and Remote Sensing*, *44*(6), 1555–1565. https://doi.org/10.1109/TGRS.2006.871564
Schubert, S. D., Suarez, M. J., Pegion, P. J., Koster, R. D., & Bacmeister, J. T. (2004). Causes of Long-Term Drought in the U.S. Great Plains. *Journal of Climate*, *17*(3), 485–503. https://doi.org/10.1175/1520-0442(2004)017<0485:COLDIT>2.0.CO;2
Senanayake, I. P., Dissanayake, D. M. D. O. K., Mayadunna, B. B., & Weerasekera, W. L. (2016). An approach to delineate groundwater recharge potential sites in Ambalantota, Sri Lanka using GIS techniques. *Geoscience Frontiers*, *7*(1), 115–124. https://doi.org/10.1016/j.gsf.2015.03.002
Sener, E., Davraz, A., & Ozcelik, M. (2005). An integration of GIS and remote sensing in groundwater investigations: A case study in Burdur, Turkey. *Hydrogeology Journal*, *13*(5–6), 826–834. https://doi.org/10.1007/s10040-004-0378-5
Shaban, A., Khawlie, M., & Abdallah, C. (2006). Use of remote sensing and GIS to determine recharge potential zones: the case of Occidental Lebanon. *Hydrogeology Journal*, *14*(4), 433–443. https://doi.org/10.1007/s10040-005-0437-6
Sheffield, J., Goteti, G., & Wood, E. F. (2006). Development of a 50-Year High-Resolution Global Dataset of Meteorological Forcings for Land Surface Modeling. *Journal of Climate*, *19*(13), 3088–3111. https://doi.org/10.1175/JCLI3790.1
Shrestha, B., Babel, M. S., Maskey, S., van Griensven, A., Uhlenbrook, S., Green, A., & Akkharath, I. (2013). Impact of climate change on sediment yield in the Mekong River basin: a case study of the Nam Ou basin, Lao PDR. *Hydrology and Earth System Sciences*, *17*(1), 1–20. https://doi.org/10.5194/hess-17-1-2013
Siebert, S., Burke, J., Faures, J. M., Frenken, K., Hoogeveen, J., Döll, P., & Portmann, F. T. (2010). Groundwater use for irrigation – a global inventory. *Hydrology and Earth System Sciences*, *14*(10), 1863–1880. https://doi.org/10.5194/hess-14-1863-2010
Sigvaldson, O. T. (1976). A simulation model for operating a multipurpose multireservoir system. *Water Resources Research*, *12*(2), 263–278. https://doi.org/10.1029/WR012i002p00263
Solomon, S., & Quiel, F. (2006). Groundwater study using remote sensing and geographic information systems (GIS) in the central highlands of Eritrea. *Hydrogeology Journal*, *14*(5), 729–741. https://doi.org/10.1007/s10040-005-0477-y
Son, N. T., Chen, C. F., Chen, C. R., Chang, L. Y., & Minh, V. Q. (2012). Monitoring agricultural drought in the Lower Mekong Basin using MODIS NDVI and land surface temperature data. *International Journal of Applied Earth Observation and Geoinformation*, *18*, 417–427. https://doi.org/10.1016/J.JAG.2012.03.014
Spruce, J., Bolten, J., Srinivasan, R., Lakshmi, V., Spruce, J., Bolten, J., et al. (2018). Developing Land Use Land Cover Maps for the Lower Mekong Basin to Aid Hydrologic Modeling and Basin Planning. *Remote Sensing*, *10*(12), 1910. https://doi.org/10.3390/rs10121910
Spruce, J., Bolten, J., Mohammed, I. N., Srinivasan, R., & Lakshmi, V. (2020). Mapping Land Use Land Cover Change in the Lower Mekong Basin From 1997 to 2010. *Frontiers in Environmental Science*, *8*, 21. https://doi.org/10.3389/fenvs.2020.00021

Sridhar, V. (2013). Tracking the Influence of Irrigation on Land Surface Fluxes and Boundary Layer Climatology. *Journal of Contemporary Water Research & Education*, *152*(1), 79–93. https://doi.org/10.1111/j.1936-704X.2013.03170.x

Sridhar, V., & Anderson, K. A. (2017). Human-induced modifications to land surface fluxes and their implications on water management under past and future climate change conditions. *Agricultural and Forest Meteorology*, *234–235*, 66–79. https://doi.org/10.1016/j.agrformet.2016.12.009

Sridhar, V., Billah, M. M., & Hildreth, J. W. (2018). Coupled Surface and Groundwater Hydrological Modeling in a Changing Climate. *Groundwater*, *56*(4), 618–635. https://doi.org/10.1111/gwat.12610

Sridhar, V., Ali, S. A., & Lakshmi, V. (2019). Assessment and validation of total water storage in the Chesapeake Bay watershed using GRACE. *Journal of Hydrology: Regional Studies*, *24*, 100607. https://doi.org/10.1016/J.EJRH.2019.100607

Sridhar, V., Kang, H., & Ali, S. A. (2019). Human-Induced Alterations to Land Use and Climate and Their Responses for Hydrology and Water Management in the Mekong River Basin. *Water*, *11*(6), 1307. https://doi.org/10.3390/w11061307

Stackhouse, P. W., Gupta, S. K., Cox, S. J., Mikowitz, J. C., Zhang, T., & Chiacchio, M. (2004). 12-year surface radiation budget data se. *GEWEX News*, *14*(4), 10–12.

Stone, R. (2016). Dam-building threatens Mekong fisheries. Retrieved from http://science.sciencemag.org/content/354/6316/1084.summary

Stone, Richard. (2011a). Mayhem on the Mekong. *Science*, *333*(6044), 814–818. https://doi.org/10.1126/science.333.6044.814

Stone, Richard. (2011b, August 12). Mayhem on the Mekong. *Science*. https://doi.org/10.1126/science.333.6044.814

Subba Rao, N. (2006). Groundwater potential index in a crystalline terrain using remote sensing data. *Environmental Geology*, *50*(7), 1067–1076. https://doi.org/10.1007/s00254-006-0280-7

Sun, S., Yan, X., Cui, P., & Feng, J. (2011). A four-step method for optimising the normal water level of reservoirs based on a mathematical programming model--a case study for the Songyuan backwater dam in Jilin Province, China. *International Journal of Environmental Research and Public Health*, *8*(4), 1049–60. https://doi.org/10.3390/ijerph8041049

Tatsumi, K., & Yamashiki, Y. (2015a). Effect of irrigation water withdrawals on water and energy balance in the Mekong River Basin using an improved VIC land surface model with fewer calibration parameters. *Agricultural Water Management*, *159*, 92–106. https://doi.org/10.1016/J.AGWAT.2015.05.011

Tatsumi, K., & Yamashiki, Y. (2015b). Effect of irrigation water withdrawals on water and energy balance in the Mekong River Basin using an improved VIC land surface model with fewer calibration parameters. *Agricultural Water Management*, *159*, 92–106. https://doi.org/10.1016/j.agwat.2015.05.011

Te, N. (2007). *Drought management in the Lower Mekong Basin*. The 3rd Southeast Asia Water Forum, Kuala Lumpur, Malaysia.

Teeuw, R. M. (1995). Groundwater Exploration Using Remote Sensing And A Low-Cost Geographical Information System. *Hydrogeology Journal*, *3*(3), 21–30. https://doi.org/10.1007/s100400050057

Thanh, T. N., Tri, V. P. D., Kim, S., Phuong, T. N., Mong, T. L., & Tuan, P. V. (2020). A

subregional model of system dynamics research on surface water resource assessment for paddy rice production under climate change in the Vietnamese mekong delta. *Climate*, *8*(3). https://doi.org/10.3390/cli8030041

Thiery, W., Visser, A. J., Fischer, E. M., Hauser, M., Hirsch, A. L., Lawrence, D. M., et al. (2020). Warming of hot extremes alleviated by expanding irrigation. *Nature Communications*, *11*(1), 1–7. https://doi.org/10.1038/s41467-019-14075-4

Thilakarathne, M., & Sridhar, V. (2017). Characterization of future drought conditions in the Lower Mekong River Basin. *Weather and Climate Extremes*, *17*, 47–58. https://doi.org/10.1016/J.WACE.2017.07.004

Thu, H. N., & Wehn, U. (2016). Data sharing in international transboundary contexts: The Vietnamese perspective on data sharing in the Lower Mekong Basin. *Journal of Hydrology*, *536*, 351–364. https://doi.org/10.1016/j.jhydrol.2016.02.035

Tran, H., Tran, T., Kervyn, M., Tran, H., Tran, T., & Kervyn, M. (2015). Dynamics of Land Cover/Land Use Changes in the Mekong Delta, 1973–2011: A Remote Sensing Analysis of the Tran Van Thoi District, Ca Mau Province, Vietnam. *Remote Sensing*, *7*(3), 2899–2925. https://doi.org/10.3390/rs70302899

Tsur, Y., Dinar, A., Doukkali, R. M., Roe, T. L., Tsur, Y., Dinar, A., et al. (2004). Irrigation water pricing: policy implications based on international comparison. *Environment and Development Economics*, *9*(6), 735–755.

Västilä, K., Kummu, M., Sangmanee, C., & Chinvanno, S. (2010). Modelling climate change impacts on the flood pulse in the Lower Mekong floodplains. https://doi.org/10.2166/wcc.2010.008

van Vuuren, D. P., Edmonds, J., Kainuma, M., Riahi, K., Thomson, A., Hibbard, K., et al. (2011). The representative concentration pathways: An overview. *Climatic Change*, *109*(1), 5–31. https://doi.org/10.1007/s10584-011-0148-z

Wang, W., Lu, H., Ruby Leung, L., Li, H.-Y., Zhao, J., Tian, F., et al. (2017). Dam Construction in Lancang-Mekong River Basin Could Mitigate Future Flood Risk From Warming-Induced Intensified Rainfall. *Geophysical Research Letters*, *44*(20), 10,378-10,386. https://doi.org/10.1002/2017GL075037

Winemiller, K. O., McIntyre, P. B., Castello, L., Fluet-Chouinard, E., Giarrizzo, T., Nam, S., et al. (2016). Balancing hydropower and biodiversity in the Amazon, Congo, and Mekong. *Science*, *351*(6269), 128–129. https://doi.org/10.1126/science.aac7082

Wood, E. F., Lettenmaier, D. P., & Zartarian, V. G. (1992). A land-surface hydrology parameterization with subgrid variability for general circulation models. *Journal of Geophysical Research*, *97*(D3), 2717. https://doi.org/10.1029/91JD01786

Wu, C. S., Chen, Y., Jeng, M. R., Hwong, J. L., & Lee, K. C. (2004). Evaluating the economic benefit of water resource nourishment by forests. *Taiwan Journal of Forest Science*, *19*(3), 187–197.

Wu, L., Feng, J., & Miao, W. (2018). Simulating the Impacts of Irrigation and Dynamic Vegetation Over the North China Plain on Regional Climate. *Journal of Geophysical Research: Atmospheres*, *123*(15), 8017–8034. https://doi.org/10.1029/2017JD027784

Yang, B., Zhang, Y., Qian, Y., Tang, J., & Liu, D. (2016). Climatic effects of irrigation over the Huang-Huai-Hai Plain in China simulated by the weather research and forecasting model. *Journal of Geophysical Research: Atmospheres*, *121*(5), 2246–2264. https://doi.org/10.1002/2015JD023736

Yang, Y., Zhang, M., Zhu, L., Liu, W., Han, J., & Yang, Y. (2017). Influence of Large

Reservoir Operation on Water-Levels and Flows in Reaches below Dam: Case Study of the Three Gorges Reservoir. *Scientific Reports*, *7*(1), 15640. https://doi.org/10.1038/s41598-017-15677-y

Zargar, A., Sadiq, R., Naser, B., & Khan, F. I. (2011). A review of drought indices. *Environmental Reviews*, *19*(NA), 333–349. https://doi.org/10.1139/a11-013

Zatarain Salazar, J., Reed, P. M., Quinn, J. D., Giuliani, M., & Castelletti, A. (2017). Balancing exploration, uncertainty and computational demands in many objective reservoir optimization. *Advances in Water Resources*, *109*, 196–210. https://doi.org/10.1016/J.ADVWATRES.2017.09.014

Zhao, R., & Chen, S. (2008). Fuzzy pricing for urban water resources: Model construction and application. *Journal of Environmental Management*, *88*(3), 458–466. https://doi.org/10.1016/j.jenvman.2007.03.004

Zhou, T., Haddeland, I., Nijssen, B., & Lettenmaier, D. P. (2016). Human-Induced Changes in the Global Water Cycle (pp. 55–69). American Geophysical Union (AGU). https://doi.org/10.1002/9781118971772.ch4

Zhou, T., Nijssen, B., Gao, H., Lettenmaier, D. P., Zhou, T., Nijssen, B., et al. (2016). The Contribution of Reservoirs to Global Land Surface Water Storage Variations. *Journal of Hydrometeorology*, *17*(1), 309–325. https://doi.org/10.1175/JHM-D-15-0002.1

Ziolkowska, J. R. (2015). Shadow price of water for irrigation-A case of the High Plains. *Agricultural Water Management*, *153*, 20–31. https://doi.org/10.1016/j.agwat.2015.01.024

Ziv, G., Baran, E., Nam, S., Rodriguez-Iturbe, I., & Levin, S. A. (2012). Trading-off fish biodiversity, food security, and hydropower in the Mekong River Basin. *Proceedings of the National Academy of Sciences*, *109*(15), 5609–5614. https://doi.org/10.1073/pnas.1201423109

Ziv, Guy, Baran, E., Nam, S., Rodríguez-Iturbe, I., & Levin, S. A. (2012). Trading-off fish biodiversity, food security, and hydropower in the Mekong River Basin. *Proceedings of the National Academy of Sciences of the United States of America*, *109*(15), 5609–14. https://doi.org/10.1073/pnas.1201423109

# Chapter 6
# Summary and Conclusion

The Mekong river basin (MRB) is one of the largest transboundary basins in the world shared between six countries, viz. China, Myanmar, Thailand, Lao PDR, Cambodia, and Vietnam, supporting more than sixty million people. Apart from being a lifeline for the people and ecosystems of half a dozen countries, the Mekong river hosts a huge unharnessed hydropower potential, which led to the development of water resources and construction of large dams with the catastrophic effects on the agriculture, fisheries, and ecosystem. The overarching objective of our study was to understand the changing hydrological conditions and develop a framework for assessing the water management by linking food-energy-water nexus for present and future conditions in fulfilling the demands of the irrigation, hydropower, domestic and ecological systems. The tasks were sequentially executed to achieve the objective and that included the following: 1) analyzing streamflow in the Mekong mainstem and tributaries considering the reservoir operation and climate change, 2) estimating net irrigation water requirement (NIWR) for the seven subbasins in the MRB, 3) quantifying hydropower production potential of the existing dams in the MRB and analyzing supply-demand scenarios considering the effect of irrigation growth on hydropower generation, and 4) developing a system dynamics model to simulate water allocation to the irrigation, domestic, hydropower generation, and ecological sectors, taking into account the effects of climate and land use and land cover change and satisfying the multiple criteria through feedback loops. The critical findings for each chapter are as follows:

Chapter 2: The land use and land cover change analysis was carried out using the high-resolution Earth's Change Atmosphere – Climate Change Initiative (ESA-CCI) maps from 1992 to 2015 suggested the expansion of the agriculture land over the forest area in the MRB. High resolution ($0.05^{o}$) Variable Infiltration Capacity (VIC) model was used to accurately simulate the streamflow of the Mekong river mainstem and tributaries with the Nash-Sutcliffe model efficiency coefficient (NSE) more than 0.6 and coefficient of correlation (r) more than 0.7 as compared to the observed inflow. The seasonal variation in the streamflow was governed by the monsoon precipitation with the peak flow occurring

during July-October. Streamflows varied substantially with the peak monthly streamflow gradually increasing from Chiang Saen in the upstream region to Kratie in the lower portion of the basin ranging from 4000 $m^3$/sec to more than 40,000 $m^3$/sec. On the other hand, the inflow to the dams located on the tributaries of the river was substantially less than the mainstem flow ranging from 10 $m^3$/sec to 2500 $m^3$/sec. The climate forecast using the four general circulation models (GCMs), namely GFDL-ESM2M, IPSL-CM5A-LR, MIROC-ESM-CHEM, and NorESM1-M, under RCP 4.5 and RCP 8.5 projected a wide range of temperatures (1-6 $^oC$) and precipitation changes (-5 to 20 %) in the basin between 2020 and 2099. The impact of climate change will be experienced by the dams through an increase in projected inflow from 1.2% to 25% under RCP 4.5 and a decrease of 28.5% - 74.7% under RCP 8.5 during 2020-2099 as compared to the long-term historic mean with a reduction during the dry season (March-May). In order to overcome the problem of data availability, the variation of the total storage of the reservoirs was simulated exclusively by regression analysis using the remote sensing products viz, LandSat8 satellite imagery for the estimation of the surface area fluctuation and altimetry datasets (ERS-1, T/P, ERS-2, GFO, Jason-1, Envisat, Jason-2, and Saral/Altika) defining the water level change. The simulated total storage precisely depicted the observed storage with NSE and r values of 0.90 or higher. The total storage of the reservoir was minimum during May-June, prior to the onset of the monsoon. The storage gradually increased and reached the maximum values by the monsoon termination (October-November); however, storages declined to satisfy water demand for domestic and irrigation purposes. The monthly comparison of the inflow to and outflow from the reservoirs showed the influence of dam operation on the streamflow by a general reduction in outflows. The seasonal cycle of the inflow and outflow from the reservoirs exhibited the lesser outflow during the wet period (June-November) and more outflow during the dry period (December-May) as compared to inflow.

Chapter 3: The growing population of the MRB is dependent on the expanding and intensifying agriculture for the food security of the region. The water requirement for irrigation plays a crucial role in water resource management as the finite available water needs to be distributed for various purposes such as energy generation, domestic water

needs, and industrial demands. A major portion of the MRB is covered with the croplands (40%) and the total irrigated area was estimated as 66,000 $km^2$ in 2004 hosted mainly by Delta (52%), Mun Chi (30%), and Middle Mekong (12%) subbasins. NIWR was estimated for the MRB using the improved VIC model with the irrigation scheme developed by Haddleland et al. (2006). The irrigation process was designed to initiate when soil moisture of the top layer falls below the level at which transpiration is limited and continues till the moisture reaches field capacity and the analysis showed reasonable estimates of NIWR. For instance, the simulated NIWR for the Mun Chi subbasin for 2007 estimated as 2268 million $m^3$ showed comparable volume to the observed estimates of 2452 million $m^3$ obtained from the AQUASTAT database. The irrigation water requirement for the MRB was calculated as 65,000 million $m^3$ for the observed period (1981-2019). Moreover, the NIWR for the Delta, Middle Mekong, Tolne Sap, Mun Chi, Vietnamese, Siem Bok, and Upper Mekong regions were estimated as 54,000 million $m^3$, 5000 million $m^3$, 3000 million $m^3$, 2500 million $m^3$, 450 million $m^3$, 3.6 million $m^3$, and 1.3 million $m^3$, respectively. The climate is expected to positively affect the MRB with the decrease in the NIWR as 0.25% for the future period as compared to the historic period. Similarly, the projected NIWR will reduce for Delta, Siem Bok, Vietnamese, and Middle Mekong with values ranging from 0.53% to 0.24%. On the other hand, the Upper Mekong and Mun Chi will face an increase of 5% in the projected NIWR. The seasonal variation of the NIWR is expected to increase during the summer season (March-May) and fall during the monsoon season (July-October). The exploration of the additional source of water to satisfy the growing demand is the key to the sustainable management of the MRB and groundwater remains largely underutilized in the MRB. A weighted overlay analysis was utilized to explore groundwater potential zones considering the topographical, hydrological, meteorological, and geoenvironmental characteristics of the MRB. A total of seven factors were determined and prepared as thematic layers to be integrated and processed in a GIS environment. Based on the analytical hierarchy principle, it was found that the drainage density, land cover, slope, and precipitation were the most effective indicators of the subsurface conditions and therefore aided in deciphering groundwater conditions in the area. A majority portion of the lower MRB showed the moderate potential for the groundwater availability, with areas of Laos and Thailand indicated high groundwater potentiality.

Chapter 4: The enormous flow of the Mekong river, combined with the strong topographic gradient, projects the MRB as the ideal site for the large-scale hydropower generation. The MRB has the hydropower potential of approximately 53,000 MW in the mainstem Mekong and 35,000 MW in the tributaries. The potential for hydropower from the multipurpose and hydropower reservoirs was estimated based on monthly release using generic regulation rules as described in Hanasaki *et al.* (2006), which was modified to better simulate the storage variation of the reservoirs. The high-resolution VIC model (0.05 deg spatial resolution) was employed for the estimation of the inflows and NIWR for the reservoirs. The simulated storage was able to precisely capture the observed variation in the storage and outflows. The multipurpose reservoirs were able to generate the desired annual energy ranging from 15 GWh to 400 GWh along with satisfying more than 80% of the irrigation water demand. Similarly, the irrigation reservoirs also satisfied more than 80% of the water demand for irrigation and hydropower reservoirs to generate the required energy between 2 GWh and 18990 GWh. Climate change will enhance the hydropower potential of the multipurpose dams with an average increase of 7.3% and 5.3% in the energy generation in the future under RCP 4.5 and RCP 8.5, respectively. But the irrigation water supply will suffer a decrease of 1.3% in fulfilling the future water demand as compared to the historic period. While the efficacy of the irrigation dams in meeting the irrigation water demand is expected to fall by 1%, despite meeting more than 93% of the irrigation water demand. The hydropower dams are expected to continue producing the same energy volume in the future under RCP 4.5 as during the historic period, but the energy potential will reduce by 2% under RCP 8.5. The investigation of the response of the six multipurpose and four irrigation dams under different conditions of agriculture expansion was explored by the development of six scenarios corresponding to 5% and 10% increase in irrigated area by incorporating two-crop cycles or three-crop cycles per year in the GoldSim environment. The increase in the irrigated area reduces the energy generation of the multipurpose dams by 1.5%, however, the addition of a crop cycle lowers the energy generation by more than 10%. The dam operation during the monsoon period executes the required performance but the November-January period shows more than a 38% reduction in energy generation. The impacts of climate change are found to be generally beneficial in this basin, suggesting the

possibility for dam operations with an increase in the energy potential of 31% under RCP 4.5 and 27% under RCP 8.5. The irrigation sector is marginally affected by climate change and anthropogenic activities with the irrigation water supply more than 88% and 100% of the demand from multipurpose and irrigation dams, respectively.

Chapter 5: A systems dynamic model was developed for the sustainable optimization of water allocation to the irrigation, domestic, hydropower generation, and ecological sectors, thereby taking into account the effects of climate and land use and land cover change and satisfying the multiple criteria through feedback loops in the MRB. Dynamic optimization and scenario analysis capabilities of GoldSim provides the mechanism to support the decision making under transforming conditions based on the available information. The system dynamic model of the Mekong river basin was able to accurately simulate the operation of the multipurpose, hydropower, and irrigation reservoir with the Nash-Sutcliffe model efficiency coefficient (NSE) more than 0.6 and coefficient of correlation (r) more than 0.8 between the simulated and observed monthly storage. The model incorporates the cascading effect of the upstream dams, projected irrigation water demand in the future, and population growth under the influence of climate change. The multipurpose dams produced an annual energy generation of 316 GWh accounting 97% of the demand and satisfied more than 60% of the water demand from the irrigation, municipal, and industrial sectors during 2006-2019. Sirindhorn and Ubol Ratana dams are able to perform better than other reservoirs in generating surplus hydropower energy due to large storage capacity. Similar efficiency was observed for the irrigation dams supplying more than 60% of the irrigation water demand and 50% of the demand from municipal and industrial sectors. The hydropower dams produced 35% more energy than the desired quantity accounting for an annual generation of 2863 GWh while satisfying more than 80% of the water demand of the municipal and industrial sectors. Climate change has a positive influence on the performance of the multipurpose dams with an enhancement of 24% and 20% in the energy generation during 2021-2009 under RCP 4.5 and RCP 8.5, respectively, as compared to the observed period. In addition, the increase in the demand satisfaction of the water demand from the other sectors is projected to be 6% and 4% under RCP 4.5 and RCP 8.5, respectively. Likewise, the irrigation dams are expected to have improved demand satisfaction with an increase of 10% for the irrigation demand and 12% for the municipal

and industrial water demands. The energy generation of the hydropower dams are forecasted to increase by 4% in the future under RCP 4.5 as compared to the observed period, however, the RCP 8.5 scenario will cause the dams to suffer a marginal decrease of 0.4%. The reservoirs were classified into four classes based on the stress index value defining the intensity of the flood and low flow events survived by the system. Most of the multipurpose dams are projected to shift from the medium or high class to medium or very high-stress class for the flood events in the future, on the other hand, the stress class for the low flow events remained as high for the observed and future period. However, the irrigation reservoirs fell under the low or high flood stress class and expected to move to medium or very high classes, while the low flow stress class to shift from low to high in the future. On the other hand, the flood stress class for the hydropower dams is expected to remain as low in the future under RCP 8.5 or change to medium under RCP 4.5, while the shift is from low to high class for low flow stress under RCP 8.5 or remain as low under RCP 4.5.

# Appendix A

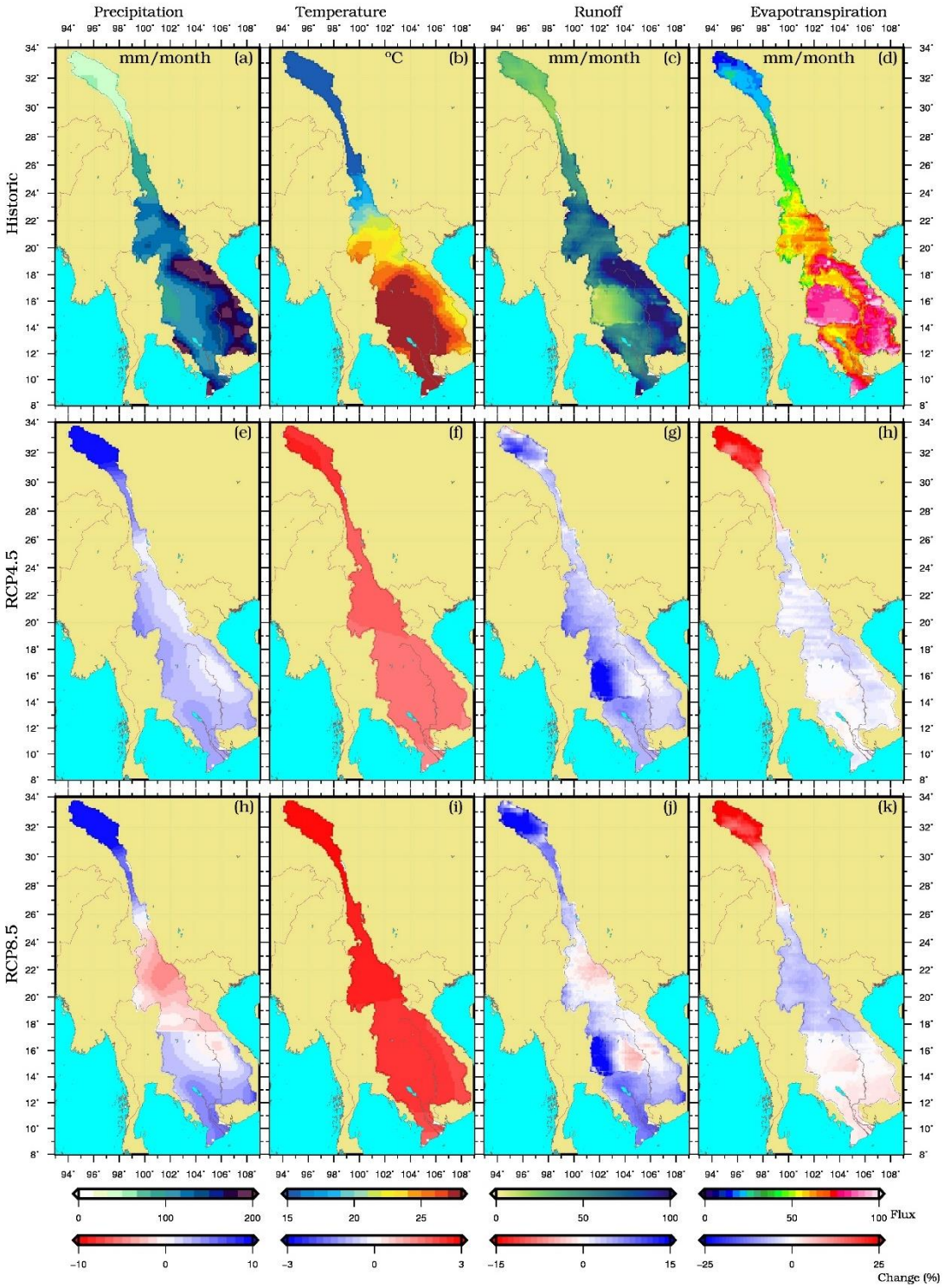


*Figure A1: Spatial distribution of precipitation, temperature, runoff, and evapotranspiration for the Mekong River basin for the historic period (1951-2005), and change in future (2006-2099) under RCP 4.5 and RCP 8.5*